

Winter 12-15-2018

Anodic Cyclization Reaction: Manipulation of Reaction Pathway and Efforts to Radical Cation and Radical Intermediate

Ruozhu Feng

Washington University in St. Louis

Follow this and additional works at: https://openscholarship.wustl.edu/art_sci_etds



Part of the [Chemistry Commons](#)

Recommended Citation

Feng, Ruozhu, "Anodic Cyclization Reaction: Manipulation of Reaction Pathway and Efforts to Radical Cation and Radical Intermediate" (2018). *Arts & Sciences Electronic Theses and Dissertations*. 1710.

https://openscholarship.wustl.edu/art_sci_etds/1710

This Dissertation is brought to you for free and open access by the Arts & Sciences at Washington University Open Scholarship. It has been accepted for inclusion in Arts & Sciences Electronic Theses and Dissertations by an authorized administrator of Washington University Open Scholarship. For more information, please contact digital@wumail.wustl.edu.

WASHINGTON UNIVERSITY IN ST. LOUIS

Division of Chemistry

Dissertation Examination Committee:

Kevin Moeller, Chair

Vladimir Birman

Marcus Foston

John-Stephen Taylor

Timothy Wencewicz

Anodic Cyclization Reaction: Manipulation of Reaction Pathway
and Efforts to Radical Cation and Radical Intermediate

by

Ruozhu Feng

A dissertation presented to
The Graduate School
of Washington University in
partial fulfillment of the
requirements for the degree
of Doctor of Philosophy

December 2018
St. Louis, Missouri

© 2018, Ruozhu Feng

Table of Contents

List of Schemes.....	vi
List of Tables.....	xii
List of Figures.....	xiii
List of Abbreviations	xvi
Acknowledgments	xix
Abstract of the Dissertation.....	xxi
Chapter 1: Introduction	1
1.1 Organic Electrochemistry	1
1.1.1 Nernst Equation.....	2
1.1.2 Cyclic Voltammetry.....	4
1.2 Anodic Cyclization Reaction	6
1.2.1 General Application of Anodic Cyclization Reaction	7
1.2.2 Reaction Experimental Apparatus.....	10
1.2.3 Constant Potential and Constant Current Electrolysis.....	12
1.2.4 The Influence of Substrate Concentration.....	14
1.3 Mechanism Related Topics in Anodic Cyclization Reactions.....	18
1.3.1 Curtin-Hammett Controlled Reaction.....	18
1.3.2 Thermodynamic Control and Kinetic Control.....	20

1.3.3	Reversible Radical Cyclization	21
1.3.5	conclusion	26
	Reference	27
Chapter 2: Anodic Cyclization Mechanism Study		30
2.1	Anodic Cyclization Reaction Mechanism Structure	31
2.1.1	Step One: The Reversible Cyclization.....	32
2.1.2	The Second Oxidation.....	36
2.2	Efforts to oxidatively construct enriched 1,4-dicarbonyl moieties and an observation about k_3 :.....	39
2.2.1	Retrosynthetic Analysis	39
2.2.2	Model Substrate.....	41
2.2.3	Conclusion	45
2.3	Experimental Section.....	46
2.4	Spectra Data	55
	Reference	56
Chapter 3: Pathway Control and the Formation of Seven Membered Rings		57
3.1	Synthesis of Artemisolide.....	57
3.2	Seven Membered Ring Formation in 5-7-5 System.....	59
3.2.1	Problems Constructing the Seven Membered Ring.....	59
3.2.2	Historical Approaches.....	62
3.3	Change of the Nature of Reactive Intermediate.....	64

3.3.1	Transformation to Radical Intermediate	64
3.3.2	Oxidative Radical Pathways and Seven-Membered Ring Formation.....	67
3.3.3	Constrained Radical Intermediate in Seven-Member Ring Formation.....	71
3.3.4	Constrained Radical Cation Intermediate in Seven-Membered Ring Formation	74
3.3.5	Discovered Alternative Pathway for Seven-Membered Ring Formation	81
3.4	Conclusions and control of pathway	83
3.5	Experimental Section.....	84
3.6	Spectra Data	97
	Reference	98
Chapter 4: Tandem Cyclization using Radical Pathway.....		100
4.1	Tandem Cyclization Reactions in the Literature.....	100
4.1.1	Paniculatine	101
4.1.2	Dankasterone	103
4.2	Initial Tests on Anodic Tandem Cyclization	104
4.2.1	Kolbe Approach.....	105
4.2.2	Double Michael Sequence.....	106
4.3	Enol Ether Substrate via Thiophene Route leading to Radical Cation Pathway	108
4.3.1	Enol Ether Substrate via Thiophene Route	108
4.3.2	Enol Ether Substrate Electrolysis	111
4.4	Alcohol Substrate leading to Radical Pathway	116
4.4.1	Synthesis of an enediol based tandem cyclization substrate:	116

4.4.2	Electrochemical Studies.....	125
4.5	Conclusions.....	133
4.6	Experimental Section.....	135
4.7	Spectra Data.....	156
	Reference.....	157
Chapter 5: Chan-Lam Coupling on Microelectrode Array Application.....		158
5.1	Micro Electrode Array.....	158
5.2	Binding Studies with C-Glycosides.....	160
5.3	Experimental Section.....	170
5.4	Spectra Data.....	173
	Reference.....	174
Chapter 6: Conclusion and Future Work.....		175
6.1	An Overview.....	175
6.2	Continuing Studies.....	176
Appendix A.....		194
Appendix B.....		203
Appendix C.....		218
Appendix D.....		247

List of Schemes

Scheme 1.1 Reduction Couple Reaction.....	3
Scheme 1.2 Anode Material Impact.....	15
Scheme 1.3. The Influence of a double layer on the reaction	17
Scheme 1.4 Electrolyte Effect in Reaction.....	18
Scheme 1.5 Curtin-Hammett Controlled Reaction.....	19
Scheme 1.6 Thermodynamic Product vs Kinetic Product	20
Scheme 1.7 α -silyl Radical over β -silyl Radical.....	22
Scheme 1.8 Radical Type vs Electrophilic Type Trapping.....	23
Scheme 1.9 Parallel Experiments on Cyclization.....	23
Scheme 1.10 Steady State Impact on Oxidation Potential ⁴⁴	26
Scheme 2.1 Anodic Cyclization Reaction Mechanism Model.....	31
Scheme 2.2 Steric Effect on Cyclization.....	33
Scheme 2.3 Polar Radical Cation Favors C-C Bond Formation	35
Scheme 2.4 Less Polar Radical Cation favors C-X Formation	36
Scheme 2.5 Stable Cation Increase k_2	38
Scheme 2.6 Aberrarone Retro-Analysis.....	40

Scheme 2.7 Proposed oxidation/hydrolysis route to higher-oxidized 1,4-dicarbonyls	41
Scheme 2.8 Proposed decomposition pathway for model substrates	42
Scheme 2.9 Electrophilic cyclization.....	43
Scheme 2.10. Addition of a bulky trityl protecting group dramatically improves conversion to product.....	43
Scheme 2.11. Water scavenges the unstable intermediate cation, avoiding overoxidation.....	45
Scheme 2.12 Synthesis of Electrolysis Substrate 25	46
Scheme 3.1 Retro-Analysis of Artemisolide.....	58
Scheme 3.2 Model Substrate Test on Seven Member Ring Formation.....	59
Scheme 3.3 Gem-dialkyl effect on seven-member ring formation.....	60
Scheme 3.4 Fused seven member ring containing allylic proton electrolysis test	61
Scheme 3.5 Total synthesis of Guanacastepene	62
Scheme 3.6 Gem substitution effect on seven member ring formation.....	63
Scheme 3.7 Radical Intermediate	65
Scheme 3.8 Literature using acetal as Michael Acceptor	67
Scheme 3.9 Radical Intermediate on Seven-Membered Ring Formation.....	68
Scheme 3.10 six member ring ene diol substrate electrolysis.....	70
Scheme 3.11 Radical Intermediate causing HAT (Hydrogen Atom Transfer).....	70

Scheme 3.12 constrained ene diol substrate synthesis.....	73
Scheme 3.13 Constrained Radical Intermediate Pathway Cyclization.....	73
Scheme 3.14 Michael addition to ketone to access constrained intermediate.....	75
Scheme 3.15 Michael condition test.....	76
Scheme 3.17 Electrolyte Influence.....	82
Scheme 3.18 Radical Pathway VS Radical Cation Pathway.....	83
Scheme 3.19 Synthesis of 59.....	84
Scheme 3.20 Synthesis of Electrolysis Substrate 47.....	85
Scheme 3.21 Electrolysis of 47.....	90
Scheme 4.1 Paniculatine Synthesis.....	102
Scheme 4.2 Paniculatine Synthesis via Anodic Cyclization.....	103
Scheme 4.3 Retro-Analysis of Dankasterone via Anodic Cyclization.....	104
Scheme 4.4 Tandem Cyclization via Anodic Condition.....	105
Scheme 4.5 Decarboxylation during Anodic Condition Tandem Cyclization.....	106
Scheme 4.6 Double Michael Sequence to Enol Ether Substrate.....	107
Scheme 4.7 Initial Test on Enol Ether Substrate.....	108
Scheme 4.8 Enol Ether 32 Synthesis via Thiophene Route.....	109

Scheme 4.9 Synthesis of 29.....	109
Scheme 4.10 Synthesis of 30.....	110
Scheme 4.11 Synthesis of 30- bromination step.....	110
Scheme 4.12 Synthesis of 32a/b.....	111
Scheme 4.13 Enol Ether Substrate 32a-b Electrolysis.....	113
Scheme 4.14 Acetylene as trapping group behavior.....	114
Scheme 4.15 Trisubstituted alkene as terminating group.....	115
Scheme 4.16 Retro analysis of ene diol 44.....	117
Scheme 4.17 Two Attempts to Alcohol Substrate.....	118
Scheme 4.18 Acetalization condition.....	119
Scheme 4.19 Michael addition to ketene acetal model substrate test.....	121
Scheme 4.20 Acyclic ene diol substrate synthesis.....	123
Scheme 4.21 Michael-type addition condition optimization.....	124
Scheme 4.22 Initial Tandem Cyclization Test on 44a.....	125
Scheme 4.23 Substrate 45 Electrolysis Test.....	126
Scheme 4.24 Substrate 46 Electrolysis Test.....	130
Scheme 4.25 Possible Pathway.....	133

Scheme 4.26 MOM protected substrate under anodic condition.....	135
Scheme 4.27 Electrolysis Substrate Synthesis Route	135
Scheme 4.28 Synthesis of side chain 29	136
Scheme 4.29 Synthesis of side chain 30	139
Scheme 4.30 Bromination Reagent Screening for 30.....	141
Scheme 4.31 Synthesis of Enol Ether Substrate 32.....	142
Scheme 4.32 Electrolysis of Enol Ether Substrate 32a-b.....	146
Scheme 4.33 Route for Synthesis of 44a	147
Scheme 4.34 Acetal Transformation Condition Screening.....	148
Scheme 4.35 Substrate 44a Condition Screening	150
Scheme 4.36 Synthesis Route of 45.....	151
Scheme 4.37 Synthesis Route of 46.....	154
Scheme 5.1. A site-selective Diels-Alder reaction	161
Scheme 5.2. The first site-selective placement of a C-glycoside on the arrays	162
Scheme 5.3 Addition of a C-glycoside based alcohol nucleophile to the surface of an array. ...	164
Scheme 5.4 Sugar-Pyrene Linker	166
Scheme 5.5 Chan-Lam Coupling on Micro Electrode Array.....	167

Scheme 6.1 Acyclic version of substrates for electrochemical Tandem cyclization..... 179

List of Tables

Table 1.1 Brief Summary of Anodic Cyclization Reaction	10
--	----

List of Figures

Figure 1.1 Nernst Equation	3
Figure 1.2 Cyclic voltammetry sweep	4
Figure 1.3 Fc^+ reduction voltammogram	5
Figure 1.4 Example of chemically irreversible voltammogram	6
Figure 1.5 Electrochemical coupling reaction.....	7
Figure 1.6 Electrolysis Set-up	11
Figure 1.7 Power Source	11
Figure 1.8 Constant Current Electrolysis	13
Figure 1.9 Double Layer Model/ Helmholtz Model	16
Figure 2.1 1,4-dicarbonyl Structure	39
Figure 2.2 Model substrates	41
Figure 2.3 ^1H NMR of 34.....	51
Figure 2.4 COSY of 34	52
Figure 2.5 HMBC of 34	53
Figure 2.6 Simulated 3D structure of 34 using ChemDraw	54
Figure 3.1 Electrolysis of 33 by Robert Perkins.....	69

Figure 3.2 Constrained Radical Intermediate Substrate.....	72
Figure 3.3 Constrained ene diol substrate electrolysis. NMR of the crude product. Coumarin as internal standars	74
Figure 3.4 Constrained Radical Cation Intermediate Substrate	75
Figure 3.5 Electrolysis of 47 using trimethoxy benzene as internal standard.....	78
Figure 3.6 Material after fast chromatography following electrolysis of 47	79
Figure 3.7 HMBC for 49.....	80
Figure 3.8 HMBC of 49	93
Figure 3.9 TOCSY of 48a.....	94
Figure 4.1 Paniculatine and Dankasterone.....	101
Figure 4.3 substrate 45 electrolysis entry c.....	128
Figure 4.4 substrate 45 electrolysis entry d.....	129
Figure 4.5 substrate 46 electrolysis entry b.....	131
Figure 4.6 substrate 46 electrolysis entry c isolated 47	132
Figure 5.1 An Addressable Micro Electrode.....	159
Figure 5.2 biphenyl substituted c-glycoside.....	165
Figure 5.3. A preliminary signaling study.....	169
Figure 6.1 Cis double bond as constrain in substrate.....	177

Figure 6.2 MOM protected Tandem cyclization substrate..... 178

List of Abbreviations

A	amp
Ac	acetyl
Bn	benzyl
Bu	butyl
COSY	homonuclear correlation spectroscopy Cp cyclopentadienyl
CSA	camphorsulfonic acid
Cy	cyclohexyl
dba	dibenzylideneacetone
dppf	1,1'-bis(diphenylphosphino)ferrocene CDI carbonyl diimidazole
DBU	1,8-diazabicyclo[5.4.0]undec-7-ene DCM dichloromethane
DCM	dichloromethane
DIBAL	diisobutylaluminum hydride
DIPA	diisopropylamine
DHP	3,4-dihydro-2H-pyran
DMAP	4-(dimethylamino)pyridine
DME	1,2-dimethoxyethane
DMF	dimethyl formamide
DMPS	dimethylphenylsilyl
DMSO	dimethyl sulfoxide
E	voltage
EDTA	ethylenediaminetetraacetic acid

Ep/2	half-peak height
ESI	electrospray ionization
Et	ethyl
F	faraday
g	gram
h	hour
HMDS	bis(trimethylsilyl)amide
HMPA	hexamethylphosphoramide
HR-MS	high resolution mass spectrometry
L	liter
LAH	lithium aluminum hydride
LDA	lithium diisopropylamide
M	mole per liter
mCPBA	3-chloroperbenzoic acid
Me	methyl
mol	mole
n	quantified charge
NBS	N-bromosuccinimide
NOESY	nuclear Overhauser effect spectroscopy
NMR	nuclear magnetic resonance
PG	protecting group
Ph	phenyl
PPTS	pyridinium p-toluenesulfonate

iPr	1-methylethyl
Rn	variable functional group
RSM	recovered starting material
RVC	reticulated vitreous carbon
s	second
T	temperature
TBAF	tetrabutylammonium fluoride
TBAI	tetrabutylammonium iodide
TBS	tert-butyldimethylsilyl
TEA	triethylamine
TEMPO	(2,2,6,6-tetramethylpiperidin-1-yl)oxy
Tf	trifluoromethanesulfonyl
THP	tetrahydropyran
TIPS	triisopropylsilyl
TMS	trimethylsilyl
THF	tetrahydrofuran
Trt	triphenylmethyl
Ts	4-methylbenzylsulfonyl
V	volt
X	variable atom or group
Y	variable atom or group

Acknowledgments

Funding for this research was provided by the National Science Foundation.

Professor Kevin Moeller as my PI and my teacher, he never gave up on me and always guided me.

This research was highly influenced by Rob Perkins, Alison Redden, Jake Smith, Sakshi Uppal.

During the research, a strong support from the group was highly appreciated.

The nuclear magnetic resonance spectroscopic data presented within this work was collected with the help of Jeff Lung-Fa Kao, and the Washington University in St. Louis High Resolution NMR Facility.

The mass spectrometric data presented in this work was collected by the NIH/NIGMS-supported Biomedical Mass Spectrometry (MS) Research Resource at Washington University in St. Louis.

Ruozhu Feng

Washington University in St. Louis

December 2018

Dedicated to my love and my parents.

Abstract of the Dissertation

Anodic Cyclization Reaction: Manipulation of Reaction Pathway

and Efforts to Radical Cation and Radical Intermediate

by

Ruozhu Feng

Doctor of Philosophy in Chemistry

Washington University in St. Louis, 2018

Professor Kevin D. Moeller, Chair

In recent years, synthetic chemists have been expressing significant interest in electro-organic synthetic methods. This interest is being fueled by the existence of an increasing number of successful methods in the literature and the availability of new electrochemical equipment that removes the barrier to attempting an electrolysis reaction for the first time. Yet while these developments have fueled growth in some areas of electro-organic synthesis (the recycling of chemical catalysts for example), other areas remain underdeveloped. One such area is the exploration of reactions that can be triggered directly as an electrode surface without the use of any chemical reagent. Such reactions lead to highly reactive intermediates that allow for entirely new modes of reactivity to be explored. For example, our group has been working to develop anodic oxidation reactions that convert electron rich olefins into reactive radical cation intermediates. The reactions lead to a reversal in the polarity of the original olefin that enable the normally nucleophilic groups to be used as electrophiles. The result is an opportunity to change the entire manner in which the synthesis of a complex target is approached. Simply put, new modes of reactivity offer an opportunity to not only change the way individual steps in a

synthetic sequence are conducted but also change the overall route because groups that normally function in a certain manner no longer behave the same way. While efforts to demonstrate the power of these opportunities have been successful for a variety of reactions in the group, our ability to continue forwarding the chemistry into even newer areas relies on our continuing to expand our knowledge of the reactive intermediates involved in electrochemical oxidation reactions, how they behave, and how they can be channeled down productive pathways. With this in mind, the main focus of this dissertation is to build our understanding of the reactive intermediates involved in anodic cyclization reactions and how those intermediates can best be applied as synthetic tools. The work probes the advantage of directly using the radical cations intermediates generated at an anode for triggering bond formation relative to pushing the reactions away from pathways that utilize the radical cation and toward pathways that involve an oxidative radical pathway. Along these lines, a synthetic route that allows both pathways to be accessed from the same starting materials has been developed. Using the chemistry, reactions that generate seven membered ring products and oxidative tandem cyclization reactions have been explored. In addition to these studies, an example of how optimizing a reaction sometimes requires one to pay attention to intermediates downstream of the cyclization is reported. Finally, the electrochemical method has been extended to an example of how it can be used in the synthesis of a complex molecular surface.

Chapter 1: Introduction

This chapter covers the fundamental background of electrochemistry and anodic cyclization reactions needed for the subsequent chapters. Section 1.1 discusses organic electrochemistry in terms of physical organic chemistry basics including the understanding of Nernst Equation and the application of cyclic voltammetry. Section 1.2 covers a general introduction to anodic cyclization, the experimental apparatus required for the reactions, and the factors (including current, concentration, temperature) that can affect reaction results. This chapter serves two major functions. (1) It provides a set of basic principles for understanding the reaction observations in the rest of this thesis. (2) It serves as a quick and simplified guide to understanding electro organic synthesis in general.

1.1 Organic Electrochemistry

Organic electrochemistry shares the same fundamental principles with the larger area of electrochemistry (analytical devices, batteries, energy storage devices, etc.), but it is more focused on organic chemical transformations. The pioneering work in this area originated with Faraday, who defined the laws of electrolyses and terms like anode, cathode, etc., and Kolbe, who developed electrochemical decarboxylation reactions, in the period between 1820-1840.¹ Toward the end of the nineteenth century Tafel and Haber introduced a method for the reduction of nitrobenzene (the now famous Haber process, 1898) that contributed greatly towards our understanding of organic electrode process. The first half of the twentieth century witnessed further growth in synthetic electrochemistry. For instance, Hickling introduced a potentiostat that brought electrochemical experiments into more common practice. After World War II, most of

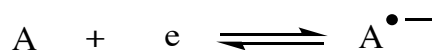
the attention was transferred to non-aqueous solvents reactions and theoretical foundations on the physical organic side¹. The first edition of *Organic Electrochemistry* (M. M. Baizer, ed., 1973) led to a more unified understanding of organic electrosynthesis and provided a foundation for future growth. Yet, while this growth was occurring, much of the larger synthetic community ignored the advantages of the technique. Most organic chemistry text books restricted their discussion of electrochemical methods to the Kolbe Electrolysis discovered in 1849. However, a series of dedicated research groups continued to press the issue. Seminal works by the groups of Schafer, Steckhan, Saveant, Simonet, Lund, Shono, Torii, Fuchigami, Yoshida, Fry, Peters, Little, and Moeller forwarded ever more synthetically relevant examples of how electrochemical methods could benefit the larger area of synthesis^{1,2}. This led to the modern-day situation where an ever-increasing number of synthetic chemists are starting to take advantage of the power of organic electrochemistry.²⁻⁸

1.1.1 Nernst Equation

Reactions at an electrode surface are at their core electron-transfer processes. As such, they fall into two major classes. Inner sphere electron transfers that involve bonding processes between two groups during an electron-transfer process and outer sphere electron transfers that exchange an electron without a bonding event. At an electrode the two processes are easy to distinguish. For an inner sphere electron transfer, the molecule becomes bound to the electrode either before or during the process. For an outer sphere electron transfer, an electron jumps between the electrode and the substrate. Most organic electrochemical processes involve outer sphere electron transfer. For example, a single electron transfer between an electrode to a carbonyl moiety to form a radical anion in solution is typically an outer sphere electron transfer. The same is true for

the one electron oxidations of electron-rich olefins that are the main focus of the thesis that follows.

All such processes are governed by the Nernst Equation. This equation defines the relationship between the potential (energy) necessary for an electron-transfer process and the equilibrium that occurs at the electrode surface. For example, consider the generic reduction shown in Scheme 1.1.



Scheme 1.1 Reduction Couple Reaction

For this transformation, the potential at the electrode can be described by the Nernst equation as follows.

$$E = E^{\circ} - \frac{RT}{nF} \ln \frac{A^{\bullet-}}{A}$$

Figure 1.1 Nernst Equation

E° reflects the standard potential. According to definition, the standard potential (reduction potential by definition) of the $A/A^{\bullet-}$ couple is the standard electromotive force when this couple is opposed to normal hydrogen electrode (NHE) whose potential is set to 0 artificially.¹ The potential E is a number that can be measured experimentally for a fully reversible system. To understand this better in terms of practical means, a brief introduction to the commonly used cyclic voltammetry technique requires.

1.1.2 Cyclic Voltammetry

Cyclic voltammetry is a common technique used to measure substance oxidation and reduction potentials. It is conducted by varying an applied potential to a solution in a linear fashion and measuring the current associated with that varied potential. The potential is swept in both directions leading to the “cyclic” part of the experiment (Figure 1.2). The voltammogram is plotted on an X,Y-axis with the X-axis being potential and the Y-axis being current. For a fully reversible electron transfer, the experiment leads to a “duck shape” voltammogram. This voltammogram allows one to measure the equilibrium oxidation potential of the substrate being studied. can be drew, which contains information of substance oxidation/reduction potential.⁹

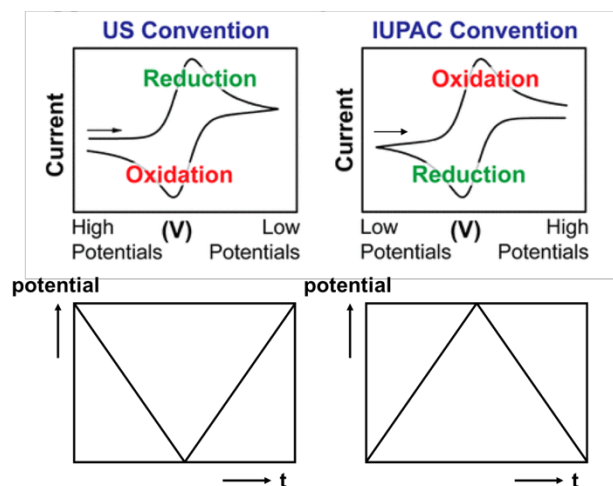


Figure 1.2 Cyclic voltammetry sweep

In the following example of reversible Fc^+ reduction (Figure 1.3), the voltammogram is achieved using 1mM Fc^+ solution at a scan rate of 100mV/s.⁹

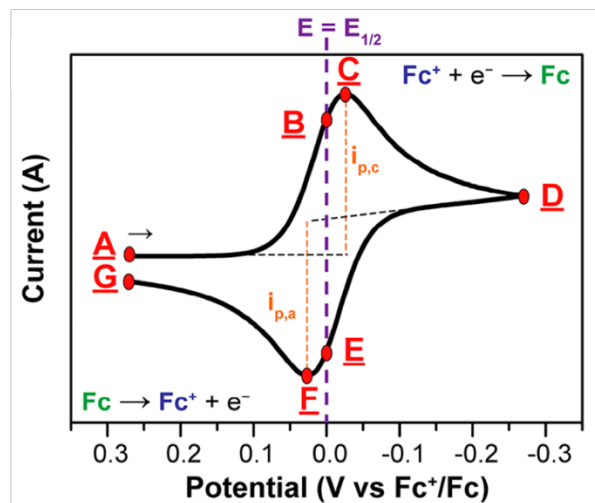


Figure 1.3 Fc^+ reduction voltammogram

In the forwarding scan, (A to D), Fc^+ is being reduced to Fc . At point C, the current reached its highest value ($i_{p,c}$). At this point, the current passed is a result of both material that was adsorbed onto the surface of the electrode and material that is diffusing to that surface. As the experiment sweeps to more negative potential, the material adsorbed on the electrode is consumed and the current falls to the diffusion control limit for the material diffusing to the surface. If the CV were continued past point D, the current would stabilize at this level. The reverse scan then show the same, but opposite trend. At point B and E, Fc^+ equals to Fc concentration. This point is the midway point between the two peak potentials that are separated by a distance of $0.059/n$ where n is the number of electrons transferred. According to Nernst Equation, the reduction potential of this process $E = E_{1/2} = 1/2 (E_{p,a} + E_{p,c})$. (The number of $E_{1/2}$ matches average potential of $E_{p,a}$ and $E_{p,c}$). The potential measured here is a thermodynamic potential. Note that, for a completely chemically reversible process, current associate with point F and point C are the same⁹.

The following example shows a chemically irreversible oxidation process.

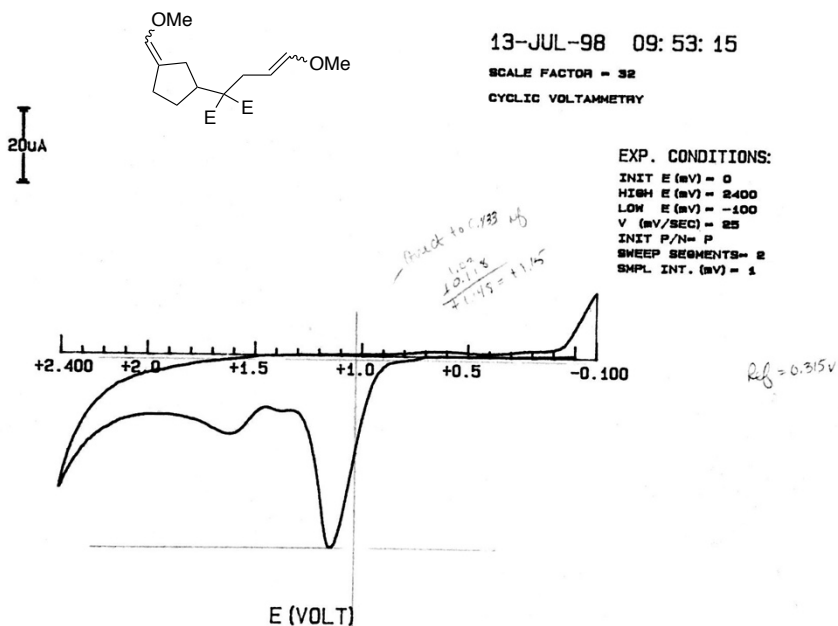


Figure 1.4 Example of chemically irreversible voltammogram

Due to its irreversibility, $E_{p/2}$ is reported as oxidation potential of this process. The value measured is a kinetic value. It depends on the concentration of the reagent, the concentration of electrolyte, the sweep rate, etc. In other words, to make comparisons between kinetic potentials of different substrates all of the other reaction parameters must be identical. The kinetic value is also dependent on the rate of a follow up reaction. This will be discussed in section 1.3.4.

1.2 Anodic Cyclization Reaction

With this backdrop, the Moeller group has been systematically studying anodic cyclization reactions and their application to organic synthesis.^{4,10} In general, anodic oxidation reactions are umpolung reactions.¹¹⁻¹⁴ For an anodic cyclization, the reactions involve a direct coupling between two nucleophiles with no need for additional transformations to convert the polarity of

one of the groups. The reactions are frequently more gentle and selective than reactions that involve a chemical oxidant,¹⁵ and they can be used to provide a straightforward method for constructing complex ring systems¹⁶.

1.2.1 General Application of Anodic Cyclization Reaction

In general, all electrochemical coupling reactions can be fit into one of two main categories (Figure 1.5) in that they are either oxidation or reduction reactions. Both are by their very nature unipolung reactions. In an oxidation reaction, an electron is removed from a substrate to convert an electron rich nucleophile into an electron poor electrophile. In a reduction reaction, an electron is added to the substrate to convert an electron poor electrophile into an electron rich nucleophile. Both can be used to trigger coupling reactions. Oxidation reactions occur at the anode in an electrolysis cell and reduction occurs at the cathode. Both reactions occur in every electrolysis, but normally one of the reactions is the primary reaction of interest and the other is an “auxiliary reaction”. In the thesis below, we will be focusing on oxidative coupling reactions. In each case, the auxiliary reaction will be the reduction of methanol to hydrogen gas and methoxide. The methoxide neutralizes the acid generated at the anode during the oxidation.

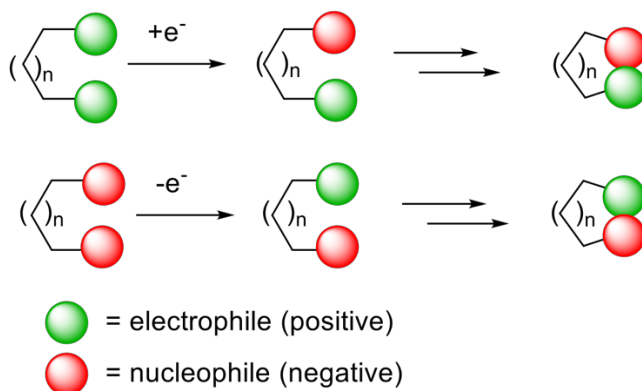


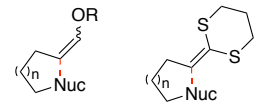
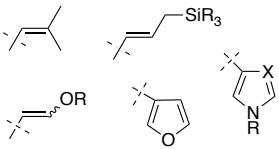
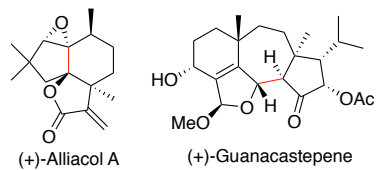
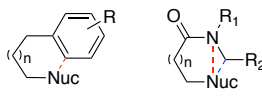
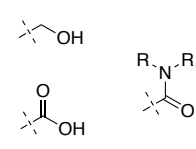
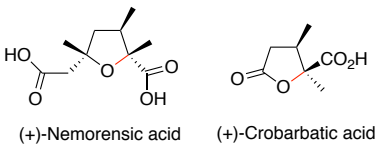
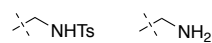
Figure 1.5 Electrochemical coupling reaction

An intramolecular anodic cyclization reaction starts when one of the electron rich moieties in a substrate is oxidized. In our group, this is typically an olefin and the electron-transfer convert the olefin into a very reactive, electrophilic radical cation intermediate. The radical cation is trapped by an internal nucleophile (the second electron-rich moiety). To accomplish this task, the initial group oxidized typically has a lower oxidation potential than any other electron rich moieties in the molecule. The qualifying word “typically” was used because there are circumstances where an electrolysis reaction is governed by the Curtin-Hammett principle.¹⁷ In these cases, a group with a low oxidation potential that does not participate in a desired coupling reaction is initially oxidized. A subsequent intramolecular electron transfer then leads to the internal oxidation of a second group. It is the reactive intermediate generated from this second group that triggers the desired coupling reaction. The coupling reaction drains the equilibrium associated with the intramolecular electron transfer toward the desired cyclization product. For the most part, we will treat these situations as special cases as they arise. A more detailed discussion of the general mechanism and how we think about the reactions will be presented below in Section **2.1**.

For now, it is important to point out that our group along with others have explored anodic cyclization reactions that arise from a series of substrates. In these substrates, the initial sites of oxidation and the trapping groups for the subsequent intermediates have been varied so that an empirical feel for the reactions has been developed. Those results have provided a mechanistic model for how to think about the reactions and how to address problems with new cyclization reactions as they arise. Since all anodic coupling reactions proceed through similar types of mechanisms, the details of the reactions studied to date provide valuable insight into how new reactions can be designed and optimized.

With this in mind, the groups oxidized in such reactions have been electron rich aryl rings¹⁸, enol ethers^{15,16,18-26}, ketene acetals^{15,17,27-34}, and amides (generating N-acyliminium ions^{35,36} and amidyl radicals³⁷). The reactive intermediates generated from these oxidation reactions have been combined with a variety of different trapping partners based on the nature of the products one has wanted to generate. For C-C bond formation, trapping partners have been di- and tri-substituted olefins^{21,22}, allylsilanes^{24,28,31}, enol ethers^{18,20-22,31,33}, heterocycles^{4,17,27,38}, and electron-rich aromatic rings¹⁸. For C-O bond formation, trapping partners can be primary alcohols^{15,19,23,29,39,40}, amides³⁴ and carboxylic acids⁴¹. For C-N bond formation, trapping partners can be sulfonamides^{39,40,42,43} and amines⁴⁴. During these studies, a number of total syntheses have been completed including with respect to C-C bond formation, Alliacol A⁴⁵, Arteannuin ring skeleton²⁷, Cyathin core⁴⁶, Heptemrone B¹⁶, and Guanacastepene¹⁶. For C-O bond formation, (+)-Nemorensic acid¹⁵ and (-)-Crobarbatic acid²⁹ have been made along with a series of C-glycoside derivatives. *(make sure that you have the main references here)*. For C-N bond formation, a series of amino acids derivatives and peptidomimetics have been synthesized.⁴¹ A brief summary of reaction types based on substrates and trapping partners that have been used is presented in **Table 1.1**. Some of the more interesting observations made in connection with these reactions will be discussed in the rest of this chapter.

Table 1.1 Brief Summary of Anodic Cyclization Reaction

substrate	bond formation	trapping group	application
	C-C		 (+)-Alliacol A (+)-Guanacastepene
	C-O		 (+)-Nemorensic acid (+)-Crobarbatic acid
	C-N		amino acids derivatives peptidomimetics

The first of these observations is that the electrochemical reactions can not only be used during the early stages of a synthesis for establishing synthetic building blocks, but also at the end of multi-step syntheses generating complex ring structures.⁴⁷ The method is both gentle and very versatile.

1.2.2 Reaction Experimental Apparatus

Before undertaking any further discussion of key reaction observations, it is important to examine how the reactions are actually conducted. Organic electrolysis set up are relatively straightforward. The reaction cell can be as simple as a three-neck round bottom flask or a vial for an undivided cell reaction (one where the anode and the cathode are in the same chamber, Figure 1.6).¹ The flask is then fitted with two carbon rods as electrodes that are attached to a direct current (DC) power source. This is the setup used for most of the reactions discussed in

this thesis in Chapter 2, 3 and 4. The two half reactions (oxidation of the substrate at the anode and reduction of methanol at the cathode) occur automatically when a constant current is applied to the reaction. The key then is the power supply used to apply that current.

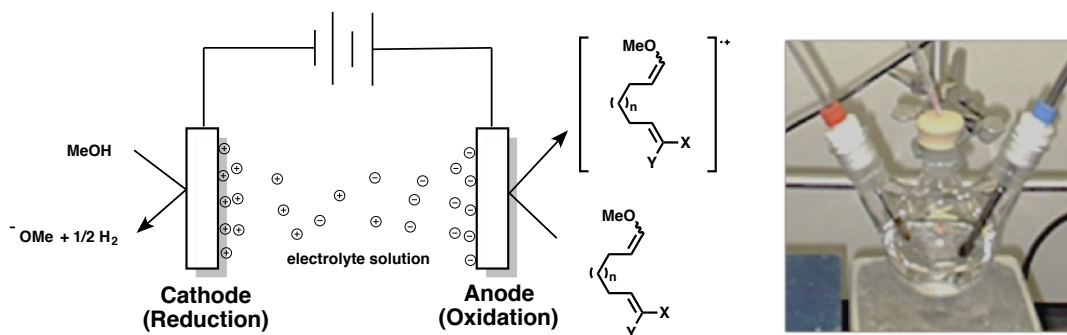
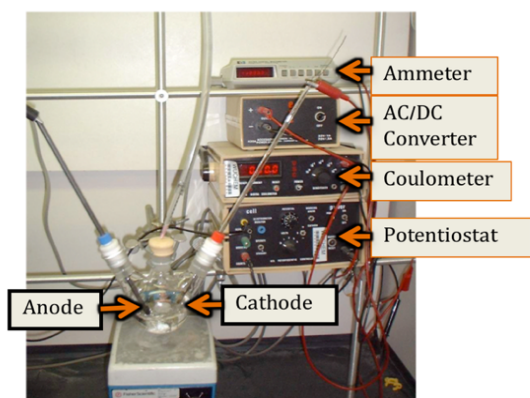
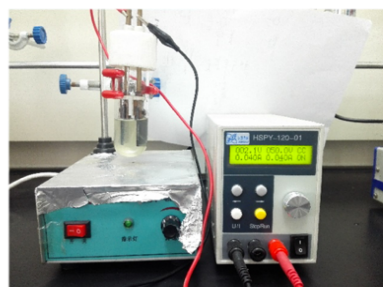


Figure 1.6 Electrolysis Set-up



Moeller, K.D. lab



Zeng, C. lab



ElectroSyn from IKA

Figure 1.7 Power Source

As for this DC power source, **Figure 1.7** shows several different types of options that can be used. The system shown in top left has been used in Moeller lab for over 30 years, an indication of the durability associated with electrochemical equipment. This set up is comprised of an AC/DC converter, a potentiostat that regulates the current that is allowed to flow through the electrochemical cell, an ammeter that monitors that current, and a coulometer that is used to record the quantity of electric charge that is passed through a reaction. The reaction setup on the bottom left is shown to illustrate how the power source for an electrochemical reaction can be as simple as a toy photovoltaic. The point is that any power source can be used to push current through a reaction. The yields obtained for reactions using this simple reaction setup are not significantly lower than those obtained using the more complex setup. On the right are more modern commercial setups that take advantage of a condensed engineering designs to provide compact, versatile power supplies for numerous electrochemical applications and experiments. (All commercially available, top is from B&K Precision, bottom is from IKA)

1.2.3 Constant Potential and Constant Current Electrolysis

With a power supply identified, an electrolysis reaction can be conducted as either a constant current or constant potential experiment. In our group, we mainly take advantage of constant current electrolyses. We do so primarily because a constant current electrolysis does not require the use of a reference electrode. This makes the reaction easier to conduct, and therefore easier to adopt by others. In addition, constant current conditions can provide advantages in some aspects over a constant potential electrolysis, which will be discussed later. In a constant current electrolysis, a constant current is passed through the electrolysis cell and the working potential at

the electrodes (the potential needed to reduce and oxidize the species in the medium) is allowed to float (**Figure 1.8**).

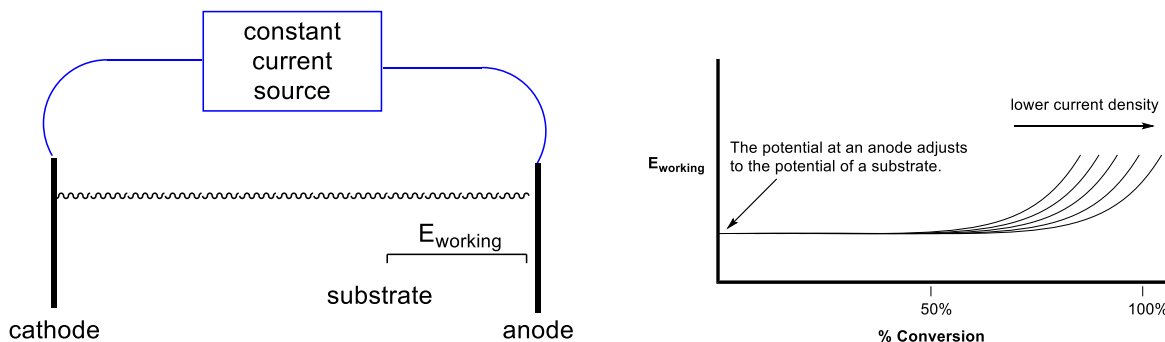


Figure 1.8 Constant Current Electrolysis

The result is that the working potential at each electrode (E_{working}) automatically adjusts to the oxidation potential of the substrate at the anode and the reduction potential of the substrate at the cathode. This is illustrated in the right hand “cartoon” presented that illustrates the working potential at the anode during a constant current electrolysis. In the reaction, the potential climbs until it matches that of the potential associated with the most easily oxidized group in solution. The potential then stays at that level until the oxidation of the substrate approaches completion. At that point, the amount of the initial substrate present at the electrode is not high enough to satisfy the flow of current. This causes the working potential at the anode to climb until it reaches the potential of the group with the next lowest oxidation potential in solution. It will then hold at that position as long as the need to pass current through the cell is satisfied. One can put off the rise in potential by running the reaction at low current density, a situation that lowers the amount of material needed to satisfy the demand for current.⁸ This can be seen in the figure as the change in percent conversion before the climb in current occurs. The lower the current density, the higher the percent conversion that can be obtained before any loss in selectivity. In

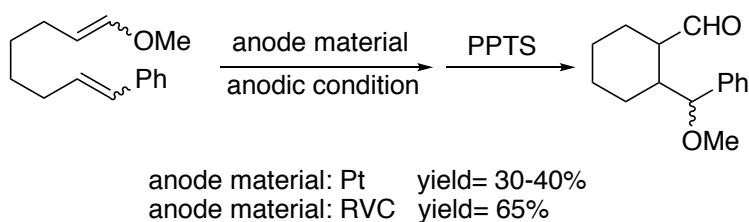
this system, the automatic adjustment of the potential allows for the selective oxidation of a wide variety of substrates with the exact same reaction setup.

The second method is the use of a controlled potential setup. In such experiments, the working potential at the anode (or cathode) is set to have a specific value relative to a reference electrode. The value selected matches that of the group one wants to oxidize. That value is then held constant for the duration of the experiment, a scenario that leads to a specific selectivity that does not change during the course of the reaction. However, as the substrate is consumed in such an experiment, the resistance across the cell increases and the current decreases. Due to this phenomenon, it takes longer time for the reaction to finish and it is very difficult to get the reaction to proceed to completion. This is a disadvantage for a typical laboratory experiment, but it can be very advantageous for industrial processes that utilize continuous flow cells that maintain a constant presence of substrate.⁴⁸

1.2.4 The Influence of Substrate Concentration

When thinking about concentration, we need to consider electrode materials, electrode surface double layer phenomena, substrate, and electrolyte. Simply put, radical cations are highly reactive intermediates, and their effective concentration at the surface of an electrode and the environment of the reaction in the region of that electrode can both play a large role in the reactions that follow. For starters, too high of a concentration of radical cation can lead to polymerization reactions and decrease the amount of intramolecular cyclization. For this reason, the nature of the electrode surface used can be important. Take for example the reaction illustrated in Scheme 1.2. In this case, the reaction outcome was significantly influenced by the nature of the anode material.²⁶ There are two potential causes for this discrepancy. First, the use

of the high surface area reticulated vitreous carbon anode (RVC) dramatically reduces the effective concentration of the radical cation at the surface of the anode. Two reactions run at the same current will lead to different current densities (the effective concentration of the oxidant) depending in the surface area of the anode. A high surface area means a low effective concentration of the oxidant and hence a low effective concentration of the resulting radical cation. This favors the intramolecular reaction. Second, high surface area RVC anodes favor two electron oxidations relative to Pt electrode.²⁶ We have seen in a number of reactions, that the rate of the second oxidation step in an electrolysis can play a significant role in the success of the reaction, a topic that will be discussed in detail later on.⁴⁹ In the reaction shown, it is likely that the RVC electrode plays both roles in optimization of the yield.



Scheme 1.2 Anode Material Impact

Another phenomenon that can prove very important in an electrochemical reaction is the formation of a “Double Layer” involving the electrolyte. **Figure 1.9** shows a double layer model for the solution around an anode (an outer Helmholtz Layer for physical chemists).

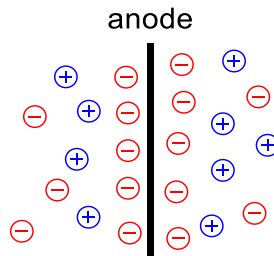
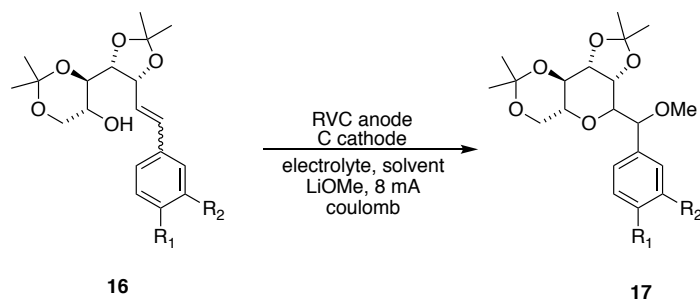


Figure 1.9 Double Layer Model/ Helmholtz Model

Due to electrical field imposed during an electrolysis, the anode surface/solution interfacial region forms compact layers of ions, negative ions and positive ions alternatively stacking layer by layer. In the Figure, a layer of negative ions is shown stacking next to the anode which is positively charged. Since the electric field decreases as the distance from the electrode increases, the layers become more diffuse as the distance increases. The first two layer are relatively well-defined leading to the “Double Layer” term. This phenomenon together with the nature of the actual electrolyte can be used to control the region of the reaction solution close to the electrode; a region in which many electrochemical reactions occur. This is important because double layers can be used as a to (1) exclude MeOH solvent that would trap a reactive intermediate too quickly and (2) control the concentration of substrate (forming radical cation) due to its solubility in the double layer generated. For example, a more polar electrolyte would lead to a high concentration of a polar substrate, etc. Consider the chemistry highlighted in Scheme 1.3 showing the effect of electrolyte on the generation of a C-glycoside derivative.⁴⁹

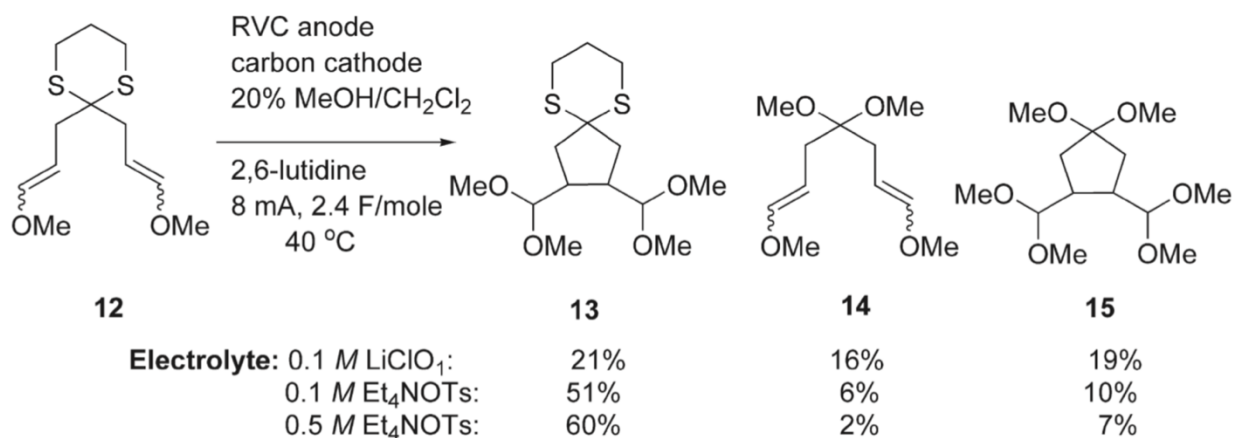


entry	electrolyte	solvent	coulomb	yield
1	Et4NOTs	MeOH:THF(3:7)	10.0F	22%
2	Et4NOTs	MeOH:THF(6:4)	5.5F	30%
3	Et4NOTs	MeOH	5.5F	40%
4	LiClO4	MeOH	2.6F	85%

Scheme 1.3. The Influence of a double layer on the reaction

Note how the use of a non-polar electrolyte and solvent led to poor current efficiencies for the reaction (2 F/mole being the theoretical amount of charge required for the reactions. Entry 3 and 4 in the table directly compare the role of the electrolyte. The substrate is polar in this case and not as soluble in a double layer comprised of a “greasy” hydrophobic electrolyte. Hence, the current efficiency of the reaction is poor with the current being drained off toward the oxidation of methanol solvent as background oxidation. As can be seen in entry 4, the use of a more polar electrolyte (less greasy) improves the solubility of the polar substrate in the double layer thus improving the current efficiency of the reaction. The less polar electrolyte can be used very favorably with a less polar substrate.

In another case, the effect of the double layer could be clearly seen in terms of its ability to limit the amount of methanol present at the electrode surface.



Scheme 1.4 Electrolyte Effect in Reaction

By utilizing a hydrophobic electrolyte such as Et₄NOTs, the concentration of methanol in double layer was greatly decreased. This decreased the rate in which methanol trapped sulfur radical cation allowing more time for the necessary electron-transfer and desired cyclization. The result was a higher yield of the desired product.¹⁷

1.3 Mechanism Related Topics in Anodic Cyclization

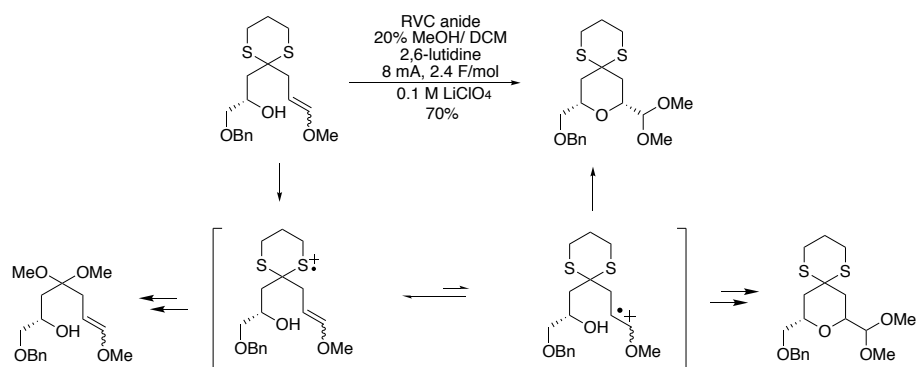
Reactions

A systematic mechanism model will be described in **Chapter 2** because the project described there helped to define the last set of principles we currently use to guide the development on new anodic coupling reactions. The topics in this section are relatively independent of each other, but all relate to the anodic cyclization discussed in Chapter 3 and 4.

1.3.1 Curtin-Hammett Controlled Reaction

When a substrate is oxidized at an anode, it is not always clear where the radical cation generated is located. When a substrate contains several electron rich functional moieties, intramolecular

electron-transfer reactions can occur leading to equilibrium structures that may in fact be resonance structures (no movement of atoms between the two or more alternatives). One case of such a reaction was shown above in Scheme 1.4. This example was an extension of the initial dithioketal example studied (Scheme 1.5).



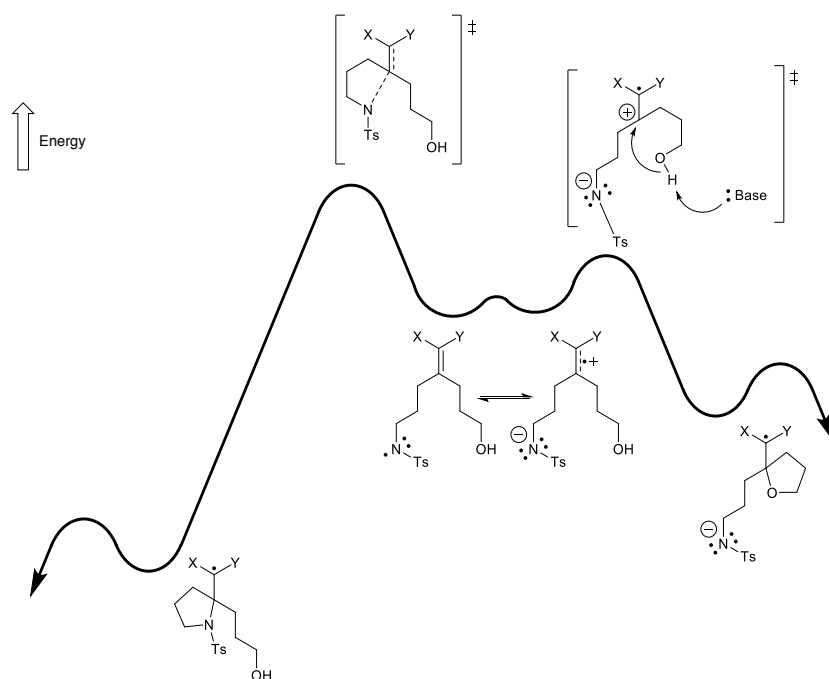
Scheme 1.5 Curtin-Hammett Controlled Reaction

In this reaction, the dithioketal has a lower oxidation potential ($E_{p/2} = +1.1$ V vs Ag/AgCl) than the enol ether ($E_{p/2} = +1.4$ V vs Ag/AgCl). Hence, the initial oxidation at the anode occurs at the sulfur atoms again leading to a sulfur based radical cation. An intramolecular electron transfer reaction can lead to the formation of an enol ether radical cation that is by definition (the oxidation potential) higher in energy. However, the enol ether radical cation can be trapped by the alcohol in the molecule, a reaction that we know to be very fast³⁹. This drains the equilibrium toward the desired cyclization product. This is an example of the Curtin Hammett principle in action. *The barrier for the cyclization is far lower in energy than the barrier for methanol trapping of the sulfur based radical cation.* Hence, the product is determined by the fast cyclization reaction. When the intramolecular alcohol trapping group was protected with a silane, then the only product generated was trapping of the sulfur based radical cation by methanol¹⁷.

This type of Curtin-Hammett control of an anodic oxidation reaction has been seen on numerous occasions including the oxidation of amides in the presence of much more electron-rich aromatic rings.⁵⁰

1.3.2 Thermodynamic Control and Kinetic Control

While it was tempting to suggest that all electrochemical reactions are governed by the Curtin-Hammett principle, this turns out to not be the case. For example, when a competition study was set up between a sulfonamide anion and an alcohol trapping group to test their ability to undergo an oxidative cyclization with a dithioetene acetal, a different scenario was found (scheme 1.6)³⁹.



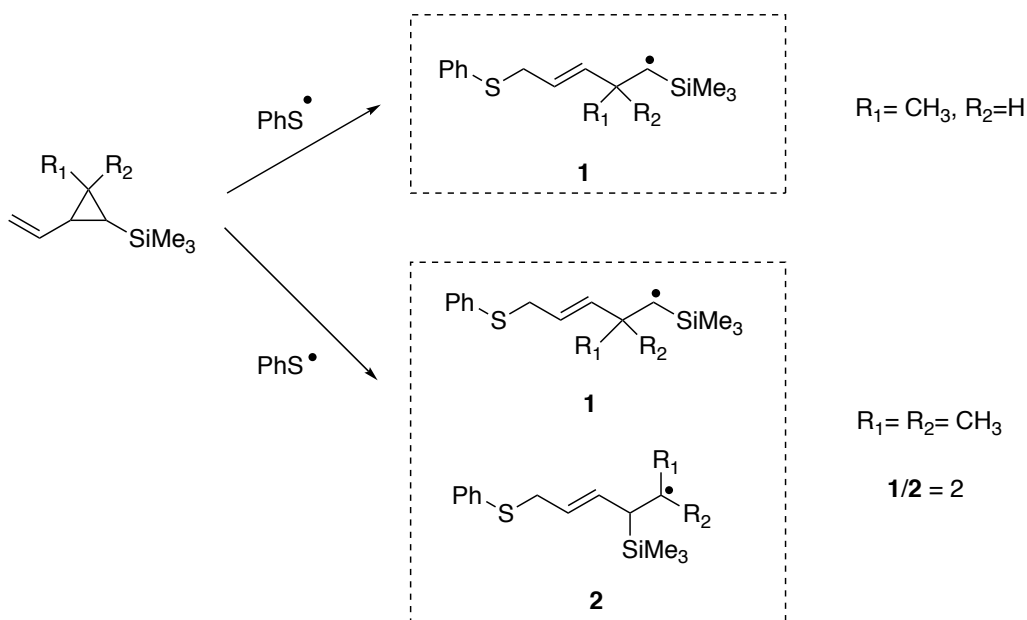
Scheme 1.6 Thermodynamic Product vs Kinetic Product

Under basic anodic oxidation conditions, the sulfonamide is deprotonated and the N anion is formed⁴⁰. This led to a question as to whether the oxidative coupling of a sulfonamide anion and an olefin involved an oxidation of the nitrogen anion to form a nitrogen-based radical that adds

to the olefin or a trapping of the olefin radical cation by the nucleophilic nitrogen-anion. It was thought that the two intermediates might equilibrate as illustrated in the center of the Scheme provided. To test this idea, an alcohol nucleophile was added to the mix. If the reaction was simply the result of a nitrogen-based radical adding to the olefin, then no alcohol trapping would occur. However, if the reaction led to the formation of the olefin radical cation, then an alcohol trapping might occur. In the event, the alcohol trapping occurred and the reaction was shown to involve the olefin radical cation. Initially, it was thought that the reaction was controlled by the Curtin-Hammett Principle in analogy to other reactions. However, further study showed that the N-trapping product was the result of thermodynamic control. Its formation was favored by non-polar reaction conditions (slow down kinetic alcohol trapping), lower current (a slower second oxidation that drives the reaction to completion) and increased temperature. The alcohol trapping product was the kinetic product. Its formation was enhanced by polar reaction conditions, low temperature (the cyclization is exothermic), and higher currents. So, in this case the reaction product obtained was not completely controlled by Curtin-Hammett kinetics.

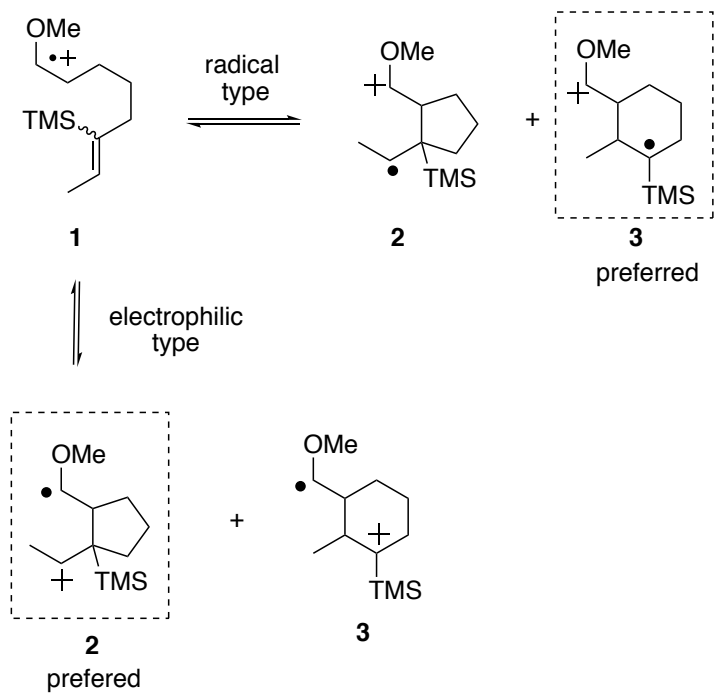
1.3.3 Reversible Radical Cyclization

In general, the cyclization of a radical cation with a carbon-based nucleophilic group is regarded as a potentially reversible radical process. The key to the word potentially is the second oxidation step that follows the cyclization. This understanding of the reactions was first formed by observing cyclization between enol ether derived radical cations and allyl- and vinylsilane trapping groups. Key was an early observation of Miura and Oshima that indicated that α -silyl radicals were formed in preference to β -silyl radicals (Scheme 1.7).⁵¹



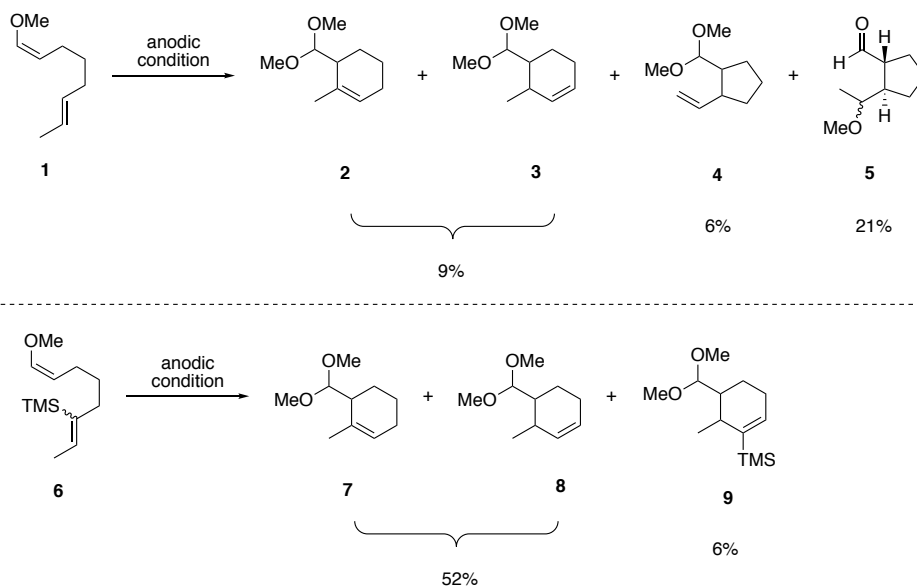
Scheme 1.7 α -silyl Radical over β -silyl Radical

This observation was determined by examining the addition of a thiol radical to a silyl-substituted vinyl cyclopropane. In the upper case shown, only the α -silyl radical was generated. In the lower case shown, the substrate was designed to further stabilize the β -silyl radical. Even so, the α -silyl radical was still the preferred product. With this piece of information (silyl radical was preferred), experiments were designed to probe the preferences of a radical cation-based reaction (Scheme 1.8). In this experiment, it was thought that if the chemistry proceeded through a radical-type addition, a six-membered ring would be preferred. If the reaction proceeded through an electrophilic-like addition, then then the five membered ring product would be preferred. The result of this experiment would be compared to a molecule that had no silyl group to establish the role of the silyl group.



Scheme 1.8 Radical Type vs Electrophilic Type Trapping

The comparison of the two reactions are shown in Scheme 1.9.²⁵



Scheme 1.9 Parallel Experiments on Cyclization

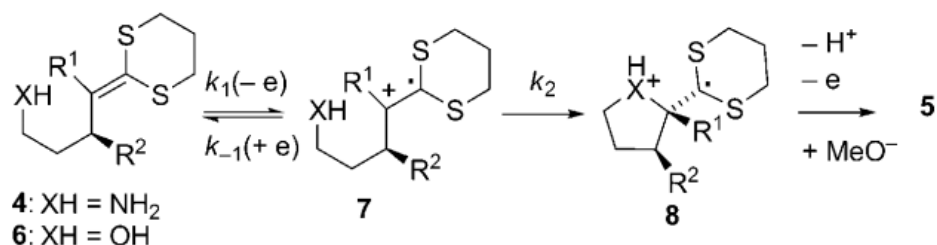
In the upper case, the oxidation took advantage of a substrate missing the silyl group. As with many such reactions, the yield of product obtained was poor. The reaction leads to products from methanol trapping, proton or hydrogen atom elimination reactions, polymerization reactions, etc. In the past, we showed that the presence of an allylsilane group to channel the reaction down the elimination pathway was needed for synthetically useful yields. Nevertheless, the baseline reaction was informative in that it led to a mixture of five and six-membered ring products with the five being obtained in slightly higher yield. With this background, the substrate with the added silyl group was submitted to the oxidation. The reaction led to an increase in yield and the exclusive isolation of 6-member ring product. This observation was consistent with a radical type cyclization according to the proposal outlined in Scheme 1.8.

With this observation, the formation of the six-membered ring product in the parent reaction and the complete lack of five-membered ring product in the reaction containing the silyl group (substrate **6**) was notable. For a radical type cyclization, the five-exo product is kinetically favored with the six membered ring product being thermodynamically favored. This suggested that in the top case there was evidence for a reversible type cyclization. With the silyl substitution on the bottom case, it is not clear that the six-endo product would not be favored kinetically as well. However, the complete lack of five-membered ring would also be more consistent with a reversible reaction, although the exact nature of this particular reaction remains a matter of speculation. In the end, it was concluded that the reaction was best viewed as a radical type reaction that was potentially reversible. Subsequent studies have shown that the initial cyclization of a radical cation is often reversible depending on the rate at which a second electron is removed from the cyclized substrate. The competition study described above was an example of this type of behavior³⁹.

The observation of radical type of cyclization discussed here is associated with behavior of intermediate discussed in chapter 3 and 4. Even though the working mechanism proposed a radical type cyclization, the radical cation intermediate still behaves different from a completely radical intermediate, as will described in chapter 3.

1.3.4 Substrate Selectivity and Steady State Kinetics

In Section 1.2.3, we included a discussion on constant potential vs constant current electrochemical reactions. In general, during constant current condition, the oxidation potential at electrode surface is maintained at the level of lowest substrate oxidation potential and climbs up once this substrate is consumed. This maintains the substrate selectivity. Within this context, it is important to note that the oxidation potential of the substrate is not only dependent on the nature of the functional group being oxidized, but also the rate of following up transformation (Scheme 1.10). As highlighted by the Nernst equation, the oxidation potential of a molecule represents the position of an equilibrium at the electrode surface between the substrate and the radical cation intermediate generated. Anything that drains the radical cation away from the electrode surface, like a rapid cyclization reaction, then shifts the equilibrium toward the radical cation and lowers the oxidation potential. This can be mathematically described by treating the reaction as a steady state kinetics situation with the radical cation being the reactive intermediate. With this approximation, one can solve for the concentration of the radical cation and plug it back into the Nernst equation. This leads to equation 1, and the observation that the faster the cyclization (k_2) the lower the observed potential.



If "steady state", then...

$$[7] = \frac{k_1[4 \text{ or } 6]}{(k_{-1} + k_2)}$$

...and the Nernst equation becomes:

$$E_{\text{obsv}} = E^\circ - (RT/(nF)) \ln \left(\frac{[4 \text{ or } 6]}{[7]} \right)$$

$$E_{\text{obsv}} = E^\circ - (RT/(nF)) \ln \left(\frac{(k_{-1} + k_2)}{k_1} \right) \quad (1)$$

Scheme 1.10 Steady State Impact on Oxidation Potential⁴⁴

This effect can be seen for the substrates shown in Scheme 1.10. An isolated dithioketal functional group has an oxidation potential of $E_{p/2} = +1.06$ V vs Ag/AgCl. The measured oxidation potential of substrate **6** with an alcohol trapping group is $E_{p/2} = +0.95$ V vs Ag/AgCl. The oxidation potential for substrate **4** was measured to be $E_{p/2} = +0.60$ V vs Ag/AgCl.⁴⁴ The drop in potential reflects the relative rates of the cyclization showing that the amine based cyclization occurs more quickly than the alcohol based cyclization.

1.3.5 conclusion

With all the observation and concepts described in this chapter, a foundation for understanding the reaction observation has been built. We are able to conduct a structure/activity study as described in the rest of this thesis, based on the advantage of constant current electrolysis. (The reactivity will change based on the structure of substrate).

Reference

- (1) Hammerich, O.; Speiser, B. *Organic Electrochemistry, Fifth Edition: Revised and Expanded*; CRC Press, 2015.
- (2) Yan, M.; Kawamata, Y.; Baran, P. S. Synthetic Organic Electrochemical Methods Since 2000: On the Verge of a Renaissance. *Chemical Reviews* **2017**, *117* (21), 13230.
- (3) Horn, E. J.; Rosen, B. R.; Baran, P. S. Synthetic Organic Electrochemistry: An Enabling and Innately Sustainable Method. *ACS Central Science* **2016**, *2* (5), 302.
- (4) Feng, R.; Smith, J. A.; Moeller, K. D. Anodic Cyclization Reactions and the Mechanistic Strategies That Enable Optimization. *Accounts of Chemical Research* **2017**, *50* (9), 2346.
- (5) Francke, R.; Little, R. D. Redox catalysis in organic electrosynthesis: basic principles and recent developments. *Chemical Society Reviews* **2014**, *43* (8), 2492.
- (6) Fu, N.; Sauer, G. S.; Saha, A.; Loo, A.; Lin, S. Metal-catalyzed electrochemical diazidation of alkenes. *Science* **2017**, *357* (6351), 575.
- (7) Sperry, J. B.; Wright, D. L. The application of cathodic reductions and anodic oxidations in the synthesis of complex molecules. *Chemical Society Reviews* **2006**, *35* (7), 605.
- (8) Yoshida, J.-i.; Kataoka, K.; Horcajada, R.; Nagaki, A. Modern Strategies in Electroorganic Synthesis. *Chemical Reviews* **2008**, *108* (7), 2265.
- (9) Elgrishi, N. m.; Rountree, K. J.; McCarthy, B. D.; Rountree, E. S.; Eisenhart, T. T.; Dempsey, J. L. A Practical Beginner's Guide to Cyclic Voltammetry. *Journal of Chemical Education* **2017**.
- (10) Moeller, K. D. Intramolecular Anodic Olefin Coupling Reactions: Using Radical Cation Intermediates to Trigger New Umpolung Reactions. *Synlett* **2009**, *2009* (08), 1208.
- (11) Beeson, T. D.; Mastracchio, A.; Hong, J.-B.; Ashton, K.; MacMillan, D. W. C. Enantioselective Organocatalysis Using SOMO Activation. *Science* **2007**, *316* (5824), 582.
- (12) Jang, H.-Y.; Hong, J.-B.; MacMillan, D. W. C. Enantioselective Organocatalytic Singly Occupied Molecular Orbital Activation: The Enantioselective α -Enolation of Aldehydes. *Journal of the American Chemical Society* **2007**, *129* (22), 7004.
- (13) Kim, H.; MacMillan, D. W. C. Enantioselective Organo-SOMO Catalysis: The α -Vinylolation of Aldehydes. *Journal of the American Chemical Society* **2008**, *130* (2), 398.
- (14) Sibi, M. P.; Hasegawa, M. Organocatalysis in Radical Chemistry. Enantioselective α -Oxyamination of Aldehydes. *Journal of the American Chemical Society* **2007**, *129* (14), 4124.
- (15) Liu, B.; Duan, S.; Sutterer, A. C.; Moeller, K. D. Oxidative Cyclization Based on Reversing the Polarity of Enol Ethers and Ketene Dithioacetals. Construction of a Tetrahydrofuran Ring and Application to the Synthesis of (+)-Nemorensic Acid. *Journal of the American Chemical Society* **2002**, *124* (34), 10101.
- (16) Miller, A. K.; Hughes, C. C.; Kennedy-Smith, J. J.; Gradl, S. N.; Trauner, D. Total Synthesis of (-)-Heptemerone B and (-)-Guanacastepene E. *Journal of the American Chemical Society* **2006**, *128* (51), 17057.
- (17) Redden, A.; Moeller, K. D. Anodic Coupling Reactions: Exploring the Generality of Curtin-Hammett Controlled Reactions. *Organic Letters* **2011**, *13* (7), 1678.

- (18) New, D. G.; Tesfai, Z.; Moeller, K. D. Intramolecular Anodic Olefin Coupling Reactions and the Use of Electron-Rich Aryl Rings¹. *The Journal of Organic Chemistry* **1996**, *61* (5), 1578.
- (19) Duan, S.; Moeller, K. D. Anodic Coupling Reactions: Probing the Stereochemistry of Tetrahydrofuran Formation. A Short, Convenient Synthesis of Linalool Oxide. *Organic letters* **2001**, *3* (17), 2685.
- (20) Reddy, S. H. K.; Moeller, K. D. Intramolecular anodic olefin coupling reactions: The construction of bridged bicyclic ring skeletons. *Tetrahedron letters* **1998**, *39* (44), 8027.
- (21) Moeller, K. D.; Tinao, L. V. Intramolecular anodic olefin coupling reactions: the use of bis enol ether substrates. *Journal of the American Chemical Society* **1992**, *114* (3), 1033.
- (22) Moeller, K. D.; Marzabadi, M. R.; New, D. G.; Chiang, M. Y.; Keith, S. Oxidative organic electrochemistry: A novel intramolecular coupling of electron-rich olefins. *Journal of the American Chemical Society* **1990**, *112* (16), 6123.
- (23) Sutterer, A.; Moeller, K. D. Reversing the polarity of enol ethers: An anodic route to tetrahydrofuran and tetrahydropyran rings. *Journal of the American Chemical Society* **2000**, *122* (23), 5636.
- (24) Frey, D. A.; Krishna Reddy, S. H.; Moeller, K. D. Intramolecular anodic olefin coupling reactions: The use of allylsilane coupling partners with allylic alkoxy groups. *The Journal of organic chemistry* **1999**, *64* (8), 2805.
- (25) Hudson, C. M.; Moeller, K. D. Intramolecular Anodic Olefin Coupling Reactions and the Use of Vinylsilanes. *Journal of the American Chemical Society* **1994**, *116* (8), 3347.
- (26) Hudson, C. M.; Marzabadi, M. R.; Moeller, K. D.; New, D. G. Intramolecular anodic olefin coupling reactions: a useful method for carbon-carbon bond formation. *Journal of the American Chemical Society* **1991**, *113* (19), 7372.
- (27) Wu, H.; Moeller, K. D. Anodic coupling reactions: A sequential cyclization route to the arteannuin ring skeleton. *Organic letters* **2007**, *9* (22), 4599.
- (28) Huang, Y.-t.; Moeller, K. D. Anodic coupling reactions: The use of N, O-ketene acetal coupling partners. *Organic letters* **2004**, *6* (23), 4199.
- (29) Xu, H.-C.; Brandt, J. D.; Moeller, K. D. Anodic cyclization reactions and the synthesis of (–)-crobarbatic acid. *Tetrahedron Letters* **2008**, *49* (24), 3868.
- (30) Duan, S.; Moeller, K. D. Anodic cyclization reactions: Capitalizing on an intramolecular electron transfer to trigger the synthesis of a key tetrahydropyran building block. *Journal of the American Chemical Society* **2002**, *124* (32), 9368.
- (31) Huang, Y.-t.; Moeller, K. D. Anodic cyclization reactions: probing the chemistry of N, O-ketene acetal derived radical cations. *Tetrahedron* **2006**, *62* (27), 6536.
- (32) Sun, Y.; Liu, B.; Kao, J.; d'Avignon, D. A.; Moeller, K. D. Anodic Cyclization Reactions: Reversing the Polarity of Ketene Dithioacetal Groups. *Organic letters* **2001**, *3* (11), 1729.
- (33) Sun, Y.; Moeller, K. D. Anodic olefin coupling reactions involving ketene dithioacetals: evidence for a 'radical-type' cyclization. *Tetrahedron letters* **2002**, *43* (40), 7159.
- (34) Brandt, J. D.; Moeller, K. D. Oxidative cyclization reactions: Amide trapping groups and the synthesis of furanones. *Organic letters* **2005**, *7* (16), 3553.
- (35) Sun, H.; Martin, C.; Kesselring, D.; Keller, R.; Moeller, K. D. Building functionalized peptidomimetics: use of electroauxiliaries for introducing N-acyliminium ions into peptides. *Journal of the American Chemical Society* **2006**, *128* (42), 13761.

- (36) Sun, H.; Moeller, K. D. Silyl-substituted amino acids: new routes to the construction of selectively functionalized peptidomimetics. *Organic letters* **2002**, *4* (9), 1547.
- (37) Xu, H.-C.; Campbell, J. M.; Moeller, K. D. Cyclization Reactions of Anode-Generated Amidyl Radicals. *The Journal of Organic Chemistry* **2014**, *79* (1), 379.
- (38) Smith, J. A., Washington University in St. Louis, 2015.
- (39) Campbell, J. M.; Xu, H.-C.; Moeller, K. D. Investigating the Reactivity of Radical Cations: Experimental and Computational Insights into the Reactions of Radical Cations with Alcohol and p-Toluene Sulfonamide Nucleophiles. *Journal of the American Chemical Society* **2012**, *134* (44), 18338.
- (40) Xu, H.-C.; Moeller, K. D. Intramolecular Anodic Olefin Coupling Reactions: Using Competition Studies to Probe the Mechanism of Oxidative Cyclization Reactions. *Organic Letters* **2010**, *12* (8), 1720.
- (41) Xu, H. *Intramolecular anodic olefin coupling reactions: Synthesis of nitrogen-and oxygen-heterocycles*; Washington University in St. Louis, 2010.
- (42) Xu, H.-C.; Moeller, K. D. Intramolecular Anodic Olefin Coupling Reactions and the Synthesis of Cyclic Amines. *Journal of the American Chemical Society* **2010**, *132* (8), 2839.
- (43) Xu, H.-C.; Moeller, K. D. Intramolecular Anodic Olefin Coupling Reactions: The Use of a Nitrogen Trapping Group. *Journal of the American Chemical Society* **2008**, *130* (41), 13542.
- (44) Xu, H.-C.; Moeller, K. D. Intramolecular Anodic Olefin Coupling Reactions: Use of the Reaction Rate To Control Substrate/Product Selectivity. *Angewandte Chemie International Edition* **2010**, *49* (43), 8004.
- (45) Mihelcic, J.; Moeller, K. D. Oxidative Cyclizations: The Asymmetric Synthesis of (–)-Alliacol A. *Journal of the American Chemical Society* **2004**, *126* (29), 9106.
- (46) Wright, D. L.; Whitehead, C. R.; Sessions, E. H.; Ghiviriga, I.; Frey, D. A. Studies on Inducers of Nerve Growth Factor: Synthesis of the Cyathin Core. *Organic Letters* **1999**, *1* (10), 1535.
- (47) Wright, P. M.; Seiple, I. B.; Myers, A. G. The Evolving Role of Chemical Synthesis in Antibacterial Drug Discovery. *Angewandte Chemie International Edition* **2014**, *53* (34), 8840.
- (48) Moeller, K. D. Using Physical Organic Chemistry To Shape the Course of Electrochemical Reactions. *Chemical Reviews* **2018**, DOI:10.1021/acs.chemrev.7b00656 10.1021/acs.chemrev.7b00656.
- (49) Smith, J. A.; Moeller, K. D. Oxidative Cyclizations, the Synthesis of Aryl-Substituted C-Glycosides, and the Role of the Second Electron Transfer Step. *Organic Letters* **2013**, *15* (22), 5818.
- (50) Moeller, K. D.; Wang, P. W.; Tarazi, S.; Marzabadi, M. R.; Wong, P. L. Anodic amide oxidations in the presence of electron-rich phenyl rings: evidence for an intramolecular electron-transfer mechanism. *The Journal of Organic Chemistry* **1991**, *56* (3), 1058.
- (51) Miura, K.; Oshima, K.; Utimoto, K. Stabilizing effect of trialkylsilyl group on carbon radical: Radical induced ring opening of 1-trialkylsilyl-2-vinylcyclopropanes. *Tetrahedron letters* **1989**, *30* (33), 4413.

Chapter 2: Anodic Cyclization Mechanism

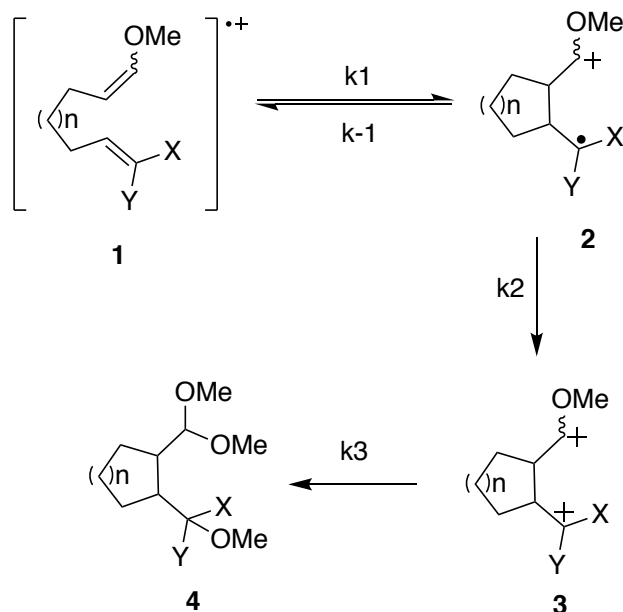
Study

In this chapter, we will discuss the mechanistic model that has been developed for anodic olefin coupling reactions, and our recent contributions to that model. The chapter is based on a paper we published that highlights how to think about and optimize the yield anodic coupling reactions.¹ As shown in Scheme 2.1, the reactions involve three steps (k_1/k_{-1} , k_2 , and k_3) that can each play a key role in defining the success of the reactions. A summary will be given for all three steps, but particular attention will be given in this chapter to the third step and how to identify and solve problems at this juncture. My role in the work was in connection with those issues. With that in mind, a brief discussion of the first two steps in the reaction (k_1/k_{-1} and k_2) will be provided in section 2.1. Section 2.2 will then present the background of my project and how we moved forward with our understanding of the third phase of the reaction. Section 2.3 will provide a conclusion for the effort, section 2.4 experimental details for the work, and section 2.5 the supporting spectra data.

(Sections of this chapter were taken from our paper: Feng, R.; Smith, J. A.; Moeller, K. D. Anodic Cyclization Reactions and the Mechanistic Strategies That Enable Optimization. Accounts of Chemical Research 2017, 50 (9), 2346)

2.1 Anodic Cyclization Reaction Mechanism Structure

As described in Chapter 1, anodic coupling reactions typically fit the mechanistic paradigm forwarded in Scheme 2.1.



Scheme 2.1 Anodic Cyclization Reaction Mechanism Model

In general, the anodic oxidation of a substrate leads to radical cation **1** that can then undergo a reversible cyclization reaction (k_1/k_{-1}). The cyclized radical cation will undergo a second oxidation forming a di-cationic intermediate **3**. At this point, there is no direct evidence for the generation of the dication intermediate. However, the reversibility of the cyclization and the dependence of that reversibility on the rate of the second oxidation is most consistent with the mechanism shown.

Following the second oxidation step, methanol trapping of the cations or a combination of methanol trapping and elimination (as in the case of an allylsilane trapping group) leads to the final product. These steps that occur after the second oxidation are typically assigned as k_3 .

During this stage of the reaction, the order of the steps that occur is frequently not clear, but controlling them can be critical for reaction success. For example, in Chapter 1 it was pointed out in connection with the use of a disubstituted olefin trapping group for the radical cation that reactions led to poor yields of product. This was the result of not providing a suitable reaction pathway for the intermediates generated after the second oxidation step.

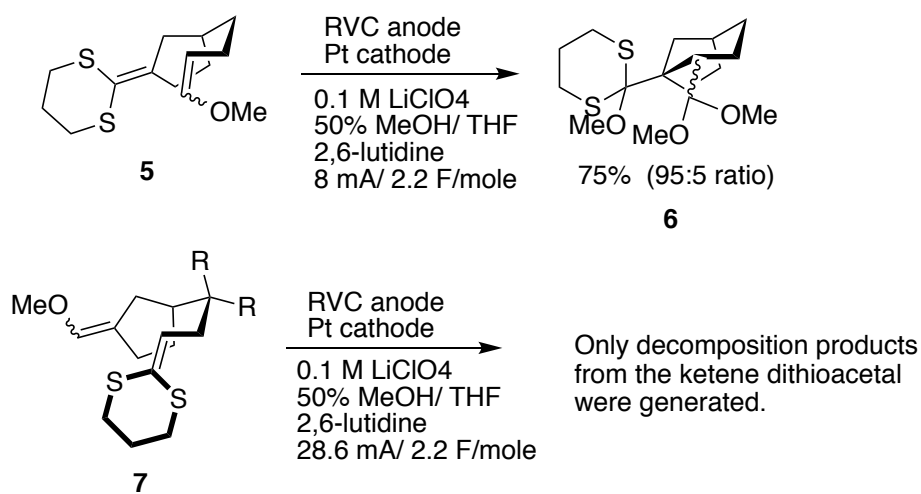
The key for conducting a successful anodic cyclization is understanding how the three steps that govern the reactions fit together and how to recognize when any one of the steps does not go according to plan.¹

2.1.1 Step One: The Reversible Cyclization

There are several factors that influence a cyclization reaction such as steric barriers in the substrate, the polarity of the radical cation intermediate, and the nature of the trapping group. In terms of steric barriers in the substrate, consider the pair of reactions illustrated in Scheme 2.2.³ Both reactions targeted the formation of a bridged bicyclic ring skeleton. Due to the lower oxidation potential of dithiol ketene acetal relative to the enol ether present in the substrates, the ketene acetal provides the site for radical cation formation and the enol ether the trapping group. In the first case, the cyclization works beautifully. In the second case, it does not. This observation is consistent with a radical-type cyclization and supported the conclusion reached in the work described in Chapter 1. Radical cyclization reactions are very sensitive to sterics on the double bond being attacked but not sterics at the site of the initial radical. Note how in Scheme 2.2, steric substitution at the site of the radical cation does not impede the cyclization, but extra sterics at the site of the terminating enol ether does. The formation of decomposition products

refers to decomposition of the reactive radical cation. Such products usually result from elimination and polymerization pathways.

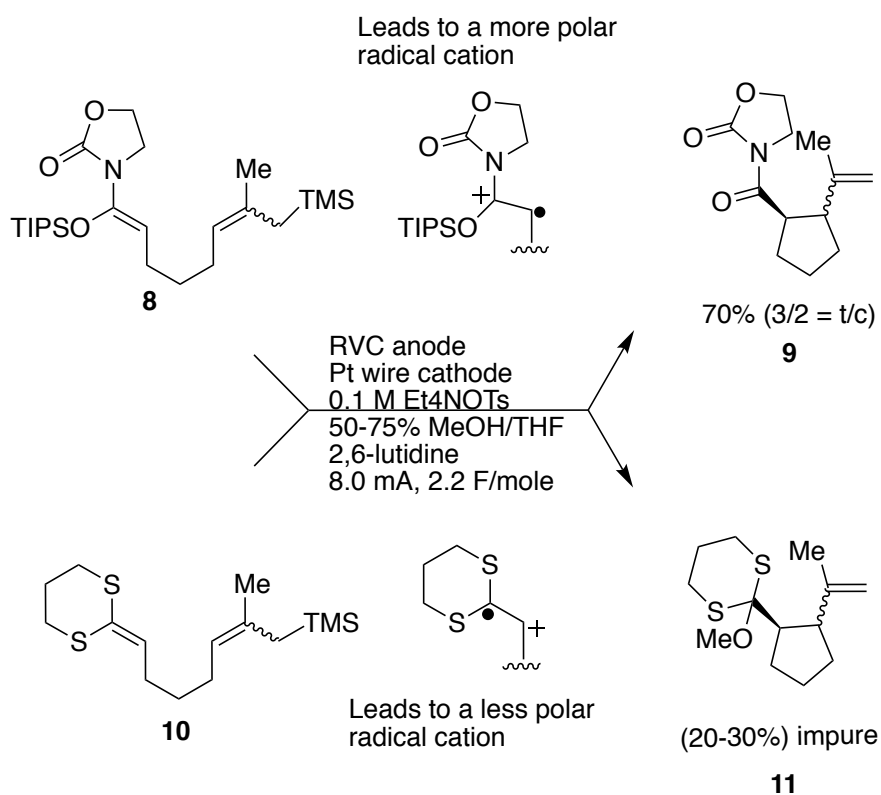
In a reaction not shown here but of significance for Chapter 3 (where the observation will be detailed), it was also found that anodic cyclization reactions can be highly dependent on the nature of the trapping group. For example, if the first reaction shown in Scheme 2.2 utilizes an allylsilane trapping group instead of the enol ether, then it fails. The reaction shown in Scheme 2.2 is challenging in that it forms a six-membered ring and a quaternary carbon at the same time. The use of an allylsilane trapping group which is less reactive toward the radical cation does not overcome this twin challenge.²



Scheme 2.2 Steric Effect on Cyclization

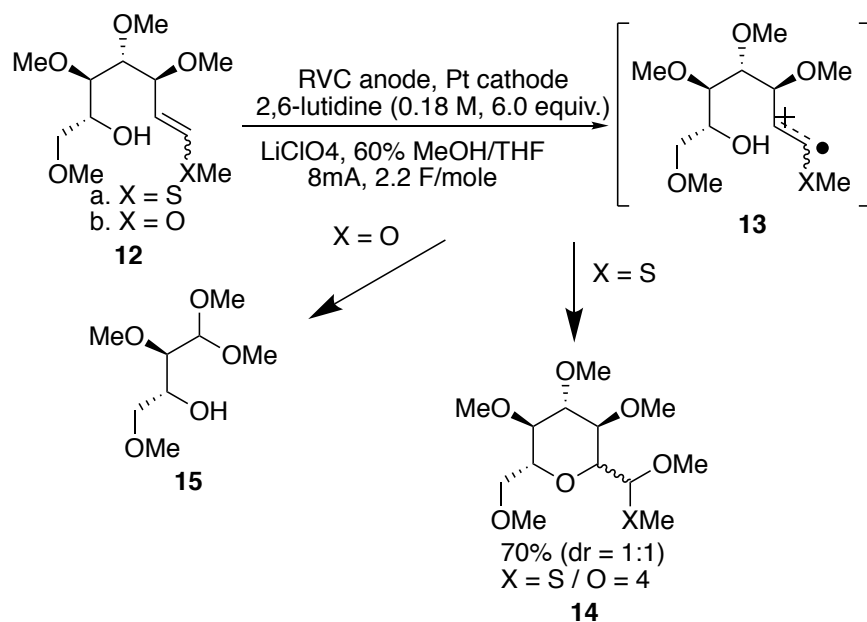
Another key observation concerning the cyclization reaction has to do with the polarity of the radical cation intermediate. As mentioned in the previous chapter, the fact that the working potential of an anode will automatically adjust to the oxidation potential of a substrate under

constant current conditions enables the use of structure-activity studies to examine how the nature of a radical cation influences the subsequent cyclization reactions. During these studies, *it was found that polar radical cations favor C-C bond formation while less polar radical cations favor heteroatom trapping reactions*. For example, consider the two oxidation reactions shown in Scheme 2.3. In these reactions, oxidation of the dithiol ketene acetal **10** leads to a less polar radical cation while the oxidation of N,O-ketene acetal **8** leads to a more polar radical cation. The polarity of the radical cation can be assessed by ^{13}C -NMR of the starting olefin. Interestingly, the two olefinic carbons of vinyl sulfide have the same chemical shift illustrating the effect of the sulfur having the same electronegativity as carbon. That case forms the base non-polar radical cation for the subsequent studies. In this case, the more polar radical cation leads to a much higher yield in the subsequent C-C bond forming cyclization³.



Scheme 2.3 Polar Radical Cation Favors C-C Bond Formation

For a counter example, the chemistry highlighted in Scheme 2.4 can be used. In this case, oxidation of a less polar vinyl sulfide substrate **12a** is compared with the oxidation of enol ether substrate **12b** in the presence of an alcohol nucleophile. In the vinyl sulfide case, the desired intramolecular trapping reaction occurs leading to desired cyclization product **14**. On the other hand, in enol ether case the intramolecular trapping is not fast enough and the radical cation leads to fragmentation product **15**.⁴ It is important to note that when the alcohol in substrate **12a** was protected with a silyl group, the oxidation led to the fragmentation product as well. So, the use of the vinyl sulfide radical cation did not make the fragmentation impossible, it only changed the relative rate of the cyclization vs. fragmentation reaction to favor the cyclization. This result was consistent with a variety of other reactions that all indicated that the use of a non-polar radical cation accelerated the heteroatom trapping reaction.⁵



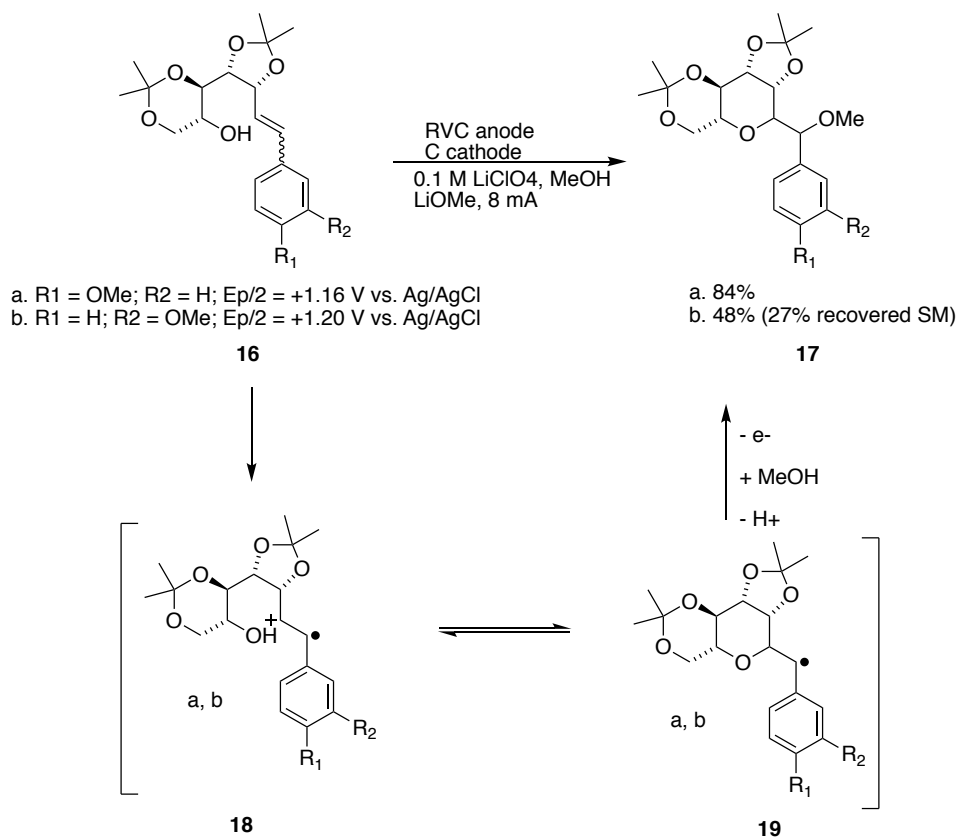
Scheme 2.4 Less Polar Radical Cation favors C-X Formation

2.1.2 The Second Oxidation

While the observations above point to the critical nature of the cyclization reaction, the removal of a second electron from the cyclized radical cation intermediate also plays an important role in the success of the reaction¹. This is especially true given that the cyclization is frequently reversible. In such cases, the second oxidation is needed to drain the reaction toward the desired product in order to avoid either poor current efficiency (re-reduction of the initial radical cation at the cathode) or decomposition of the radical cation.

When these situations arise, there are a number of strategies that can be used to aid the removal of a second electron from the cyclic radical cation intermediate (**2** in Scheme 2.1). First, higher current densities increase the effective concentration of oxidant in the reactions, and this change can lead to faster oxidation of both the substrate and the removal of the second electron (k_2 in

Scheme 2.1). Second, substrate modification strategies can be a very effective way to increase k_2 . The most common way to accomplish this is to generate a more stable cation after the second oxidation (or viewed alternatively – generate a more electron rich electron following the cyclization, which can easily be oxidized). This has been done using tri-substituted olefins, allylsilanes, and para-substituted aromatic rings. In the case shown in Scheme 2.5,⁶ an example of this approach is shown using the para-methoxy substituted phenyl substrate **16a** and its meta substituted derivative **16b** for comparison. As expected, the effect of the para-substituent was dramatically better than that seen with the meta-substituent due to its better overlap with the benzylic radical and subsequent cation after the second oxidation step. Note that effect was attributed to the second oxidation step because of the similarities in the initial oxidation potential, a value that indicates that the initial removal of an electron and the rate of the cyclization reaction are similar for the two substrates.



Scheme 2.5 Stable Cation Increase k_2

Another approach that has been effective is increasing the electrolyte in the reactions. This provides more of the anionic counter ion needed for the cation generated during the second oxidation step. This approach was also very effective for the formation of C-glycosides in connection with the chemistry shown in Scheme 2.5⁶

2.2 Efforts to oxidatively construct enriched 1,4-dicarbonyl moieties and an observation about k_3 :

Our efforts to probe the role of the third step in the mechanistic scheme above originated with efforts to develop an oxidative strategy for structure like those illustrated in Figure 2.1. The chemistry was based on the observation that anodic coupling reactions are frequently good tools for making 1,4-carbonyl derivatives⁷. Both of the structures shown contain the types of 1,4-dicarbonyl structures synthesized in the past, but in this case require the generation of molecules having a higher net oxidation state. With this in mind, the group was working on a general strategy to access these types of molecules.

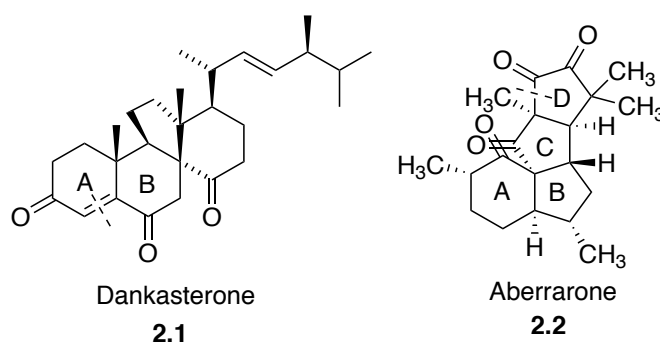
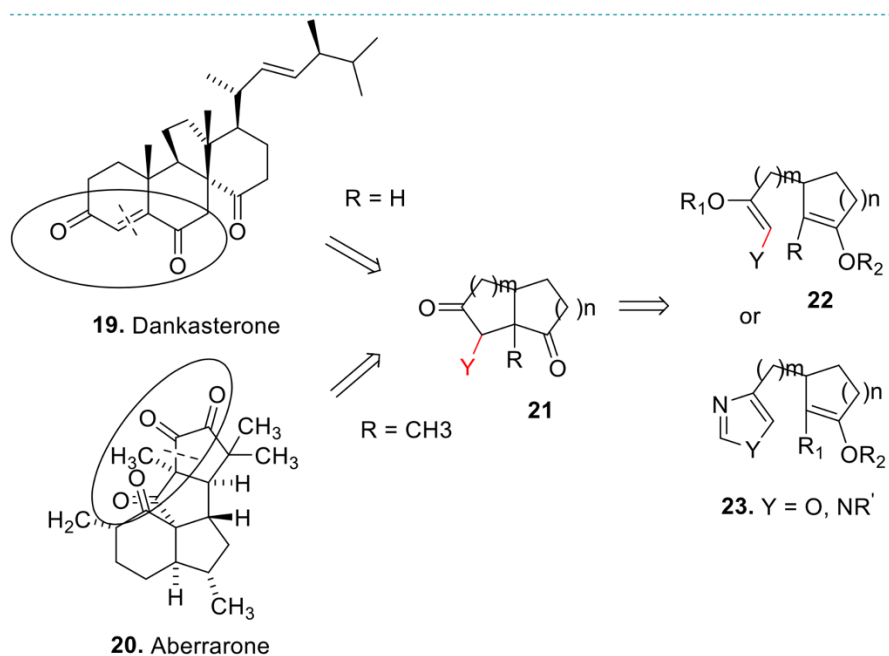


Figure 2.1 1,4-dicarbonyl Structure

2.2.1 Retrosynthetic Analysis

Dankasterone (2.1) is a target that has intrigued our group for a number of years both because of the 1,4-dicarbonyl group and because of the unique angularly fused ring system contained within its skeleton. The molecule, isolated from a marine sponge, is a member of a novel class of rearranged steroid derivatives with significant cytotoxicity against tumor cells⁸. Because of the group's interest in the molecule, a number of attempts have been made concerning its synthesis.

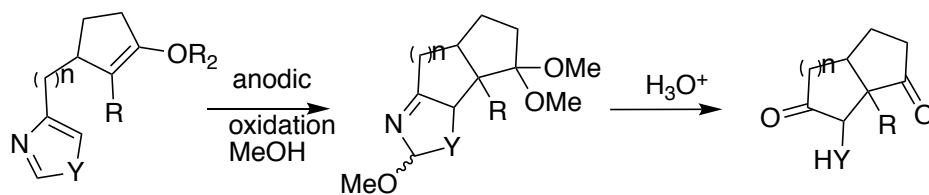
While none of these attempts has been particularly successful in terms of assembling the angularly fused core of the molecule, interest remains in a general strategy for the molecule and for the oxidized 1,4-dicarbonyl system. The interest in the oxidized 1,4-dicarbonyl portion of the molecule is fueled by its relationship to other molecules such as aberrarone (**2.2**). Aberrarone is from a novel class of terpenoid that has anti-malarial activity.⁹ In this case, the C,D-rings of the natural product contain an oxidized 1,4-dicarbonyl motif. It was hoped that a common route might be developed to synthesize both the A,B-ring system of dankesterone and the C,D-ring system of aberrarone. This route is shown in Scheme 2.6.



Scheme 2.6 Aberrarone Retro-Analysis

In principle, both product types can be made from a common intermediate (**21**) that would be generated from the anodic oxidation of a functionalized substrate like **22** or **23**. The initial plan was to use substrates like **22** for the oxidation, but problems with the synthesis quickly led to the choice of substrates with the general structure of **23**. In these cases, the idea was to conduct the

oxidation and then hydrolyze the resulting heterocyclic product to the desired functionalized 1,4-dicarbonyl (Scheme 2.7).



Scheme 2.7 Proposed oxidation/hydrolysis route to higher-oxidized 1,4-dicarbonyls

2.2.2 Model Substrate

With this in mind, model substrates **24**, **25**, and **26** (Figure 2.2) were synthesized for

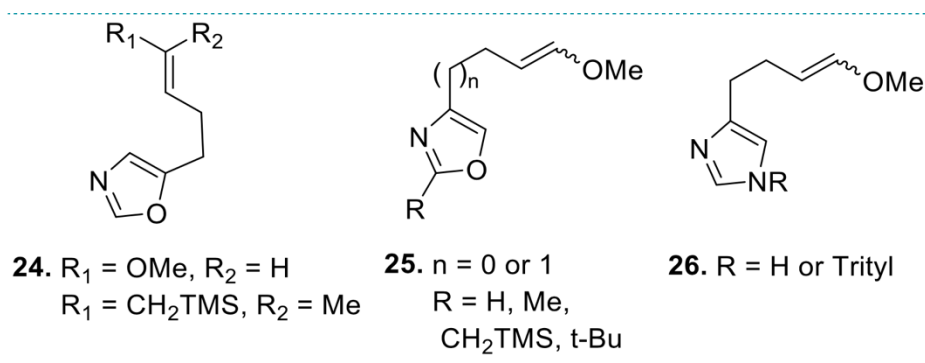
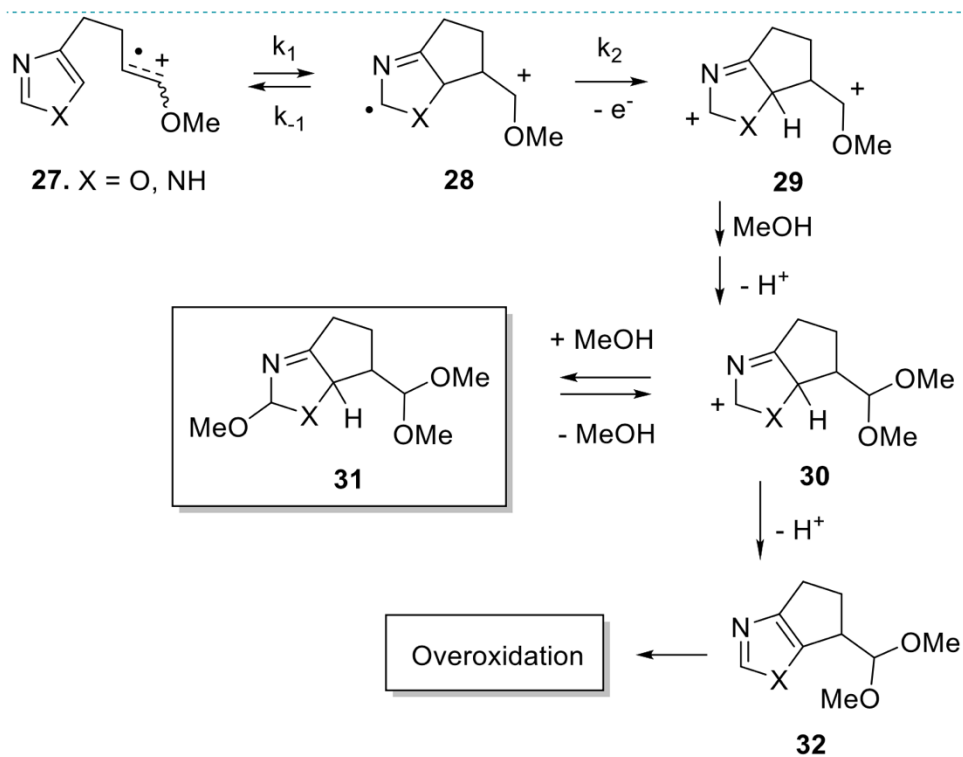


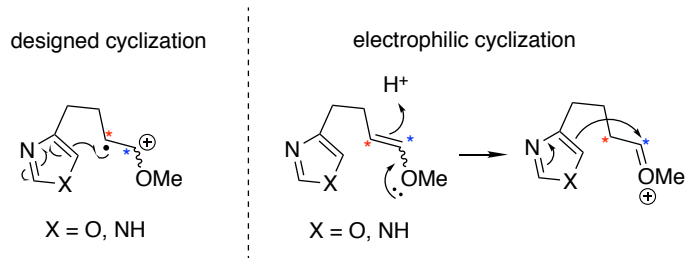
Figure 2.2 Model substrates

study. In general, the desired oxidative cyclization of these substrates failed. Instead, the reactions afforded polymeric materials. It appeared that the cation resulting from the second oxidation and subsequent methanol trapping (**30**) (Scheme 2.8) was unstable and underwent an elimination reaction to form an electron-enriched heterocycle (**32**) instead of trapping a second equivalent of methanol to form the desired product **31**. This was problematic because the heterocycle **32** had an oxidation potential lower than that of the initial substrate. This led to overoxidation of the product.



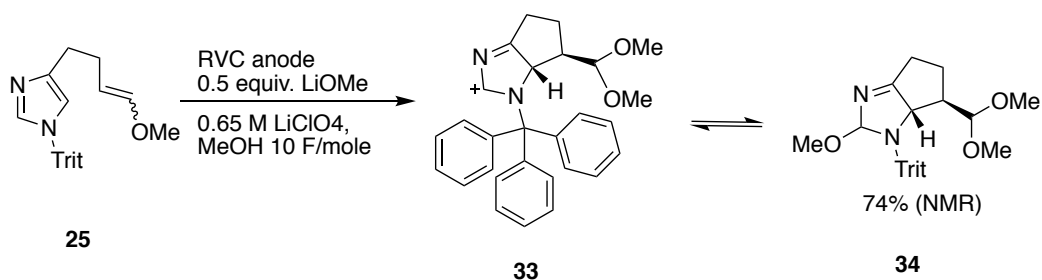
Scheme 2.8 Proposed decomposition pathway for model substrates

Problems of this nature can be challenging to avoid because the reactions do require mildly basic conditions that can favor elimination reactions. While electrochemical reactions do remain neutral overall, acid is generated at the anode and base at the cathode. Hence, in the absence of a base to shuttle protons away from the surface of the anode, substrates like **24-26** can undergo acid catalyzed electrophilic cyclization that afford the wrong regiochemical addition to the enol ether (Scheme 2.9).



Scheme 2.9 Electrophilic cyclization

The plan to avoid the elimination and overoxidation observed for the reaction in Scheme 2.8 was to introduce steric bulk onto the heterocycle. The hope was that this hindrance would reduce the amount of overoxidation by either hindering the ability of the heterocycle to approach the anode, slowing the rate of elimination to **32**, or perhaps both. The addition of a t-Bu group to the ring in substrate **26** was ineffective, and overoxidation occurred in a manner similar to the other substrates studied. However, the addition of a trityl protecting group to substrate **26** dramatically improved the reaction (Scheme 2.10). The idea that the newly added steric bulk slowed the elimination was supported by the observation that **34** could be isolated without



Scheme 2.10. Addition of a bulky trityl protecting group dramatically improves conversion to product

formation of the aromatic ring. With the protecting group in place, the reaction led to a 74% yield of product as determined by NMR-integration of the product relative to an internal standard

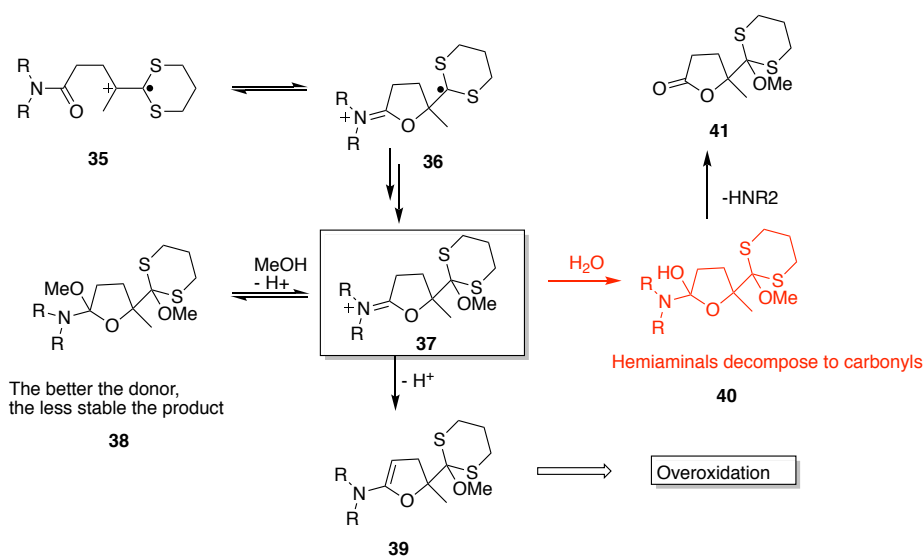
that was added to the crude reaction product.¹ The product could be isolated in a 55% yield, with the loss of material attributable to instability of the product to chromatography through silica gel.

The optimized reaction conditions shown in Scheme 2.10 did require excess current to go to completion. At this point, it is not known whether this excess current is needed because the substrate has difficulty reaching the anode due to sterics (a situation that would lead to background oxidation of the solvent), or if the initial cyclization is reversible and the second oxidation of an intermediate **28** (Scheme 2.8) is slow. Such scenarios lead to poor current efficiency due to migration of the radical cation intermediate to the cathode followed by reduction of the intermediate back to the starting material⁶. In either event, protecting intermediates like **33** from elimination did allow for isolation of the desired product.

This was not the first time that consideration of a cation generated downstream of the second oxidation proved critical for optimization of an anodic cyclization reaction¹⁰. Earlier studies conducted by John Brandt in the group examined the trapping of ketene dithioacetal derived radical cations (**35**) by amides to form lactones (Scheme 2.11). In this case, the product from the second oxidation **37** was trapped by methanol to reversibly form product **38** (which in the initial plan was to be hydrolyzed to the desired lactone upon workup). The reversibility of the reaction led to intermediate **37** persisting in solution. This allowed time for an elimination to generate the very electron-rich ketene aminal **39**. The oxidation of **39** led to a significant decrease in the yield of the desired lactone product. One key observation was that the more electron rich the N of the amide, the poorer the yield of product. This was initially confusing, because more donating N-groups were viewed as making the amide in **35** a better nucleophile, accelerating the radical cation trapping step. In short, the first attempt to fix the yield of the anodic oxidation reaction

focused on improving the rate of cyclization (k_1 in the mechanistic model shown in Scheme 2.1).

This solution pushed the reaction in the wrong direction.



Scheme 2.11. Water scavenges the unstable intermediate cation, avoiding overoxidation

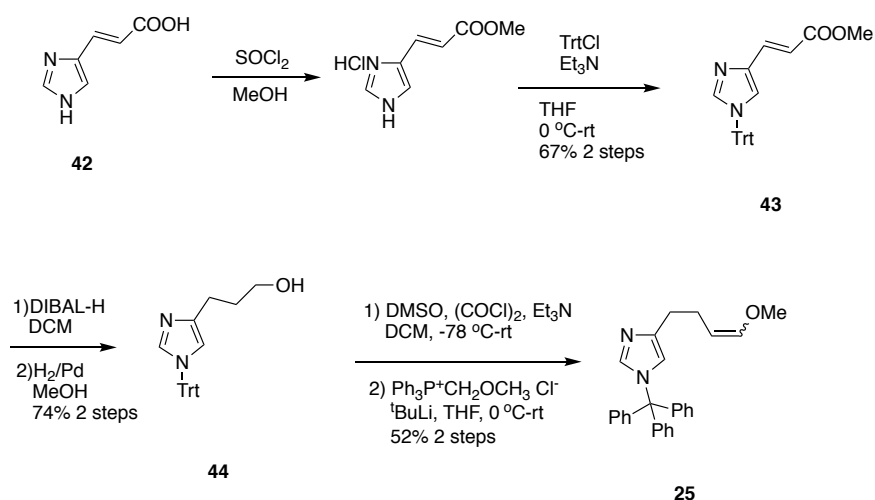
The problem was eventually resolved by the addition of water to the reactions. When the cation **37** was trapped with water, hemiaminal **40** was generated. The hemiaminal then eliminated the amine to form a stable lactone product (**41**), which could not undergo a subsequent oxidation reaction. So as with the reaction shown in Scheme 2.10, optimization of this reaction involved controlling an intermediate generated downstream of the oxidations rather than optimizing either the initial cyclization or second oxidation step.

2.2.3 Conclusion

In the end, it became clear that the overoxidation of a product in an anodic coupling reaction is likely caused by an unwanted elimination reaction involving either the product or frequently the cation generated from the final oxidation. In such cases, optimization of the anodic cyclizations rests with channeling the final cation generated down a productive pathway.

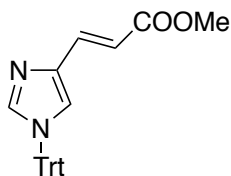
2.3 Experimental Section

Synthesis of electrolysis substrate 25 was as followed.



Scheme 2.12 Synthesis of Electrolysis Substrate 25

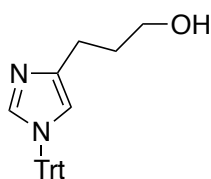
Synthesis of 43 (methyl (E)-3-(1-trityl-1H-imidazol-4-yl)acrylate)



To a solution of (E)-3-(1H-imidazol-4-yl)acrylic acid **41** (2 g, 14.5 mmol, 1.0 eq) in MeOH (15 mL) at 0 °C was added thionyl chloride (1.05 mL, freshly distilled) dropwise. The suspension was warmed to room temperature, stirred for 1h, and brought to reflux for 3h. The reaction

mixture was then transferred into a 250 mL round bottom flask under argon and diluted with 50 mL of THF (50 mL) and 5.5 mL of triethylamine (2.5 eq) was added in at 0 °C. To the resulting solution was added TritCl (4.67 g, 1.15 eq) in 50 mL of THF in small portions. The reaction mixture was stirred overnight. Upon completion, the reaction mixture was quenched by water and then diluted with CH₂Cl₂. The organic layer was separated, and the aqueous layer was washed with CH₂Cl₂. The combined organic layers were dried over MgSO₄, concentrated, and the crude product purified by recrystallization with EtOAc to afford **25** (3.87 g, 67% yield). Spectra data for **25**: ¹H NMR (300 MHz, Chloroform-d) δ 7.47 (s, 1H), 7.38 – 7.31 (m, 10H), 7.17 – 7.10 (m, 7H), 7.02 (d, J = 1.3 Hz, 1H), 6.55 (d, J = 15.6 Hz, 1H), 3.75 (s, 3). This data matched the previously published ¹H NMR. (Refence from Smith, J. A. Ph.D. Dissertation, Washington University in St. Louis, **2015**)

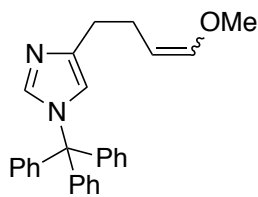
Synthesis of **44** (3-(1-trityl-1H-imidazol-4-yl)propan-1-ol)



To a solution of **25** (2.2 g, 5.59 mmol, 1.0 eq) in dichloromethane (100 mL) under argon at -78 °C was added DIBAL-H (1M in hexane) dropwise over 1h. Mixture was stirred at rt for 2h. Upon completion, the reaction was diluted with 15 mL of EtOAc and then treated with 30 mL of a saturated Rochelle's salt solution. The mixture was stirred overnight before being quenched with water and then diluted with CH₂Cl₂. The organic layer was separated, and the aqueous layer was washed with CH₂Cl₂. The combined organic layers were dried over MgSO₄, concentrated, and

carried onto next step. To this end, the crude mixture was placed into 100 mL round bottom flask under argon and then diluted with 12 mL of methanol. The resulting solution was sonicated for 10 min until everything had been completely dissolved and then treated with 0.12 g of 10% by weight Pd/C. The reaction was then placed under a H₂ atmosphere and was stirred for 20h. Upon completion, the reaction mixture was filtered through celite, washed with CH₂Cl₂, and concentrated. The crude product was purified by chromatography through silica gel using Hexane: EtOAc: MeOH (5:4:1) as the eluent to afford **43** (0.785g, 74% yield). Spectra data for **43**: ¹H NMR (300 MHz, Chloroform-d) δ 7.43 – 7.30 (m, 10H), 7.19 – 7.05 (m, 7H), 6.55 (s, 1H), 4.33 (s, 1H), 3.74 (t, J = 5.6 Hz, 2H), 2.68 (t, 2H), 1.86 (p, J = 6.0 Hz, 2H). This data matched the previously published ¹H NMR. (Refence from Smith, J. A. Ph.D. Dissertation, Washington University in St. Louis, **2015**)

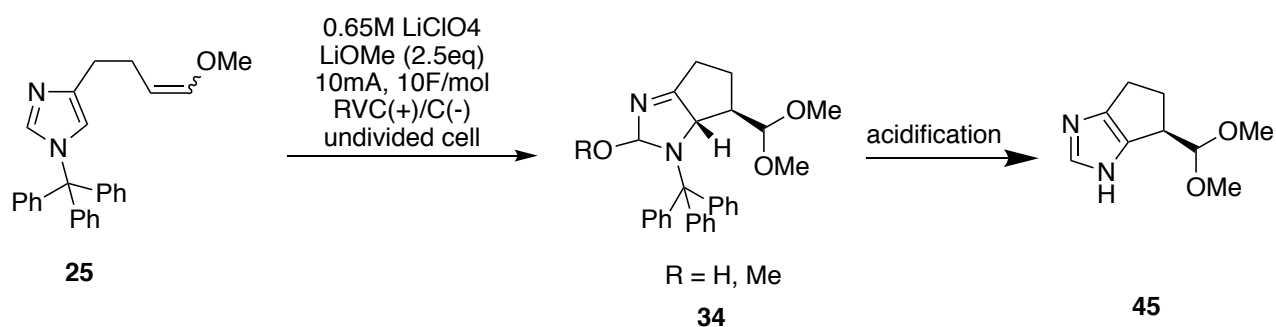
Synthesis of **25** (4-(4-methoxybut-3-en-1-yl)-1-trityl-1H-imidazole)



To a solution of **43** (1.75g, 4.77 mmol, 1.0 eq) in CH₂Cl₂ (30 mL) under argon was added DMSO (0.42 mL, 1.25 eq). The mixture was cooled to -78 °C and then freshly distilled oxalyl chloride (0.49 mL, 1.2 eq) was added in a dropwise fashion. The solution was allowed warm to -60 ~ -50 °C and stirred for 30 min before triethyl amine (3.3 mL 5 eq) was added to the flask. The reaction was allowed to warm to was allowed warm to rt before being quenched with water and diluted with CH₂Cl₂. The organic layer was separated, and the aqueous layer was washed with CH₂Cl₂. The combined organic layers were dried over MgSO₄, concentrated, and carried

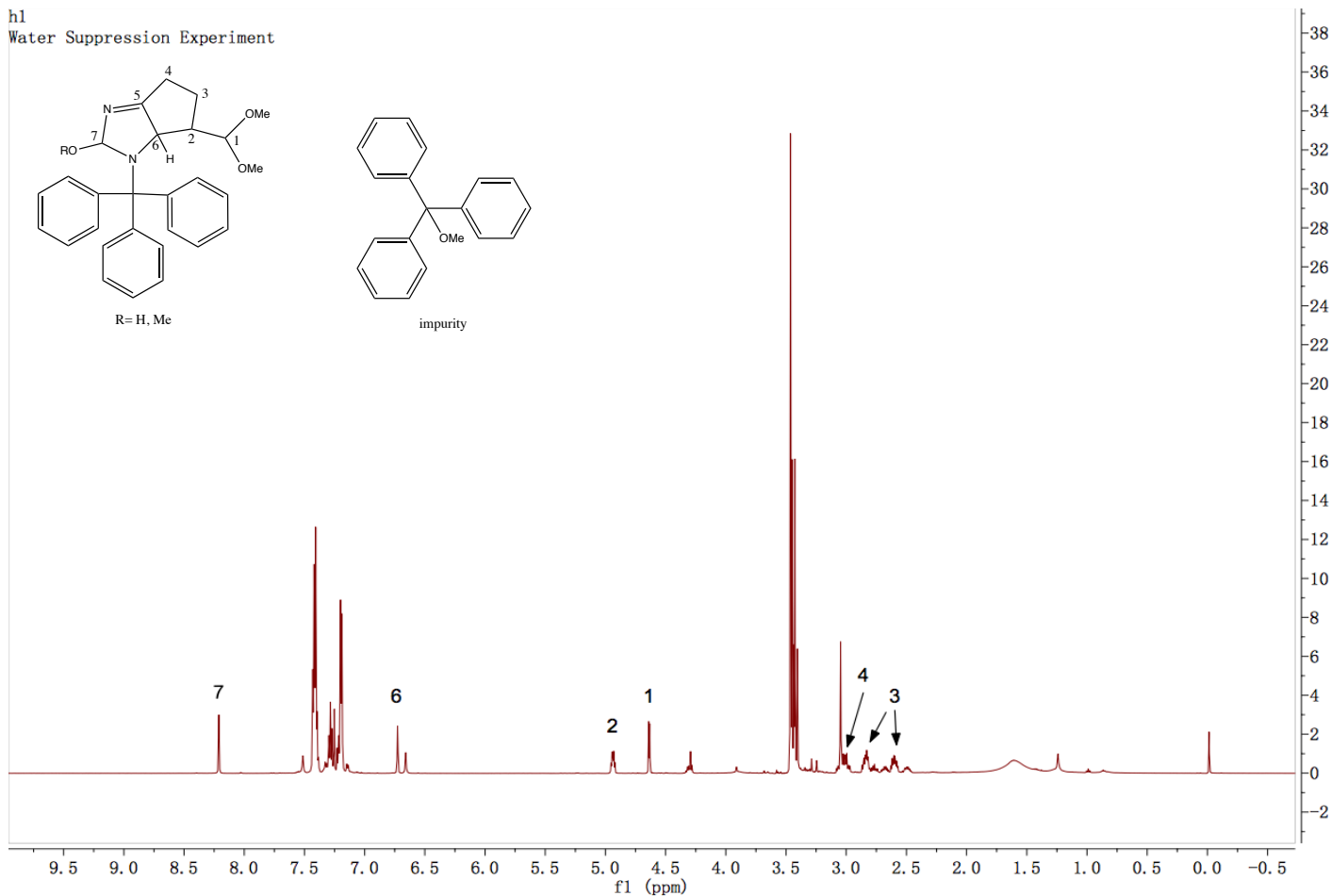
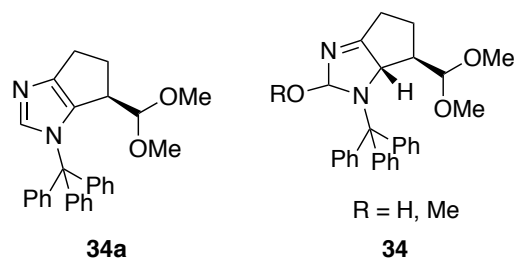
onto next step. To this end, methoxymethyl phosphonium chloride (3.27 g, 2 eq) was dissolved in 26 mL of THF and cooled to 0 °C. t-BuLi (5.61 mL, 2 eq) was added to this solution in a dropwise fashion before stirring the mixture for 1h. At this point the aldehyde from the previous step, was dissolved in 7 mL THF. The resulting aldehyde solution was added into newly generated ylide solution in a dropwise fashion. The resulting solution was stirred overnight. Upon completion, reaction mixture was quenched by water and then diluted with ethyl ether. The organic layer was separated, and the aqueous layer was washed with ethyl ether. The combined organic layers were dried over MgSO₄, concentrated, purified by chromatography through silica gel using Hexane: EtOAc (5:5) as the eluent to afford **25** (0.97 g) in a 52% yield. Spectra data for **25**: ¹H NMR (300 MHz, CDCl₃) δ 7.51 – 7.25 (m, 10H), 7.22 -7.09 (m, 6H), 6.55 (s, 0.34H), 6.50 (s, 0.48H), 6.27 (d, J = 12.7 Hz, 0.41H), 5.83 (d, J = 6.2 Hz, 0.27H), 4.74 – 4.65 (dt, 0.48H), 4.36 (q, J = 7.0 Hz, 0.28H), 3.50 (s, 0.87H), 3.45 (s, 1.64H), 2.58 (t, J = 7.5 Hz, 2H), 2.44 – 2.09 (m, 2H); ¹³C NMR (75 MHz, CDCl₃) δ 147.4, 146.1, 142.6, 138.2, 129.8, 127.9, 118.1, 106.4, 102.2, 59.4, 55.7, 29.8, 28.7, 27.6, 23.6. IR (neat, cm⁻¹): 3052, 2925, 2847, 2825, 2361, 2157, 1654, 1491, 1445, 1207, 1130, 1107, 1035, 1001, 748, 701. HRMS (ESI) calcd for C₂₇H₂₆N₂O [M + Na]⁺ 395.2110, found 395.2118.

General Procedure for Electrolysis:



Compound **25** (72.9 mg, 0.184 mmol) and 5 mL of a 0.65 M LiClO₄ in THF were placed in a 25 mL, 3-neck round bottom flask. To this solution was added LiOMe (0.5 mmol). The mixture was sonicated for 10 min, and then the flask equipped with carbon cathode and RVC anode. Current (10 mA, 10 F/mol) was passed through the cell until the starting material disappeared by TLC. At that point, the reaction mixture was diluted with NaHCO₃ (sat. aq), the layers separated, and the aqueous layer washed three times with CH₂Cl₂. The combined organic layer was dried over MgSO₄ and then concentrated. A ¹H NMR was taken of the crude product and the yield of the product present calculated to be 74% using 2,6-ludidine which had been added to the crude material following the reaction as internal standard. The crude product was purified by flash chromatography through silica gel to afford **34** (45 mg, 55% yield). The same material was applied to same second time chromatography, the yield dropped to 43%, proving the evidence of losing material during chromatography. ¹H NMR (600 MHz, Chloroform-d) δ 8.21 (s, 1H), 7.42 - 7.17 (m, 15H), 6.73 (d, J = 1.6 Hz, 1H), 4.96 - 4.91 (m, 1H), 4.64 (d, J = 4.9 Hz, 1H), 3.48 - 3.39 (m, 9H), 3.06 - 2.98 (m, 2H), 2.83 (td, J = 8.8, 4.7 Hz, 1H), 2.70 - 2.50 (m, 1H). ¹³C NMR (151 MHz, Chloroform-d) δ 146.59, 142.37, 142.29, 134.56, 132.27, 131.79, 131.47, 131.36, 130.37, 129.52, 121.64, 118.11, 108.02, 107.09, 65.11, 60.78, 59.22, 59.06, 57.80, 57.15, 54.71, 53.42, 34.10, 31.84, 25.28, 23.46. HRMS (ESI) calcd for C₂₈H₂₈N₂O₂ [M + H]⁺ 425.2219, found 425.2224.

The structure was originally assigned as **34a**. (Reference from Smith, J. A. Ph.D. Dissertation, Washington University in St. Louis, **2015**). The mass matched this structure, but compound **34** would be expected to lose the OR group during the mass spectrometry experiment. Hence, mass spectrometry was not a good way to differentiate the two compounds. However, during the 2D NMR analysis, the existence of an extra proton leading to the assignment of **34**.



In the 2D NMR analysis, initially, proton NMR, carbon NMR, and HSQC were used to assign the position of proton and carbon using the logic described below: Following an initial estimation of proton assignment, HSQC was used to find the corresponding carbon. (Appendix A). Then COSY was used to confirm the correlation between protons (see below).

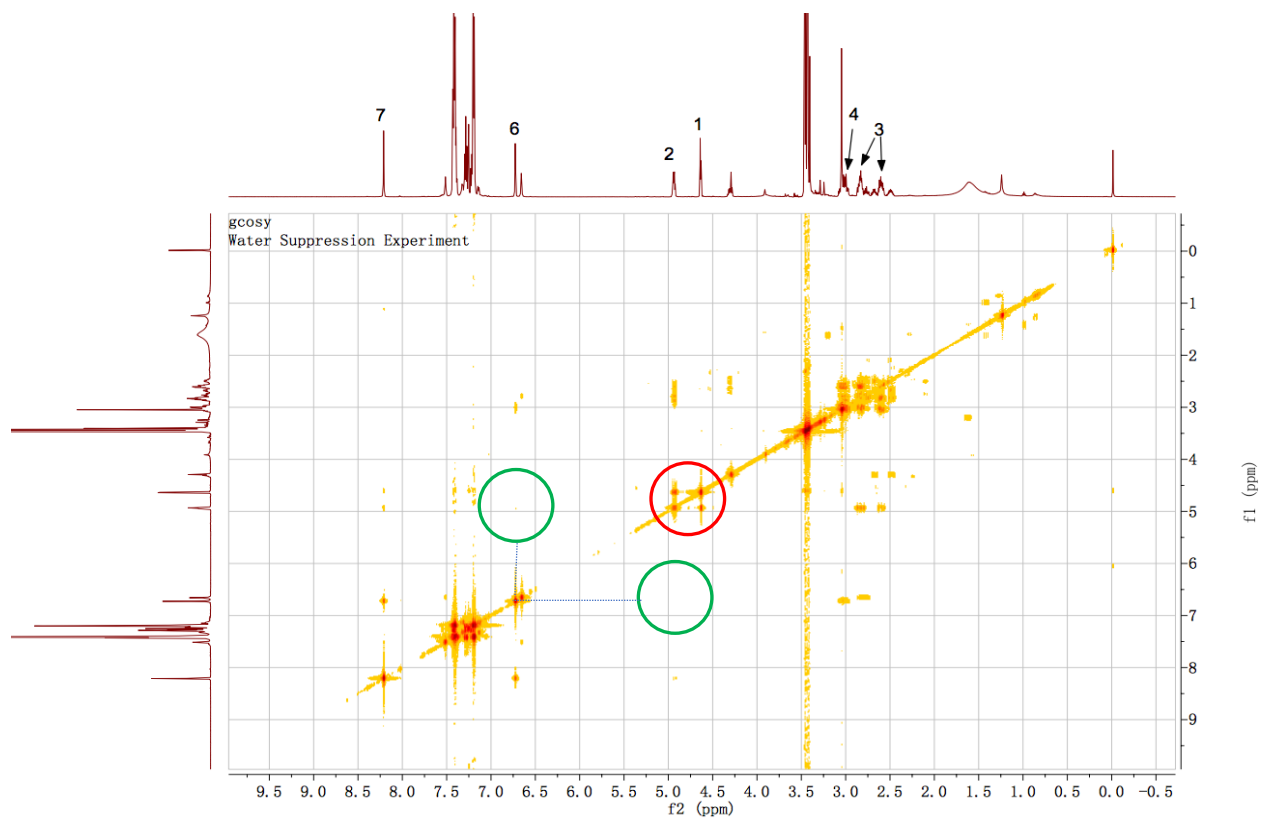


Figure 2.4 COSY of 34

In red circle, the correlation shows coupling between proton 1 and proton 2. In green circle and dashed line shows no coupling between proton 2 and proton 6 which is common in ring. To further confirm the structure, HMBC was analyzed (see below). The purple circle and red line showed the multiband correlation between carbon 5 and proton 2, which proves the key evidence for the formation of C6-C2 bond.

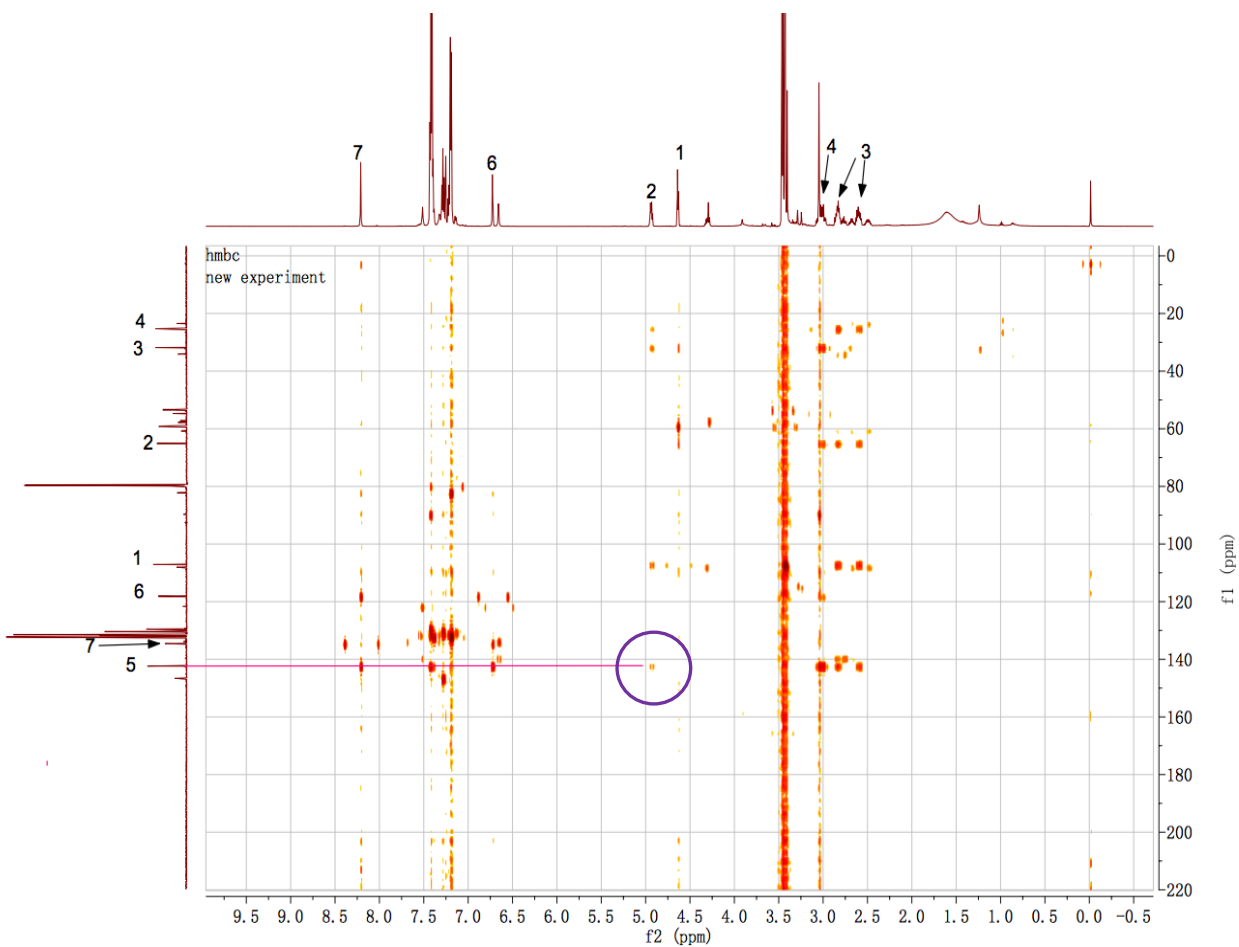


Figure 2.5 HMBC of 34

Simulated 3D molecule structure (using ChemDraw 3D generating lowest energy structure) was provided below to show the stereochemistry generated from this transformation. The C1-C2 bond winds up at the convex face of the molecule due to a reversible cyclization leading to the most stable product. (circled in blue)

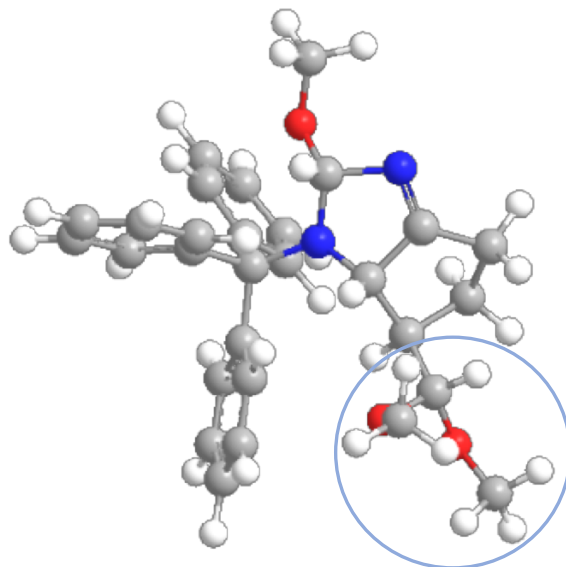


Figure 2.6 Simulated 3D structure of 34 using ChemDraw

During repeating experiments, **25** (105 mg) was used to conduct same electrolysis reaction, after same work up procedure as described before, product **34** was directly dissolved in DCM/TFA (10 mL/ 2 mL), the mixture was stirred overnight. The reaction was quenched with 2M NaOH aqueous solution. The layer was separated, aqueous layer was extracted with DCM by three times. The combined organic layer was dried over MgSO₄. The mixture was purified through flash chromatography using 30% Ethyl Acetate in hexane as eluting solvent to give 32.6 mg product (estimated 68%). NMR showed a mixture of product and impurity not able to characterized at 4.5 ppm and trityl region. The material was conducted a second time flash chromatography (same condition) was conducted to give 8 mg of product **45** (loss of material during chromatography). ¹H NMR (300 MHz, Chloroform-d) δ 7.56 (d, J = 5.6 Hz, 1H), 6.70 (s, 1H), 4.29 (d, J = 1.6 Hz, 1H), 3.43 (d, J = 8.9 Hz, 6H), 2.96 – 2.21 (m, 5H). HRMS (ESI) calcd for C₉H₁₄N₂O₂ [M + H]⁺ 183.2201, found 183.1131.

2.4 Spectra Data

See Appendix A.

Reference

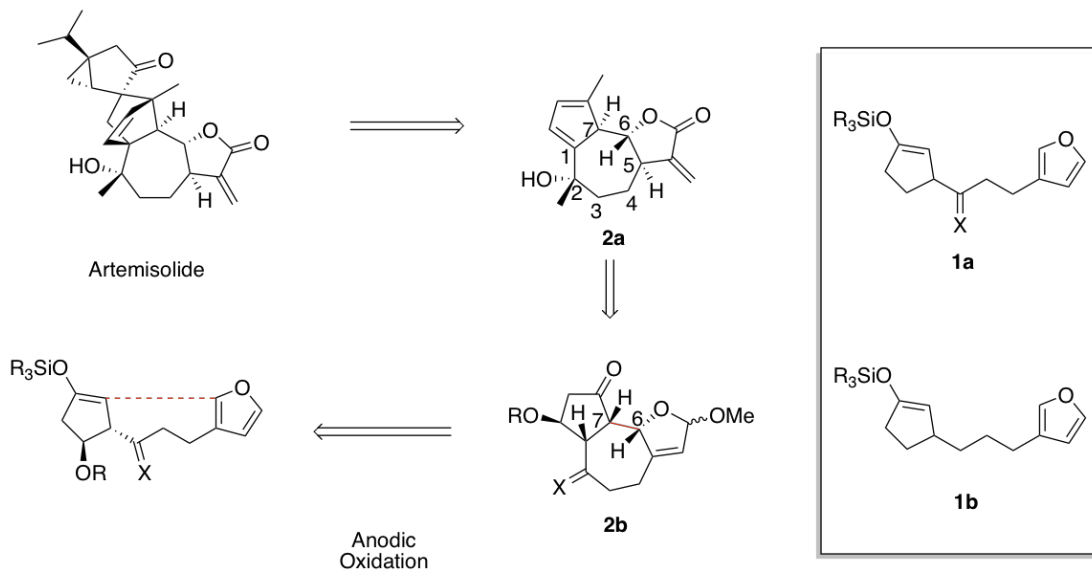
- (1) Feng, R.; Smith, J. A.; Moeller, K. D. Anodic Cyclization Reactions and the Mechanistic Strategies That Enable Optimization. *Accounts of Chemical Research* **2017**, *50* (9), 2346.
- (2) Reddy, S. H. K.; Chiba, K.; Sun, Y.; Moeller, K. D. Anodic oxidations of electron-rich olefins: radical cation based approaches to the synthesis of bridged bicyclic ring skeletons. *Tetrahedron* **2001**, *57* (24), 5183.
- (3) Huang, Y.-t.; Moeller, K. D. Anodic coupling reactions: The use of N, O-ketene acetal coupling partners. *Organic letters* **2004**, *6* (23), 4199.
- (4) Xu, G.; Moeller, K. D. Anodic Coupling Reactions and the Synthesis of C-Glycosides. *Organic Letters* **2010**, *12* (11), 2590.
- (5) Tang, F.; Moeller, K. D. Intramolecular anodic olefin coupling reactions: The effect of polarization on carbon– carbon bond formation. *Journal of the American Chemical Society* **2007**, *129* (41), 12414.
- (6) Smith, J. A.; Moeller, K. D. Oxidative Cyclizations, the Synthesis of Aryl-Substituted C-Glycosides, and the Role of the Second Electron Transfer Step. *Organic Letters* **2013**, *15* (22), 5818.
- (7) Tino-Wooldridge, L. V.; Moeller, K. D.; Hudson, C. M. Intramolecular anodic olefin coupling reactions: a new approach to the synthesis of angularly fused, tricyclic enones. *The Journal of Organic Chemistry* **1994**, *59* (9), 2381.
- (8) Amagata, T.; Doi, M.; Tohgo, M.; Minoura, K.; Numata, A. Dankasterone, a new class of cytotoxic steroid produced by a *Gymnascella* species from a marine sponge. *Chem Commun* **1999**, (14), 1321.
- (9) Rodríguez, I. I.; Rodríguez, A. D.; Zhao, H. Aberrarone: A gorgonian-derived diterpene from *Pseudopterogorgia elisabethae*. *The Journal of organic chemistry* **2009**, *74* (19), 7581.
- (10) Brandt, J. D.; Moeller, K. D. Oxidative cyclization reactions: Amide trapping groups and the synthesis of furanones. *Organic letters* **2005**, *7* (16), 3553.

Chapter 3: Pathway Control and the Formation of Seven Membered Rings

While in the last chapter we focused on the three-step mechanism involved in an anodic coupling reaction with a special emphasis on the last step, it is important to remember that the first cyclization step is in many ways the most critical. After all, if the cyclization reaction does not work, then the other steps are not in play at all. With that in mind, this chapter will focus on the cyclization reaction and the nature of the reactive intermediate that triggers it. The chemistry described focuses on our efforts to establish the seven-membered ring core structure of the natural product artemisolide with the use of an anodic cyclization reaction.

3.1 Synthesis of Artemisolide

Artemisolide is a sesquiterpene–monoterpene lactone isolated from Artemisia Species. It is used in traditional Chinese medicine for the treatment of malaria, hepatitis, inflammation, and infections caused by bacteria, fungi and virus¹. From the standpoint of our group, we have been working on incorporating synthetic electrochemistry into a broader range of applications and in so doing introducing synthetic electrochemistry to broader range of organic chemists. In this context, artemisolide represented an appealing target because of its novel structure and biological activity, and its apparent compatibility with a concise and innovative use of both an anodic cyclization reaction and the Curtin-Hammett principle (Scheme 3.1).



Scheme 3.1 Retro-Analysis of Artemislide

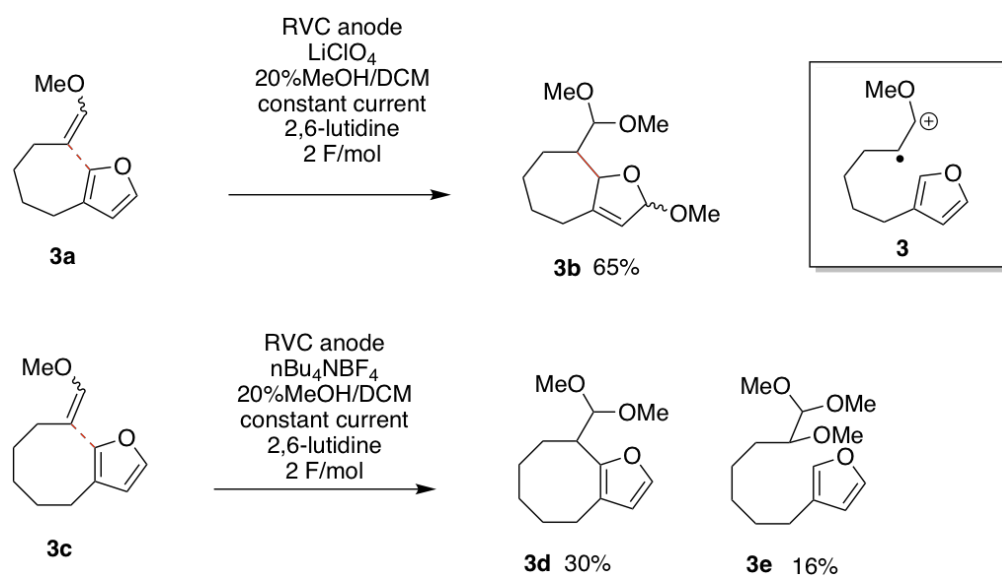
The planned approach for constructing artemislide is shown in Scheme 3.1. In the first step of the retrosynthetic analysis presented, the molecule is reduced to a core 5-7-5 ring structure through a retro Diels-Alder reaction. The forward Diels-Alder reaction is known²⁻⁵. Therefore, the synthesis of the tricyclic intermediate (**2a**) would represent a formal total synthesis of the natural product. From this point, the retrosynthetic analysis tracks back to a potential anodic coupling reaction between an enol ether and a furan to construct the bond between C6 and C7. Key to this notion was the use of a protecting group to mask the functionality at C2 of the key intermediate. This protecting group was selected to be a dithioketal that would stabilize an anion for construction of the substrate, accelerate the cyclization to form the seven membered ring through a gem-substituent effect,⁶ and then afford a carbonyl after deprotection. Of course, the sulfurs of the ketal would undergo an oxidation reaction prior to oxidation of either the enol ether or the furan, but we had previously shown in a similar substrate bearing both a dithioketal and an

enol ether that an intramolecular electron-transfer and Curtin-Hammett control of the reaction would lead to products generated from the enol ether radical cation.⁶

3.2 Seven Membered Ring Formation in 5-7-5 System

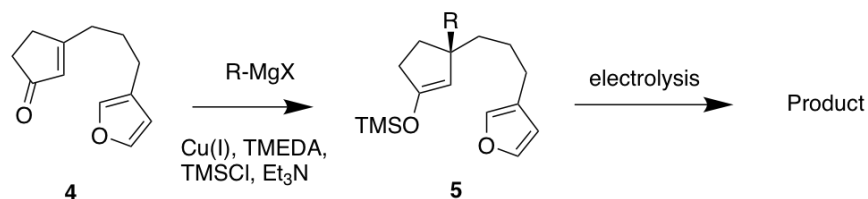
3.2.1 Problems Constructing the Seven Membered Ring

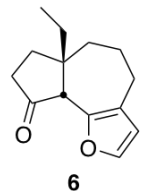
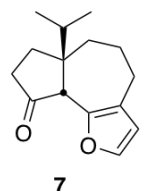
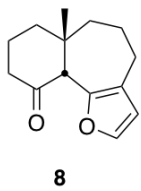
When this project was started, two key preliminary results were of interest (Scheme 3.2). In the first, it had been demonstrated that the anodic cyclization was compatible with the formation of a seven-membered ring.⁷ In this paper, a disubstituted methoxy enol ether was coupled to the furan ring to make the seven-membered ring in a 62% isolated yield. Interestingly, when the chain between the enol ether and the furan ring was extended to make an eight membered ring, the reaction led to a mixture of some cyclized product and an acyclic product (Scheme 3.2). The acyclic product was clearly formed from an enol ether oxidation. No product derived for a furan product was observed.



Scheme 3.2 Model Substrate Test on Seven Member Ring Formation

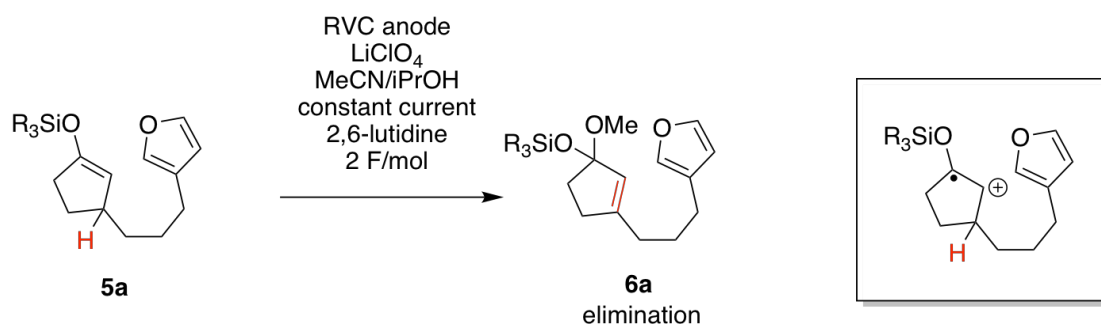
In the second example, the Wright group studied the formation of seven-membered rings in the context of building similar tricyclic ring skeletons. They found that when the group at the allylic carbon was a hydrogen ($R = H$) the reaction failed to generate a cyclic product. When this group was an alkyl ($R = \text{Me}$, Ethyl, etc), the reaction proceeded nicely to the desired product. The conclusion reached by Wright and Sperry was that the addition of the alkyl group accelerated the cyclization through a gem-dialkyl affect thereby enabling the chemistry⁸⁻¹⁰.



entry	enoether	R	product	yield
1	5a	Et		60%
2	5b	iPr		63%
3	5c	Me		61%

Scheme 3.3 Gem-dialkyl effect on seven-member ring formation

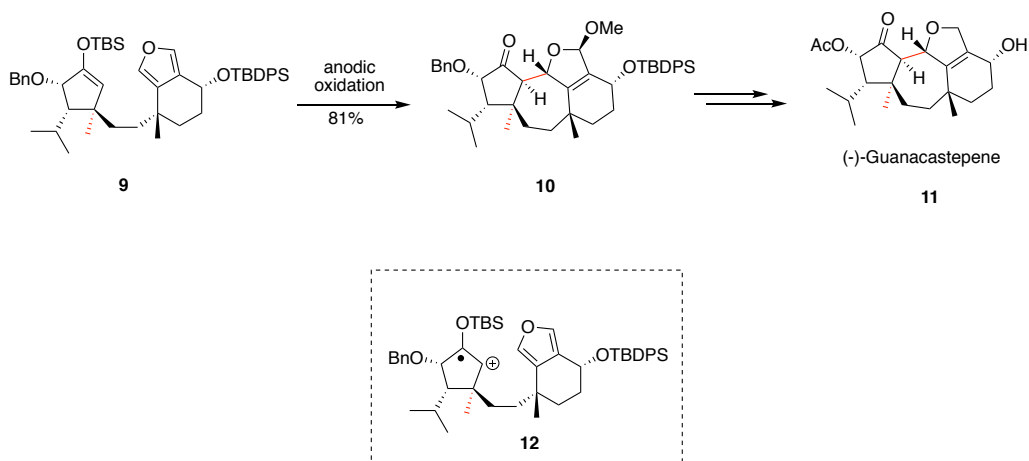
This result from the Wright group was a bit of a surprise based on our earlier finding that the reactions could lead to seven-membered ring formation. Hence, Rob Perkins in the group remade the Wright-substrate with the proton on the allylic carbon and studied its oxidation chemistry¹¹. We found that the byproducts formed were consistent with the types of radical cation-based elimination reactions that plague other slow anodic cyclization reactions.



Scheme 3.4 Fused seven member ring containing allylic proton electrolysis test

This elimination reaction would be enhanced by the direct overlap of the allylic hydrogen with a radical cation in the cyclic enol ether substrate **5a**. It was slower and unobserved when the enol ether was not contained within a ring (Scheme 3.2, substrate **3a**). In the end, it was our conclusion that the alkyl groups in the Wright case most likely blocked the elimination along with making the cyclization faster.

The use of an alkyl group to block the elimination reaction appears to be a general solution. In their reported total synthesis of **11** ((-)-Guanacastepene)¹², the Trauner group took advantage of methyl group at the allylic position of the enol ether/radical cation to enable the synthesis of a central seven-membered ring. This reaction proceeded through key intermediate **12** (Scheme 3.5).

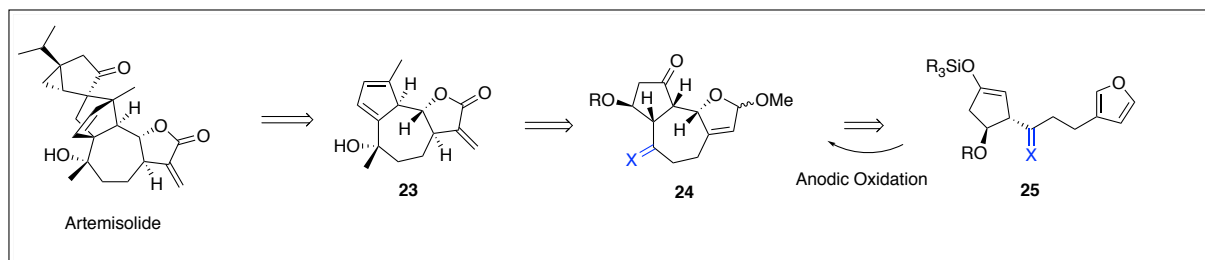
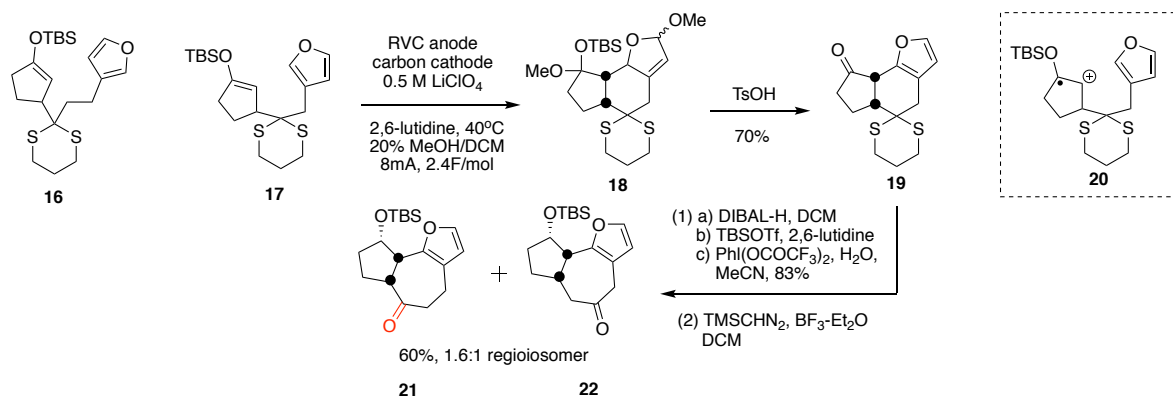


Scheme 3.5 Total synthesis of Guanacastepene

While this approach works, the structure of artemisolide (Scheme 3.1) does not have a alkyl group at the position allylic to the radical cation to be generated. In fact, this position in the molecule (C1) plays an important role in constructing the diene in **3a** (Scheme 3.1) that is needed for the final Diels-Alder reaction. As a result, we needed an alternative approach to either accelerate the cyclization, stop the elimination, or both.

3.2.2 Historical Approaches

Our first approach, initially pursued by Alison Redden in the group, sought to accelerate the cyclization with a different geminal substituent as described in the discussion of the retrosynthesis above. The plan was to incorporate a dithioketal at a point consistent with the functionality at C2 in the key tricyclic intermediate. Two attempts at this approach are worth mentioning here (Scheme 3.6).³



Scheme 3.6 Gem substitution effect on seven member ring formation

Initially, an attempt at directly making the seven membered-ring via the oxidation of substrate **16** was examined. The reaction failed and led to elimination products and polymeric material in a fashion again consistent with a slow cyclization step. Clearly, the effect of this particular gem substitution on the rate of the cyclization was not sufficient to overcome decomposition of the radical cation. It did appear that the Curtin-Hammett step⁶ had worked as planned (Scheme 3.5) because the products formed arose from the enol ether radical cation and not a dithioacetal based radical cation, a reaction that leads to cleavage of the carbon sulfur bonds and formation of a dimethoxy ketal.

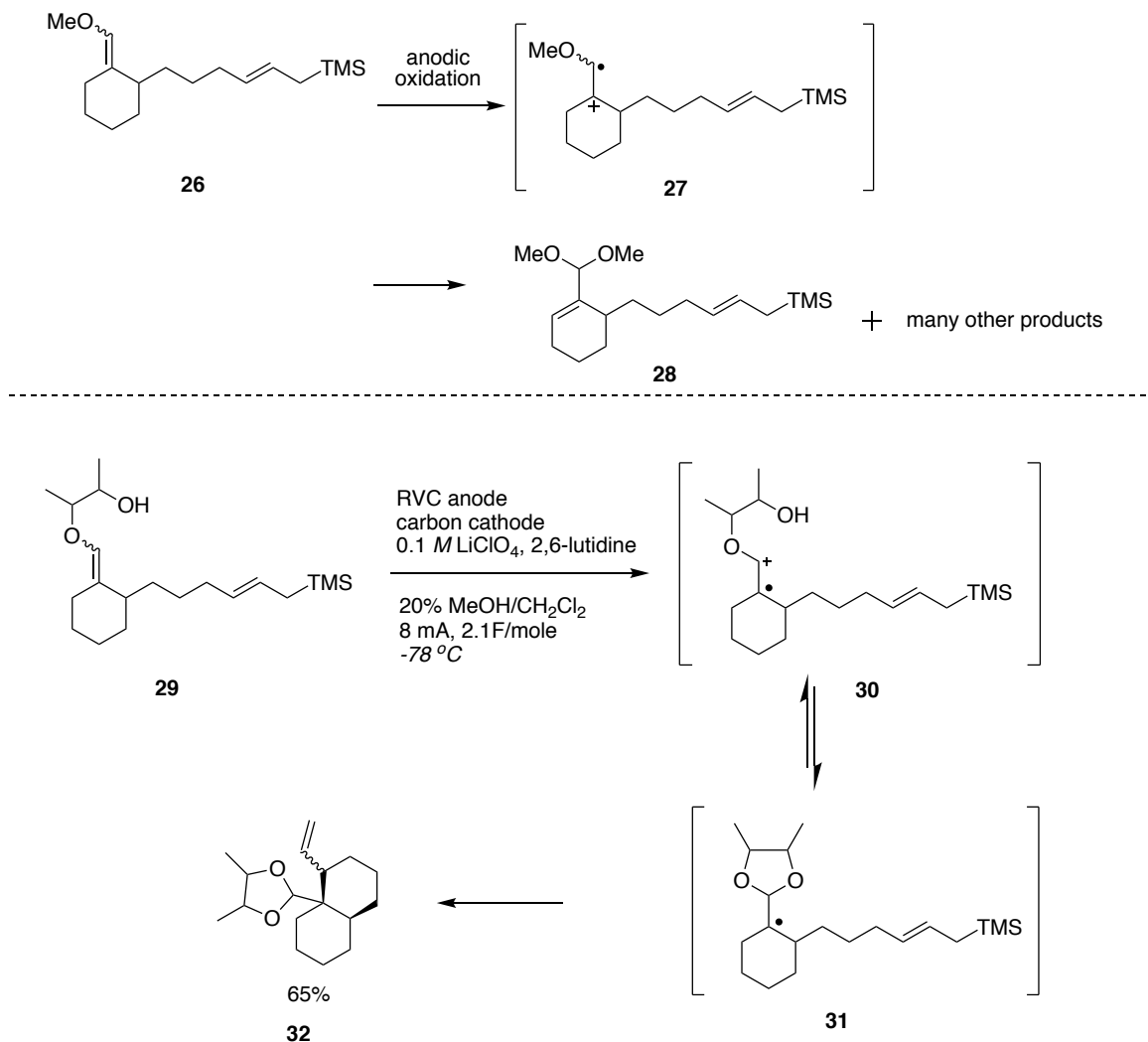
The success of the Curtin-Hammett approach in these reactions was demonstrated more convincingly with the use of substrate **17**. In this case, Dr. Redden demonstrated that the reaction proceeded smoothly to afford the six-membered ring product¹³. The product from the cyclization was then used in a ring expansion reaction to generate the desired tricyclic system. This ring expansion was only partially successful leading to a mixture of regioisomers (**21** and **22**). This was obviously problematic for the total synthesis. With that said, the route was also problematic from a conceptual point of view. It represented an indirect synthesis of the ring system. A more desirable approach would be a direct synthesis of the seven-membered ring. In other words, our desire was not to find a “work around” for a failed electrolysis, but rather to fix the electrolysis.

3.3 Change of the Nature of Reactive Intermediate

3.3.1 Transformation to Radical Intermediate

With the failure to accelerate the seven-membered ring formation with a geminal substituents consistent with the desired total synthesis, the group’s interests changed to examine an approach to slowing the elimination reaction. It is important to remember that while radical cations can do radical-like cyclizations¹⁴ (Chapter 1), they do have significant cationic character. It is this cationic character that leads to the problematic elimination reaction. To address this, Alison Redden and Robert Perkins developed a method for neutralizing this cationic character and channeling the anodic oxidation reactions down an oxidative radical pathway.¹³

Their approach was first illustrated in the context of forming six-membered rings and quaternary carbons with an allylsilane terminating group (Scheme 3.7).



Scheme 3.7 Radical Intermediate

The first reaction in Scheme 3.7 was included as background. In this reaction, the oxidation generated a radical cation from a methoxy enol ether. The subsequent cyclization was too slow leading to the elimination of a proton from the radical cation along with polymerization reactions. This observation paralleled the ones made in connection with the seven membered ring forming reactions described above.¹⁵ To address this issue, the substrate (**29**) was modified by

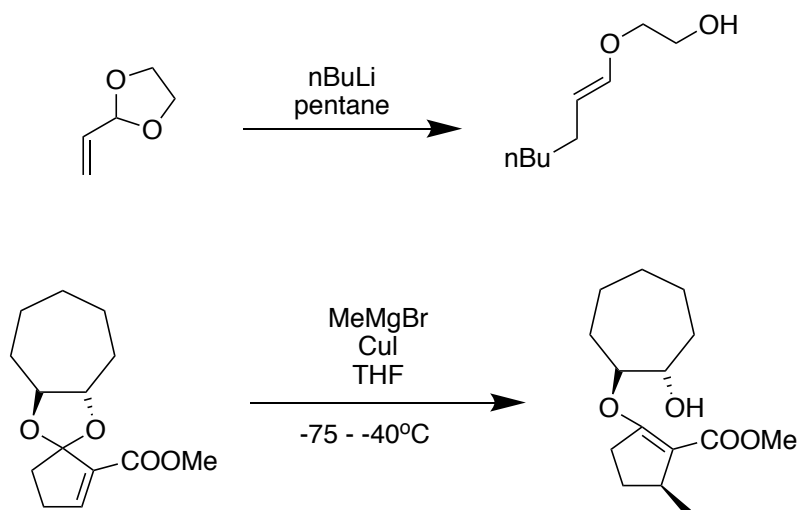
changing the simple enol ether to a glycol based enediol ether that contained a free hydroxy group. This provided the substrate with a second nucleophile that had the potential to quickly trap the radical cation intermediate in **30**, remove the possibility for the proton elimination side reaction arising from the cationic character of the intermediate, and leave behind a radical intermediate that could still undergo the desired cyclization.

The initial test of this idea was conducted at room temperature. The reaction formed a low yield of product (10-25%), but still formed mainly products from decomposition of the radical cation. Fortunately, work ongoing in the group at the time showed that the trapping of a radical cation by an alcohol was both reversible and exothermic.¹⁶ If alcohol trapping of intermediate **30** is reversible, then some cation character would remain and the possibility for a competing elimination reaction would persist. However, since the alcohol trapping is exothermic¹⁶, the formation of the cyclized product would be favored by lowering the temperature. Hence, the oxidative cyclization was repeated at -78 °C. At this low temperature, the isolated yield of the cyclized product was raised to 65%. Clearly, the allylsilane could be used as a trapping group to simultaneously form a six-membered ring and a quaternary carbon if the reaction was channeled down an oxidative radical pathway and a persistent radical cation intermediate avoided.¹³

The success of this reaction suggested that maybe the approach would provide a general route to anodic carbon-carbon bond forming reactions that involved slow cyclization reactions. Certainly, it was reasonable to suggest that the same approach might solve the challenges associated with the formation of seven-membered rings outlined above.

3.3.2 Oxidative Radical Pathways and Seven-Membered Ring Formation

To test this idea, we needed a rapid route to make the substrates. As shown in Scheme 3.3, the Wright group had developed a Michael reaction/electrolysis sequence for exploring similar silyl enol ether based substrates.¹⁷ A survey of the literature suggested that a related approach utilizing a Michael-type addition to an unsaturated acetal (Scheme 3.8) might provide a useful route to the enediol ether substrates. The work built upon observations made by the Manna group using organolithium reagents,¹⁸ and the Sakai group using cuprate reagents¹⁹ as the nucleophiles for the additions.

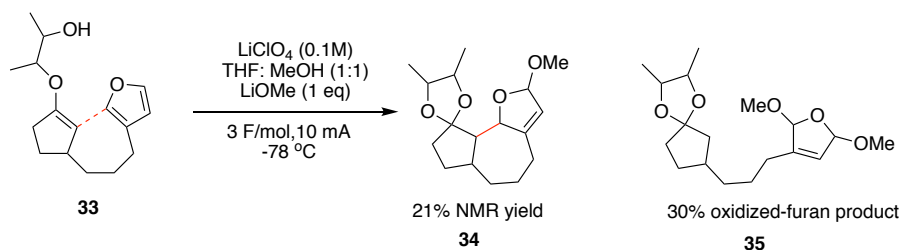


Scheme 3.8 Literature using acetal as Michael Acceptor

We thought this approach might prove very general since Grignard reagents needed for generating the necessary cuprate reagents should be accessible and in principle unsaturated ketals can be synthesized from a variety of available enones. The real key was carrying the furan through the Grignard process, but again the Wright group's efforts indicated that this was possible. The approach would potentially provide access to a large number of ene diol

electrolysis substrates. This was also an initiation point for me build a series of substrates required in chapter 4.

In the beginning, Robert Perkins expended significant effort to optimize both the reaction conditions and workup procedure to make the reactions possible.¹¹ Substrate **33** was synthesized and oxidized by Dr. Perkins.



Scheme 3.9 Radical Intermediate on Seven-Membered Ring Formation

The oxidation reaction was partially successful. It did lead to the formation of some cyclized product (21%), but the reaction was messy and the product difficult to isolate. Hence, the yield was determined by NMR analysis of the crude reaction product. In addition to the desired product, approximately 30% of product (**35**) derived from furan oxidized was obtained. The initial ene diol ether did lead to a cyclic ketal in this product. Many attempts to optimize the reaction also led to formation of the oxidized furan as the major product.

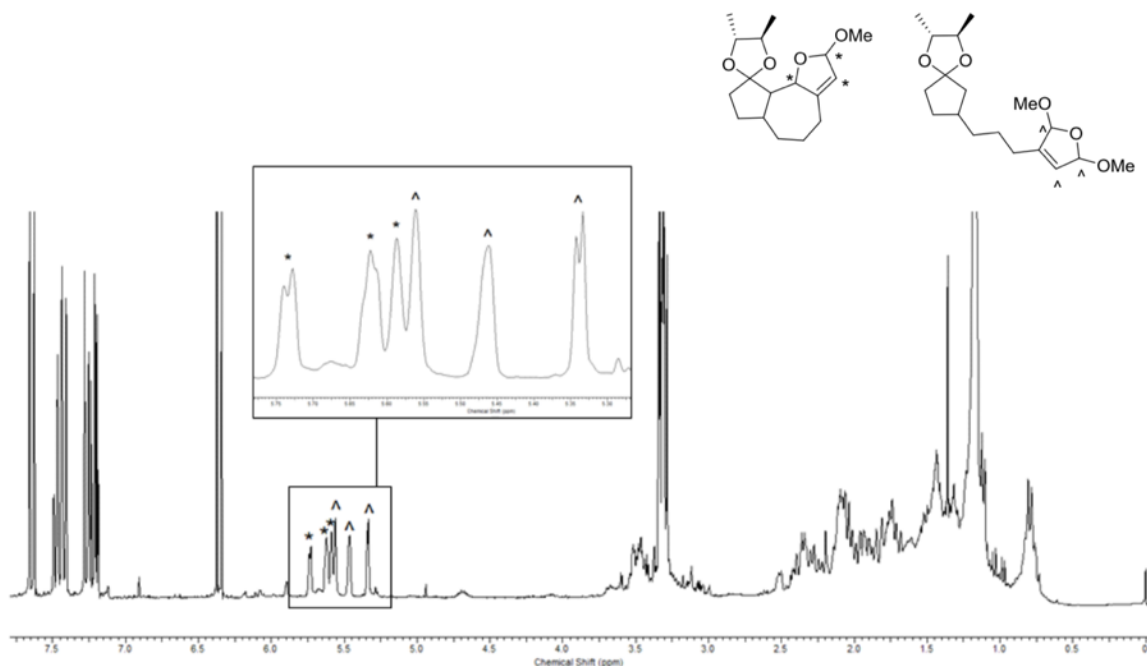
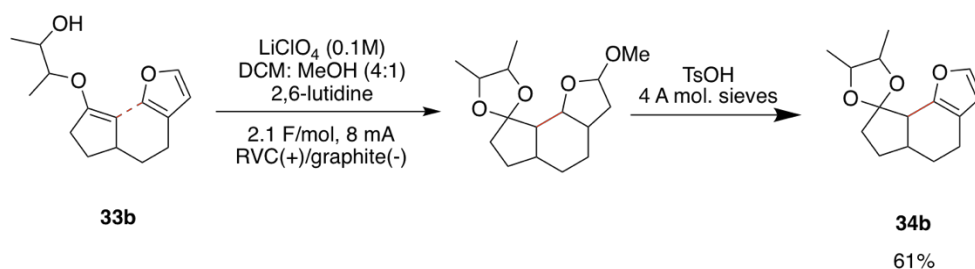


Figure 3.1 Electrolysis of 33 by Robert Perkins

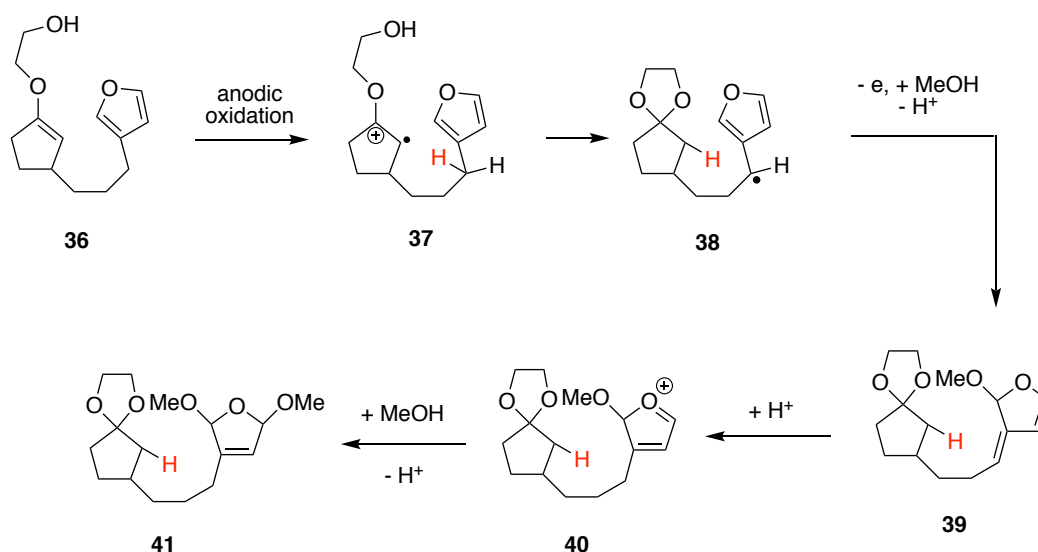
The oxidation of the furan was a surprise since the previous studies had clearly demonstrated that enol ethers are preferentially oxidized in the presence of a furan ring, even when the enol ether is less electron-rich than the one utilized in substrate.⁷ For example, consider the oxidation of substrate **3c** mentioned earlier (Scheme 3.2). In this reaction, the only non-cyclized products obtained were the result of enol ether oxidation. No products from furan oxidation were observed even though it is clear from the current reaction that they can be isolated. In addition, the oxidation of enol ether substrate shown in Schemes 3.2, 3.3, 3.4, 3.5 had not led to any furan oxidation product. Nor had the reaction originating from substrate **33b** (Scheme 3.10), an observation that ruled out any suggestion of an initial proton induced cyclization of the enol ether in the substrate to form the cyclic ketal prior to the oxidation¹³.



Scheme 3.10 six member ring ene diol substrate electrolysis

Interestingly, the ratio of the two products shown in Scheme 3.9 did not depend on the pH of the reaction, another observation that was inconsistent with decomposition of the enol ether prior to the oxidation.

In light of these observations, it seems more likely that the desired radical for the oxidative radical cyclization led to a hydrogen atom abstraction as shown in Scheme 3.11¹¹.



Scheme 3.11 Radical Intermediate causing HAT (Hydrogen Atom Transfer)

In the proposed mechanism, once radical cation **37** was trapped by internal hydroxyl group, the radical was in position to abstract a proton alpha to the furan ring through a six-membered ring

transition state. This HAT (Hydrogen Atom Transfer) reaction would result in radical **38**. A second oxidation followed by methanol trapping and a methanolysis reaction would lead to the observed product **41**.

While such a hydrogen atom abstraction should not have been a surprise, it caught us off guard because the previous successful anodic cyclization reactions leading to seven-membered rings showed no such behavior (Schemes 3.2 and 3.3). Is it possible that radical cation intermediates (which does not require low temperature) simply do not undergo such hydrogen atom abstraction reactions? This is a question we will address below.

3.3.3 Constrained Radical Intermediate in Seven-Member Ring Formation

With it becoming clear that slowing down the competitive elimination reaction was not an option; the key question became whether or not we could accelerate the cyclization to form a seven membered ring without putting a quaternary carbon next to the radical cation. Our hope was that we could accelerate either the oxidative radical pathway enough to overcome the hydrogen atom abstraction, the radical cation pathway enough to overcome the problematic elimination from the radical cation, or both.

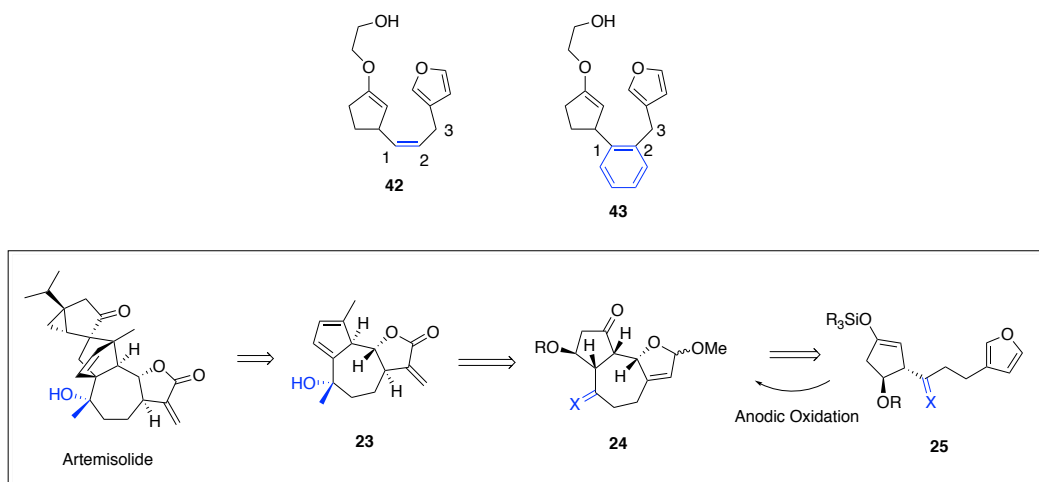
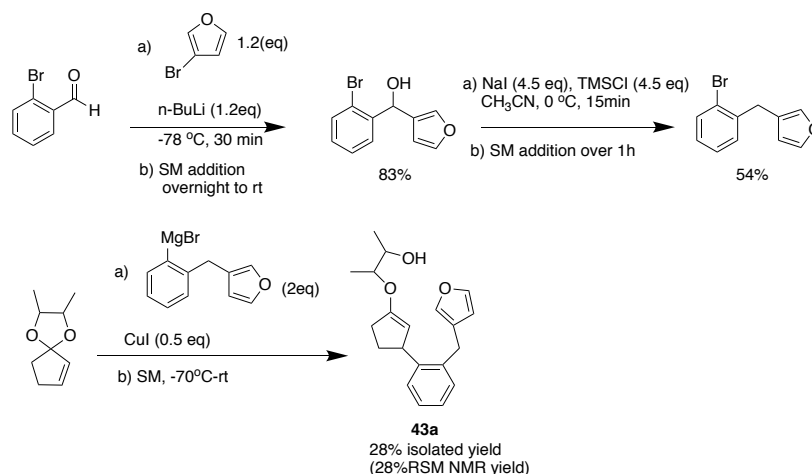


Figure 3.2 Constrained Radical Intermediate Substrate

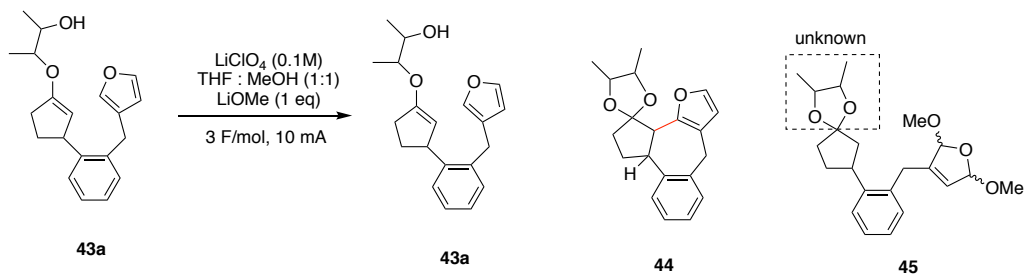
With this in mind, the two substrates shown in Figure 3.2 were designed. The design was guided by two main thoughts. First, the more rigid side chain would decrease the rotational degrees of freedom associated with the tether and should lead to a significant increase in the rate of the cyclization reaction. In addition, the presence of the sp^2 -hybridized atoms would reduce any transannular interactions that might slow the cyclization. Second, while the phenyl group would not be compatible with the synthesis of artemislide, the use of a cis olefin as the constraint would potentially be compatible with the synthesis because it could be used to mask the functionality needed at C2 of intermediate **23**. It was hoped in both cases that the rate of the cyclization might overcome the HAT reaction, although we did worry that the presence of the constraint might also accelerate the HAT reaction.

With this in mind, we made substrate **43a** using the chemistry shown in Scheme 3.12.



Scheme 3.12 constrained ene diol substrate synthesis

The electrolysis substrate was chromatographed through silica gel. While the material was unstable and chromatography led to lower yields, the substrate could be isolated in an amount that allowed for examination of the electrolysis.



Scheme 3.13 Constrained Radical Intermediate Pathway Cyclization

The oxidation led to a significant amount of recovered starting material along with a collection of oxidation products (Figure 3.3 Three of the peaks (labeled with asterisks) seem consistent with the cyclized product. However, the smaller peaks upfield of these signals would be consistent with the furan oxidation product. Much of the rest of the spectrum was consistent with a messy electrolysis and the formation of polymer type products. Note the very messy methoxy region between 3 and 4 that is often associated with these types of problems in an electrolysis.

Certainly, an extensive optimization of the reaction would be needed for there to be a chance for obtaining a significant amount of the desired cyclized product. There was little evidence that the reaction would lead to a high yield of cyclized product if optimized for conversion. This optimization was not conducted due to the success of the reaction channeled down the radical cation pathway.

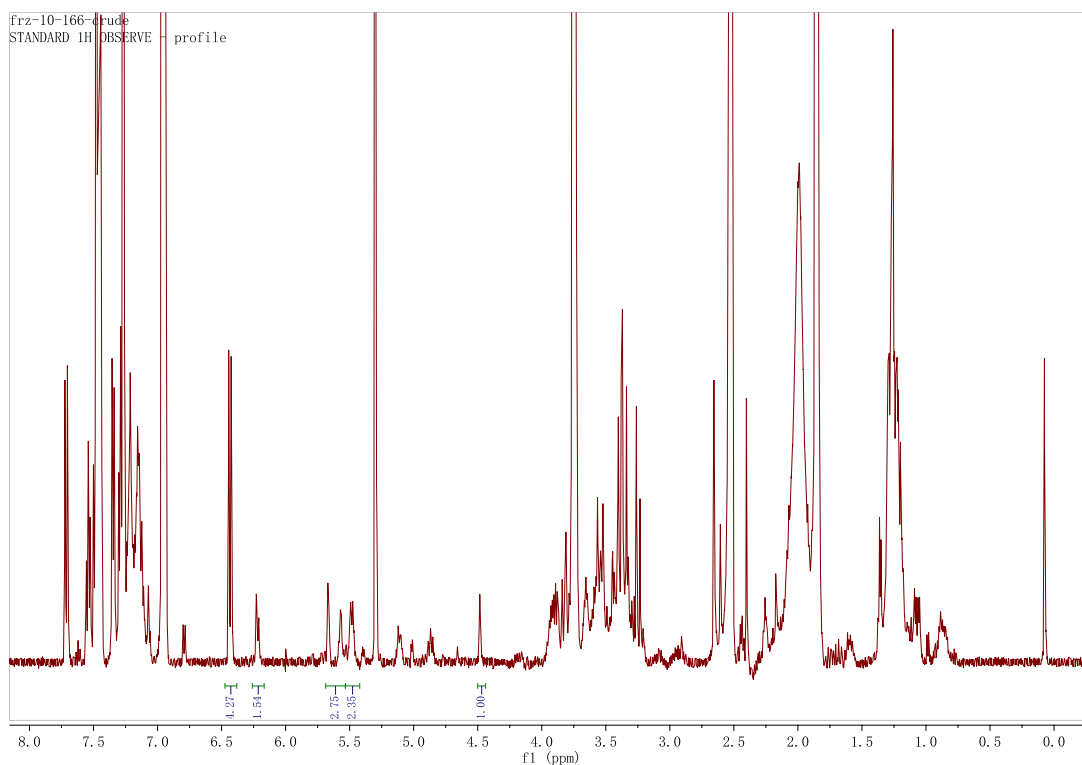


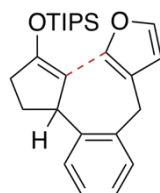
Figure 3.3 Constrained ene diol substrate electrolysis. NMR of the crude product. Coumarin as internal standars

3.3.4 Constrained Radical Cation Intermediate in Seven-Membered Ring Formation

The lack of cleanliness in the reaction channeled down the oxidative radical pathway made it clear that the added constraint had not fixed the problems encountered with the previous

oxidative radical pathway. Hence, we turned our attention to the radical cation pathway and the twin questions of whether or not radical cation reactions were subject to the HAT transfer reaction and whether or not the presence of the phenyl ring in the tether would increase the rate of the desired cyclization relative to the elimination reactions that typically plague slow radical cation-based cyclizations reactions? It was noted that the phenyl ring would also accelerate the elimination reaction of the allylic, and now benzylic hydrogen from the radical cation?

To address these questions, substrate **47** was synthesized and oxidized. The TIPS group was chosen in order to increase the stability of the substrate with respect to methanolysis during

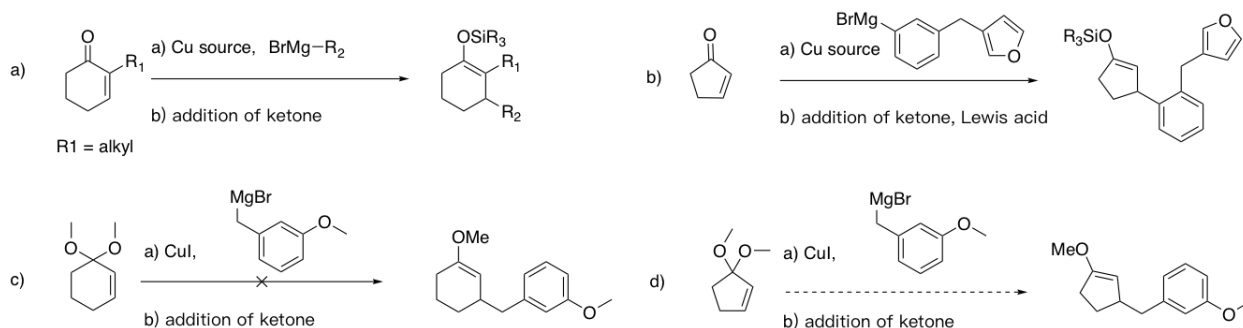


47

Figure 3.4 Constrained Radical Cation Intermediate Substrate

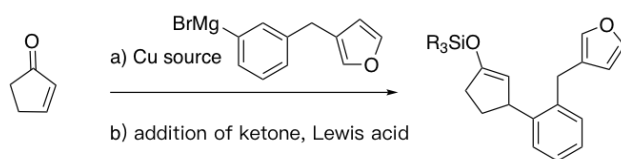
electrolysis reaction. As with the synthesis of the enediol ether substrates, we examined the generality of an approach to make the silyl enol ether substrates (Scheme 3.14).

Model substrate plan



Scheme 3.14 Michael addition to ketone to access constrained intermediate

Plan (a) and (b) were both selected for this study so we could examine the generality of our earlier observation about the effect of fused ring size on the reactions. The reaction highlighted in equation (a) will be detailed in chapter 4 since the substrates synthesized were part of the project outlined there. In Plan (b), different conditions were tested in order to optimize both the yield of the reaction and the stability of the substrate for the electrolysis. This stability was important so that we could obtain pure material for testing the electrolysis reaction. The Grignard-reagent was synthesized as shown previously in Scheme 3.12. Different conditions were then tested for the Michael addition.



entry	Cu source	grignard	step (a) temperature	additive	Lewis acid	yield
1	CuI (0.5eq)	~1.5eq	-20°C	HMPA(3eq)	TBSCl (2.4eq)	19%
2	CuI (0.5eq)	~1.5eq	-78°C	HMPA(2.5eq)	TBSCl (3eq)	13% enol ether (21% ketone form)
3	CuBr-Me ₂ S	~1.5eq	-78°C	HMPA(2eq)	TBSOTf (2.4eq)	clean crude NMR lost during chromatography
4	CuI (0.5eq)	~1.5eq	(a)0°C (b)-78°C	HMPA(2eq)	TipsOTf (2.4eq)	60%

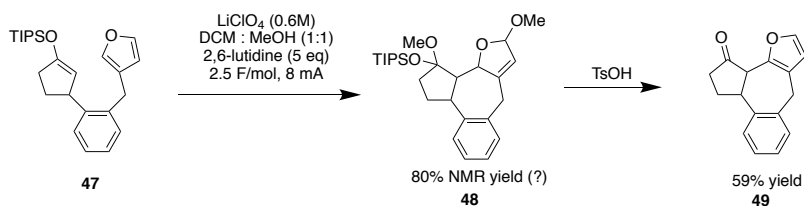
Scheme 3.15 Michael condition test

The chart shown in Scheme 3.15 summarizes selected examples of conditions probed that combined taught us critical items about the reaction. First, generation of the cuprate benefited from a temperature that was higher than the -78 °C used for the actual addition reaction. Second, the reaction benefited from a slow addition of the ketone to the cuprate at low temperature before

warming the reaction temperature back to room temperature following the addition (a detail prescription can be found in Experimental Section). Third, the reaction benefited from the use of a triisopropyl silyl group on the enol ether. With this TIPS group, the product was more stable and could be purified by silica gel chromatography.

The reactions shown in equations (c) and (d) represented a back-up plan in case the silyl enol ethers could not be isolated. Unfortunately, both of these reactions failed. The example shown in equation (c) did not work when the conditions above were employed, and the substrate for equation (d) proved too difficult to make. The routes were abandoned because of the successful synthesis of triisopropylsilyl enol ether substrate **47**.

With the substrate **47** in hand, the electrolysis reaction was attempted. For this reaction, the five-membered ring enol ether was utilized because of its relationship to the targeted natural product. In this case, the phenyl ring constraint proved very successful, and the oxidation reaction led cleanly to oxidized product. In the proton NMR spectrum of the crude product obtained (Figure 3.5), note the cleanliness of the methoxy region. This region is at a chemical shift consistent with ketal and acetal based methoxy ethers (ca. 3.2 – 3.4 ppm). Isolation of the product proved to be difficult due to hydrolysis reactions and elimination to the furan ring. So, the success of the cyclization was first evaluated by NMR integration using the crude reaction product.



Scheme 3.16 Constrained Radical Cation Intermediate

To get a rough approximation of yield, the signals at 5.5 were integrated relative to trimethoxy benzene as internal standard. These signals were selected because a fast chromatography of the crude material did lead to the isolation of the material (tentatively assigned as **48**) shown in Figure 3.6. This material could be hydrolyzed to generate a fully characterized cyclization product **49**. Clearly, the material that gave rise to Figure 3.6 might only represent part of the isomeric mixture that could have been formed in the reaction. However, the integration of this region of Figure 3.5 indicated that the yield of cyclized material might be as high as 80%. However, this number is very crude, and it likely only indicates that a significant portion of the oxidized material was the desired cyclized product.

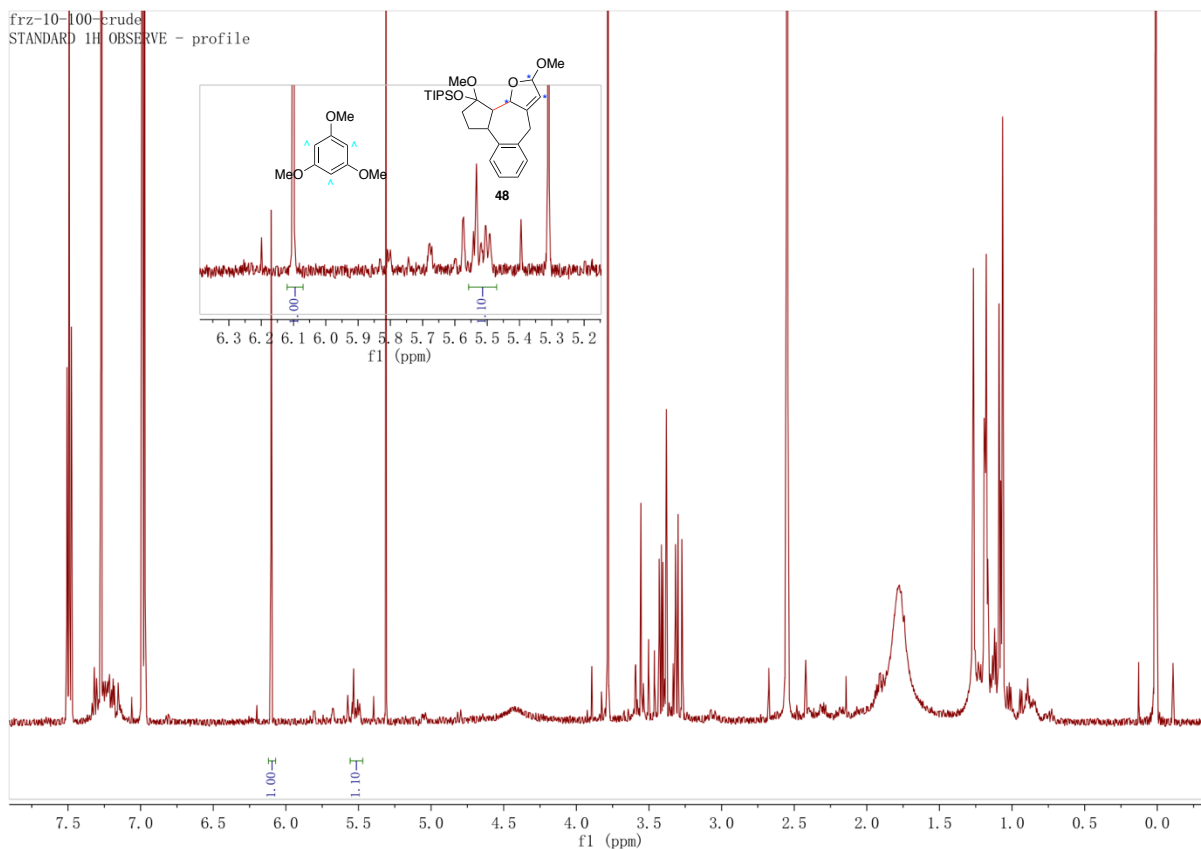


Figure 3.5 Electrolysis of 47 using trimethoxy benzene as internal standard

More evidence for the formation of cyclized product was obtained by the hydrolysis of the material shown in Figure 3.6 to form a cyclized product containing both a ketone and the furan (49). Product 49 was formed in a 59% isolated overall yield from the oxidation substrate 47.

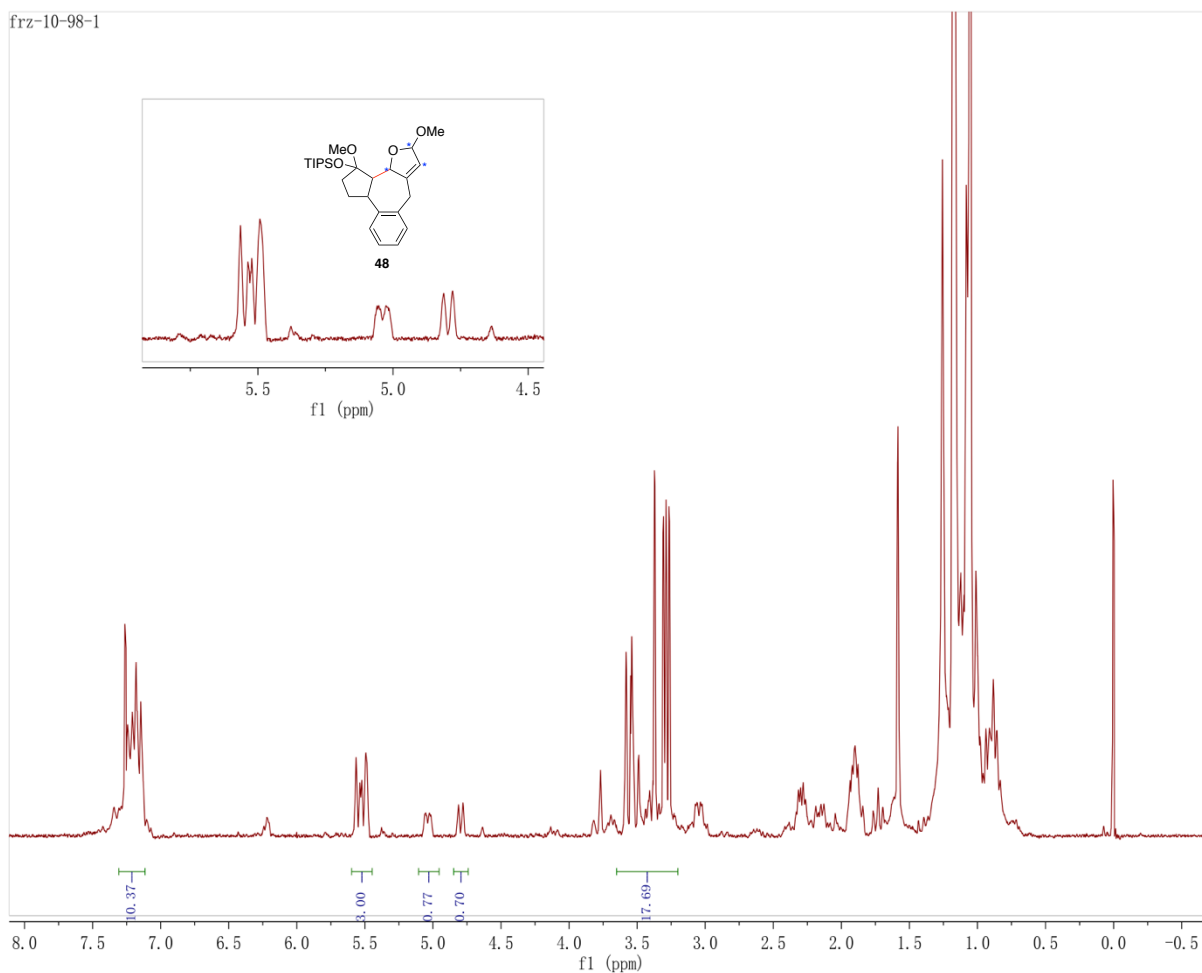


Figure 3.6 Material after fast chromatography following electrolysis of 47

The yield is currently tentative because of the scale of transformation (14 mgs). (A larger scale reaction is on under investigation). It was characterized as a cyclization product with the use of 2D NMR. The HMBC spectrum is included in Figure 3.7. Note the correlation between the

hydrogen on atom eight and carbon nine that indicates formation of the desired carbon-carbon bond.

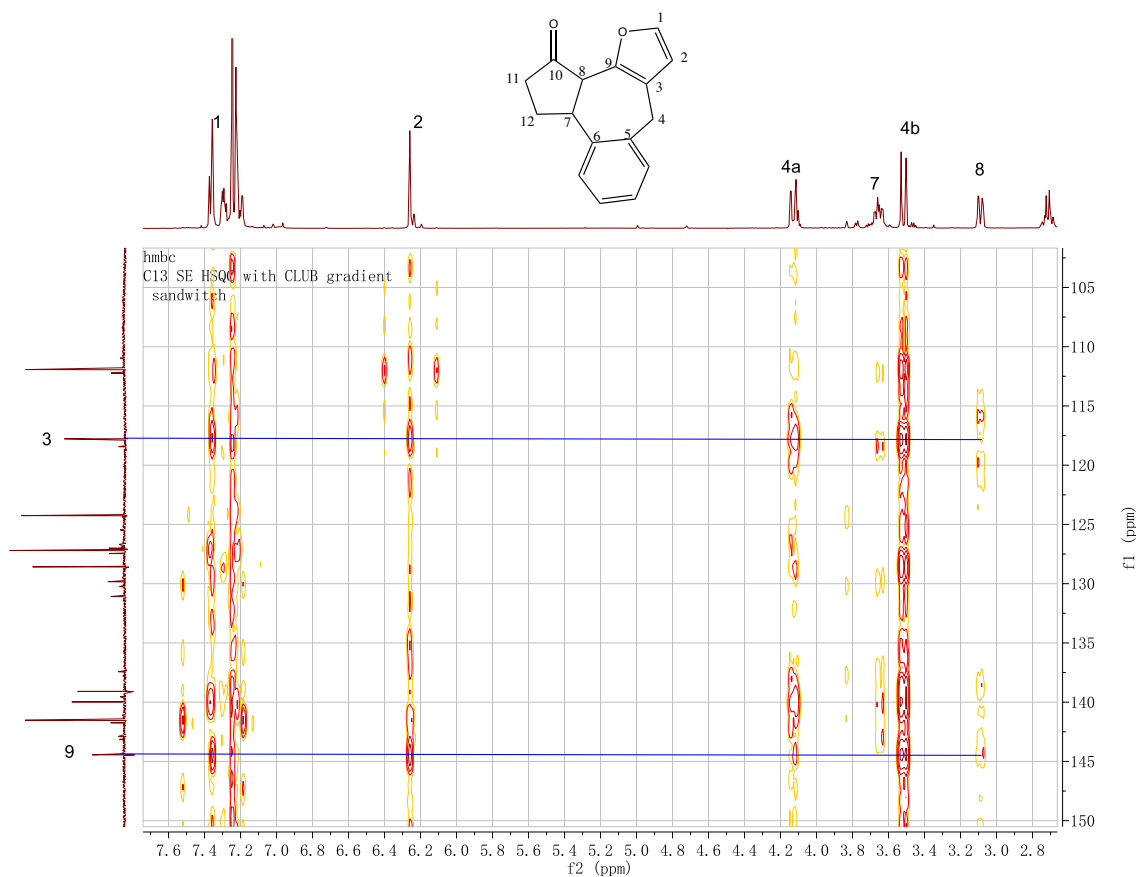


Figure 3.7 HMBC for 49

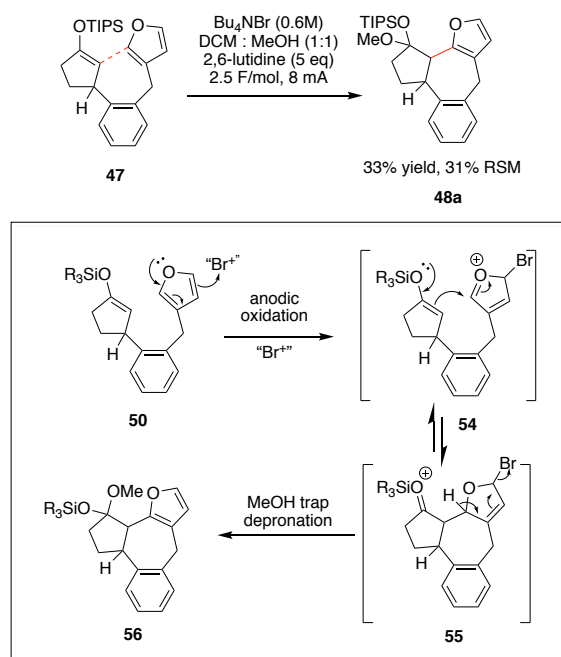
The conditions for the overall conversion of **47** to **49** were not optimized since this was a model system and not compatible with the natural product synthesis (the presence of the phenyl ring is not consistent with the ring system of artemiside). However, the oxidation of **47** when compared with the reaction resulting from the oxidation of substrate **43** did provide compelling evidence that this reaction benefited from the use of a radical cation intermediate. The oxidation led to no evidence of a product derived from the elimination of a proton next to the initial radical

cation. In addition, we did not isolate any product that would result from the competitive H-atom abstraction or furan oxidation, although the proton NMR of the crude material leaves open the possibility that a minor amount of material from a H-atom abstraction may have formed. With that said, the use of the conformational constraint with the radical cation pathway eliminated the need to block a potential elimination reaction from the radical cation with a methyl group as seen in the earlier related seven-membered ring forming reactions, and it avoided the need to employ the more difficult to synthesize and handle enediol ether substrate. The reaction suggests that the anodic coupling reaction might be compatible with the synthesis of artemisolide if channeled down the radical cation pathway in the presence of an appropriate conformational constraint.

Furthermore, a comparison of the reactions resulting from oxidation of **43** and **47** suggests that *radical cation intermediates do not rapidly undergo H-atom abstraction reactions and that the reaction is overall a much cleaner process*. This led to the conclusion that we cannot simply channel a reaction down an oxidative radical pathway to overcome a slow cyclization as previously thought. There are times (a competitive H-atom abstraction) where the use of a radical cation intermediate dramatically improves the oxidative cyclization. Of course, this does not change the earlier observations that there are times (a competitive proton elimination from the radical cation) when the oxidative radical approach is needed).

3.3.5 Discovered Alternative Pathway for Seven-Membered Ring Formation

During the process of reaction condition optimization, we chose the use of tetrabutylammonium bromide as an electrolyte and stumbled onto an alternative pathway for the generation of a seven-membered ring product. This pathway involved an initial oxidation of the bromide electrolyte to form a source of Br⁺ as previously reported in the literature.^{20,21}



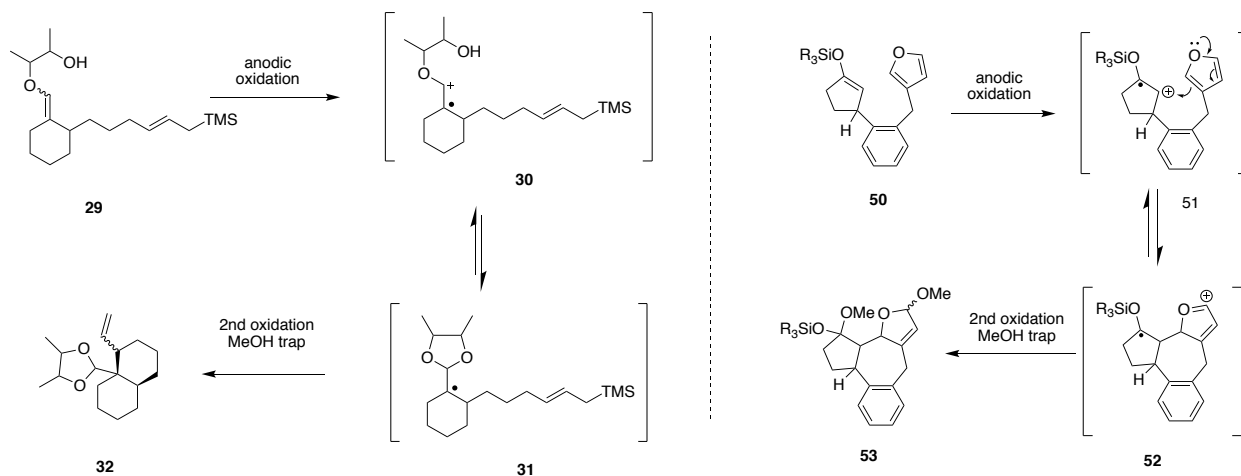
Scheme 3.17 Electrolyte Influence

The Br^+ can then brominate the furan ring leading to the cyclization as outlined in Scheme 3.17. In this case, the reaction would lead directly to the furan product following the elimination of HBr . When substrate **47** was oxidized using similar CCE (Constant Current Electrolysis) conditions with the use of the tetrabutylammonium bromide, product **48** was achieved in a 33% isolated yield along with 31% RSM. Remember that without the Br^- -based electrolyte the product generated from the reaction was not the furan but a methoxylated dihydrofuran derivative that needed to be converted into the furan with a subsequent oxidation step.

Since this alternative approach did not relate to the main topic of our work in this area (a more general look at the role of radical cation and oxidative radical pathways in oxidative cyclization) it was not pursued in detail as part of this study. However, this alternative approach might provide an interesting alternative for other classes of reactions that would benefit from the use of a Br^+ catalyst²¹.

3.4 Conclusions and control of pathway

It is clear that both the oxidative radical pathway and the radical cation pathway have situations where they represent the preferred approach for an oxidative cyclization reaction. For example, consider the chemistry shown in Scheme 3.18 which highlights the conclusions reached above.



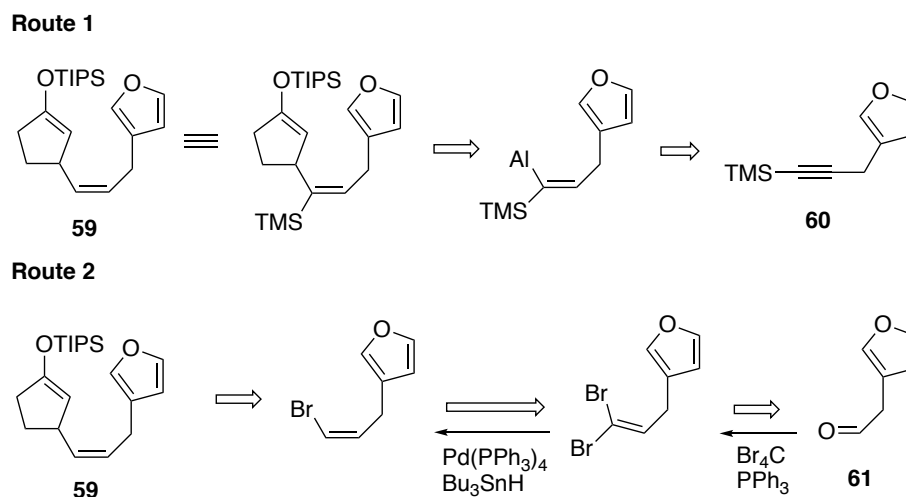
Scheme 3.18 Radical Pathway VS Radical Cation Pathway

In the cyclization originating from the oxidation of substrate **29** use of the oxidative radical pathway was essential in order to avoid elimination reactions from the radical cation. Here, the intramolecular HAT pathway was not competitive with the cyclization. However, for the oxidation of substrate **50** the intramolecular HAT reaction did prove to be problematic (presumably due to the stability of the new radical formed) and a radical cation pathway that was not susceptible to the HAT reaction required.

With it becoming clear that the nature of the reactive intermediate is important for the success of an oxidative cyclization reaction, it is important to take note of how substrates **43** and **47** were synthesized (Scheme 3.12 and scheme 3.15). Both were made from the same cuprate reagent and the same enone with slightly modification. For the formation of the substrate leading to the

radical cation pathway (**43**), the cuprate was added to the enone *via* a Michael addition. For the formation of the substrate leading to the oxidative radical pathway (**47**), the cuprate was added to a ketal derived from the enone. The point is that the same synthetic sequence can be used to access both substrates. *So, in a synthesis the same overall route can be employed to a product no matter what reactive intermediate is needed for optimizing the success of the oxidative cyclization.*

In this chapter, a major issue discussed is centered on the mechanism attempting to get access to seven-member ring. However, in the actual artemisolide synthesis, we need a double bond instead of phenyl ring. A couple of attempts were made to access these intermediates, but time ran out before we could find a successful route.^{22,23}

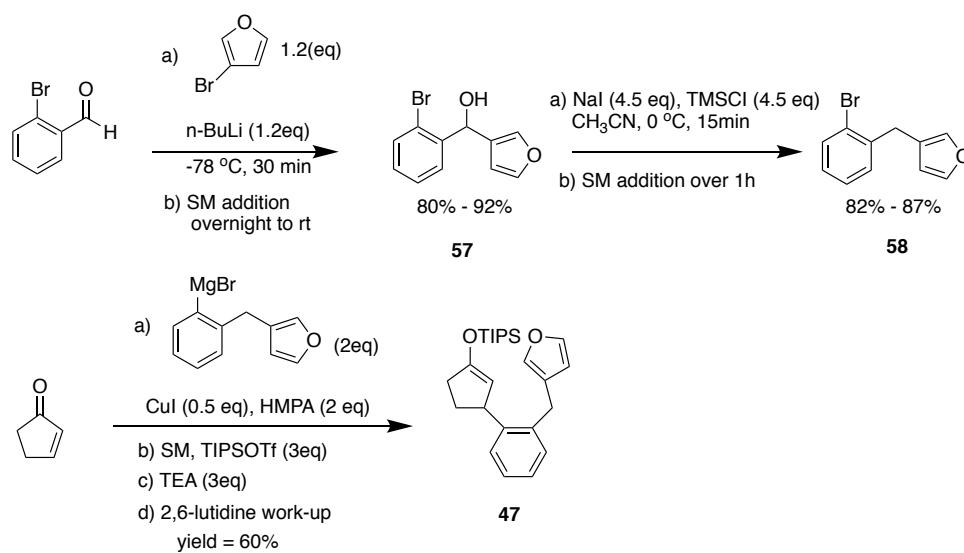


Scheme 3.19 Synthesis of **59**

3.5 Experimental Section

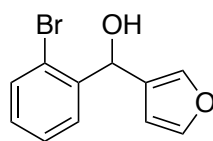
Synthesis of **47** route

The key to the synthesis of the electrolysis substrates in this chapter is Michael-addition to corresponding ketone or ketone acetal. As a sample, the synthesis of substrate **47** is detailed here. Other Grignard-reagents used in this chapter were either purchased from Sigma Aldrich or synthesized from the commercially available bromide using the procedure described below.



Scheme 3.20 Synthesis of Electrolysis Substrate **47**

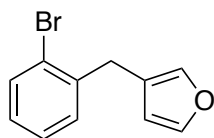
Synthesis of **57** (2-bromophenyl)(furan-3-yl)methanol



To a solution of 3-bromo furan (5.23 g, 35.6 mmol, 1.12 eq) in THF (40 mL) at -78 °C was added n-BuLi (14.2 mL of a 1.6 M solution in hexane, 1.2 eq) in a dropwise fashion. After 30min, 2-bromobenzaldehyde (3.66 mL, 31.6 mmol) in 15 mL THF was added in dropwise. The reaction mixture was allowed to warm to room temperature and then stirred overnight. The reaction was then quenched with a saturated aqueous solution of NH₄Cl and most of THF solvent

removed under reduced pressure. The residue was diluted with water and DCM, and the aqueous layer extracted with three times with dichloromethane (DCM). The combined organic layer was dried over MgSO₄, filtered, and concentrated *in vacuo*. The crude product was chromatographed through silica gel using 20% ethyl acetate in hexane as eluent to give 7.0 g of product (87% yield). The NMR data (Appendix B) matched the previously published data.¹¹

Synthesis of **58** 3-(2-bromobenzyl)furan



To a solution of NaI (5.55 g, 37 mmol, 4.5 eq) in acetonitrile (100 mL) at 0 °C, was added TMSCl (4.73 mL, 37 mmol, 4.5 eq) in a dropwise fashion. The reaction was stirred at 0 °C for 15min before adding **57** (2.08 g, 8.22 mmol, 1 eq) in 50 mL of CH₃CN dropwise over 1h at 0 °C. The reaction was then quenched with NaOH (2M). The resulting aqueous layer was extracted two times with Et₂O. The combined organic layer was dried over MgSO₄, filtered, and concentrated *in vacuo*. The crude product was chromatographed through silica gel with hexane as eluent to give 2.0 g of product (85% yield). The NMR data (Appendix B) matched the previously published data.¹¹

A procedure for making phenyl bromide Grignard:

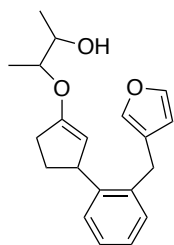
Note: In our hands, the phenyl-based Grignard-reagents generally require longer reaction time (5 h vs 3 h) and higher temperature (reflux) than the alkyl-based Grignard-reagents.

Mg ribbon (4 g, freshly sanded, freshly cut) was placed in 50 mL flask. The flask was flame dried and then cooled to room temperature. THF (12 mL) was added to the flask and the mixture sonicated for 15 min. The starting bromide (8.5 mmol) was dissolved in 8 mL of THF. The subsequent additions were made using a Sage Instruments Syringe Pump (Model number 341B). In stage one, 2 mL of the bromide solution was added to the flask with the syringe pump at a rate of 8 mL/min. A heat gun was then used to initiate a reflux. In a second stage, the remaining 6 mL of bromide solution was added to the flask at a rate of 2 mL/min while the reaction was heated with a hot plate. In the third stage of the reaction, the result mixture was refluxed for 5h. A dark red solution was obtained.

A procedure for titration of phenyl bromide Grignard:

A 5 mL flask was flame dried and placed under argon with the use of a balloon. To this flask was added 14.5 mg of menthol along with $\frac{1}{2}$ a spatula of 1,10-phenanthroline to be used as an indicator. Methanol solvent (0.5 mL) was then used to dissolve the solid. To this mixture was added the Grignard-reagent in a dropwise fashion. Upon addition, a milky white solid was formed. After 0.54 mL of the Grignard-reagent was added, the mixture became a clear, dark red solution. The titration indicated that the Grignard-reagent had a concentration of 0.18 M. This concentration varied due to a loss of solvent during the preparation of the Grignard and activation of the bromide.

Synthesis of **43a** 3-((3-(2-(furan-3-ylmethyl)phenyl)cyclopent-1-en-1-yl)oxy)butan-2-ol



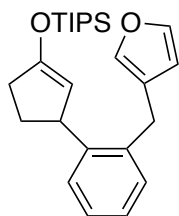
To a freshly made Grignard solution (0.69 M, 2mL) at 0 °C was added freshly recrystallized CuI (50 mg). The mixture was stirred at room temperature for 30 min until a dark red color suspension was formed. Mixture was then cooled to -78 °C. To this solution the unsaturated ketal substrate synthesized in Chapter 4 (154 mg, 1.0 mmol, 1 eq) was added in 1 mL of THF in a dropwise fashion. This was followed by a dropwise addition of BF₃-Et₂O (0.04 mL, 1 mmol, 1 eq), and then the reaction was stirred for 5 h. Prior to the workup, 2,6-lutidine (0.6 mL) was added into the mixture. The reaction was quenched with a saturated aqueous NaHCO₃ solution. The reaction was washed with EDTA solution (pH=8, 0.1 M) until no blue color remained. The layers were separated, and the aqueous layer was washed with ether three times. The combined organic layer was dried over MgSO₄, filtered, and concentrated *in vacuo*. The crude product was chromatographed on silica gel (20% EtOAc in hexane, packed with 1% TEA) to give 148 mg of **43a** and 2,6-lutidine mixture (2:1 NMR ratio) (28% product yield) and 28% RSM (NMR yield). ¹H NMR (500 MHz, Chloroform-d) δ 7.47 (t, J = 7.7 Hz, 1.79H), 7.41 – 7.03 (m, 6H), 6.97 (d, J = 7.6 Hz, 2.98H), 6.23 (d, J = 2.3 Hz, 1H), 4.49 (t, J = 1.8 Hz, 1H), 4.26 – 4.11 (m, 1H), 3.98 – 3.69 (m, 4H), 2.50 – 2.24 (m, 4H), 1.35 – 1.14 (m, 6H).

Note: This procedure was according to the development of project outlined in chapter 4.

Electrolysis of **43a**

A three-neck round bottom flask was charged with **43a** (0.14 mmol, 1 eq), LiClO₄ (200 mg), MeOH/THF (1:1, 3 mL), and 2,6-lutidine (0.1 mL, 5 eq). Into this solution was inserted a RVC anode and a carbon cathode. The reaction was electrolyzed at 8 mA until 3 F/mol current was passed through the solution at -78 °C. The reaction was then quenched with water. The layers were separated and the aqueous layer extracted two times with dichloromethane. The combined organic layers were then washed with brine, dried over MgSO₄, filtered, and concentrated *in vacuo*. This crude product gave rise to the proton NMR spectrum shown in Figure 3.3.

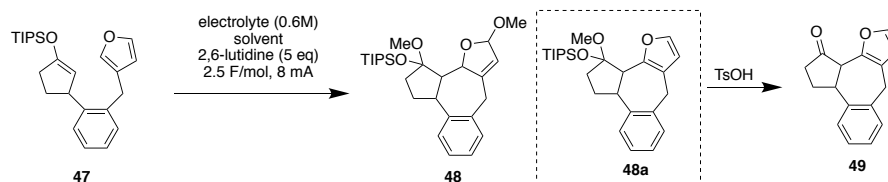
Synthesis of **47** ((3-(2-(furan-3-ylmethyl)phenyl)cyclopent-1-en-1-yl)oxy)triisopropylsilane



A Grignard solution of **58** (10 mL, 0.2 M) was freshly made using the procedure reported above. To this solution at 0 °C as added CuI (200 mg, 0.5 eq) and HMPA (0.68 mL, 2 eq). The mixture was then stirred at 0 °C for 10 min before the temperature was allowed to slowly climb to room temperature and the reaction stirred for an additional 30 min. The reaction was cooled to -78 °C, and then cyclopent-2-en-1-one (164 mg, 2 mmol) in 3 mL of THF was added to the mixture followed by the addition of TIPSOTf (1.62 mL, 3 eq). The reaction was stirred for 1 h before the addition of trimethylamine (1.6 mL, 3 eq). The resulting reaction mixture was allowed to warm to room temperature. 2,6-Lutidine (0.21 mL) was added to the reaction before work up. The reaction was then quenched with a saturated aqueous solution of NaHCO₃. The layers were separated and the organic layer then washed with an EDTA solution (0.1 M, pH=8) until no green/blue coloration remained. The aqueous layer was extracted two times with Et₂O. The

combined organic layers were dried over MgSO_4 , filtered, and concentrated *in vacuo*. A ^1H NMR of the crude reaction product was taken, using 2,6-lutidine as internal standard. Integration indicated a 60% NMR yield of the desired enol ether. The crude product was chromatographed on silica gel (using hexane as eluting solvent) to give 114 mg of product (30% yield). ^1H NMR (600 MHz, Chloroform- d) δ 7.35 (d, J = 1.8 Hz, 1H), 7.31 (d, J = 7.6 Hz, 1H), 7.24 – 7.20 (m, 1H), 7.13 (dd, J = 6.4, 1.6 Hz, 2H), 7.08 (s, 1H), 6.23 (d, J = 1.7 Hz, 1H), 4.65 (q, J = 1.8 Hz, 1H), 4.14 (dd, J = 8.5, 6.1, 2.4 Hz, 1H), 3.88 – 3.78 (m, 2H), 2.42 – 2.37 (m, 1H), 2.32 (ddd, J = 13.0, 8.6, 4.9 Hz, 1H), 1.74 (dq, J = 12.0, 6.8, 5.5 Hz, 2H), 1.23 (q, J = 7.4 Hz, 3H), 0.89 (q, J = 8.5, 7.6 Hz, 18H). ^{13}C NMR (151 MHz, CDCl_3) δ 153.87, 143.04, 140.16, 137.00, 134.43, 126.85, 124.25, 124.09, 123.20, 121.88, 108.52, 103.23, 40.50, 31.99, 30.85, 25.79, 19.99, 15.24. HRMS (ESI) for $\text{C}_{25}\text{H}_{36}\text{O}_2\text{Si}$ $[\text{M} + \text{Na}]^+$: Calcd. = 419.6282, Found 419.2369.

Electrolysis of 47



electrolyte influence					
entry	electrolyte	solvent	product	yield	acidified product yield
1	0.6M LiClO_4	DCM:MeOH (1:1)	48	80% ^a	59%
2	0.6M Bu_4NBF_4	MeOH	48	-	28%
3	0.6M Bu_4NBr	MeOH	48a	33% (31%RSM)	-

a) NMR yield

Scheme 3.21 Electrolysis of 47

Entry 1 as an example:

To a three-neck round bottom flask was charged with **47** (0.1mmol, 1eq), LiClO₄ (127 mg), MeOH/DCM (1:1, 2 mL), 2,6-lutidine (0.1 mL, 5 eq), the reaction was electrolyzed at 8 mA until 2.5 F/mol current passed. The reaction was then quenched with water. Aqueous layer was extracted with DCM twice. The combined organic layer was dried over MgSO₄, filtered, and concentrated in vacuo. 12.1 mg of 1,3,5-trimethoxybenzene was used as internal standard for crude NMR. By calculation, a crude cyclized product **48** yield was obtained of 80%. Figure 3.5 (Note: a) TsOH treatment following by NaHCO₃ work up did not lead to product, so repeating experiments were attempted; b) When using Bu₄NBr, **48a** was obtained in 33% isolated yield after electrolysis without acid treatment). In one of the repeating experiments, 14 mg starting material was used to conduct electrolysis under the condition described before. A quick chromatography was conducted following electrolysis. The material as shown in Figure 3.6 was then then dissolved in THF:Water (4:1). TsOH was added in. After stirring for 4 h, the reaction was then quenched with water. Aqueous layer was extracted with DCM twice. The combined organic layer was dried over MgSO₄, filtered, and concentrated *in vacuo*. The crude product was chromatographed on silica gel (using 20% EtOAc in hexane) to give product 5 mg **49** isolated yield 59%. In another repeating experiments (0.28 mmol scale reaction, 113.2 mg) using the same electrolysis as described before and no chromatography following electrolysis. After TsOH treatment (8 mL H₂O: THF = 1:4, 0.5 g TsOH), same aqueous work up as described before led to 18 mg, 26% isolated yield.

Compound **48**

(Note: The compound was purified through silica gel using 10% Ethyl Acetate in hexane directly after water wash, to remove huge 2,6-lutidine peak. A spectrum of after fast column can

be found in Appendix B). The spectra showed not very pure, but a clear view on the methoxylated furan peaks (5.5-5.6 ppm, 3 protons)

Compound **49**

^1H NMR (600 MHz, Chloroform- d) δ 7.37 – 7.19 (m, 5 H), 6.26 (s, 1 H), 4.13 (dd, J = 16.1, 3.1 Hz, 1 H), 3.66 (m, 1H), 3.52 (d, J = 16.2 Hz, 1H), 3.11 – 3.08 (d, J = 16.2 Hz, 1H), 2.78 – 2.69(m, 1H), 2.51 – 2.37(m, 3H). ^{13}C NMR (151 MHz, CDCl_3) δ 144.4, 141.5, 128.5, 127.2, 127.0, 124.2, 117.7, 111.9, 54.5, 42.9, 37.7, 31.2, 24.2. NMR was compared to **48a** for confirmation and 2D NMR for confirming structure was taken using similar logic as described for characterizing **48a** due to the same core ring structure. The green circle showed correlation between C9 and H8. A detailed discovery logic can be seen **48a**.

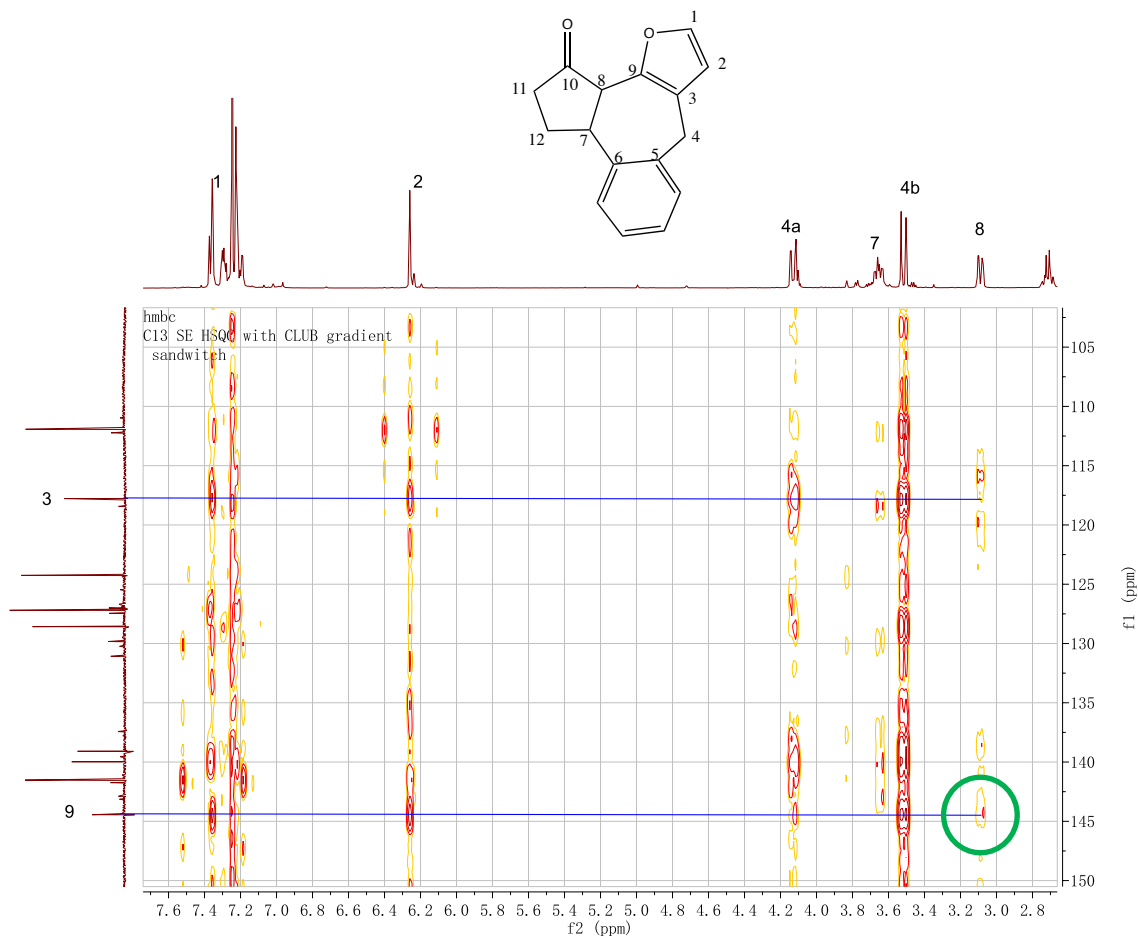


Figure 3.8 HMBC of 49

Compound **48a**

^1H NMR (600 MHz, Chloroform-*d*) δ 7.37 - 6.98 (m, 5H), 6.20 (s, 1H), 4.27 (d, $J = 10.5$ Hz, 1H), 4.02 (d, $J = 16.0$ Hz, 1H), 3.81 (m, 1H), 3.73 (d, $J = 16.4$ Hz, 1H), 3.39 (s, 3H), 2.36 – 2.18 (m, 1H), 2.00 (dd, $J = 13.3, 9.1$ Hz, 1H), 1.90 (dd, $J = 8.5, 3.9$ Hz, 1H), 1.70 (dd, $J = 13.1, 10.2$ Hz, 1H). ^{13}C NMR (151 MHz, Chloroform-*d*) δ 142.8, 141.0, 130.0, 127.1, 126.7, 125.8, 111.0, 104.8, 62.5, 48.1, 38.0, 30.6, 29.0, 18.2, 17.6, 13.2. HRMS (ESI) for $\text{C}_{26}\text{H}_{38}\text{O}_3\text{Si}$ $[\text{M} + \text{H}]^+$: Calcd 426.6645; Found 427.2664. 2D NMR was used for confirming structure.

In the 2D NMR analysis, initially, proton NMR, carbon NMR, and HSQC were used to assign the position of proton and carbon using the logic described below: Following an initial

estimation of proton assignment, HSQC was used to find the corresponding carbon. (Appendix B). Then TOCOSY was used to confirm the correlation between protons (see below).

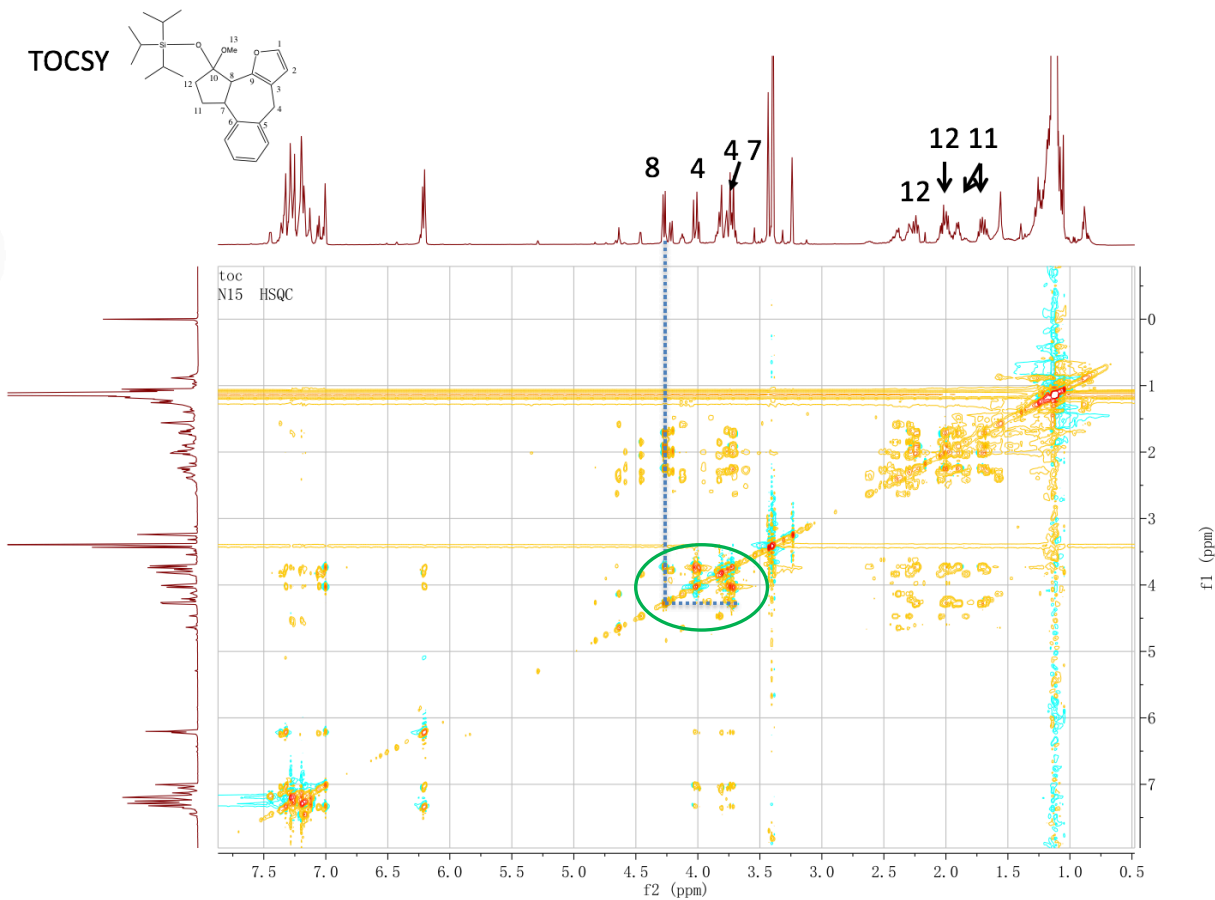


Figure 3.9 TOCSY of 48a

In green circle and linked by dashed line, the correlation shows coupling between proton 7 and proton 8. To further confirm the structure, HMBC was analyzed (see below). The green circle and arrow showed the multiband correlation between carbon 9 and proton 7, which proves the key evidence for the formation of C8-C9 bond.

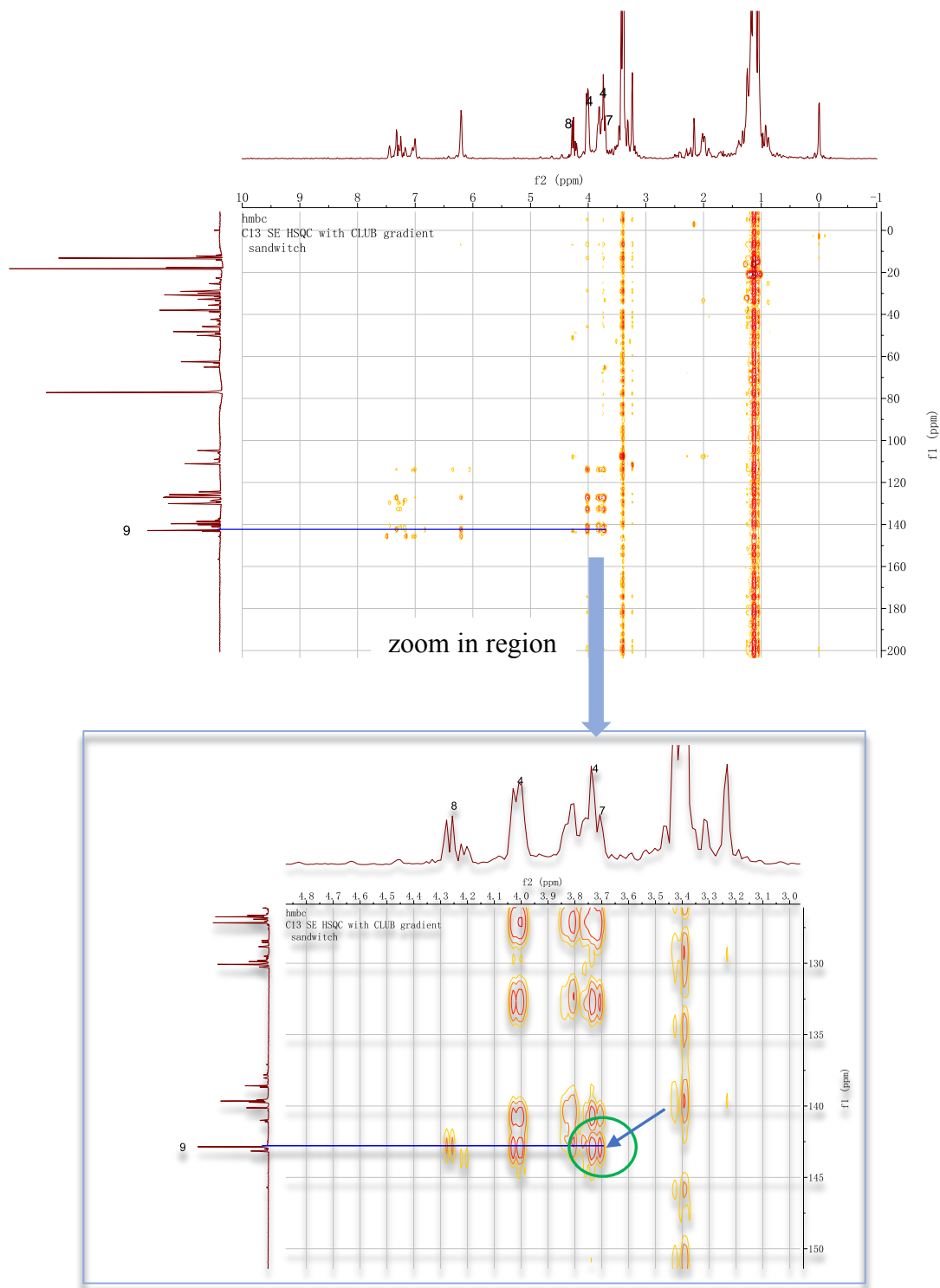
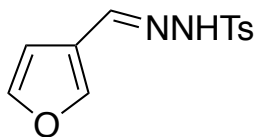


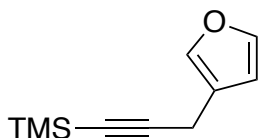
Figure 4.10 HMBC of 48a

Synthesis of **60a** (E)-N'-(furan-3-ylmethylene)-4-methylbenzenesulfonylhydrazide



A solution of TsNHNH₂ (0.93 g, 5 mmol, 1 eq) in 5 mL MeOH was stirred at 60 °C until all of the hydrazine dissolved. To this solution was added furan-3-carbaldehyde (0.43 mL, 5 mmol, 1 eq) in a dropwise fashion. After 15 min, the mixture was cooled to room temperature and the solvent removed *in vacuo*. The proton NMR of the crude product (DMSO-d₆ solvent) showed a product that was pure enough to carry on to the next step in the synthesis. The yield of the product obtained was 1.132 g (85% yield). The NMR data (Appendix B) matched the data previously reported for this compound.²⁴

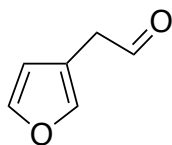
Synthesis of **60** (3-(furan-3-yl)prop-1-yn-1-yl)trimethylsilane²⁴



Compound **60a** (0.872 g, 3.3 mmol, 2.2 eq) and CuI (57 mg, 0.3 mmol, 20 mol%) were dissolved in 18 mL of dioxane. The reaction mixture was placed under argon, and then Li^tOBu (5.25 mL, 1M in THF) added. The mixture turned from a murky yellow to a dark red solution.

Ethynyltrimethylsilane (0.21 mL, 1.5 mmol, 1 eq) was added in. The mixture was stirred at 90 °C for 1 h, and then cooled to room temperature. Mixture was filtered through celite. The solvent was concentrated *in vacuo*. The crude product was chromatographed on silica gel (using 5% EtOAc in hexane as eluting solvent) to give 200 mg of product (73% yield). The NMR data (Appendix B) was corresponded to previously published data.²⁴

Synthesis of **61** 2-(furan-3-yl)acetaldehyde



A solution of (methoxymethyl)triphenylphosphonium chloride (4.64 g, 13.53 mmol, 2.9 eq) in 30 mL THF was stirred at 0°C. K^tOBu (13.5 mL, 1M in THF) was added in dropwise. The mixture was stirred at room temperature for 1 h, cooled to -78 °C, and then treated with furan-3-carbaldehyde (1.00 g, 10.4 mmol, 1 eq) in 10 mL of THF. The addition of the aldehyde was done in a dropwise fashion. The reaction was stirred at room temperature for 20 min. The reaction was monitored for the loss of the starting material using TLC. The reaction was then quenched with hexane and solvent was removed under pressure. The reaction mixture was chromatographed through silica gel eluting with hexane. This was done quickly in order to avoid decomposition of the enol ether. The collected compound (1.57 g) was dissolved in 40 mL THF and 20 mL of H₂SO₄ (1%). This mixture was refluxed overnight. The reaction was then quenched with a saturated aqueous NaHCO₃ solution. The layers were separated and the aqueous layer was extracted two times with Et₂O. The combined organic layers were dried over MgSO₄, filtered, and concentrated *in vacuo*. The product was then isolated by Kugelrohr distillation (100 °C, 0.4 mmHg) to afford a 25% yield of product the targeted aldehyde. The NMR data (Appendix B) matched that of the previously published data.²⁵

3.6 Spectra Data

See Appendix B

Reference

- (1) Kim, J. H.; Kim, H.-K.; Jeon, S. B.; Son, K.-H.; Kim, E. H.; Kang, S. K.; Sung, N.-D.; Kwon, B.-M. New sesquiterpene–monoterpene lactone, artemisolide, isolated from *Artemisia argyi*. *Tetrahedron Letters* **2002**, *43* (35), 6205.
- (2) Sohn, J.-H. [5+ 2] Oxidopyrylium Ion Cycloaddition Reaction with Vinylsilane: Construction of Core Structure of Biogenic Intermediates of Arteminolides. *Bulletin of the Korean Chemical Society* **2009**, *30* (11), 2517.
- (3) Sohn, J.-H. Studies toward Synthesis of Arteminolides: Intramolecular [5+ 2] Oxidopyrylium Ion Cycloaddition Reactions with Silicon Tether. *Bulletin of the Korean Chemical Society* **2010**, *31* (7), 1841.
- (4) Wong, H.-F.; Brown, G. D. Dimeric Guaianolides and a Fulvenoguaianolide from *Artemisia myriantha*. *Journal of Natural Products* **2002**, *65* (4), 481.
- (5) Zhang, W.; Luo, S.; Fang, Chen, Q.; Hu, H.; Jia, X.; Zhai, H. Total Synthesis of Absinthin. *Journal of the American Chemical Society* **2005**, *127* (1), 18.
- (6) Redden, A.; Moeller, K. D. Anodic Coupling Reactions: Exploring the Generality of Curtin–Hammett Controlled Reactions. *Organic Letters* **2011**, *13* (7), 1678.
- (7) New, D. G.; Tesfai, Z.; Moeller, K. D. Intramolecular Anodic Olefin Coupling Reactions and the Use of Electron-Rich Aryl Rings¹. *The Journal of Organic Chemistry* **1996**, *61* (5), 1578.
- (8) Sperry, J. B.; Wright, D. L. The gem-Dialkyl Effect in Electron Transfer Reactions: Rapid Synthesis of Seven-Membered Rings through an Electrochemical Annulation. *Journal of the American Chemical Society* **2005**, *127* (22), 8034.
- (9) Lightstone, F. C.; Bruice, T. C. Geminal dialkyl substitution, intramolecular reactions, and enzyme efficiency. *Journal of the American Chemical Society* **1994**, *116* (23), 10789.
- (10) Parrill, A. L.; Dolata, D. P. The “Facilitated Transition” hypothesis as an explanation for the gemdialkyl effect. *Journal of Molecular Structure: THEOCHEM* **1996**, *370* (2-3), 187.
- (11) Perkins, R. J. Anodic Electrochemistry: Controlling the Reactivity of Radical Cation Intermediates. **2016**.
- (12) Miller, A. K.; Hughes, C. C.; Kennedy-Smith, J. J.; Gradl, S. N.; Trauner, D. Total Synthesis of (–)-Heptemerone B and (–)-Guanacastepene E. *Journal of the American Chemical Society* **2006**, *128* (51), 17057.
- (13) Redden, A.; Perkins, R. J.; Moeller, K. D. Oxidative Cyclization Reactions: Controlling the Course of a Radical Cation-Derived Reaction with the Use of a Second Nucleophile. *Angewandte Chemie International Edition* **2013**, *52* (49), 12865.
- (14) Hudson, C. M.; Moeller, K. D. Intramolecular Anodic Olefin Coupling Reactions and the Use of Vinylsilanes. *Journal of the American Chemical Society* **1994**, *116* (8), 3347.
- (15) Moeller, K. D.; Tino, L. V. Intramolecular anodic olefin coupling reactions: the use of bis enol ether substrates. *Journal of the American Chemical Society* **1992**, *114* (3), 1033.
- (16) Campbell, J. M.; Xu, H.-C.; Moeller, K. D. Investigating the Reactivity of Radical Cations: Experimental and Computational Insights into the Reactions of Radical Cations with Alcohol and p-Toluene Sulfonamide Nucleophiles. *Journal of the American Chemical Society* **2012**, *134* (44), 18338.

- (17) Sperry, J. B.; Whitehead, C. R.; Ghiviriga, I.; Walczak, R. M.; Wright, D. L. Electrooxidative Coupling of Furans and Silyl Enol Ethers: Application to the Synthesis of Annulated Furans. *The Journal of Organic Chemistry* **2004**, *69* (11), 3726.
- (18) Mioskowski, C.; Manna, S.; Falck, J. Reactivity of α , β -unsaturated acetals and ketals toward organolithium reagents in pentane. *Tetrahedron letters* **1984**, *25* (5), 519.
- (19) Kato, K.; Suemune, H.; Sakai, K. New type of asymmetric double Michael reaction induced by chiral acetal. *Tetrahedron letters* **1993**, *34* (31), 4979.
- (20) Verkruijsse, H. D.; Keegstra, M. A.; Brandsma, L. A High-Yield Preparative-Scale Method for 2-Bromofuran. *Synthetic Communications* **1989**, *19* (5-6), 1047.
- (21) Jiang, Y.; Xu, K.; Zeng, C. Use of Electrochemistry in the Synthesis of Heterocyclic Structures. *Chemical Reviews* **2017**, DOI:10.1021/acs.chemrev.7b00271
10.1021/acs.chemrev.7b00271.
- (22) Li, C.-C.; Liang, S.; Zhang, X.-H.; Xie, Z.-X.; Chen, J.-H.; Wu, Y.-D.; Yang, Z. Exploring an Expedient IMDA Reaction Approach to Construct the Guanacastepene Core. *Organic Letters* **2005**, *7* (17), 3709.
- (23) Zweifel, G.; Steele, R. B. Novel method for the synthesis of cis- α , β -unsaturated derivatives trans-hydroalumination of disubstituted alkynes with lithium diisobutylmethylaluminum hydride. *Journal of the American Chemical Society* **1967**, *89* (19), 5085.
- (24) Ye, F.; Ma, X.; Xiao, Q.; Li, H.; Zhang, Y.; Wang, J. C (sp)–C (sp³) bond formation through Cu-catalyzed cross-coupling of n-tosylhydrazones and trialkylsilylalkynes. *Journal of the American Chemical Society* **2012**, *134* (13), 5742.
- (25) Uenishi, J. i.; Kawahama, R.; Tanio, A.; Wakabayashi, S.; Yonemitsu, O. Stereocontrolled synthesis of dehydrodendrolasin: unstable polyene furanosesquiterpenoids. *Tetrahedron* **1997**, *53* (7), 2439.

Chapter 4: Tandem Cyclization using

Radical Pathway

Having shown that the nature of the reactive intermediate in an oxidative cyclization is important for the reactions, we turned our attention toward another previously problematic transformation. Namely, the oxidative initiation of tandem cyclization reactions that generate more than one bond at a time. With the findings made in Chapter 3 the question immediately became, did the previous efforts utilize the correct reactive intermediate? In this chapter, we will outline the history of our efforts to conduct a tandem anodic cyclization and then our initial efforts to determine the nature of the reactive intermediate needed for these intriguing, potentially powerful synthetic reactions.

4.1 Tandem Cyclization Reactions in the Literature

Tandem cyclization reactions have long proven to be an effective strategy for the synthesis of complex ring skeletons.¹ It is intriguing to think about the role an oxidative cyclization reaction might play in this approach because the reactions raise the overall functionality of a molecule while making new bonds. With this in mind, the molecules paniculatine and dankasterone were selected as targets for studying the synthetic potential of oxidative tandem cyclization reactions. Both are structurally interesting natural products with significant biological activity^{1,2} as mentioned in the previous chapter (Chapter 2).

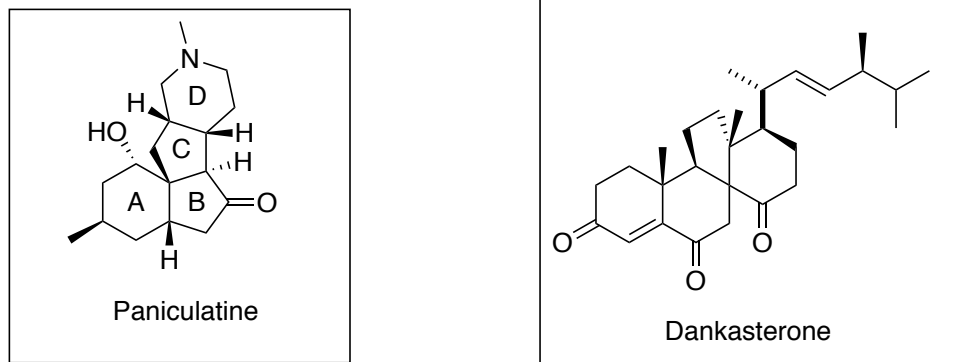


Figure 4.1 Paniculatine and Dankasterone

4.1.1 Paniculatine

Paniculatine was selected as a target because of a previous synthesis that would allow us to highlight the importance of an oxidative approach to tandem cyclization reactions. Paniculatine, along with magellanine and magellaninone, belongs to a class of *Lycopodium* alkaloids that are comprised of a tetracyclic framework. This ring skeleton has always been a challenging and appealing task for researchers. Accordingly, the family of molecules has been the subject of a number of synthetic efforts.^{1,3}

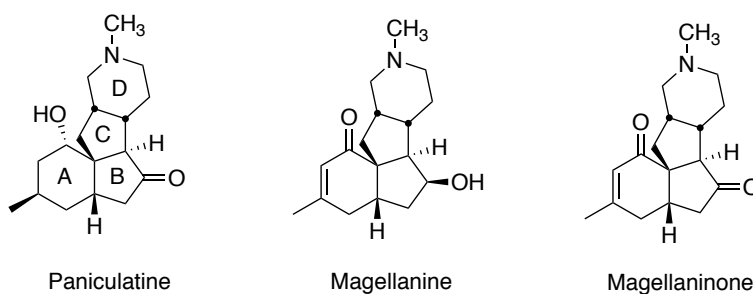
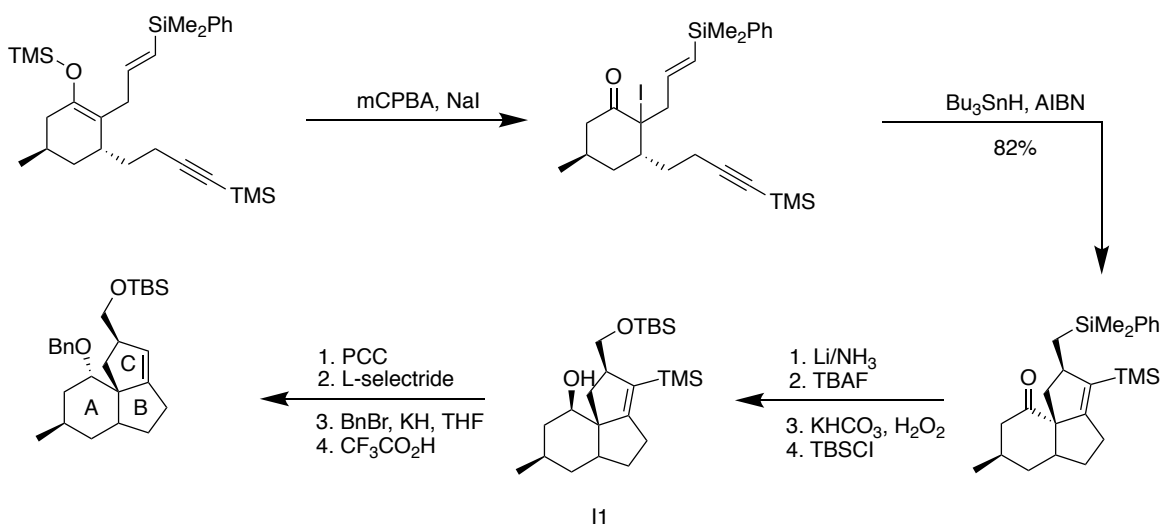


Figure 4.2 *Lycopodium* Alkaloids

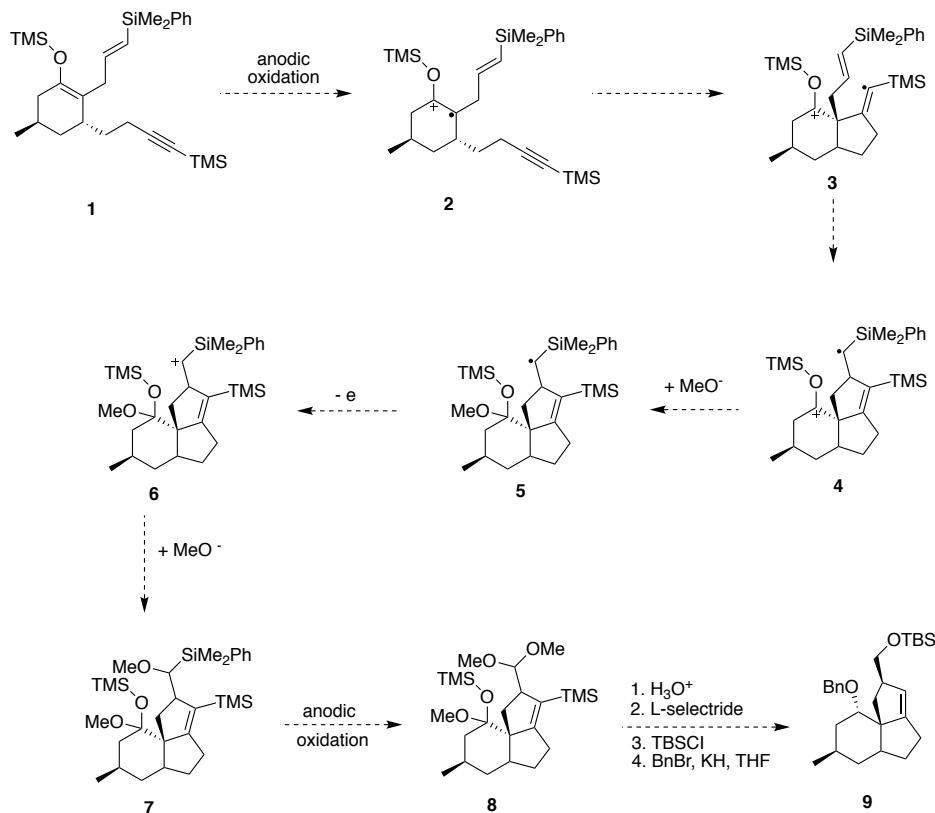
One of those synthetic efforts was very attractive for our purposes. In that regard, the paniculatine structure was achieved by the Sha group with the use of a tandem radical cyclization reaction (Scheme 4.1).¹ In this approach, a site for the initiation of the radical reaction was generated by the introduction of an iodide.



Scheme 4.1 Paniculatine Synthesis

This was accomplished by treating a Michael reaction derived silyl enol ether with mCPBA and NaI. A tandem cyclization was then triggered with the use of tributyltin hydride, and the product of the tandem cyclization eventually converted to intermediate **II**. Since the tandem radical cyclization at the heart of this scheme is a reductive process, the overall plan required an oxidation, reduction, oxidation strategy that consumed stoichiometric MCPBA, NaI, Bu₃SnH, TBAF, Li/NH₃, H₂O₂, and PCC. *In principle, all of these reagents can be avoided and the synthetic sequence dramatically shortened with the use of an oxidative radical cyclization like the one illustrated in Scheme 4.2.* The point is that the net transformation required is an oxidative

one. So, why not use an oxidation based tandem cyclization in place of a reduction-based approach?



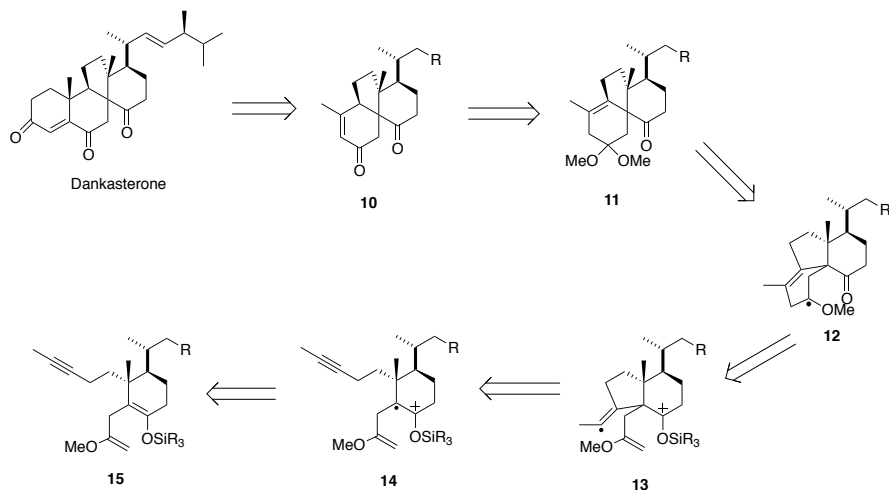
Scheme 4.2 Paniculatine Synthesis via Anodic Cyclization

Of course, the route shown would utilize a radical cation intermediate to trigger the tandem cyclization. Is this the best intermediate or would this particular reaction be best pursued using an oxidative radical approach? Since the starting substrate is made by a Michael reaction, either route could be readily implemented using the strategy highlighted in Chapter 3.

4.1.2 Dankasterone

Dankasterone also contains multi-cyclic framework which can potentially be made use the use of an oxidative tandem cyclization strategy. For that reason, the retrosynthetic analysis highlighted

in Scheme 4.3 was designed. (Reference from Scates, B.A., Ph.D. Dissertation, Washington University in St. Louis, 2006)



Scheme 4.3 Retro-Analysis of Dankasterone via Anodic Cyclization

In this case, silyl enol ether **15** would be oxidized to generate a radical cation (**14**) that would in turn trigger the tandem cyclization. As in the earlier reaction an acetylene would serve as the relay pi-system in the tandem reaction. A methoxy vinyl ether would then serve as the terminating group leading eventually to intermediate **11**.

The similarity of the routes proposed for the two natural products suggested that the development of such an oxidative approach might prove generally useful.

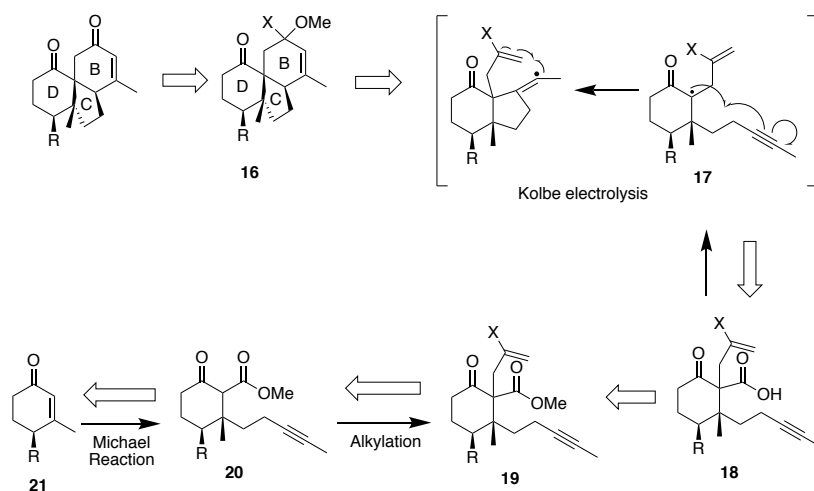
4.2 Initial Tests on Anodic Tandem Cyclization

Because of the synthetic potential of the approach, Bradley Scates and Laura Anderson both spent time during their Ph.D. thesis studies looking at this possibility. However, they did not know about the mechanistic considerations highlighted in Chapters 2 and 3. So, we decided to

take another, hopefully more informed look. Before getting to that effort, it is instructive to briefly look at Bradley and Laura's efforts.

4.2.1 Kolbe Approach

The first attempt was conducted in the context of a route to Dankesterone. It involved a Kolbe electrolysis to generate the radical needed because the acid needed for the Kolbe was already present as a result of the substrate synthesis (Scheme 4.4). (Reference from Scates, B.A., Ph.D. Dissertation, Washington University in St. Louis, **2006**.)

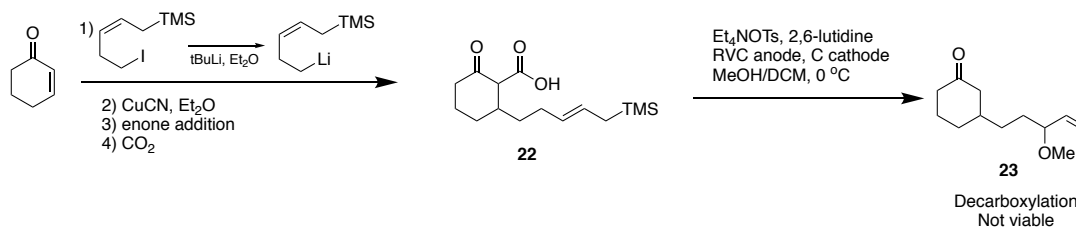


Scheme 4.4 Tandem Cyclization via Anodic Condition

The plan was to install a carboxyl group at α -position of ketone like **21** following a Michael reaction and then use the resulting 1,3-dicarbonyl to introduce the sidechain needed for terminating the tandem cyclization. This avoided problems with the alkylation and any loss of regioselectivity derived from the Michael reaction. Note how a Michael, alkylation sequence starting from **21** would require regeneration of an enolate, etc. The use of the Kolbe to generate

the radical avoided this complication. The result would still be a two-electron oxidative process that avoided a reduction based cyclization.

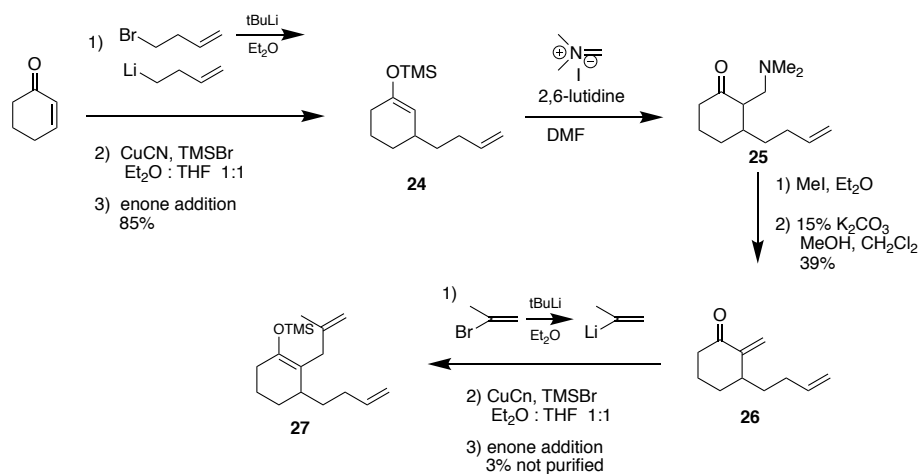
Unfortunately, in practice a non-oxidative decarboxylation could never be avoided. As soon as, the ester was saponified an immediate decarboxylation occurred after the alkylation. The quaternary carbon was simply not stable. Even when the alkylation was avoided and a simple model study without the substituent alpha to the carbonyl present subjected to the electrolysis, the molecule underwent decarboxylation prior to the oxidation (Scheme 4.5). The result was a product that resulted from oxidation of the allylsilane.



Scheme 4.5 Decarboxylation during Anodic Condition Tandem Cyclization

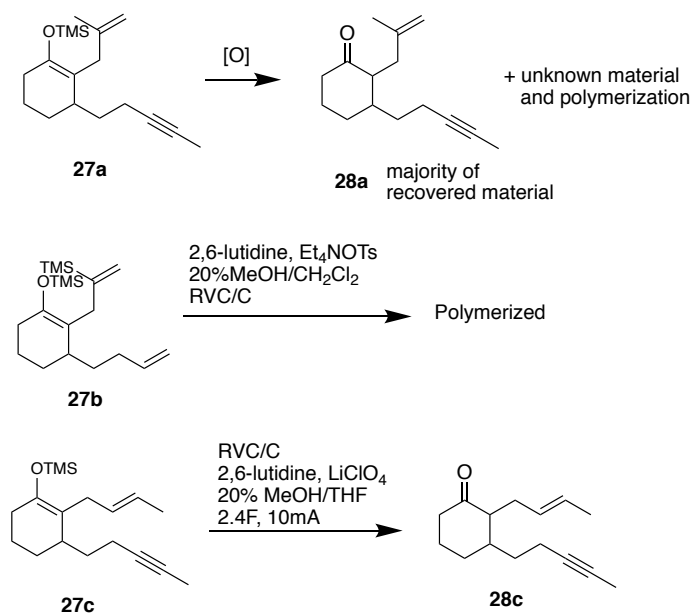
4.2.2 Double Michael Sequence

The failure of this simple approach led to an effort to make the substrate through a double Michael reaction sequence as highlighted in Scheme 4.6. (Reference from Anderson, L.A., Ph.D. Dissertation, Washington University in St. Louis, **2010**.)



Scheme 4.6 Double Michael Sequence to Enol Ether Substrate

In this trial, a monosubstituted olefin was used as the relay in order to simplify the Mannich reaction used to install the second Michael acceptor in the sequence. The terminal double bond was chosen to be a simpler disubstituted olefin in order to further simplify the substrate synthesis. However, neither change was all that effective. The yield of the electrolysis substrate **27** was never obtained in over 5% and even that amount could not be purified. Attempts were made at the cyclization, but with the lack of clean starting material little was learned. The electrolysis either afforded product from a straight hydrolysis or polymerized material that may or may not have come from the actual substrate. The route was abandoned.

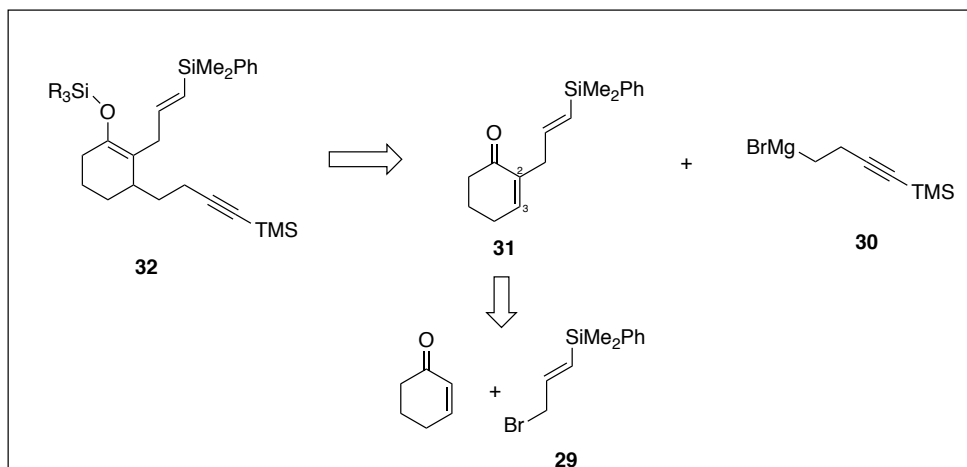


Scheme 4.7 Initial Test on Enol Ether Substrate

4.3 Enol Ether Substrate via Thiophene Route leading to Radical Cation Pathway

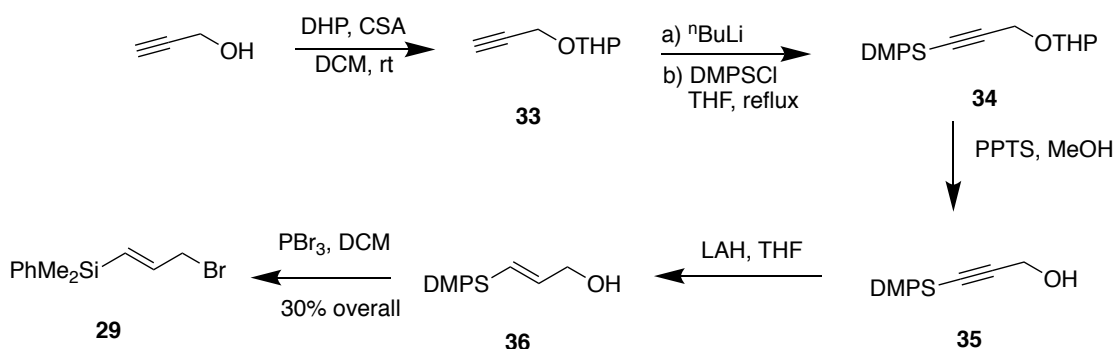
4.3.1 Enol Ether Substrate via Thiophene Route

These results led to another change in the substrate synthesis (Scheme 4.8).



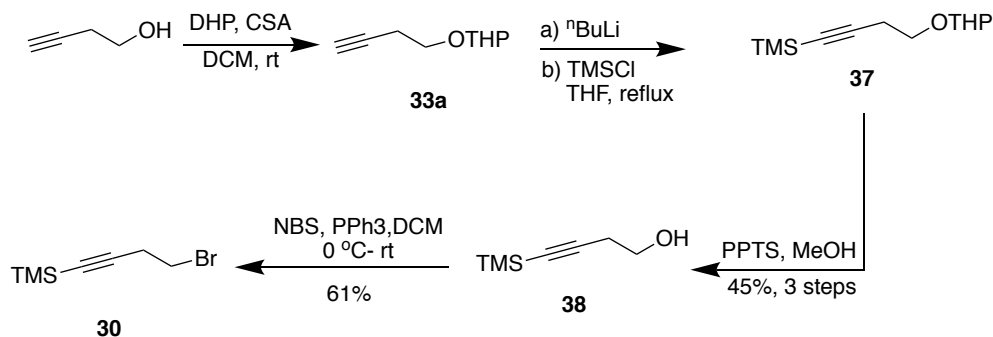
Scheme 4.8 Enol Ether 32 Synthesis via Thiophene Route

In this route, the two side chains were made separately, and then the α -position alkyl side chain **29** installed first with a net retention of double between C2-C3 via the use of the known thiol based strategy developed by Baraldi and coworkers (Scheme 4.12).⁴ The sidechains were selected to be consistent with the previous panculatine synthesis since it was known that the radical based reaction worked with those groups. Once intermediate **31** was in hand, the β alkyl chain **30** was installed via Michael addition.



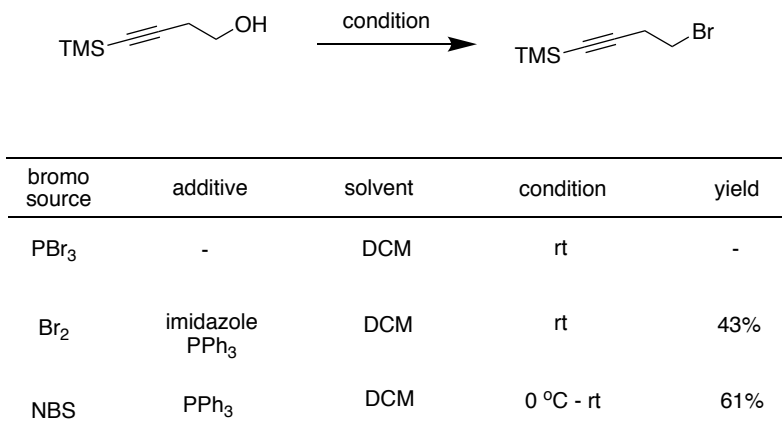
Scheme 4.9 Synthesis of 29

The synthesis of **29** was straight-forward. Using the route shown in Scheme 4.9, compound **29** was obtained in 30% yield from the starting material. No purification of the intermediates before the final bromide **29** was necessary.



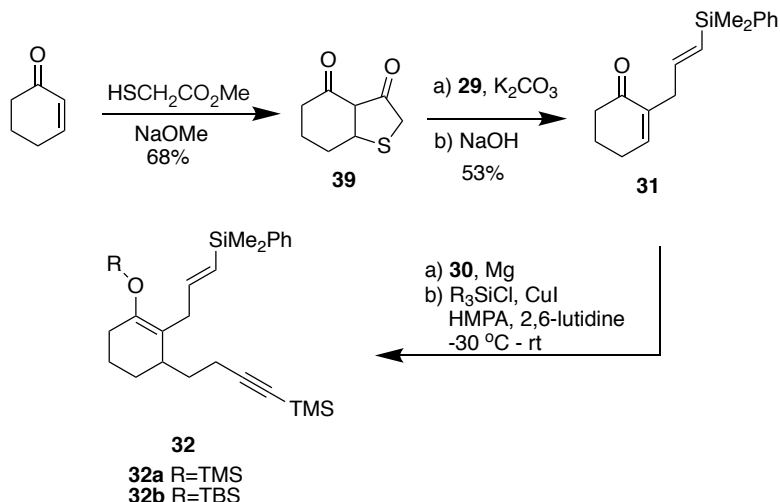
Scheme 4.10 Synthesis of **30**

The synthesis of compound **30** proved to be a bit more problematic. While the chemistry prior to the final bromination worked well, the bromination itself proved difficult even though the related bromination reaction had worked well for the synthesis of compound **29**. To solve this problem, several different reaction conditions were attempted.



Scheme 4.11 Synthesis of **30**- bromination step

The best of these conditions involved the use of NBS as the source of bromine. Because of its convenience, these conditions were used throughout the rest of the project.



Scheme 4.12 Synthesis of 32a/b

With the sidechains in place, intermediate **31** was synthesized via intermediate **39** starting from the enone and a thiolated methylacetate as shown⁴. A series of Michael reaction conditions were then explored to make the electrolysis substrate. The development of these conditions was described in Chapter 3. For this reaction, the Michael product **32a** obtained when the silyl trapping group was a TMS could only be obtained without purification as a clean mixture of the enol ether electrolysis substrate and the ketone derived from hydrolysis of the enol ether. Using a TBS based trapping group allowed for isolation of the pure silyl enol ether **32b** but only in a yield of 17% due to decomposition of the enol ether during the chromatography.

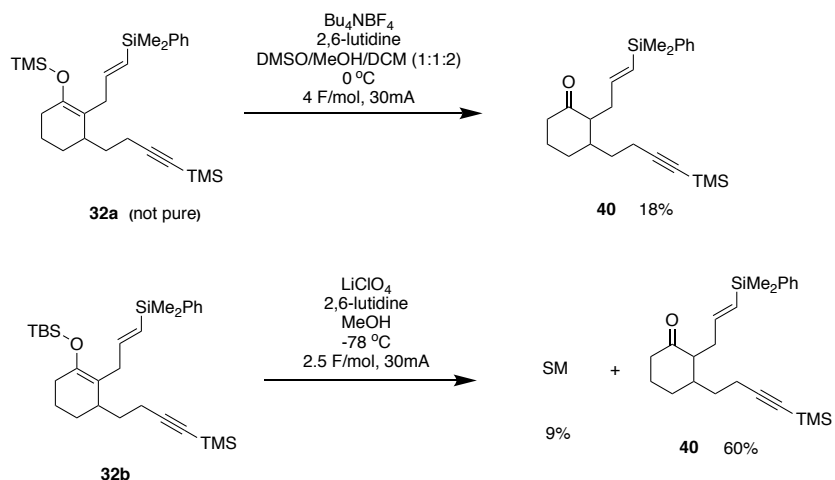
4.3.2 Enol Ether Substrate Electrolysis

The two types of silyl enol ether substrate were oxidized even though the TMS substrate was never pure and mixed with its hydrolysis product. In this work, it appeared that Dr. Bradley

Scates was able to obtain an approximately 10% yield of the desired product by NMR analysis of the crude reaction mixture. However, the product mixture was very complex and the product was never fully characterized. Hence, this assignment remains tentative.

I worked to repeat this work. However, during my efforts at the electrolysis of **32a** I was only able to obtain about an 18% yield of a ketone **40** derived from hydrolysis of the substrate (Scheme 4.13). The rest of the reaction mixture was messy, and it was impossible to tell if this was the result of an unsuccessful oxidation or our inability to generate enough of a good quality substrate for the electrolysis. Different conditions deviated from Dr. Bradley Scates's thesis were put under test in order to exclude the influence from electrolyte (Bu₄NBF₄) and temperature (0°C), still no product.

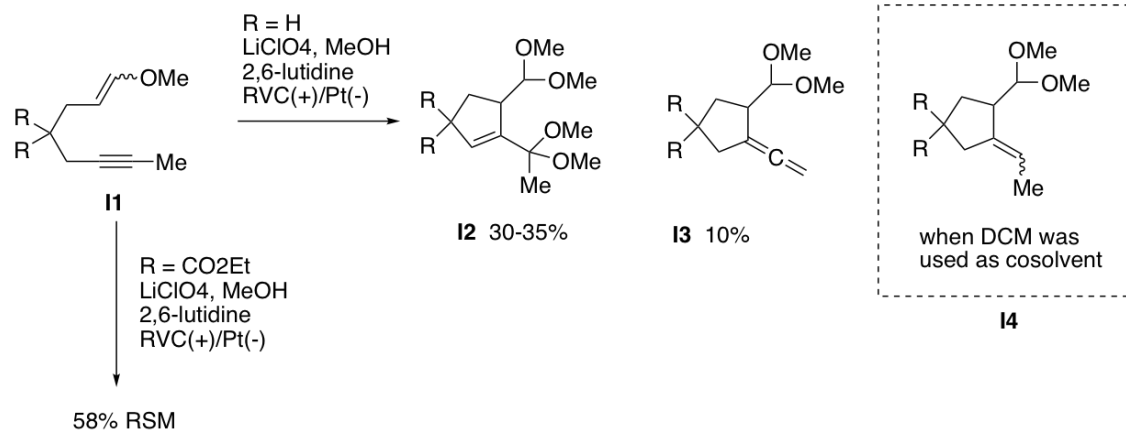
As for the TBS substrate **32b** (stable than **32a**), the conclusions reached were more trustworthy since a good quality substrate could be obtained. However, the cyclization was not successful. In the best case, the reaction led to the ketone from cleavage of the silyl enol ether in a 60% yield along with 9% of the recovered starting material. The recovery of some starting material from the reaction did hint that TBS substrate was more stable to the electrolysis conditions than the TMS substrate.



Scheme 4.13 Enol Ether Substrate 32a-b Electrolysis

In many ways, the generation of the ketone product from the reaction was a surprise since TBS enol ethers are typically stable to the electrolysis. However, it should be noted that the hydrolysis product might arise from recovered starting material, and recovered starting material does not always mean the oxidation did not occur. A reversible cyclization that leads to a stable radical cation can lead to reduction of the radical cation at the cathode⁵. This often means driving the cyclization to completion by increasing the rate of the second oxidation reaction.

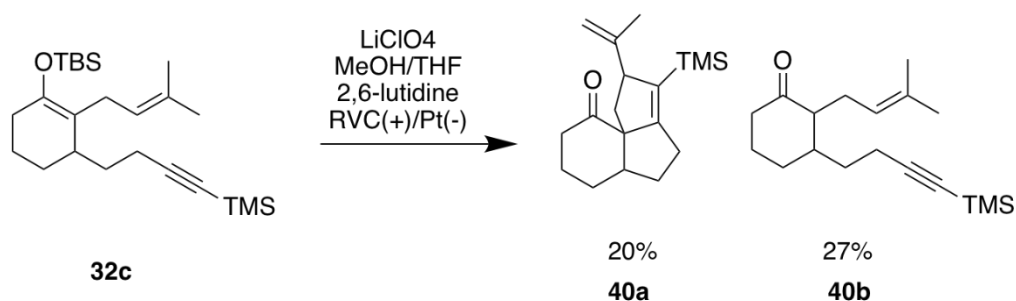
Such a conclusion would be consistent with the simple coupling of an enol ether derived radical cation and an acetylene that showed similar behavior (Scheme 4.14). (Reference from Scates, B.A., Ph.D. Dissertation, Washington University in St. Louis, **2006**.)



Scheme 4.14 Acetylene as trapping group behavior

In the first case studied ($\text{R} = \text{H}$), the reactions led to a low mass balance but did provide cyclized products. One was obtained by formation of a vinyl cation that was then trapped by methanol and oxidized to form an unsaturated acetal **I2**, and a second was formed by the elimination of a proton from the vinyl cation to make an allene **I3**. In a mechanistic study, the addition of dichloromethane to the reaction led to the formation of a hydrogen abstraction product **I3** suggesting that the reaction did lead to the formation of a vinyl radical intermediate. *Attempts to accelerate the cyclization with geminal substituents*⁶ led to recovery of the starting material. *In no case, did the reaction lead to a product showing decomposition of the enol ether radical cation even though a stoichiometric amount of current was passed through the reaction and the enol ether was clearly the group with the lowest oxidation potential functional moiety in solution.* This is important since we know oxidation of an enol ether followed by a slow cyclization leads to elimination reactions from the radical cation along with solvent trapping of the enol ether radical cation⁷. The appearance of none of these products is more consistent with oxidation of the enol ether, stabilization of the radical cation through an intramolecular trapping reaction, and then a reversible cyclization leading to reduction of the radical cation at the

cathode. This stabilization is necessary since the enol ether radical cation will not survive in methanol solvent long enough to reach the cathode. At the time of this chemistry, we did not know how to solve this problem (higher electrolyte concentrations, acceleration of the second oxidation step, etc.). However, the clear indication that the reaction did lead to a vinyl radical suggested that one way to drive the reaction to completion might be to accelerate trapping of the vinyl radical. It was concluded that the vinyl silane trapping group in substrate **32b** might not be sufficient to accomplish this task. So, a more effective trisubstituted olefin **32c** was used as the final radical trapping group. (Reference from Scates, B.A., Ph.D. Dissertation, Washington University in St. Louis, **2006**) (Scheme 4.15) This reaction was partially successful. The tandem cyclization led to a 20% yield of the desired product **40a** along with a 27% yield of a ketone derived from methanolysis or hydrolysis of the starting enol ether **40b**. As discussed above, the TBS enol ether has been shown to be stable to the electrolysis conditions so it was thought that once again the presence of this second product might be consistent with the hydrolysis of recovered starting material – a result that again might be consistent with a reversible cyclization followed by radical cation reduction to starting material. The result did suggest the possibility that the reaction could be made to work.



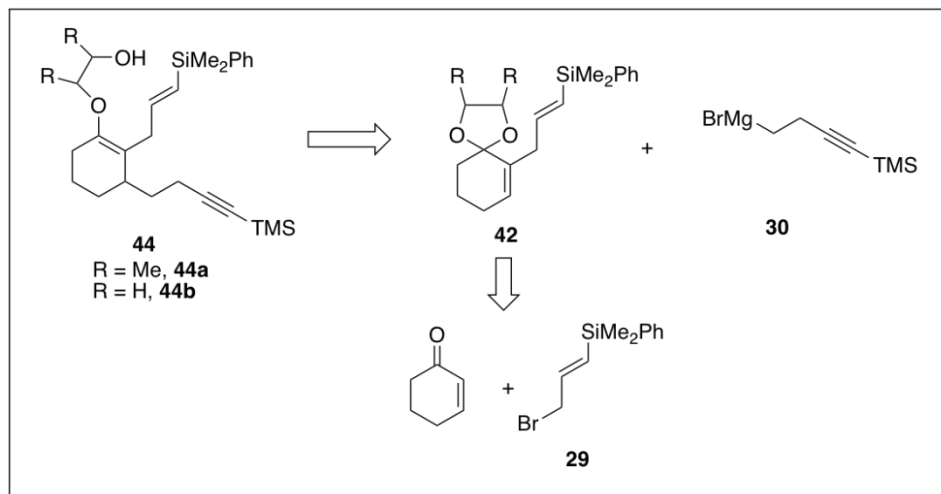
Scheme 4.15 Trisubstituted alkene as terminating group

4.4 Alcohol Substrate leading to Radical Pathway

While the chemistry did appear workable, the route to the substrates and the lack of success led to other projects in the group being pursued. The project lay dormant for several years. However, it was bothersome that the Sha chemistry had so nicely led to a tandem cyclization reaction from similar substrates using the reductive radical approach. Based the results we described in Chapter 3, we began to wonder if the problem with the previous efforts was the nature of the reactive intermediate involved. Maybe the radical cation and its propensity toward reversible reactions was not the ideal intermediate to use, and the reactions would benefit from an oxidative radical type approach where the key intermediate doing the tandem cyclization would be the same as in the Sha chemistry (Section 4.1.1). Fortunately, the chemistry discussed in Chapter 3 also meant that the oxidative radical method could be attempted.

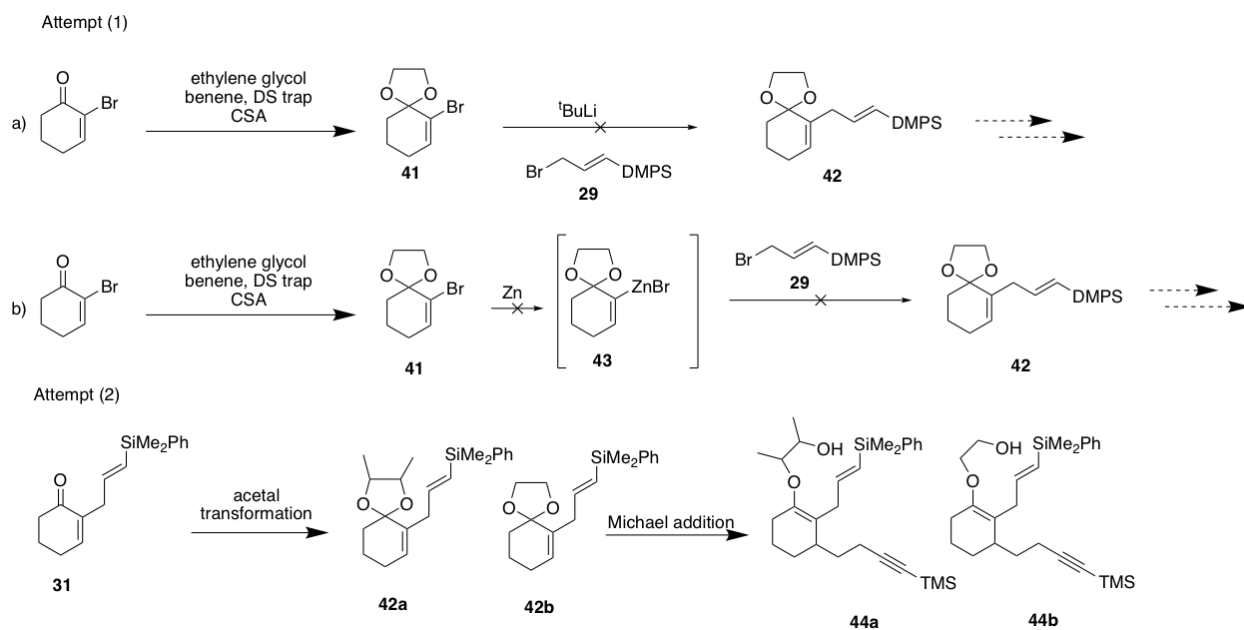
4.4.1 Synthesis of an enediol based tandem cyclization substrate:

The synthetic route to a substrate compatible with an oxidative radical cyclization was developed by modifying the route used to generate the silyl enol ether substrate **32**. The retrosynthetic analysis is shown below.



Scheme 4.16 Retro analysis of ene diol **44**

The main change was the need to introduce a cyclic ketal **42** into the substrate for the Michael reaction. Two approaches to this task were attempted. First, the ketal was installed in a 2-bromocyclohexene substrate **41** that was then used to add the sidechain **29** needed at the α -position of the electrolysis substrate. Second, the order of these steps was reversed with the α -side chain **29** being introduced first to generate **31** (Scheme 4.12). The cyclic acetal was then introduced to form intermediate **42** (Scheme 4.17).

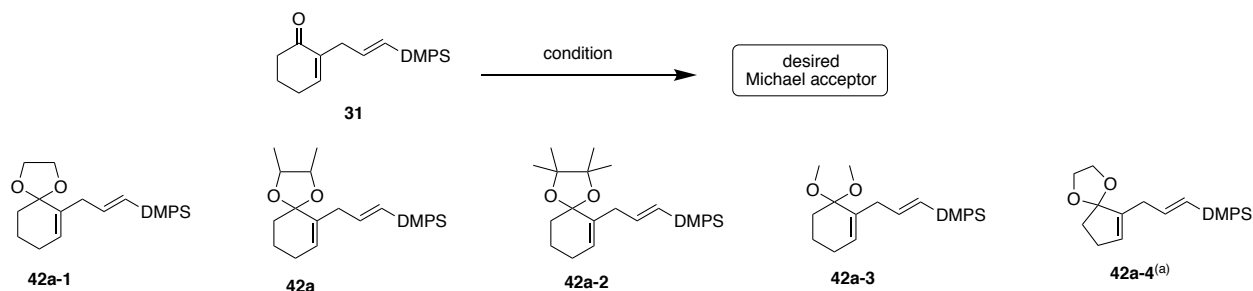


Scheme 4.17 Two Attempts to Alcohol Substrate

In the first strategy, the bromo ketal **41** could be achieved with 52 % yield. However, the installation of sidechain **29** was never successful. Initially, *t*-butyl lithium was used to generate an anion from **41** before the addition of sidechain **29**. The route failed. Starting material **41** was recovered indicating that vinyl anion was never achieved. Following this attempt, an organozinc based approach was attempted.^{8,9} The result was the same. The initial attempt to form the zinc-reagent **43** led once again to recovered starting material **41** along with some of the ketone derived from hydrolysis of **41**. With the difficulties encountered with the vinyl anion synthesis, the effort was changed to the second approach that would form the ketal from substrate **31** (Scheme 4.12).

The ketalization of compound **31** proved to be more problematic than the previous ketalization to form intermediate **41**. Compound **41** contained an inductive electron-withdrawing group at the

alpha carbon that might have made that reaction proceed more easily. With respect to the ketalization of **31**, a variety of conditions were tested.



top bridge source	additive	product	yield
ethylene glycol	TsOH, D.S. trap	42a-1	-
ethylene glycol ^a	PPTS, D.S. trap	42a-4	-
ethylene glycol	Aniline-Aldehyde Resin Salts	42a-1	-
	TMSOTf	42a-1	-
	Sc(OTf) ₃ , DCM	42a	62%
	Sc(OTf) ₃ , DCM	42a-2	52%
HC(OMe) ₃	Aniline-Aldehyde Resin Salts	42a-3	-

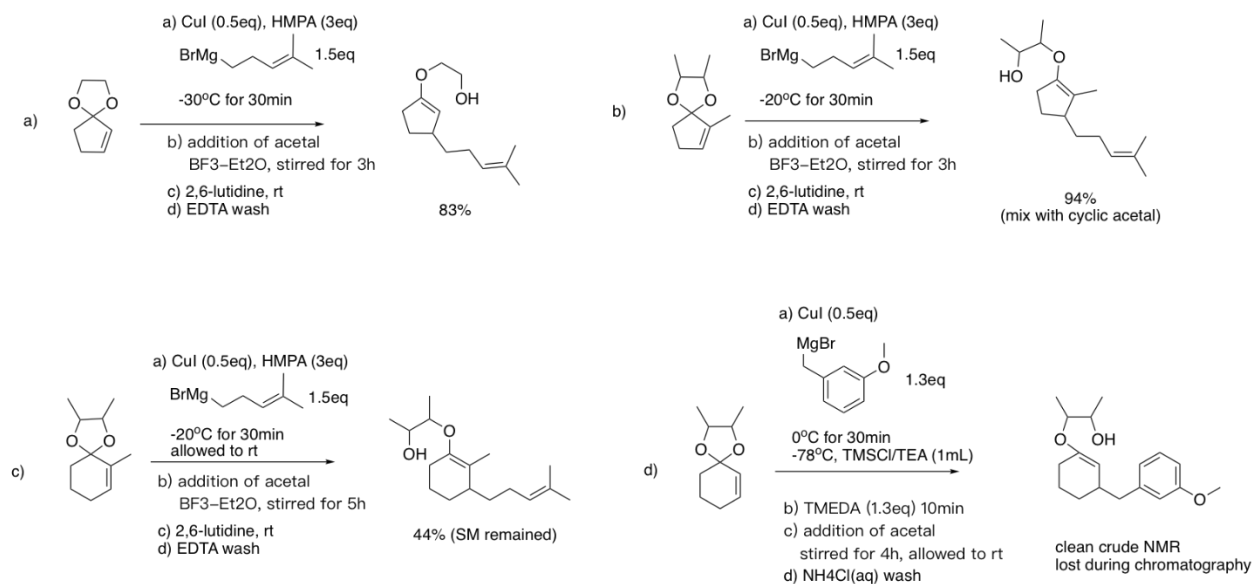
(a) five member ring ketone was used as starting material

Scheme 4.18 Acetalization condition

In entry 1-3, different Lewis acids were screened for effecting a condensation reaction between the ketone and ethylene glycol. None of the reactions led to the product. For the reaction in Entry 4, a TMS protected glycol was used in combination of a TMSOTf as Lewis acid following the procedure from R. Noyori¹⁰. It was hoped that the TMS protected glycol and TMSOTf combination would lead to increased reactivity, but the change did not improve the reaction. With the failure of the condensation type approaches, a change of mechanism was attempted. In this case, the carbonyl was used as a nucleophile to open an epoxide following the work of William J. Scott.¹¹ This was the procedure that Robert Perkins found to be effective for the

chemistry outlined in Chapter 3 and condition optimized myself. In this mechanism, the epoxide opening leads to an alkoxide and an oxonium ion that then undergo an intramolecular cyclization reaction to form the desired ketal. The initial attempts along these lines did show promise. The yield of the reaction was then optimized by examining the stoichiometry of the reaction and the relative concentration of the epoxide. It was observed that the reaction worked best when the epoxide was dissolved in the solvent to lower its overall concentration and then that solution added very slowly to the ketone and Lewis acid. This reduced the amount of epoxide polymerization that occurred. The use of the dimethyl epoxide proved superior to the tetramethyl epoxide, presumably due to the slower polymerization of the dimethyl epoxide. The mechanism is thought to have significant S_{N1} -character where the epoxide initially complexes the Lewis acid leading to a cationic intermediate. In the case of the more substituted epoxide, ring opening to a carbon cation and subsequent reaction with a second epoxide is more likely because of the longer lifetime of the carbocation. The reaction did not proceed well to form either the dimethoxy ketal or a ketal derived from an unsubstituted ethylene oxide.

The unsaturated acetal substrate was then subjected to a Michael-type addition. Initially, we looked for the best reaction conditions for this reaction with a series of model substrates (Scheme 4.19). Our starting point for the reaction conditions utilized for the reaction was to follow the lead of Robert Perkins who developed the approach during the work described in Scheme 3. For the model studies, the reactions either took advantage of unsaturated ketals that were commercially available or unsaturated ketals that could be rapidly synthesized from enone starting materials.



Scheme 4.19 Michael addition to ketene acetal model substrate test

The examples shown were chosen in order to examine the compatibility of the reactions with the methyl groups on the acetal and the size of the ring. Reactions (a) and (b) were run using the exact conditions developed by Robert Perkins. Both reactions worked well with case (b) illustrating the compatibility of the reaction with a donating alkyl substituent on the alpha carbon of the double bond.

It should be noted that the general basic work-up and EDTA wash protocol Robert Perkins developed for the reactions were essential for the success of the reactions. During my repeating experiments, I usually added 5 equivalents of 2,6-lutidine (more than used in his protocol) to the reaction before work up. The crude reaction mixture was then washed with an EDTA solution until no blue/green color remained. This was essential because either a slightly acidic crude product or a reaction product that retained some of the Cu metal from the cuprate triggered the conversion of the desired enediol to a cyclic ketal. Following the EDTA wash, the organic layers were extracted with brine. Then a regular brine extraction was conducted. Chromatography was

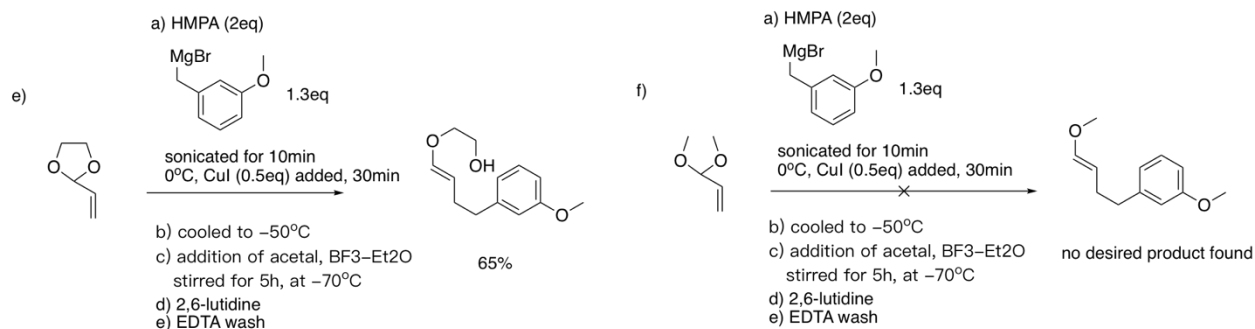
then conducted using silica gel that was pre-treated with TEA to prevent acid catalyzed decomposition of the product.

The reaction shown in part (c) of Scheme 4.19 turned out to be more sensitive to the reaction conditions and the quality of the reagents. The cuprate itself was in this case generated more efficiently at room temperature instead of the lower temperature used with the other cuprate reagents. In addition, the reaction using the six-membered ring substrate required more time and was optimally complete in 5 h instead of the 3 h employed with the five-membered ring substrate. Even with the extended reaction time, some starting material was recovered.

The example shown in Scheme 4.19 part (d) changed the Lewis acid used for the reaction. In this case, the cuprate reagent was generated at 0°C. The reaction mixture was then cooled to -78°C and TMSCl added (buffered with an equal equivalent of trimethylamine). This avoided the need for the BF₃·Et₂O used in the previous reactions. TMEDA was added to increase the nucleophilicity of the anion instead of the HMPA added to the previous reactions. This was done to avoid the toxicity of the HMPA reagent. A proton NMR of the crude reaction mixture did show a vinyl proton consistent with the enol ether product, however the product could not be isolated.

In the end, it became clear that the addition reaction with the six-membered ring substrate was slower and more challenging than the reaction with the five-membered ring substrate in terms of product isolation. We also found that in many cases the sequence of making the cuprate at 0°C, letting the reaction warm to room temperature, and then cooling it down again before adding in the acetal improved the reaction. Presumably, this sequence led to a more complete formation of the nucleophile.

Two other reactions were pursued by Ms. Kendra White and myself in order to establish the generality of the approach. These reactions used acyclic unsaturated acetal substrates.



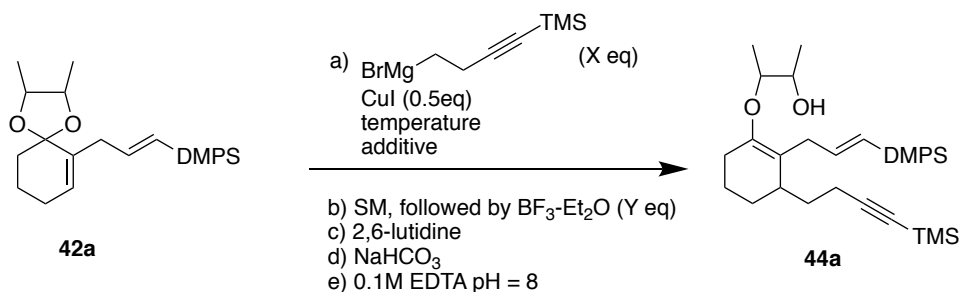
Scheme 4.20 Acyclic ene diol substrate synthesis

The overall goal was to examine the preference of the subsequent electrolysis reactions for either the oxidative radical vs. radical cation reaction pathway. The reaction shown in case (e) worked well using the same reaction conditions developed previously. However, the reaction shown in part (f) of the Scheme did not work. It appears that the dimethoxy substrate will require different conditions for generating the oxonium ion needed for the addition. While we were confident that this reaction could be optimized, the project was not a priority at the time because we wanted to answer the question being asked about the tandem oxidative cyclization. It was clear that we had the chemistry in place to make the necessary substrate for that study.

With this in mind, the key Michael-type reaction was then conducted using ketal **42a**.

Unfortunately, the optimized conditions developed for the model substrates were not successful with this substrate. The reactions were capricious, and conditions optimized for one substrate could not automatically be applied to others.

Hence, the reaction needed to be re-optimized specifically for substrate **42a**.



condition	Grignard eq	step a) teperature	step a) additive	$\text{BF}_3\text{-Et}_2\text{O}$ eq	yield
1 ^a	2eq	-20 °C	HMPA (3eq)	2eq	-
2	2eq	-20 °C	HMPA (3eq)	2eq	70% RSM
3	10eq	0 °C	HMPA (1eq)	2eq	5% 44a
4	10eq	0 °C-rt- -78°C	-	1eq	30% 44a

(a) tetramethyl bridge substrate **44a-2** used

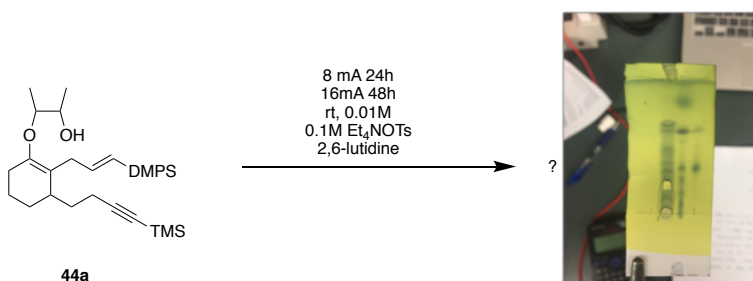
Scheme 4.21 Michael-type addition condition optimization

In many ways, this observation was not much of a surprise. The reactions are a fine balance between the generation of an oxonium ion from the ketal and then a subsequent addition to the result electron poor Michael acceptor. In previous cases, this required an activated anion that was optimized with the use of HMPA and assistance in opening the ketal with the use of $\text{BF}_3\text{-Et}_2\text{O}$ as a Lewis acid. In this case, the use of too much of the Lewis acid and the use of HMPA proved to be detrimental to the reaction. The reaction with a substrate having four methyl groups on the ketal bridge led to decomposition. It may be that the extra sterics associated with the substrate led to opening of the ketal and decomposition faster than the addition of the nucleophile could occur. The same reaction conditions with the less hindered ketal (entry 2) led to recovery of starting material. In the end, we found that the reaction benefited from raising the temperature of the reaction, avoiding HMPA, lowering the amount of Lewis acid used, and increasing the amount of the anion utilized. Eventually a yield of 30% could be obtained for the product **44a**.

While not optimal, further optimization was not pursued because we wanted to know if the oxidative cyclization was going to work before expending that additional effort. So, a similar route along with additional optimization efforts for each substrate was employed to develop a set of electrolysis substrates (as shown in next section).

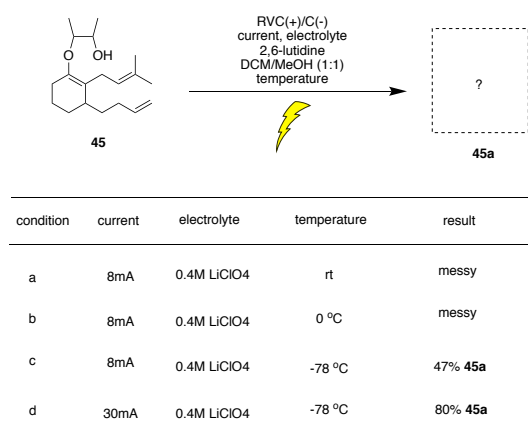
4.4.2 Electrochemical Studies

Our initial electrochemical test was conducted on substrate **44a** at room temperature (Scheme 4.22). The reaction was very messy leading to the TLC shown. The left lane was reaction spot. The Right lane was starting material. (The top spot in right lane generated due to instability, I know that because when I was doing chromatography for starting material, there was only the lower spot after chromatography) Clearly, the use of the oxidative radical pathway was not going to automatically mimic the reaction conducted by Sha. However, it was not clear where the problem was. Was the issue the initial cyclization, or was the issue downstream of that step with either the intermediate generated from the first cyclization, the intermediate from the second cyclization, the second oxidation step, etc., or a combination of one or more of these issues?



Scheme 4.22 Initial Tandem Cyclization Test on 44a

Since, we were not sure how the vinylsilane would behave as a terminating olefin for the oxidative cyclization, the next substrate tried (**45**) had a trisubstituted olefin as this terminating group. Trisubstituted olefins have functioned beautifully as terminal groups for anodic coupling reactions.¹² In addition, an olefin was used instead of the acetylene as a relay so that we could examine its involvement as relay in the reaction by proton NMR (Scheme 4.23).



Scheme 4.23 Substrate 45 Electrolysis Test

The first two conditions tried (entries a and b) led to a complex mixture with low mass balances (entry a with a 30% mass balance and entry b with a 15% mass balance). In both cases, the products that could be observed still contained the mono-substituted olefin. This result was consistent with a failure of the initial cyclization and polymerization of the radical cation intermediate generated, although no specific product from the reaction could be characterized.

This result was not totally surprising since early work by Rob Perkins in the group had shown that the oxidative radical type reactions benefited from low temperature.⁷ This kept the ketal formed from the initial radical cation trapping reaction closed and prevented unwanted side reactions from the initial radical cation. With this in mind, the reaction was run at -78 °C. The reaction shown in entry c led to a 47% isolated mass balance. Once again, the reaction did not

consume the monosubstituted double bond as can be seen in the proton NMR of the crude product shown in Figure 4.3 below. The reaction was interesting because the side chain trisubstituted olefin in the substrate appeared to be largely consumed. Note how the trisubstituted olefin proton peak (5.17ppm, 1 proton) integrated in 1:2 ratio relative to the monosubstituted olefin proton peaks (5.8ppm, 1 proton, 4.9-5.0ppm, 2 protons). This suggested that the trisubstituted olefin was consumed in at least one half of the product. It was also noted that the peaks at 3.7 ppm changed significantly relative to the starting material (compound **45** as shown in Appendix C). This indicated that a cyclic acetal may have formed during the reaction. The methoxy region of the spectrum showed some small peaks, but did not indicate that the major products not been methoxylated to a major extent. At the time, this result was surprising. Now, we think the products generated may well be derived from a three membered ring cyclization product originating from the radical. Evidence for this type of product will be presented below (Scheme 4.25).

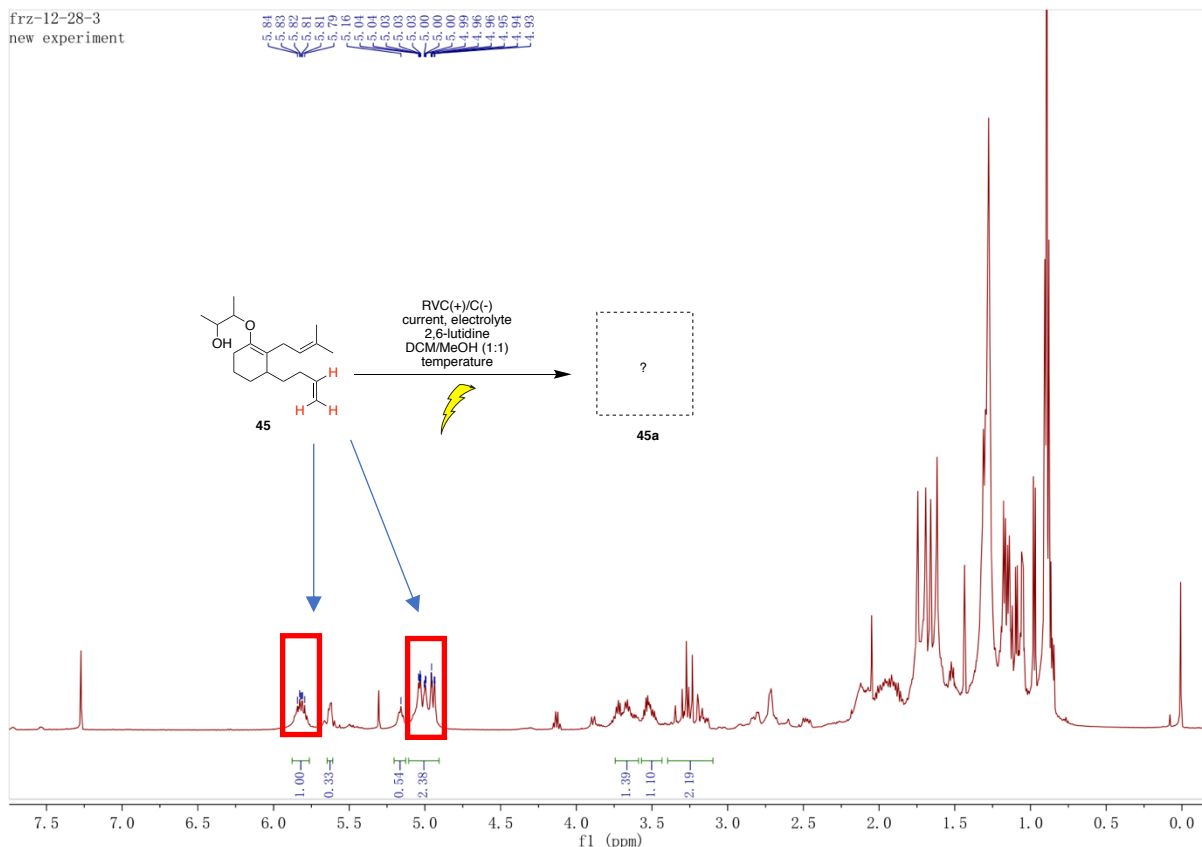


Figure 4.3 substrate 45 electrolysis entry c

At this point, the current passed through the reaction was increased in a fashion that would accelerate the loss of a second electron from the reaction (entry d). In this case, α tri-substituted olefin proton peak was completely lost, the reaction looked cleaner, and the mass balance of the reaction dramatically improved. However, once again there was clear evidence that the monosubstituted olefin was not involved in the reaction (Figure 4.4). The methoxy region of the spectrum showed a number of methoxy signals in a fashion consistent with earlier radical cation reactions that led to polymerization. Alternatively, the methoxy groups might arise from trapping of cation intermediates like **49** suggested in Scheme 4.25 below. What was clear from the spectrum is that the reaction had not led to the desired tandem cyclization reaction.

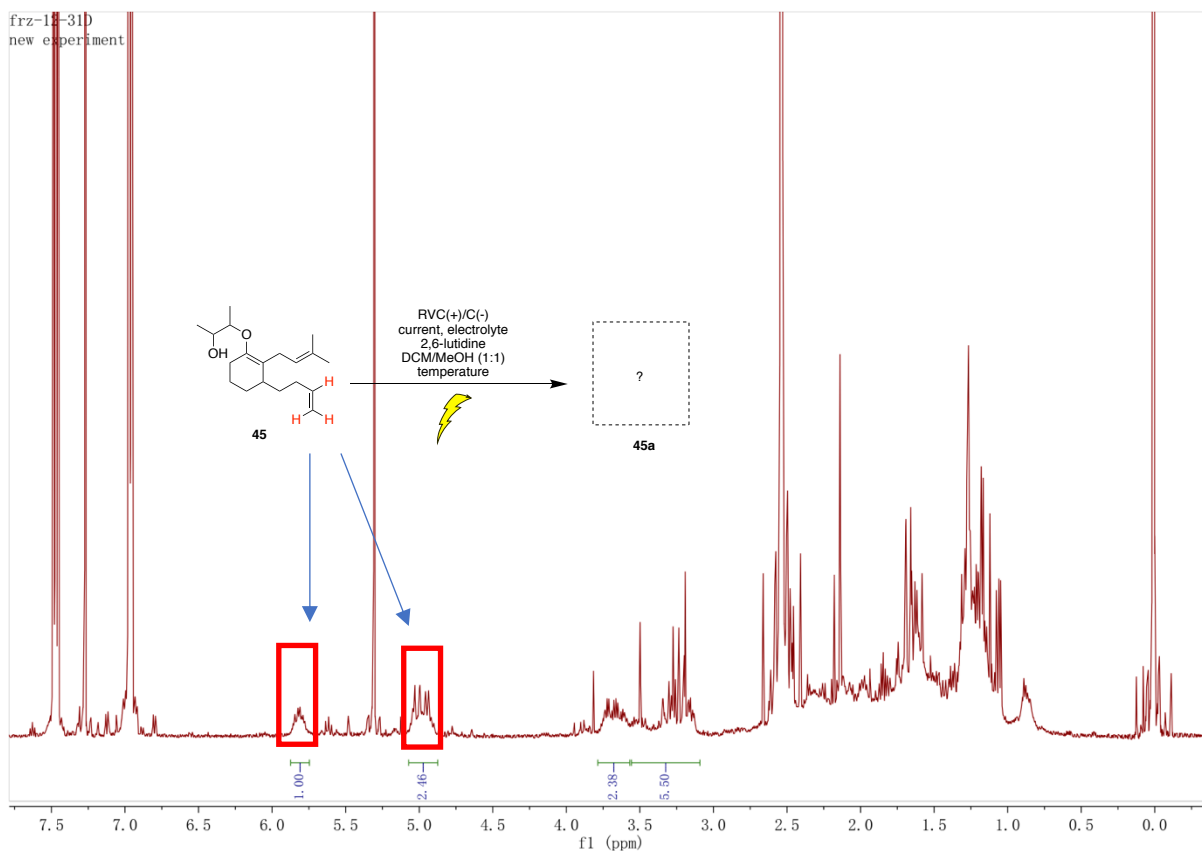
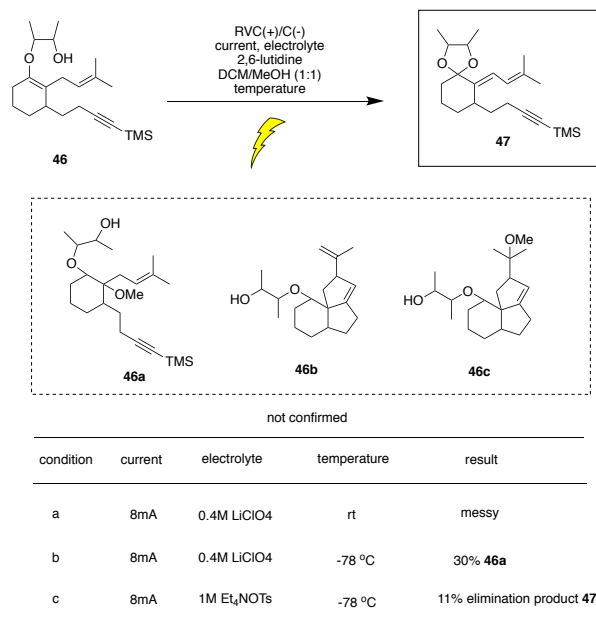


Figure 4.4 substrate 45 electrolysis entry d

The fact that in both cases the double bond of the relay did not participate in the cyclization suggested that perhaps this monosubstituted double bond was a poor enough trapping group that it led to the problems seen. For that reason, substrate **46** with the acetylene in place as the relay was utilized. It was hoped that the TMS group on the acetylene would help stabilize a vinyl radical intermediate and lead to the tandem cyclization.



Scheme 4.24 Substrate 46 Electrolysis Test

However, as shown in Scheme 4.24 the change to the acetylene did not improve the reaction. At room temperature, the reaction again led to a complex mixture with no identifiable product. For the reaction shown in entry b the temperature was decreased to -78°C . The reaction led to a 30% mass balance of material. However, in this case there appeared to be trisubstituted olefin remaining (5.17ppm, 1 proton, triplet, and asymmetric peak at 3.7ppm) indicating that the tandem cyclization reaction had not gone as expected. There was evidence of methoxylation in a manner cleaner than the previous reactions. What was missing was the expected olefinic methylene that would result from a successful tandem cyclization like in **46b**, although some tandem cyclization product trapped by methoxy group cannot be ruled out like **46c**. Such a product was not isolated from the reaction.

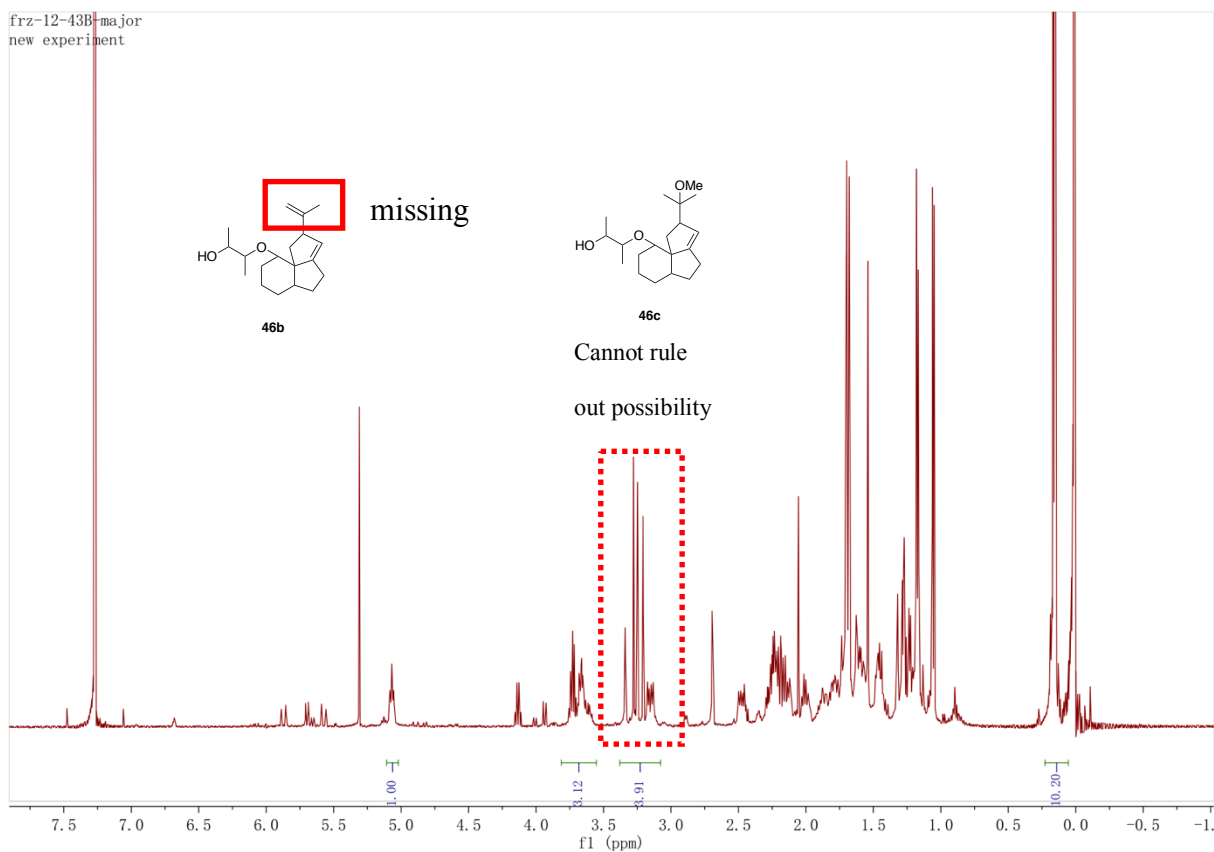


Figure 4.5 substrate 46 electrolysis entry b

We hoped to increase the yield of the oxidized product and perhaps buy more time for the cyclization with a change to a high concentration of a greasier electrolyte. The idea was to make a more defined double layer that excluded methanol solvent and bought more time for the desired tandem intramolecular reactions. The result was a cleaner reaction out of which the elimination product **47** could be isolated in an 11% yield. (NMR below)

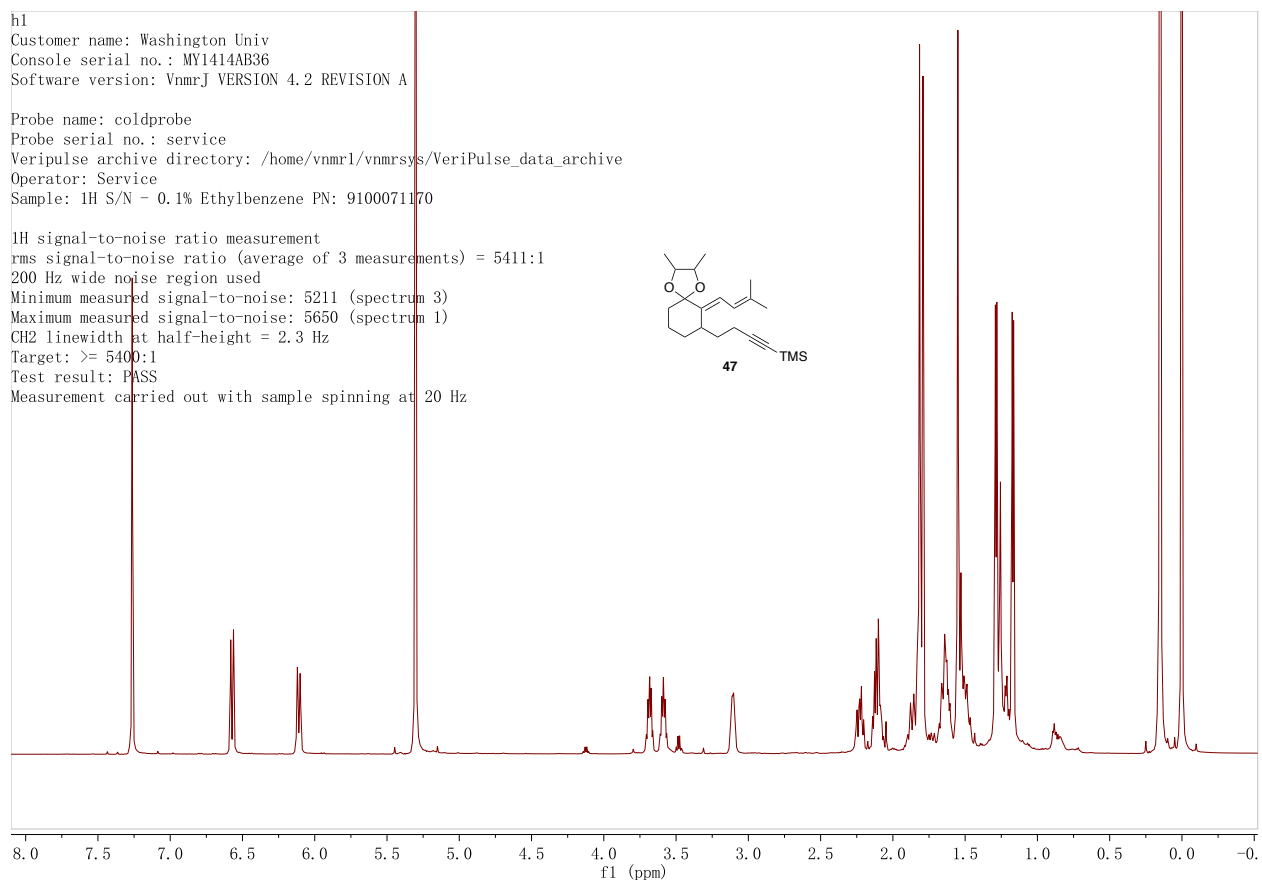
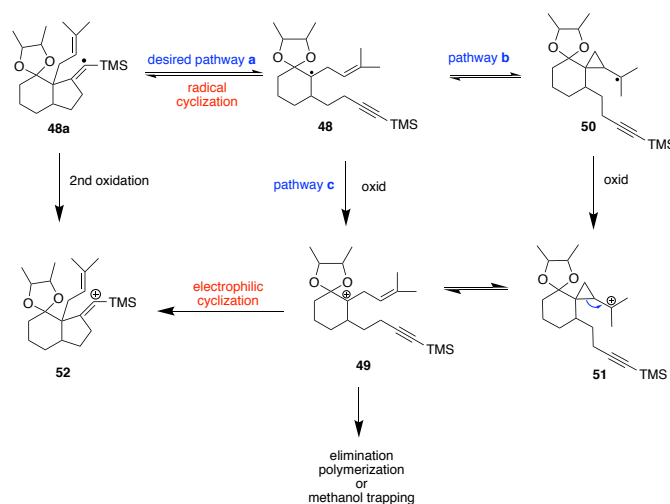


Figure 4.6 substrate 46 electrolysis entry c isolated 47

The recovery of this product (Structure confirmed by 2D NMR, Appendix C) was intriguing because it provided some insight into a potential explanation for why this particular reaction was proving to be problematic. Consider the potential mechanism highlighted in Scheme 4.25. One can imagine the formation of the desired radical (**48**) leading to either a reversible cyclization with the acetylene (pathway **a**) or a potentially fast reversible three-membered ring cyclization with the trisubstituted olefin (pathway **b**). The reversible three membered ring cyclization might stabilize the radical long enough for a second oxidation (pathway **c**) to take place generating a cationic intermediate **49** that would not readily undergo electrophilic cyclization with the acetylene to form an unstable vinyl cation **52**. The result would be elimination leading to the

observed product **47**, potential methanol trapping leading to the methoxy signal observed in the NMR, and/or polymerization reactions from the cations. Of course, some formation of a successful tandem cyclization product that might lead to a methoxylated product could not be ruled out, although once again no such product was isolated.



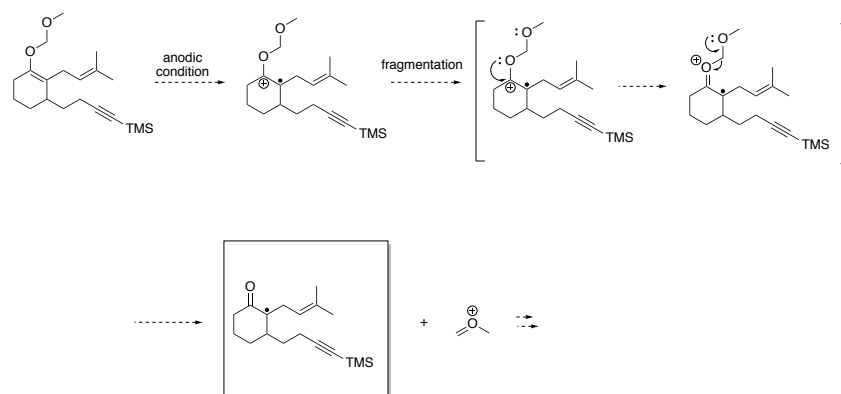
Scheme 4.25 Possible Pathway

The resulting diene could easily undergo further oxidation reactions leading to a loss of mass balance and the types of methoxylated products observed as well. It was clear that the presence of the trisubstituted olefin on the sidechain bound to the radical intermediate was problematic for the reaction. This may well have been part of the problem in the earlier cyclization attempts by Bradley Scates and Laura Anderson. The isolation of this product provides one of the first key observations needed to shape subsequent experiments in a more hypothesis driven approach.

4.5 Conclusions

It is clear at this point that we need to understand more about the oxidative tandem cyclization reactions before venturing into more complex substrates. In the case shown above, the equilibrium may well be driven by the final oxidation reaction. Hence, the behavior of the reaction may be quite different from that observed with a reductive radical reaction that is terminated by a hydrogen atom abstraction from tributyltin hydride. For example, steric hindrance might slow a hydrogen atom abstraction reaction from tributyltin hydride allowing time for a series of equilibrium steps to make multiple bonds whereas the same steric hindrance might make a radical electron rich and accelerate an oxidation that shortened the lifetime of the reaction and eliminated the opportunity for the same equilibrium steps. What is needed is a systematic study of oxidative tandem cyclization reactions so that these issues can be probed. Such a study is suggested in Chapter 6.2.3 using acyclic system probing tandem cyclization.

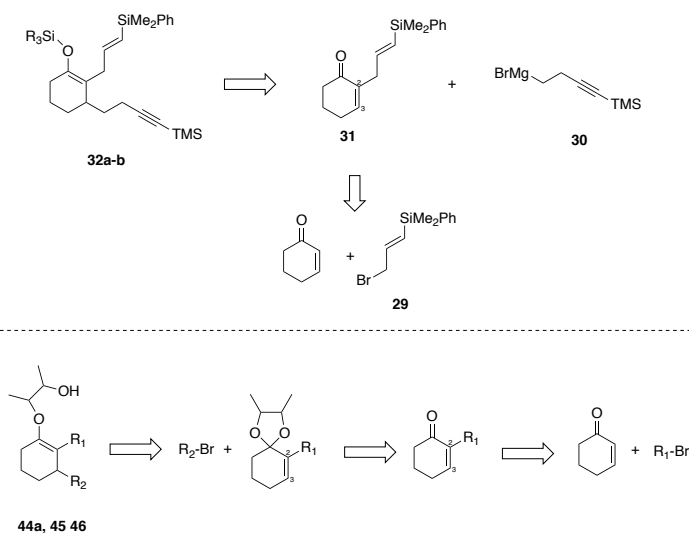
Another possible solution resides in raising the temperature of the reaction in order to accelerate the desired cyclization. One of the disadvantages of using the enediol ether substrates is the need to conduct the reactions at -78°C in order to keep the cyclic ketal generated closed. This lower temperature favors the formation of kinetic products like the three membered ring relative to the potentially more stable tandem cyclization products. Higher temperature might buy time for an equilibrium. One way to resolve this issue may be the use of a MOM-protected enol ether. In this case, the anodic oxidation would lead to a radical cation that can fragment to generate exactly the same radical used in Sha's synthesis (Scheme 4.26). This fragmentation approach would not require the lower temperature. In Sha's synthesis, the reaction was brought to reflux.¹ It is also possible to raise the temperature of an anodic cyclization reaction¹³. Would this lead to the tandem cyclization?



Scheme 4.26 MOM protected substrate under anodic condition

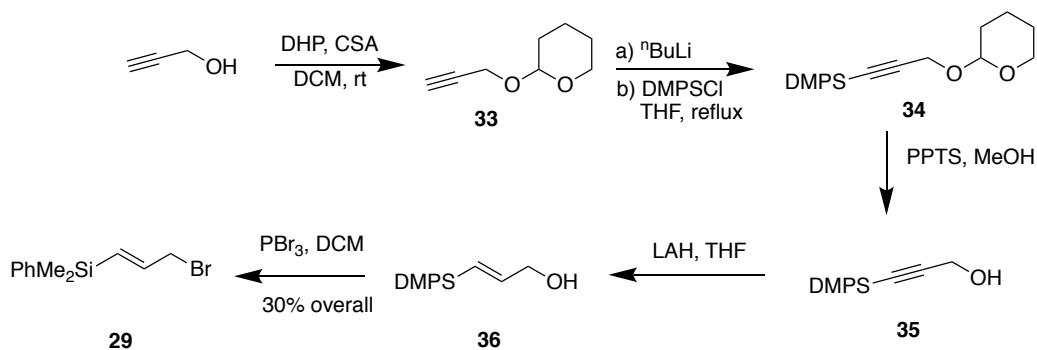
4.6 Experimental Section

The synthesis of silyl enol ether substrates **32a-b** and enediol ether substrates **44a**, **45**, **46** were accomplished using similar routes. The synthesis of substrates **32a-b** was relatively straight forward. Most of the non-standard effort focused on exploring the reaction conditions needed to form the acetylene side chain **30**. On the other hand, the synthesis of substrates **44a**, **45**, and **46** required significantly more effort.



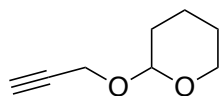
Scheme 4.27 Electrolysis Substrate Synthesis Route

4.6.1 Synthesis of 29 (E)-(3-bromoprop-1-en-1-yl)dimethyl(phenyl)silane¹⁴



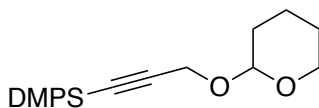
Scheme 4.28 Synthesis of side chain 29

Synthesis of 33 2-(prop-2-yn-1-yloxy)tetrahydro-2H-pyran



To a solution of camphorsulfonic acid (46 mg, 0.2 eq) and 3,4-dihydro-2H-pyran (2 mL, 22 mmol, 1.1 eq) in 10 mL of dichloromethane under Argon was added prop-2-yn-1-ol (1.15 mL, 20 mmol, 1eq). The reaction mixture was stirred for 18 h at room temperature and then quenched with a saturated aqueous solution of NaHCO₃. The layers were separated and then the aqueous layer was extracted two times Et₂O. The combined organic layer was dried over MgSO₄, filtered, and concentrated *in vacuo*. The residue was carried onto next step without further purification. The spectra data (Appendix C) matched the previously published ¹H NMR (CAS 6089-04-9).

Synthesis of 34 dimethyl(phenyl)(3-((tetrahydro-2H-pyran-2-yl)oxy)prop-1-yn-1-yl)silane



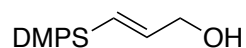
A solution of **33** from the last step in 40 mL of THF was added to a three-neck round bottom flask that was fitted with a condenser and placed under argon. The mixture was cooled to -78°C , and then n-BuLi (13.8 mL, 1.6 M in hexane, 1.1 eq) added in a dropwise fashion. The mixture was stirred for 15 min (clear brown solution) before allowing the reaction to warm to room temperature. After an addition of chlorodimethyl(phenyl)silane (4.0 mL, 24 mmol, 1.2eq), the reaction was brought to reflux for 20h. The reaction was then quenched with aqueous NaHCO_3 , and most of THF solvent was removed under reduced pressure. The residue was diluted with water and Et_2O , the layers separated, and the aqueous layer extracted three times with Et_2O . The combined organic layer was dried over MgSO_4 , filtered, and concentrated *in vacuo*. The residue was carried onto next step.

Synthesis of **35** 3-(dimethyl(phenyl)silyl)prop-2-yn-1-ol



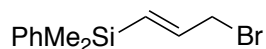
To a mixture of **34** from last step in 100 mL of MeOH was added pyridinium p-toluenesulfonate (1 g, 0.2 eq). The reaction was stirred for 20 h and then quenched with a saturated aqueous solution of NaHCO_3 . Most of solvent was removed under reduced pressure. The residue was diluted with water and dichloromethane, the layers separated, and then the aqueous layer extracted three times with dichloromethane. The combined organic layers were dried over MgSO_4 , filtered, and concentrated *in vacuo*. Once again, the residue was carried onto next step without further purification.

Synthesis of **36** (E)-3-(dimethyl(phenyl)silyl)prop-2-en-1-ol



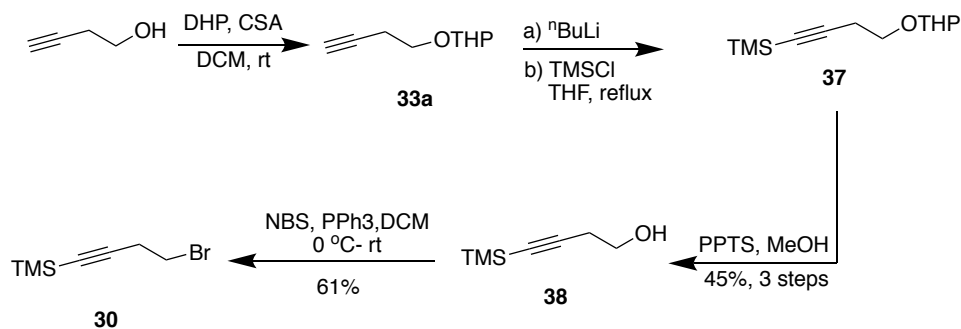
Lithium aluminium hydride (1.214 g, 1.6 eq) in 60 mL of THF was added to a round bottom flask under Argon. The mixture was cooled to 0 °C and then product **35** from last step added. The reaction was allowed to warm to room temperature and then stirred for 20 h. The reaction was quenched with a saturated Rochelle's salt solution and stirred until the layers were separated. Most of organic solvent in the mixture was removed under reduced pressure, the resulting residue was then diluted with water and Et₂O, and the aqueous layer extracted three times with Et₂O. After concentration, the residue was carried onto next step.

Synthesis of **29** (E)-(3-bromoprop-1-en-1-yl)dimethyl(phenyl)silane



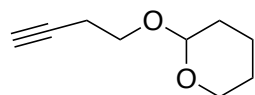
To a solution of the crude **36** from the last step in 300 mL of dichloromethane at 0 °C under argon was added PBr₃ (10 mL, 1 M in dichloromethane, 0.5 eq) in small portions. The mixture was allowed to warm to room temperature overnight. The reaction was then quenched with a saturated solution of aqueous NaHCO₃. The layers were separated and the aqueous layer extracted three times with dichloromethane. The combined organic layers were dried over MgSO₄, filtered, and concentrated *in vacuo*. The crude product was chromatographed through silica gel using 10% ethyl acetate in hexane as eluent to give 0.61 g of product (30% yield over four steps). The NMR data (Appendix C) matched the previously published data.¹⁴

4.6.2 Synthesis of 30 (4-bromobut-1-yn-1-yl)trimethylsilane



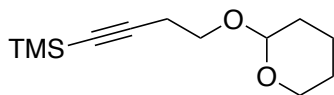
Scheme 4.29 Synthesis of side chain 30

Synthesis of 33a 2-(but-3-yn-1-yloxy)tetrahydro-2H-pyran



To a solution of camphorsulfonic acid (92 mg, 8 mmol, 0.2 eq) and 3,4-dihydro-2H-pyran (4 mL, 44 mL, 1.1 eq) in 20 mL of dichloromethane under argon was added but-3-yn-1-ol (3.03 mL, 40 mmol, 1eq). The reaction mixture was stirred for 18 h at room temperature. The reaction was quenched with a saturated aqueous solution of NaHCO_3 , the layers separated and the aqueous layer extracted two times with Et_2O . The combined organic layer was dried over MgSO_4 , filtered, and concentrated *in vacuo*. The residue was carried onto next step. The spectra data (Appendix C) matched the previously published ^1H NMR.¹⁴

Synthesis of 37 trimethyl(4-((tetrahydro-2H-pyran-2-yl)oxy)but-1-yn-1-yl)silane



A solution of **33a** from the last step in 80 mL of THF was added to a three-neck round bottom flask that was fitted with a condenser and placed under argon. The mixture was cooled to -78°C . To this solution was added n-BuLi (27.5 mL, 1.7 M in hexane, 44 mmol, 1.1 eq) in a dropwise fashion. The resulting solution was stirred for 15 min. The reaction was allowed to warm to room temperature before trimethylsilyl chloride (6.1 mL, 48 mmol, 1.2 eq) was added and the reaction brought to reflux for 20 h. The reaction was then quenched with a saturated aqueous solution of NaHCO_3 . Most of THF solvent was removed under reduced pressure before the resulting residue was diluted with water and Et_2O , the layers were separated, and the aqueous layer was extracted three times with Et_2O . The combined organic layer was dried over MgSO_4 , filtered, and concentrated *in vacuo*. The residue was carried onto next.

Synthesis of **38** 4-(trimethylsilyl)but-3-yn-1-ol



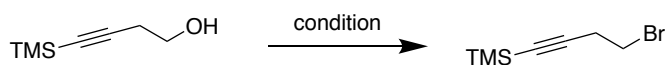
To a mixture of **34** from the last step in 200 mL of MeOH was added pyridinium p-toluenesulfonate (2 g, 8 mmol, 0.2 eq). The reaction was stirred for 20 h and then quenched with a saturated aqueous solution of NaHCO_3 . Most of solvent was removed under reduced pressure. The resulting residue was diluted with water and dichloromethane, the layers separated, and the aqueous layer extracted three times with dichloromethane. The combined organic layers were dried over MgSO_4 , filtered, and concentrated *in vacuo*. The crude product was chromatographed

through silica gel with 50% ethyl acetate in hexane as eluent to afford 2.54 g of product (45% yield over three steps). The NMR data (Appendix C) matched the previously published data (CAS 2117-12-6).

Synthesis of **30** (4-bromobut-1-yn-1-yl)trimethylsilane



A bromination reagent was screened. NBS was used for the rest of synthesis.



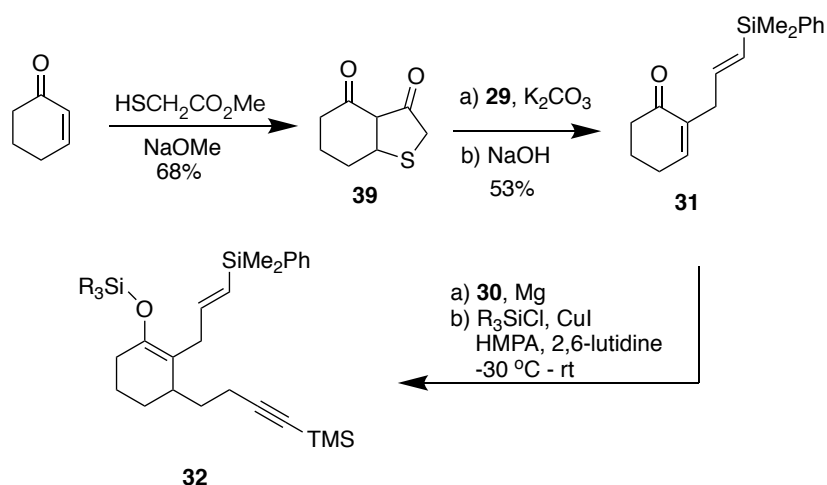
bromo source	additive	solvent	condition	yield
PBr ₃	-	DCM	rt	-
Br ₂	imidazole PPh ₃	DCM	rt	43%
NBS	PPh ₃	DCM	0 °C - rt	61%

Scheme 4.30 Bromination Reagent Screening for **30**

A solution of **38** (0.57 g, 4.03 mmol, 1 eq) in 15 mL of dichloromethane under argon was cooled to -20 °C. To this solution was added PPh₃ (1.258 g, 4.8 mmol, 1.2 eq) in 7 mL of dichloromethane, followed by a solution of NBS (0.79 g, 4.4 mmol, 1.1 eq) in 18 mL of dichloromethane. The reaction mixture was allowed to room temperature overnight during which period the color of the mixture changed from pale yellow to bright yellow. The reaction was then quenched with an aqueous, saturated solution of NaHCO₃. The layers were separated, the

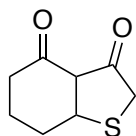
aqueous layer extracted two times with Et₂O, and the combined organic layers dried over MgSO₄, filtered, and concentrated *in vacuo*. The crude product was chromatographed through silica gel using hexane as eluent to afford 0.5 g of product (61% yield). The spectra data matched the previously published ¹H NMR (CAS 69361-41-7).

4.6.3 Synthesis of 32 enol ether electrolysis substrate



Scheme 4.31 Synthesis of Enol Ether Substrate 32

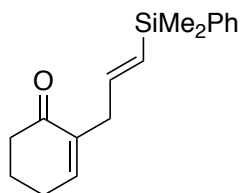
Synthesis of 39 tetrahydrobenzo[b]thiophene-3,4(2H,3aH)-dione⁴



A solution of methyl 2-mercaptoacetate (4.6 mL, 1eq) in 10 mL of MeOH was added dropwise into a freshly made NaOMe solution (Na metal, 1.31 g, 100 mL of MeOH, 1.05eq) at 0°C. To this mixture was added a solution of cyclohex-2-en-1-one (5 mL, 52 mmol, 1 eq) in an additional 10 mL of MeOH in a dropwise fashion. During this time, the reaction was maintained at 0 °C. The

reaction mixture was allowed to warm to room temperature, and then brought to reflux overnight. After the reaction was cooled, the majority of the solvent was removed under reduced pressure. The resulting residue was diluted with ether and washed with 2 N NaOH until basic (The organic layer pH was tested with regular pH testing strip). The aqueous layer was collected, acidified with 1 N HCl, and then extracted three times with Et₂O. The combined organic layers were dried over MgSO₄, filtered, and concentrated *in vacuo*. The crude product was chromatographed through silica gel using 10% EtOAc in hexane as eluent to give 6 g of the desired product (68% yield). The spectra data matched the previously published ¹H NMR. We did find that the yield of the product varied significantly during repeated scale up efforts, and at times the product was obtained in yields as low as 13%.

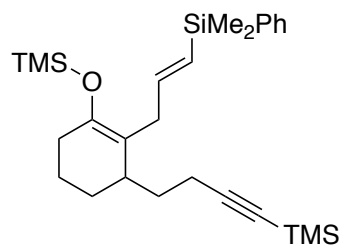
Synthesis of **31** (E)-2-(3-(dimethyl(phenyl)silyl)allyl)cyclohex-2-en-1-one



A round bottom flask fitted with a condenser was charged with compound **39** (180 mg, 1.05 mmol, 1 eq), compound **29** (0.321 g, 1.26 mmol, 1.2 eq), K₂CO₃ (0.174 g, 1.26 mmol, 1.2 eq), and 10 mL of anhydrous acetone. The mixture was brought to reflux for 16 h. After reaction, the salt was removed by filtration and the solvent removed under reduced pressure. The residue was suspended in a solution of 5% aqueous NaOH and Et₂O (1:1). This mixture was stirred for 10 h. After the reaction, the layers were separated and the aqueous layer was extracted three times with Et₂O. The combined organic layers were dried over MgSO₄, filtered, and concentrated *in vacuo*.

The crude product was chromatographed through silica gel using 20% EtOAc in hexane as the eluent to give 150 mg of product (53% yield). In this reaction, we found that the yields of product ranged from 34% to 70% with the yield frequently benefiting from a smaller reaction scale. The spectra data matched the previously published ^1H NMR. ^1H NMR (300 MHz, CDCl_3) δ 7.68 – 7.49 (m, 2H), 7.47 – 7.33 (m, 3H), 6.73 (t, $J = 4.2$ Hz, 1H), 6.31 – 5.97 (m, 1H), 5.82 (dt, $J = 18.6, 1.4$ Hz, 1H), 3.41 – 2.87 (m, 2H), 2.63 – 2.43 (m, 2H), 2.42 – 2.20 (m, 2H), 2.23 – 1.81 (m, 2H), 0.36 (s, 6H). ^{13}C NMR (75 MHz, CDCl_3) δ 198.9, 145.9, 145.7, 137.9, 133.8, 129.6, 128.8, 127.7, 38.4, 36.4, 26.1, 23.1.

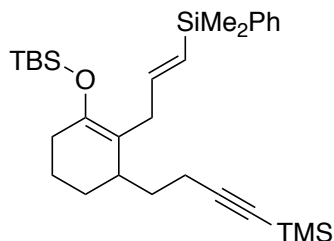
Synthesis of 32a



A Grignard solution of **30** (0.48 M, 1.68 mL, 1.5 eq) was made freshly and titration. (A procedure for Grignard and titration can be found in chapter 3 experimental). To the solution, CuI (24 mg, 0.124 mmol, 0.2 eq) and HMPA (0.28 mL, 1.612 mmol, 3 eq) were added in, the mixture was stirred at -40 °C for 30 min. The mixture was cooled to -40 °C, a solution of cyclohex-2-en-1-one (145 mg, 0.537 mmol, 1eq), TMSCl (0.164 mL, 1.28 mmol, 2.4 eq) and 0.1 mL 2,6-lutidine in 0.5 mL THF was added in dropwise. The reaction was stirred for 15 min and allowed to warm to room temperature. The reaction was then quenched with saturated NaHCO_3 (aq). The organic layer was washed with EDTA (pH=8, 0.1M) three times. And all aqueous layer

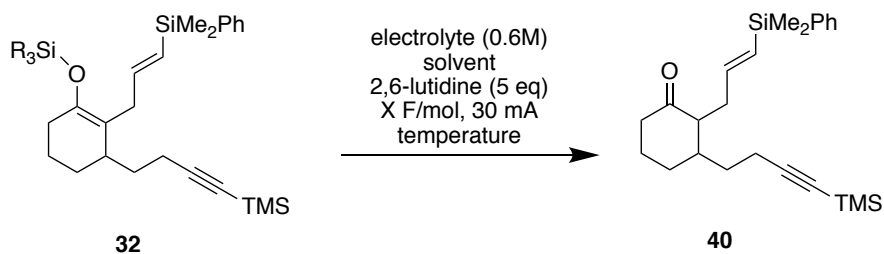
was extracted with DCM. The combined organic layer was dried over MgSO₄. The solvent was removed under reduced pressure and WITHOUT chromatography, **32a** crude can be achieved (clean reaction).

Synthesis of **32b**



A Grignard solution of **30** (0.34 M, 4.4 mL, 1.5 eq) was made freshly. To the solution, CuI (95 mg, 0.5 mmol, 0.5 eq) and HMPA (0.52 mL, 3 mmol, 3 eq) were added in, the mixture was stirred at -30 °C for 30 min. The mixture was cooled to -30 °C, cyclohex-2-en-1-one (270 mg, 1 mmol, 1 eq) was added in, followed by TBSCl (362 mg, 2.4 mmol, 2.4 eq) and 0.1 mL 2,6-lutidine. The reaction was stirred at -30 °C and allowed to warm to room temperature over 6 h. The reaction was then quenched with saturated NaHCO₃ (aq). The organic mixture was washed with EDTA (pH=8, 0.1M) three times. The combined organic layer was dried over MgSO₄, filtered, and concentrated *in vacuo*. The crude product was chromatographed through silica gel using 20% EtOAc in hexane as eluent to give 88 mg of product (17% yield).

General Procedure for Electrolysis:



initial Tandem Cyclization reaction test

entry	electrolyte	solvent	quantity of electric charge	temperature	result
1 ^a	0.6M Bu ₄ NBF ₄	DMSO/MeOH/DCM (1:1:2)	4 F/mol	0 °C	40 18%
2	0.6M LiClO ₄	MeOH	2.5 F/mol	-78 °C	40 60% (RSM 9%)

a) condition were chosen to differentiate former students condition in order to stabilize radical cation further

Scheme 4.32 Electrolysis of Enol Ether Substrate 32a-b

Entry 2 as an example

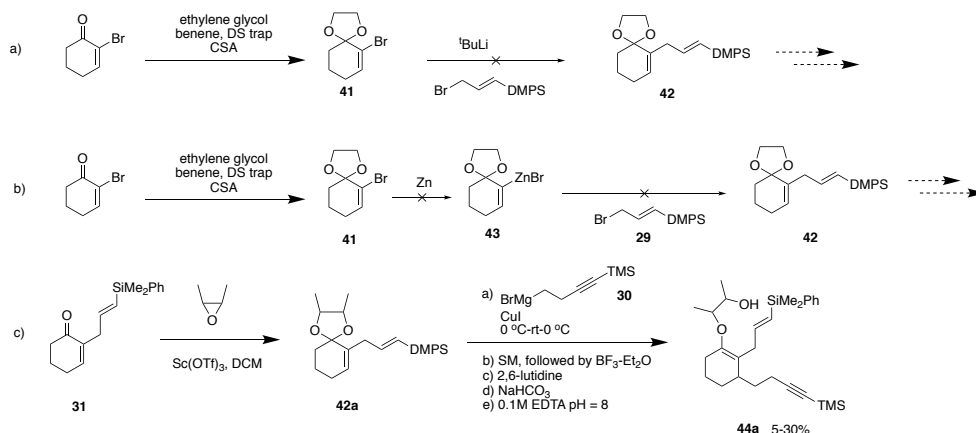
To a three-neck round bottom flask was charged with **32b** (0.173 mmol, 1eq), 0.6 M LiClO₄, 10 mL MeOH, 2,6-lutidine (0.1 mL, 0.867 mmol, 5 eq). The reaction was electrolyzed at 30 mA until 2.5 F/mol current passed using RVC as anode and graphite as cathode. The reaction was then quenched with saturated NaHCO₃ (aq). Aqueous layer was extracted with DCM three times. The combined organic layer was dried over MgSO₄, filtered, and concentrated *in vacuo*. The crude product was chromatographed through silica gel using 10% EtOAc in hexane as eluent to give 8 mg of **32b** (9% yield) and 41 mg of **40** (60% yield).

Spectra data for **40**

¹H NMR (300 MHz, CDCl₃) δ 7.57 – 7.46 (m, 2H), 7.39 – 7.32 (m, 3H), 6.11 – 5.92 (m, 1H), 5.85 – 5.54 (m, 1H), 2.65 – 2.09 (m, 9H), 2.02 – 1.91 (m, 1H), 1.87 – 1.56 (m, 4H), 0.3 (s, 6H), 0.15 (s, 9H). Appendix C

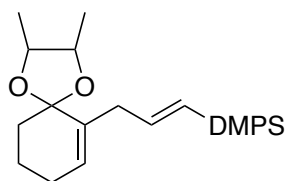
4.6.4 Synthesis of 44a alcohol electrolysis substrate

Several routes were attempted. Pathway c) was chosen as the standard route for the rest substrates synthesis. The synthesis of **31** can be found in 4.6.3.

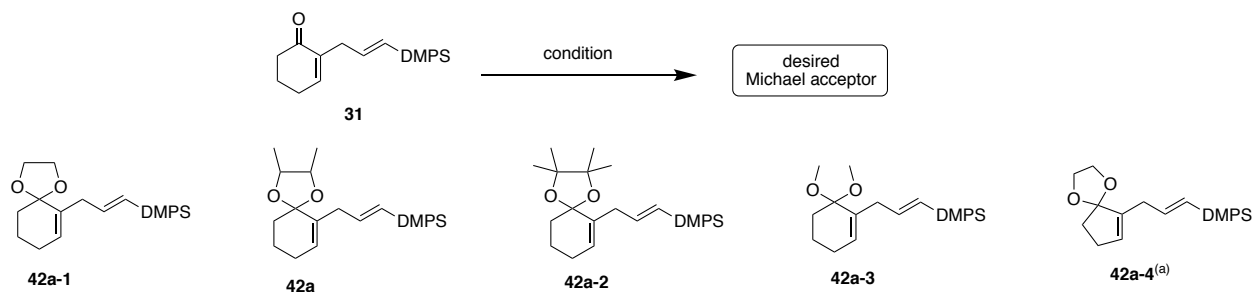


Scheme 4.33 Route for Synthesis of 44a

Synthesis of 42a (E)-(3-(2,3-dimethyl-1,4-dioxaspiro[4.5]dec-6-en-6-yl)prop-1-en-1-yl)dimethyl(phenyl)silane



A condition screening on making the acetal was conducted.



top bridge source	additive	product	yield
ethylene glycol	TsOH, D.S. trap	42a-1	-
ethylene glycol ^a	PPTS, D.S. trap	42a-4	-
ethylene glycol	Aniline-Aldehyde Resin Salts	42a-1	-
	TMSOTf	42a-1	-
	Sc(OTf) ₃ , DCM	42a	62%
	Sc(OTf) ₃ , DCM	42a-2	52%
HC(OMe) ₃	Aniline-Aldehyde Resin Salts	42a-3	-

(a) five member ring ketone was used as starting material

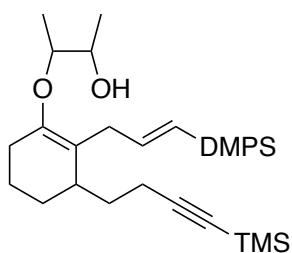
Scheme 4.34 Acetal Transformation Condition Screening

(2R,3S)-2,3-dimethyloxirane was used as a general synthesis for the rest of the synthesis.

To a round bottom flask was charged with **31** (0.6 g, 2.22 mmol, 1 eq), Sc(OTf)₃ (109 mg, 10mol%), Na₂SO₄ (0.86 g) under Argon. 2 mL DCM was added in, the mixture was cooled to 0 °C. (2R,3S)-2,3-dimethyloxirane (0.48 g, 6.66 mmol, 3 eq) (cis leads to same result) in 2 mL DCM was added in dropwise with syringe pump (Model as described in chapter 3) over 6 h. Reaction was stirred overnight at room temperature. The reaction was quenched with 1 mL TEA and stirred for 10 min. The reaction was then quenched with saturated NaHCO₃ (aq). Aqueous layer was extracted with DCM three times. The combined organic layer was dried over MgSO₄, filtered, and concentrated *in vacuo*. The crude product was chromatographed through silica gel using 10% EtOAc in hexane as eluent to give 0.47 g of **42a** (62% yield). ¹H NMR (300 MHz,

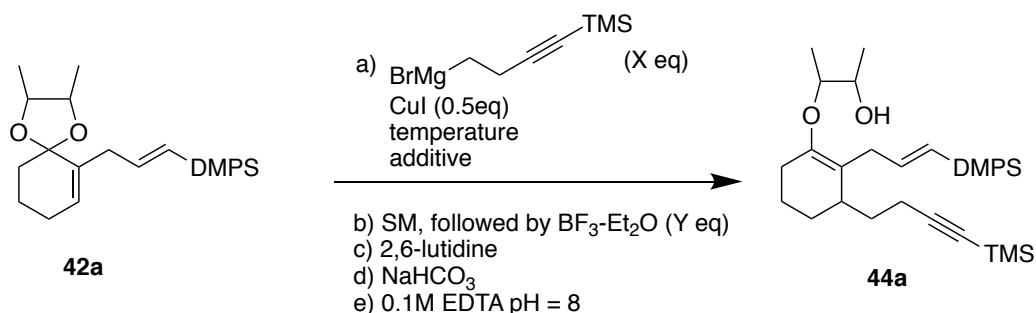
CDCI₃) δ 7.59 – 7.47 (m, 2H), 7.39 – 7.30 (m, 3H), 6.26 – 6.02 (m, 1H), 5.80 (dt, $J = 18.5, 1.4$ Hz, 1H), 5.67 – 5.58 (m, 1H), 3.81 – 3.48 (m, 2H), 3.03 – 2.79 (m, 2H), 2.06 – 1.97 (m, 2H), 1.93 – 1.59 (m, 4H), 1.33 – 1.13 (m, 6H), 0.33 (s, 6H). HRMS (ESI) for C₂₁H₃₀O₂Si [M + H]⁺ calc. 343.5558, found 343.2069, [M + Na]⁺ calc. 365.5376, found 365.1887.

Synthesis of 44a (E)-3-((2-(3-(dimethyl(phenyl)silyl)allyl)-3-(4-(trimethylsilyl)but-3-yn-1-yl)cyclohex-1-en-1-yl)oxy)butan-2-ol



A condition screening on the Michael reaction was conducted.

For future substrate synthesis, condition (4) was used as standard operation except with better quality of Grignard solution and larger scale reaction.



condition	Grignard dose	step a) teperature	step a) additive	$\text{BF}_3 \cdot \text{Et}_2\text{O}$ dose	yield
1 ^a	2eq	-20 °C	HMPA (3eq)	2eq	-
2	2eq	-20 °C	HMPA (3eq)	2eq	70% RSM
3	10eq	0 °C	HMPA (1eq)	2eq	5% 44a
4	10eq	0 °C-rt- -78°C	-	1eq	30% 44a

(a) tetramethyl bridge substrate **44a-2** used

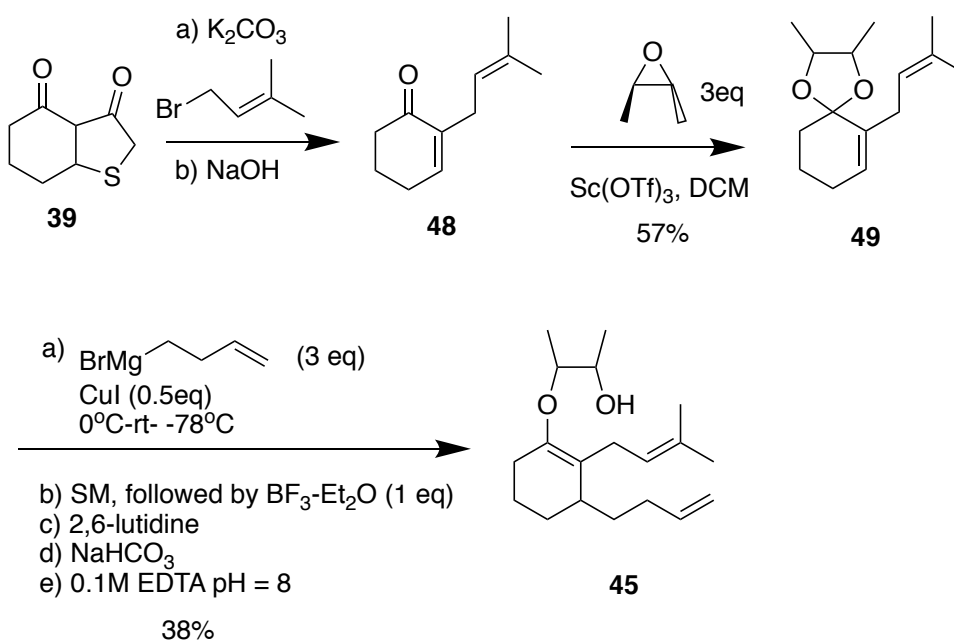
Scheme 4.35 Substrate **44a** Condition Screening

To a freshly made Grignard solution (0.53 M, 3.5 mL, >10 eq) at 0°C was added CuI (recrystallized, 50 mg). Mixture was stirred at room temperature for 30 min, a coffee color suspension was formed. Mixture was then cooled to -78 °C. **42a** (56.6 mg, 0.16 mmol, 1 eq) in 3 mL THF was added in dropwise, followed by dropwise addition of $\text{BF}_3 \cdot \text{Et}_2\text{O}$ (0.02 mL, 0.16 mmol, 1eq). Reaction was stirred for 15 h. 2,6-lutidine (0.2 mL) was added into the mixture before work up. The organic mixture was quenched with saturated NaHCO_3 , washed with EDTA solution (pH=8, 0.1M) until no blue color. Aqueous layer was washed with ether three times. The combined organic layer was dried over MgSO_4 , filtered, and concentrated *in vacuo*. The crude product was chromatographed through silica gel (packed with 1% TEA) using 10% EtOAc in hexane as eluent to give 22 mg of **44a** (30% yield) and 18% RSM. ^1H NMR (500 MHz, Chloroform-d) δ 7.59 – 7.47 (m, 2H), 7.35 (dd, J = 3.8, 2.5 Hz, 3H), 6.08 – 5.99 (m, 1H), 5.77

(dt, $J = 18.4, 1.6$ Hz, 1H), 3.79 – 3.59 (m, 2H), 3.25 (ddd, $J = 14.9, 5.3, 1.8$ Hz, 1H), 2.70-2.5 (2H), 2.34 – 1.96 (m, 4H), 1.91 – 1.36 (m, 6H), 1.34 – 1.21 (m, 6H), 0.33 (dd, $J = 4.0, 1.7$ Hz, 6H), 0.26 – 0.12 (m, 9H). HRMS (ESI) for $C_{28}H_{44}O_2Si_2$ $[M + Na]^+$ calc. 491.8093, found 491.2737.

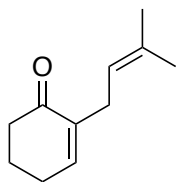
4.6.5 Synthesis of 45 alcohol electrolysis substrate

Based on the work discussed in 4.6.4, the synthesis of 45 was straight forward.



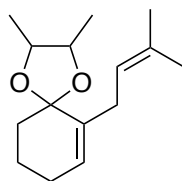
Scheme 4.36 Synthesis Route of 45

Synthesis of 48 2-(3-methylbut-2-en-1-yl)cyclohex-2-en-1-one



A round bottom flask with condenser was charged with **39** (0.7 g, 4 mmol, 1 eq), 1-bromo-3-methylbut-2-ene (0.55 mL, 4.8 mmol, 1.2 eq), K_2CO_3 (0.663 g, 4.8 mmol, 1.2 eq) in 40 mL anhydrous acetone. The mixture was brought to reflux over 16 h. After reaction, the salt was filtered and solvent was removed under reduced pressure. Residue was suspension in a mixture of 5% NaOH/Et₂O (1:1). The mixture was stirred for 10 h. Mixture was extracted with ether by three times. The organic layer was dried over $MgSO_4$, filtered, and concentrated *in vacuo*. The crude product was chromatographed through silica gel using 20% EtOAc in hexane as eluent to give 0.9 g of **48** can be achieved (<100% pure). The spectra data matched the previously published ¹H NMR. (Reference from Scates, B.A., Ph.D. Dissertation, Washington University in St. Louis, 2006)

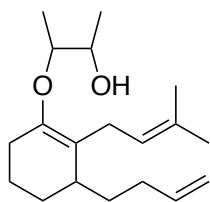
Synthesis of 49 2,3-dimethyl-6-(3-methylbut-2-en-1-yl)-1,4-dioxaspiro[4.5]dec-6-ene



To a round bottom flask was charged with **48** (4 mol), $Sc(OTf)_3$ (200 mg, 10mol%), Na_2SO_4 (1.5 g) under Argon. 3.5 mL DCM was added in, the mixture was cooled to 0°C. (2R,3S)-2,3-dimethyloxirane (0.86 g, 12 mmol, 3 eq) in 3.5 mL DCM was added in dropwise with syringe pump over 6 h. Reaction was stirred overnight at room temperature. The reaction was quenched with 2 mL TEA and stirred for 10 min (Mixture turned from bright red to bright yellow). The reaction was then quenched with saturated $NaHCO_3$ (aq). Aqueous layer was extracted with DCM three times. The combined organic layer was dried over $MgSO_4$, filtered, and concentrated

in vacuo. The crude product was chromatographed through silica gel using 10% EtOAc in hexane as eluent to give 0.535 g of **49** (57% yield). ¹H NMR (500 MHz, Chloroform-d) δ 5.64 (dt, J = 4.0, 2.0 Hz, 1H), 5.37 – 5.11 (m, 1H), 3.85 – 3.54 (m, 2H), 2.77 (d, J = 7.3 Hz, 2H), 2.01 (d, J = 3.7 Hz, 2H), 1.91 – 1.58 (10H), 1.40 – 1.01 (m, 6H). HRMS (ESI) for C₁₅H₂₄O₂ [M + H]⁺ calc. 237.3583, found 237.1839, [M + Na]⁺ calc. 259.3402, found 259.1657.

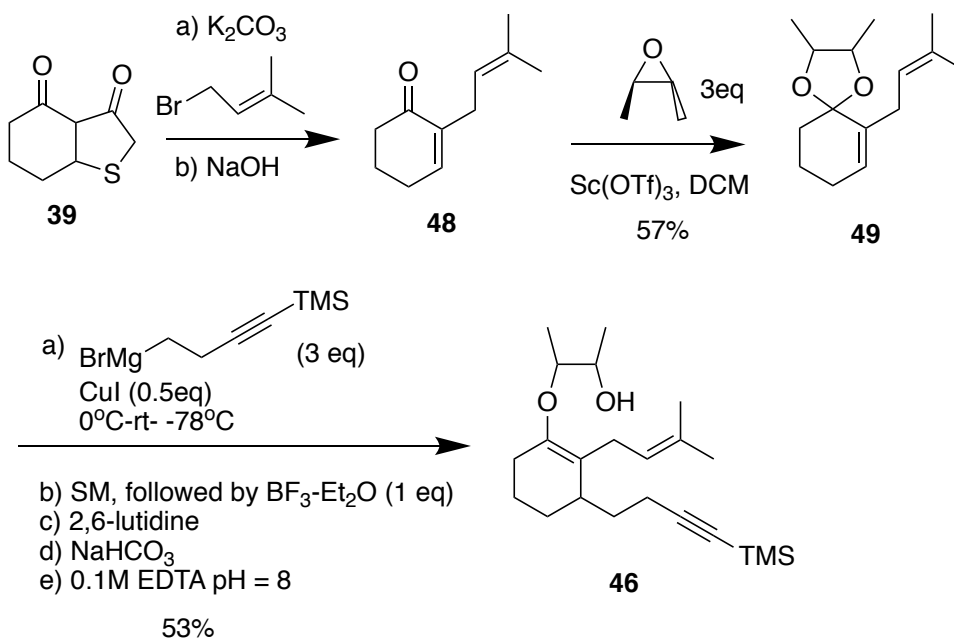
Synthesis of 45 (E)-3-((3-(but-3-en-1-yl)-2-(3-(dimethyl(phenyl)silyl)allyl)cyclohex-1-en-1-yl)oxy)butan-2-ol



To a freshly made Grignard solution (0.8 M, 8.4 mL) at 0°C was added CuI (recrystallized, 130 mg, 0.3 eq). Mixture was stirred at room temperature for 30 min, a coffee color suspension was formed. Mixture was then cooled to -78 °C. **49** (2.26 mmol, 1 eq) in 15 mL THF was added in dropwise, followed by dropwise addition of BF₃-Et₂O (0.3 mL, 1 eq). Reaction was stirred for 15 h. 2,6-lutidine (1.3 mL) was added into the mixture before work up. The organic mixture was quenched with saturated NaHCO₃, washed with EDTA solution (pH=8, 0.1M) until no blue color. Aqueous layer was washed with ether three times. The combined organic layer was dried over MgSO₄, filtered, and concentrated *in vacuo*. The crude product was chromatographed through silica gel (packed with 1% TEA) using 10% EtOAc in hexane as eluent to give 0.47 g of **44a** and 2,6-lutidine mixture (22% yield product) and 54% RSM. (Note: During repeating experiments, product yield could be increased to 38%). ¹H NMR (500 MHz, Chloroform-d) δ 5.82 (ddt, J = 16.9, 10.2, 6.6 Hz, 1H), 5.09 – 4.89 (m, 3H), 3.78 – 3.60 (m, 2H), 3.15 (dd, J =

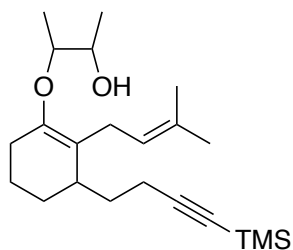
14.8, 6.6 Hz, 1H), 2.72 (d, $J = 2.7$ Hz, 1H), 2.58 (d, $J = 7.8$ Hz, 1H), 2.19 – 1.80 (6H), 1.70-1.66 (6H), 1.77-1.57 (4H), 1.28 (3H), 1.17 (3H). HRMS (ESI) for $C_{19}H_{32}O_2$ $[M + Na]^+$ calc. 315.4466, found 315.2278.

4.6.6 Synthesis of 46 alcohol electrolysis substrate



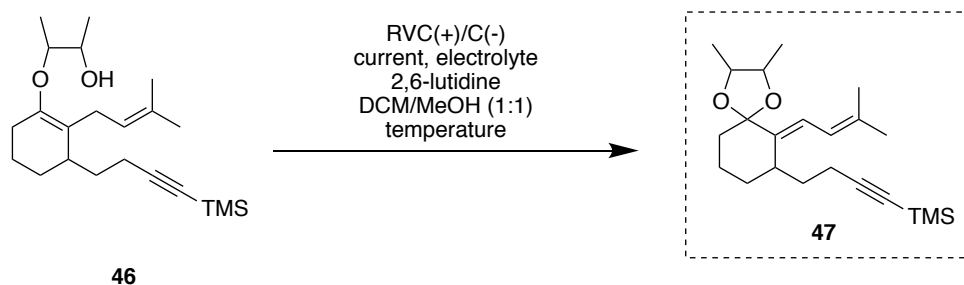
Scheme 4.37 Synthesis Route of 46

Synthesis of 46 3-((2-(3-methylbut-2-en-1-yl)-3-(4-(trimethylsilyl)but-3-yn-1-yl)cyclohex-1-en-1-yl)oxy)butan-2-ol



To a freshly made Grignard solution (0.4 M, 10 mL) at 0 °C was added CuI (recrystallized, 174 mg). Mixture was stirred at room temperature for 30 min, a coffee color suspension was formed. Mixture was then cooled to -78 °C. **49** (0.63 g, 2.66 mmol) in 15 mL THF was added in dropwise, followed by dropwise addition of BF₃-Et₂O (0.3 mL, 1 eq) was added in. Reaction was stirred for 15 h. 2,6-lutidine (1.55 mL, 5 eq) was added into the mixture before work up. The organic mixture was quenched with saturated NaHCO₃, washed with EDTA solution (pH=8, 0.1 M) until no blue color. Aqueous layer was washed with ether three times. The combined organic layer was dried over MgSO₄, filtered, and concentrated *in vacuo*. The crude product was chromatographed on silica gel (packed with 1% TEA) using 10% EtOAc in hexane as eluent to give 0.65 g of **46** and 2,6-lutidine mixture (53% yield product). ¹H NMR (500 MHz, Chloroform-d) δ 5.07 (t, 1H), 3.76 – 3.61 (m, 2H), 3.15 (dd, J = 14.7, 6.9 Hz, 1H), 2.72 – 2.66 (m, 1H), 2.48 (dd, J = 14.8, 7.4 Hz, 1H), 2.32 – 2.08 (m, 4H), 2.00 (dt, J = 15.8, 7.1 Hz, 1H), 1.86 – 1.74 (m, 1H), 1.73 – 1.65 (6H), 1.65 – 1.54 (m, 2H), 1.51 – 1.40 (m, 2H), 1.20 – 1.03 (6H). HRMS (ESI) for C₂₂H₃₈O₂Si [M + Na]⁺ calc. 385.6119, found 385.2511.

Electrolysis of **46** leading to **47**



A general electrolysis procedure (described before) was utilized, with reaction flask cooled at -78 °C. 11% of **47** can be isolated and characterized. ¹H NMR (500 MHz, Chloroform-d) δ 6.58 (d, J = 11.5 Hz, 1H), 6.12 (dt, J = 11.6, 1.6 Hz, 1H), 3.64 (ddq, J = 48.4, 7.9, 5.9 Hz, 2H), 3.12

(d, $J = 7.5$ Hz, 1H), 2.30 – 2.04 (m, 3H), 1.93-1.85 (1H), 1.85 – 1.77 (m, 6H), 1.71 – 1.58 (m, 2H), 1.57 – 1.45 (m, 4H), 1.24 (dd, $J = 57.8, 6.0$ Hz, 6H), 0.16 (s, 9H). HRMS (ESI) for $C_{22}H_{36}O_2Si$ $[M + H]^+$ calc. 361.6141, found 361.2538, $[M + Na]^+$ calc. 383.5960, found 383.2356.

Notes:

- (1) The additive to facilitate Michael condition serves as counter effect for cuprate, a sweet ratio of the reagent used need to be discovered.
- (2) A good quality of Grignard is required.

4.7 Spectra Data

See Appendix C

Reference

- (1) Sha, C.-K.; Lee, F.-K.; Chang, C.-J. Tandem Radical Cyclizations Initiated with α -Carbonyl Radicals: First Total Synthesis of (+)-Paniculatine. *Journal of the American Chemical Society* **1999**, *121* (42), 9875.
- (2) Amagata, T.; Doi, M.; Tohgo, M.; Minoura, K.; Numata, A. Dankasterone, a new class of cytotoxic steroid produced by a *Gymnascella* species from a marine sponge. *Chem Commun* **1999**, (14), 1321.
- (3) Hirst, G. C.; Johnson, T. O.; Overman, L. E. First total synthesis of Lycopodium alkaloids of the magellanane group. Enantioselective total syntheses of (-)-magellanine and (+)-magellaninone. *Journal of the American Chemical Society* **1993**, *115* (7), 2992.
- (4) Baraldi, P. G.; Achille, B.; Simoneta, B.; Gian Piero, P.; Vinicio, Z. 2,3a,5,6,7,7a-Hexahydro-3h,4h-benzothiophene-3,4-dione and cyclopenta [b]-tetrahydrothiophene-3,4-dione enolate anions as synthetic equivalents to cyclohex-2-enone and cyclopent-2-enone *c*-2-carbanions. *Tetrahedron Letters* **1984**, *25* (38), 4291.
- (5) Smith, J. A.; Moeller, K. D. Oxidative Cyclizations, the Synthesis of Aryl-Substituted C-Glycosides, and the Role of the Second Electron Transfer Step. *Organic Letters* **2013**, *15* (22), 5818.
- (6) Sperry, J. B.; Wright, D. L. The gem-Dialkyl Effect in Electron Transfer Reactions: Rapid Synthesis of Seven-Membered Rings through an Electrochemical Annulation. *Journal of the American Chemical Society* **2005**, *127* (22), 8034.
- (7) Redden, A.; Perkins, R. J.; Moeller, K. D. Oxidative Cyclization Reactions: Controlling the Course of a Radical Cation-Derived Reaction with the Use of a Second Nucleophile. *Angewandte Chemie International Edition* **2013**, *52* (49), 12865.
- (8) Yorimitsu, H.; Oshima, K. Recent progress in asymmetric allylic substitutions catalyzed by chiral copper complexes. *Angewandte Chemie International Edition* **2005**, *44* (29), 4435.
- (9) Goldsmith, P. J.; Teat, S. J.; Woodward, S. Enantioselective Preparation of β , β -Disubstituted α -Methylenepropionates by MAO Promotion of the Zinc Schlenk Equilibrium. *Angewandte Chemie International Edition* **2005**, *44* (15), 2235.
- (10) Tsunoda, T.; Suzuki, M.; Noyori, R. A facile procedure for acetalization under aprotic conditions. *Tetrahedron letters* **1980**, *21* (14), 1357.
- (11) Torok, D. S.; Figueroa, J. J.; Scott, W. J. 1,3-Dioxolane formation via Lewis acid-catalyzed reaction of ketones with oxiranes. *The Journal of Organic Chemistry* **1993**, *58* (25), 7274.
- (12) Hudson, C. M.; Marzabadi, M. R.; Moeller, K. D.; New, D. G. Intramolecular anodic olefin coupling reactions: a useful method for carbon-carbon bond formation. *Journal of the American Chemical Society* **1991**, *113* (19), 7372.
- (13) Redden, A.; Moeller, K. D. Anodic Coupling Reactions: Exploring the Generality of Curtin-Hammett Controlled Reactions. *Organic Letters* **2011**, *13* (7), 1678.
- (14) Smith, J. A., Washington University in St. Louis, 2015.

Chapter 5: Chan-Lam Coupling on

Microelectrode Array Application

While the chemistry in the previous chapters has been focused on the use of oxidative cyclization reactions in synthesis, it is important to note that the electrochemical methods have a broad range of applications. To broaden my own expertise with these systems, I undertook a side project aimed at using a mediated electrolysis reaction to selectively functionalize a complex microelectrode array. The key was to see how the same constant current electrolysis conditions employed in the studies above would automatically adjust to a completely different set of parameters. In this case, the potential at the anode would need to automatically adjust to the precursor for a Cu(II)-catalyst as opposed to an electron-rich olefin. But at its core the electrochemistry is the same.

(Sections of this chapter were taken from our paper: A., S. J.; Guoxi, X.; Ruozhu, F.; W., J. J.; D., M. K. C-Glycosides, Array-based Addressable Libraries, and the Versatility of Constant Current Electrochemistry. *Electroanalysis* **2016**, *28* (11), 2808)

5.1 Micro Electrode Array

To begin, the chemistry to be discussed will take advantage of microelectrode arrays that have 12544 electrodes/ cm². The electrodes are separated from each other by a distance of 33 microns¹. Each one of the electrodes can be independently used as a cathode, an anode, or as the working electrode for sweeping potential. Our group has been developing methods to build and

analyze libraries of molecules on these arrays². Because our emphasis is on synthesis, we will only discuss use of synthetic methods on the arrays here.

All synthetic methods on an array begin with a polymer that is used to coat the array and provides the functionality needed to add groups to the surface of the electrodes (Figure 5.1).

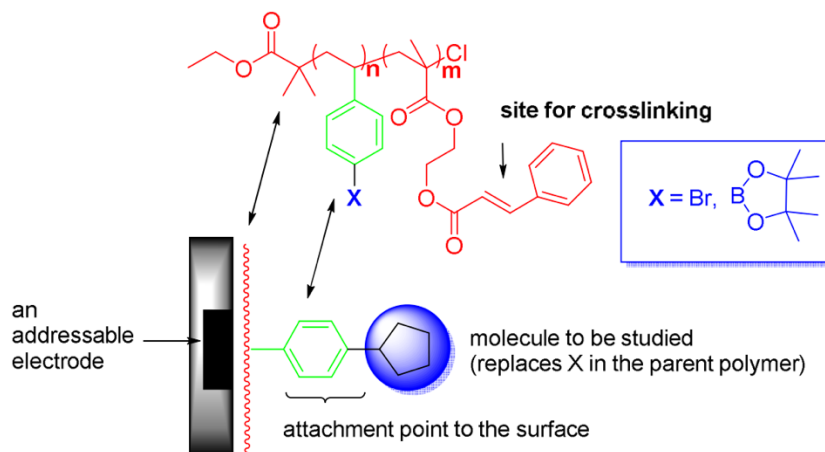


Figure 5.1 An Addressable Micro Electrode

The polymer we typically use contains two important sections. One is aryl bromide or aryl boronic ester that allows for modification of the surface, and the other is a cinnamate modified styrene moiety for cross-linking and adding stability to the surface¹.

Reactions are run on the surface of the array by utilizing the electrodes in the array to generate specific catalysts, substrates, or chemical reagents. An example of this chemistry will be highlighted below. For now, let's focus on the use of a catalyst on the array (the chemistry we will need below) and simply say that reactions are conducted on the array by taking a precursor for the catalyst and either reducing it or oxidizing it to form the catalyst at the electrodes surface. A "confining agent" is then added to the solution above the array that returns the catalyst to its

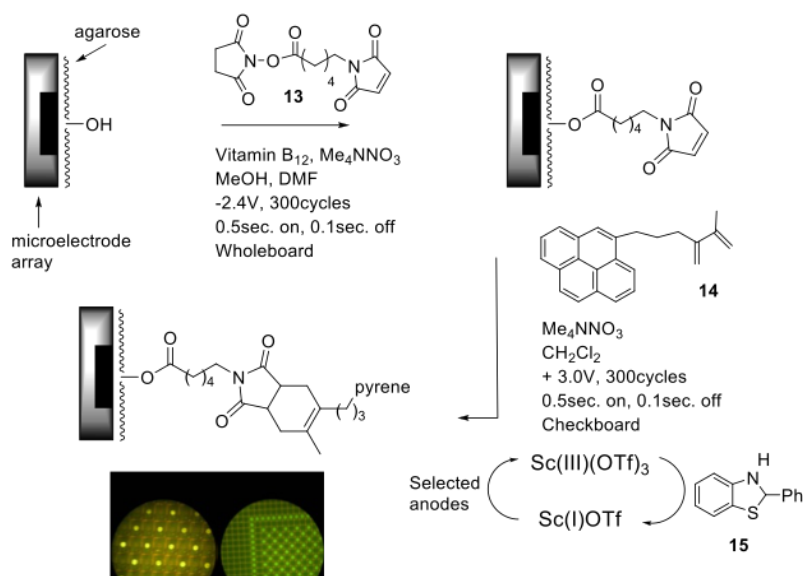
pre-catalyst state before it can migrate to sites on the array not selected for the reaction. By controlling the relative rates at which the catalyst is made at the electrodes and destroyed in solution one controls how far the catalyst can migrate from its site of origin. Again, an example of this approach will be presented below.

5.2 Binding Studies with C-Glycosides

The goal of the project I joined was to examine the chemistry of C-glycosides and in particular the chemistry between phenyl substituted C-glycosides that were antagonists of FimH³. To this end, Jake Smith in the group developed a synthesis of C-glycosides, built some of the molecules for testing, and had begun developing a strategy to probe their activity using the arrays.

5.2.1 Array-based metal catalyzed cross coupling method development

One of the first approaches taken for the placement of the C-glycosides on the array was the use of an array-based Diels-Alder reaction.^{2,3} The Diels-Alder reaction has been used on multiple occasions to attach biomolecules to the surface of electrodes because of its orthogonality to the functional groups found in peptides, DNA, or sugars.⁴ On an array, the reaction is confined to selected electrodes by using those electrodes to generate a Lewis acid. Scheme 5.1



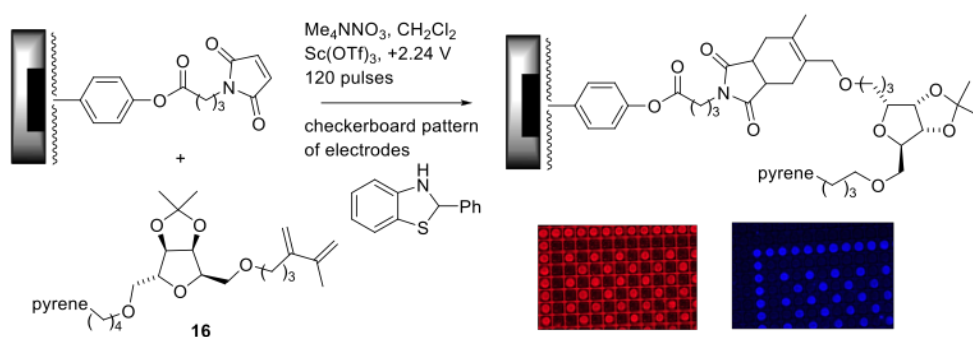
Scheme 5.1. A site-selective Diels-Alder reaction

The array was first coated with an agarose polymer that provided attachment sites from molecules above each electrode in the array. All of the electrodes in the array were then functionalized with a dienophile (**13**), using the previously reported esterification reaction strategy⁵. Once the dienophile was attached to the surface of every electrode in the array, the array was treated with the diene (**14**) and a solution that contained a Sm(I)-species, an electron-rich aryl ring (**15**) and an electrolyte for the subsequent electrolysis reaction. A checkerboard in a box pattern of electrodes were then used as anodes to oxidize the Sm(I)-species to the Sm(III)-Lewis acid needed to trigger the Diels-Alder reaction. The electron-rich aryl ring (**15**) served as a confining agent for the reaction by reducing the Sm(III)-Lewis acid generated at the selected electrodes before it could migrate to sites on the array that were not selected for the reaction.

The whole process amounted to a nice example of the versatility associated with a constant current electrolysis. The electrochemical cell for the array reaction is a simple, thin-film flow cell that consists of the array on one side, a Pt-counter electrode on the other, and the solution in

between. The array potential is then set as being either positive or negative relative to the counter electrode, and then a constant current passed between the electrodes. The potential at the electrodes is allowed to float to match that of the substrate in solution. To place the dienophile on the array, the array was set at a potential negative to the counter electrode and then allowed to float so that it matched the reduction of vitamin B12 leading to a base needed for esterification. To conduct the Diels-Alder reaction, the array was set at a potential positive to the counter electrode and then allowed to float so that it matched the oxidation potential of the Sm(I). The electrochemical experiments were essentially identical to the direct, bulk electrolyses described in the previous chapters.

In order to use the Diels-Alder reaction to place a sugar onto an array, both the surface of the array and the C-glycoside derivative needed to be altered accordingly. In this case, the array was functionalized with a dienophile in a manner directly analogous to the previous experiment with one exception (Scheme 5.2). In this case, the diblock copolymer that contained a cinnamate



Scheme 5.2. The first site-selective placement of a C-glycoside on the arrays

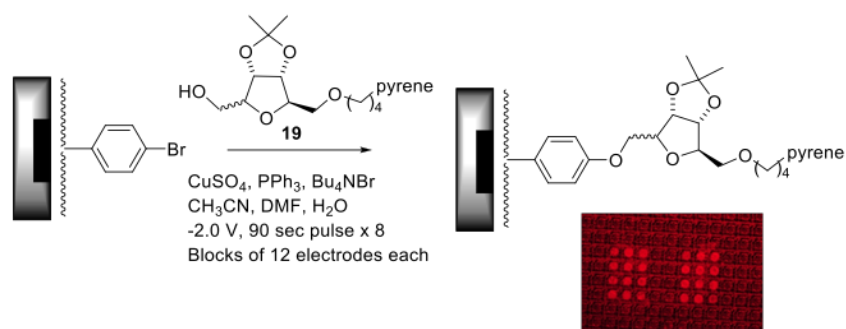
functionalized methacrylate block and a hydroxylated polystyrene block described above was used in place of the agarose coating on the array^{6,7}. The hydroxyl-substituted aryl ring of the polystyrene block was then used to attach molecules to the surface of the array. The dienophile was attached to the coating proximal to every electrode in the array and then the Diels-Alder reaction with a “properly functionalized” C-glycoside diene (**16**) conducted with a checkerboard in a box pattern of electrodes in the same manner as described above. The C-glycoside was labeled with a pyrene group so that the success of the reaction could be determined with the use of a fluorescence microscope. The quality of the reaction can be seen in the image provided. A bright fluorescent spot appears by each electrode used for the oxidation. The red fluorescence from the array is indicative of a pyrene dimer and therefore consistent with a high concentration of the C-glycoside by the selected electrodes. At the same time, no fluorescence appears in between the electrodes or at any unwanted site on the array, even when the array was examined for the presence of pyrene monomer (blue). Clearly, both the reaction and the confinement strategy worked perfectly.

While the Diels-Alder strategy worked well, the overall approach was less than ideal, in that both the array and the C-glycoside had to be pre-functionalized. While this was not a large problem with respect to the array, the use of a “properly functionalized” C-glycoside (**16**) required a multistep synthesis of the substrate. Clearly, it would be better if such a separate synthesis could be avoided and a method for directly placing a fluorescently labeled C-glycoside derivative on the array developed.

At the time the Diels-Alder reaction was being developed, other methods for functionalizing diblock copolymer coating on the arrays were taking hold. One in particular was quite intriguing. In this chemistry, alcohol substrates were directly added to the diblock copolymer coating on the

array that contained a bromostyrene block. In this case, a Cu(I)-catalyst generated on the arrays by the reduction of a Cu(II) salt triggered addition to the surface. Once again, the reactions only occurred on the surface proximal to the electrodes used to generate the active catalyst. Oxygen was used as the confining agent to oxidize the Cu(I)-catalyst in the solution above the array, before it could migrate to a non-selected site.

The extension of this chemistry to the use of a C-glycoside is illustrated in Scheme 5.3. The reaction used the pyrene labeled alcohol (**19**) already available from the earlier synthesis.



Scheme 5.3 Addition of a C-glycoside based alcohol nucleophile to the surface of an array.

With the nucleophile in hand, an array having 12,544 electrodes/ cm² was coated with the diblock copolymer, and then blocks of twelve electrodes each, used for the generation of Cu(I) in the presence of the alcohol nucleophile and air. The success of the reaction can be seen in the image provided. Once again, the C-glycoside was placed onto the array by the electrodes selected, and once again the presence of the confining agent kept the C-glycoside from being placed at sites not selected for the reaction. The same reductive constant current reaction setup used on the arrays for the generation of base (Scheme 5.1), was this time used to make Cu(I), with the potential at the electrode surface automatically adjusting to match that needed for the reduction of Cu(II).

5.2.2 Fluorescence Linker Synthesis

While the chemistry looked very reasonable, it was not directly compatible with the glycosides desired for the initial study. These molecules are shown in Figure 5.2.

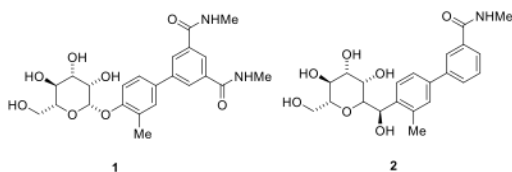
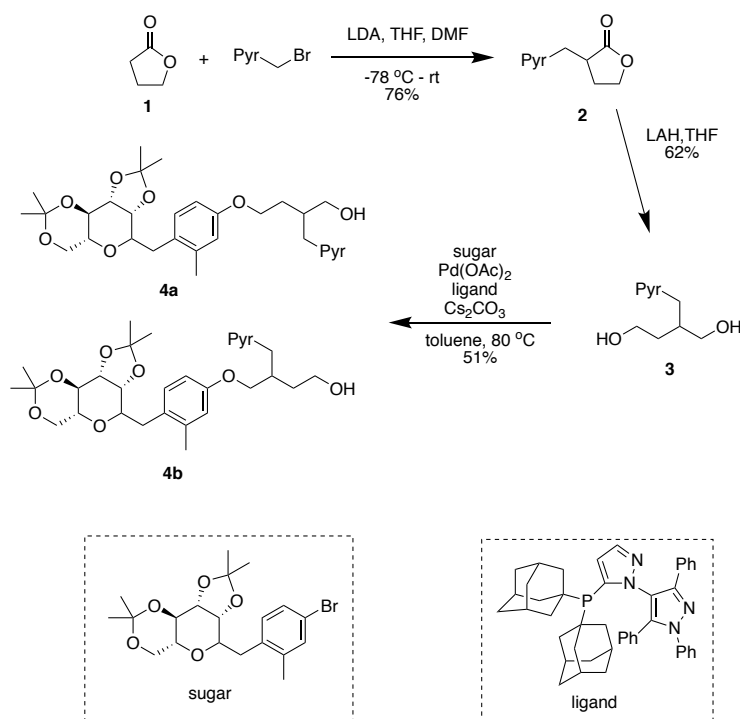


Figure 5.2 biphenyl substituted C-glycoside

Both of these molecules contained a phenyl substituent on the anomeric carbon with 2 being stable C-glycoside derivative. The mannose part of the sugar is responsible for binding. If the primary alcohol is added to the array, then there is no place to attach a fluorescent group for determining if a reaction to place the molecules on the array has been successful. In fact, efforts along these lines met with failure during subsequent signaling experiments, and it was unclear as to whether the molecules no longer bound because of the surface of the array or whether the molecules were never placed on the array.

It was at this point that I joined the project. We figured that the most direct method for resolving these issues would be to design and build a linker that would allow for both removal of the C-glycoside from immediate contact with the surface and for determining its presence on the array (Scheme 5.4).



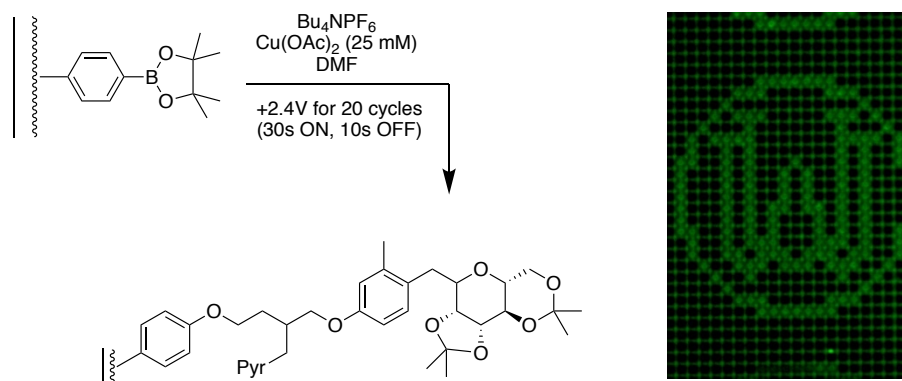
Scheme 5.4 Sugar-Pyrene Linker

The linker was made by alkylating lactone **1** with pyrene bromide in 76% yield followed by reduction to the diol in a yield of 62%. The diol then can be coupled to the C-Glycoside through Pd catalyzed Buchwald type coupling⁹ to yield **4a/4b** with 51% yield. In this case, synthetic expediency led to the formation of a mixture of labeled molecules. However, the two molecules differed only in the specific location of the fluorescent label, a detail that was not important for the subsequent study. The key was that the C-glycoside was both tagged with a fluorescent group so that the quality of the array reaction could be monitored, and that the nucleophile used was a simple alcohol. Hence, in future efforts there would be no need to conduct extra synthetic steps to add the functionality for attachment to an array.

5.2.3 Placement of C-Glycoside onto the Array via Chan-Lam coupling

At this point, we decided to utilize the borate ester surface for the placement reaction because it is superior for use in signaling studies. The placement of alcohols onto a borate ester functionalized array does not require utilization of a Cu(I)-catalyst (like in the addition to the bromostyrene derived surface), but rather a Cu(II)-catalyst and the Chan-Lam coupling reaction. Cu(II) is known to oxidize alcohols, so in this case the presence of excess nucleophile can serve as a confining agent to make sure that the Chan-Lam coupling reaction only occurs at sites selected for the oxidative catalytical cycle conversion of Cu(I) to the required Cu(II)-catalyst. The reaction worked very well with the more complex sugar and borate ester surface (Scheme 5.5, a “W” in a circle pattern of electrodes was used for the oxidation). As in the earlier reactions, the fluorescently labeled C-glycoside was only placed by the electrodes used for the reaction.

Once again, the chemistry demonstrated the versatility of the constant current electrolysis. To change from a Cu(I)-catalyzed reaction on the array to a Cu(II)-catalyzed reaction on the array, one only needs to reverse the polarity of the electrodes, pass current through the reaction, and allow the working electrodes on the array to automatically adjust to the substrate in solution.



Scheme 5.5 Chan-Lam Coupling on Micro Electrode Array

5.2.4 Binding Study Between C-Glycoside and Protein

This study is not a major work for this chapter. Reference can be found below.

With the ability to both make C-glycosides and place them by selected electrodes in an addressable microelectrode array, attention was quickly turned toward determining if the resulting C-glycoside modified arrays were compatible with the analytical experiments the arrays are being developed for^{2,11}. In these experiments, a microelectrode array that has been functionalized with potential ligands for a receptor is typically inserted into a solution that contains a redox mediator and a specific concentration of a targeted receptor. A current is established for the redox mediator at each of the electrodes in the array. If the receptor in solution binds a molecule on the surface of the array, it changes the capacitance of the surface above the electrode associated with the molecule. This causes a change in current that can then be monitored. By varying the concentration of the receptor in solution, a plot of the change in current relative to the amount of receptor used can be accumulated and information about the strength of the interaction between the molecule and the receptor obtained.

A preliminary look at signaling

The compatibility of the C-glycoside functionalized surface with this experiment was demonstrated by taking the array functionalized in Scheme 5.3, treating it with a solution containing both a ferrocyanide/ ferricyanide redox couple, and varying concentrations of streptavidin, and then monitoring the current associated with the redox mediator at various sites on the array. Streptavidin is known to undergo strong non-specific binding interactions with sugar surfaces, enough to interfere with streptavidin–biotin interactions¹². In fact, we learned that we could not use the streptavidin–biotin interaction to probe the use of arrays with sucrose

surfaces because of the extent of background binding observed. The data for the current experiment is shown in Figure 5.3. In this figure, the current measured at three blocks of electrodes functionalized with the C-glycoside is plotted along with data taken from three blocks of electrodes that are only functionalized with the diblock copolymer coating used for the synthetic experiment. The currents measured are given as relative currents with the highest current measured on the array given a value of zero and the lowest a value of 1. In this way, interactions between the streptavidin and the C-glycoside functionalized surface that block the redox mediator from reaching the electrode below afford positive changes to the curve. The data for the interaction between the streptavidin and the C-glycoside functionalized surface is shown in blue. The error bars show the spread in data from the three blocks of electrodes.

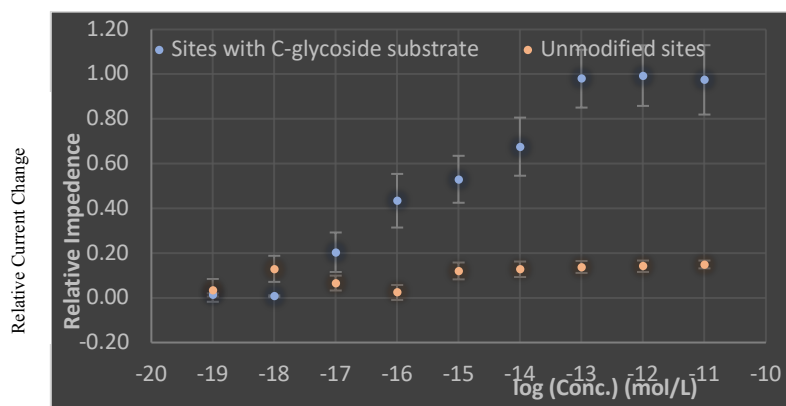


Figure 5.3. A preliminary signaling study.

The red line was generated from three blocks of electrodes that were left unfunctionalized. Once again, the error bars show the spread in data associated with those blocks of electrodes.

From the start it was clear that the presence of the C-glycoside functionalized diblock copolymer did lead to an increased interaction between streptavidin and the surface. The data showed a clear difference in current between the blocks of electrodes functionalized with the C-glycosides and

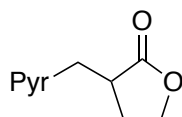
the blocks of electrodes that were not similarly functionalized. No binding occurred with the unfunctionalized polymer and the same maximum current for the redox mediator was obtained for each concentration of receptor used. Initially, roughly the same current was measured for the blocks of electrodes functionalized with the C-glycoside, indicating that the polymer was easily permeable to the redox mediator. However, this changed as the concentration of receptor was increased indicating that a binding event between streptavidin and the functionalized surface did occur. The strength of this binding interaction was not a complete surprise since there are multiple C-glycosides associated with the surface of the electrodes. Multiple ligands on the surface of an electrode have been shown to amplify binding signals.

While determining the exact nature of the binding interaction between the surface and the streptavidin (a direct interaction with the sugar or an interaction with the swelled polymer) would require additional studies, the data presented does demonstrate that the presence of the C-glycoside on the array is compatible with the analytical approach taken. When combined with the synthetic studies described, it is clear that the chemistry needed for using the arrays to examine binding interactions, like the one between mannose derivative **2** and the FimH receptor

Reference from Smith, J., Ph.D. Dissertation, Washington University in St. Louis, **2015**.

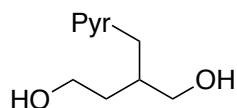
5.3 Experimental Section

Synthesis of 2 5-(2-(2-oxotetrahydrofuran-3-yl)acetyl)pyrrolidin-2-one



To a solution a triethylamine (1.55 mL, 1.1 equiv) in 80 mL THF at -78 °C, nBuLi (6.88 mL, 1.6 M in hexane, 1.1 equiv) was added in dropwise. Mixture was stirred for 15 min. Dihydrofuran-2(3H)-one **1** (0.76 mL, 1 equiv) in 13 mL THF was added in. Mixture was stirred for 30 min. Pyrene-CH₂-Br (2.95 g, 1 equiv) in 43 mL DMF was added in. Mixture was stirred for 4 h. Upon completion, the mixture was quenched with NH₄Cl (aq) and diluted with CH₂Cl₂. Organic layer was separated and aqueous layer was extracted with CH₂Cl₂ by 3 times. Combined organic layers were dried over MgSO₄. The crude product was purified by flash chromatography through silica gel to afford **2** (78% yield). The spectra data matched the previously published ¹H NMR.

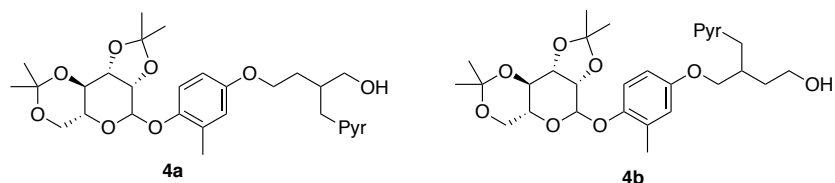
Synthesis of **3** 5-(5-hydroxy-3-(hydroxymethyl)pentanoyl)pyrrolidin-2-one



To a flask containing lithium aluminum hydride powder (0.584 g, 2.5 equiv) in 142 mL THF solution, under argon, at 0 °C, **2** in 43 mL THF was added in dropwise. Reaction mixture was stirred overnight. 80 mL Rochella salt (half saturated) was added in. Mixture was stirred overnight. Most THF was removed on rotovap. Residue was extracted with DCM. Organic layer was separated and aqueous layer was extracted with DCM by 3 times. Combined organic layers were dried over MgSO₄. The crude product was purified by flash chromatography through silica gel to afford **3** (1.54 g, 82% yield). ¹H NMR (300 MHz, CDCl₃) δ 8.29 (d, J = 9.3 Hz, 1H), 8.10-8.18 (m, 4H), 8.06 – 7.96 (m, 3H), 7.87 (d, J = 7.8 Hz, 1H), 3.88 – 3.57 (m, 4H), 3.36 (ddd, J = 48.2, 13.8, 7.6 Hz, 2H), 2.29 (m, 1H), 1.81(dt, J = 7.4, 4.5 Hz, 2H); ¹³C NMR (75 MHz, CDCl₃) δ 134.7, 131.4, 130.8, 130.0, 129.1, 128.2, 127.5, 127.4, 126.8, 125.9, 125.1, 125.0, 124.8, 124.6,

123.4, 109.9, 65.5, 61.2, 41.5, 35.7, 35.6; IR (neat, cm⁻¹) 3294, 2903, 2847, 1051, 1006, 953, 838, 753, 706, 680; HRMS (ESI) calcd for C₂₁H₁₈O₂ [M + H]⁺ 305.1532, found 305.1536.

Synthesis of 4a/4b



To a flask containing sugar bromide (79.9 mg, 1 equiv) and **3** (165 mg, 3 equiv) was added Pd(OAc)₂ (4 mg, 10 mol%), ligand (24 mg, 20 mol%) as well as Cs₂CO₃ (87.9 mg, 1.5 equiv). System was charged under argon. 0.5 mL of toluene was added in. The reaction mixture was brought to reflux for 20 h. Upon completion, the mixture was quenched with water and diluted with DCM. Organic layer was separated and aqueous layer was extracted with DCM by 3 times. Combined organic layers were dried over MgSO₄. The crude product was purified by flash chromatography through silica gel (eluted 30% EtOAc in hexane) to afford **4a** and **4b** mixture (62 mg, 51% yield). ¹H NMR (300 MHz, CDCl₃) δ 8.32 (d, J = 9.2 Hz, 1H), 8.23 – 7.93 (m, 7H), 7.85 (d, J = 7.9 Hz, 1H), 7.24 (d, J = 10.1 Hz, 1H), 6.76 (s, 1H), 6.64 (s, 1H), 4.99 (d, J = 6.0 Hz, 1H), 4.92 – 4.72 (m, 1H), 4.49 (s, 1H), 4.40 – 4.22 (m, 1H), 4.22 – 3.94 (m, 5H), 3.89 (s, 1H), 3.83 – 3.71 (m, 1H), 3.71 – 3.49 (m, 1H), 3.41 (dd, J = 23.3, 13.6 Hz, 1H), 3.19 (d, J = 12.8 Hz, 2H), 2.56 (s, 1H), 2.36 (s, 1H), 2.29 – 2.14 (m, 3H), 2.05 (s, 1H), 1.91 (d, J = 6.3 Hz, 2H), 1.72 (s, 1H), 1.46 (d, J = 9.4 Hz, 5H), 1.42 – 1.30 (m, 5H), 1.26 (t, J = 7.1 Hz, 2H); ¹³C NMR (75 MHz, CDCl₃) δ 171.1, 158.1, 137.3, 136.9, 134.4, 131.3, 130.8, 130.0, 129.0, 128.6, 128.3, 127.8, 127.4, 126.9, 126.7, 126.1, 125.8, 124.9, 124.8, 124.6, 123.4, 116.4, 112.4, 112.2, 112.0, 109.1, 109.0, 87.1, 86.4, 83.2, 81.5, 73.6, 67.1, 60.9, 60.4, 57.1, 56.9, 37.7, 35.2, 26.9, 25.1,

14.2; IR (neat, cm⁻¹) 3338, 2930, 2360, 1726, 1604, 1453, 1380, 1288, 1073; HRMS (ESI) calcd for C₄₂H₄₈O₈ [M + Na]⁺ 703.3241, found 703.3245.

Reactions Performed on 12K-microelectrode Array: Cu(II)

3.0 mg of C-glycoside **4a/4b** and 15 mg tetrabutylammonium hexafluorophosphate were dissolved into 300 μ L of DMF in an Eppendorf tube as well as 15 μ L of 25 mM solution of Cu(OAc)₂. The 12K-array chip coated with diblock copolymer (with aryl bromide unit) was exposed to 125 μ L of the reaction solution and selected electrodes were grounded (WashU pattern), while a potential of +2.4 V was applied to the auxiliary electrode for 20 pulses. The slide was washed with EtOH. The whole process was repeated to get a bright enough image under the observation of a fluorescence microscope.

5.4 Spectra Data

See Appendix D

Reference

- (1) Yeh, N.-H.; Medcalf, M.; Moeller, K. D. Organic Electrochemistry and a Role Reversal: Using Synthesis To Optimize Electrochemical Methods. *Journal of the American Chemical Society* **2018**, *140* (24), 7395.
- (2) Graaf, M. D.; Moeller, K. D. Introduction to Microelectrode Arrays, the Site-Selective Functionalization of Electrode Surfaces, and the Real-Time Detection of Binding Events. *Langmuir* **2015**, *31* (28), 7697.
- (3) A., S. J.; Guoxi, X.; Ruozyu, F.; W., J. J.; D., M. K. C-Glycosides, Array-based Addressable Libraries, and the Versatility of Constant Current Electrochemistry. *Electroanalysis* **2016**, *28* (11), 2808.
- (4) Palomo, J. M. Diels–Alder Cycloaddition in Protein Chemistry. *European Journal of Organic Chemistry* **2010**, *2010* (33), 6303.
- (5) Stuart, M.; Maurer, K.; Moeller, K. D. Moving known libraries to an addressable array: A site-selective hetero-Michael reaction. *Bioconjugate chemistry* **2008**, *19* (8), 1514.
- (6) Bains, G. K.; Kim, S. H.; Sorin, E. J.; Narayanaswami, V. The extent of pyrene excimer fluorescence emission is a reflector of distance and flexibility: analysis of the segment linking the LDL receptor-binding and tetramerization domains of apolipoprotein E3. *Biochemistry* **2012**, *51* (31), 6207.
- (7) Bartels, J.; Lu, P.; Maurer, K.; Walker, A. V.; Moeller, K. D. Site-Selectively functionalizing microelectrode arrays: The use of Cu (I)-catalysts. *Langmuir* **2011**, *27* (17), 11199.
- (8) Fellet, M. S.; Bartels, J. L.; Bi, B.; Moeller, K. D. Site-selective chemistry and the attachment of peptides to the surface of a microelectrode array. *Journal of the American Chemical Society* **2012**, *134* (40), 16891.
- (9) Gowrisankar, S.; Sergeev, A. G.; Anbarasan, P.; Spannenberg, A.; Neumann, H.; Beller, M. A General and Efficient Catalyst for Palladium-Catalyzed C–O Coupling Reactions of Aryl Halides with Primary Alcohols. *Journal of the American Chemical Society* **2010**, *132* (33), 11592.
- (10) Rao, K. S.; Wu, T.-S. Chan–Lam coupling reactions: synthesis of heterocycles. *Tetrahedron* **2012**, *38* (68), 7735.
- (11) Smith, J. A., Washington University in St. Louis, 2015.
- (12) Houen, G.; Hansen, K. Interference of sugars with the binding of biotin to streptavidin and avidin. *Journal of immunological methods* **1997**, *210* (2), 115.

Chapter 6: Conclusion and Future Work

6.1 An Overview

In general, the work reported here has sought to provide improved insight into how we think about and optimize anodic cyclization reactions. After laying a foundation for this effort in the first chapter, the second chapter focused on detailing the importance of controlling the reactivity of the intermediate generated downstream of the second oxidation step in a two-electron oxidative cyclization. Specifically, we noted that an elimination reaction involving the cation generated from the second oxidation can lead to over-oxidation products. Trapping the cationic intermediate or slowing the elimination can prevent these issues. The observations made completed the picture of a three-step working model for the reactions that allows us to make observations about the products obtained from any given reaction and then propose the step in the reaction that is problematic along with a potential solution. While all three steps in the reaction can play a critical role in a cyclization, the first step is still the most critical. If it does not go well, then the others have no chance. With that in mind, Chapter 3 focused on the role the key reactive intermediate plays in the success of the initial cyclization. Anodic coupling reactions can be channeled down pathways that involve either radical cations or radical intermediates. Previous work had shown situations where the radical intermediate was preferred. In this thesis, we highlight an example that benefits from the use of a radical cation pathway and a strategy by which the same overall synthetic route can be used to access either approach. In Chapter 4, work toward determining whether an oxidative radical or a radical cation pathway is preferred for oxidative cascade type reactions is presented. While a successful tandem

cyclization has not yet been accomplished, preliminary data suggested that the specific substrates studied were hampered by a reversible cyclization and competitive reactions involving the initially generated reactive intermediate and the trapping group that was supposed to terminate the final cyclization. This result indicated the need for a more general approach to studying the possibility of a tandem cyclization. Chapter 5 departs from the chemistry of oxidative cyclization reactions and applies the same constant current electrolysis strategy to the synthesis of complex molecular surfaces on a microelectrode array. The goal was to show how electrochemical methods that are traditionally used in solution phase synthesis can be expanded to include applications of the surface of a microelectrode array destined for application in bioanalytical chemistry.

6.2 Continuing Studies

6.2.1 A final solution to synthesis of Artemisolide

In Chapter 3, we concluded that the coupling of an enol ether and a furan could be used to synthesize seven-membered rings like the one in the natural product artemisolide if the substrate contained a conformational constraint in the tether between the enol ether and the furan that could accelerate the reaction enough to overcome the competitive elimination of a proton from the carbon alpha to the radical cation. We demonstrated that the reaction might need to be channeled down the radical cation pathway since an oxidative radical approach led to a competitive H-atom abstraction reaction that could not be avoided. For these studies, the conformational constraint used was a phenyl ring. However, the actual structure of artemisolide lacks this phenyl ring, and instead has a tertiary alcohol group on the central seven-membered ring. Hence, an alternative conformational constraint is needed. In principle, a cis-double bond

would accomplish the same thing as the phenyl ring and provide a more relevant synthetic handle for the natural product synthesis.

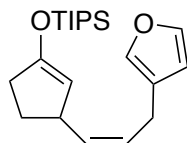


Figure 6.1 Cis double bond as constrain in substrate

6.2.2 An remain-questioned solution to electrochemical Tandem Cyclization with α , β disubstituted moieties

As concluded in chapter 4, the tandem cyclization reaction derived from **46** was conducted at low temperature in order to keep the initial trapping of the radical cation by an alcohol closed and thus furnish the radical intermediate. The reaction led to product **47** suggesting the presence of a cyclopropane formation pathway that competed successfully with the desired pathway. It is possible that the reaction represents the formation of kinetic products that would be favored by the use of lower temperature. This suggests that it may be possible to gain access to the desired product if it is the thermodynamically favored product. To test this question would require a higher temperature. To this end, a methoxymethyl (MOM) protected enol ether substrate would provide an alternative way to generate radical intermediate. The decomposition of this substrate would lead to the radical intermediate in a fashion that would not be reversible. Hence, there would be no need to lower the temperature of the reaction. One potential pathway forward would be to pursue this substitution pattern for the substrate.

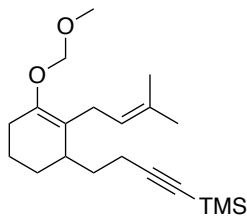
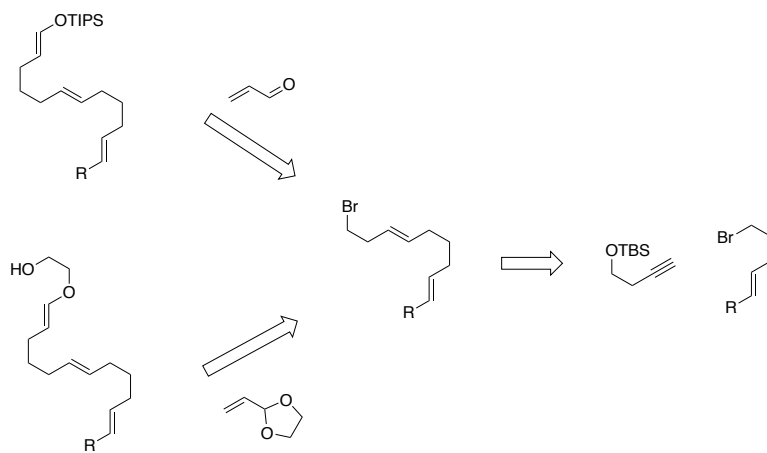


Figure 6.2 MOM protected Tandem cyclization substrate

6.2.3 A fast and systematic way to study electrochemical Tandem Cyclization

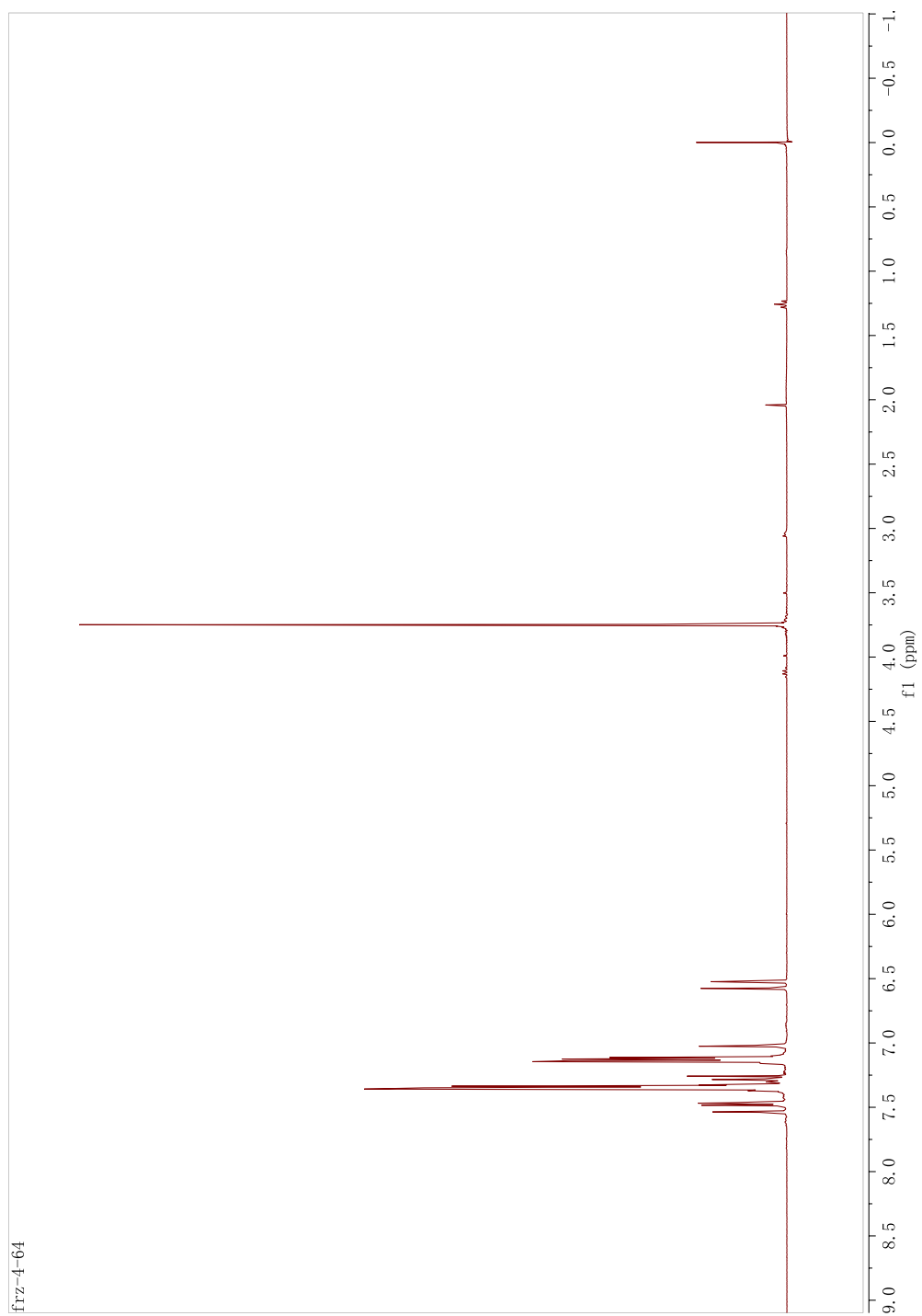
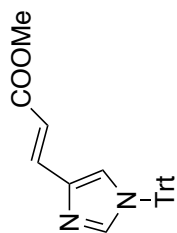
As described in chapter 4, efforts to determine the parameters needed to control an oxidative cascade type reaction have been hampered by the nature of the substrates utilized. They were selected because of their relationship to known processes. However, the synthesis of the substrates proved complex and hindered exploration of the reactions, and the location of the terminating olefin in the substrate complicated the study.

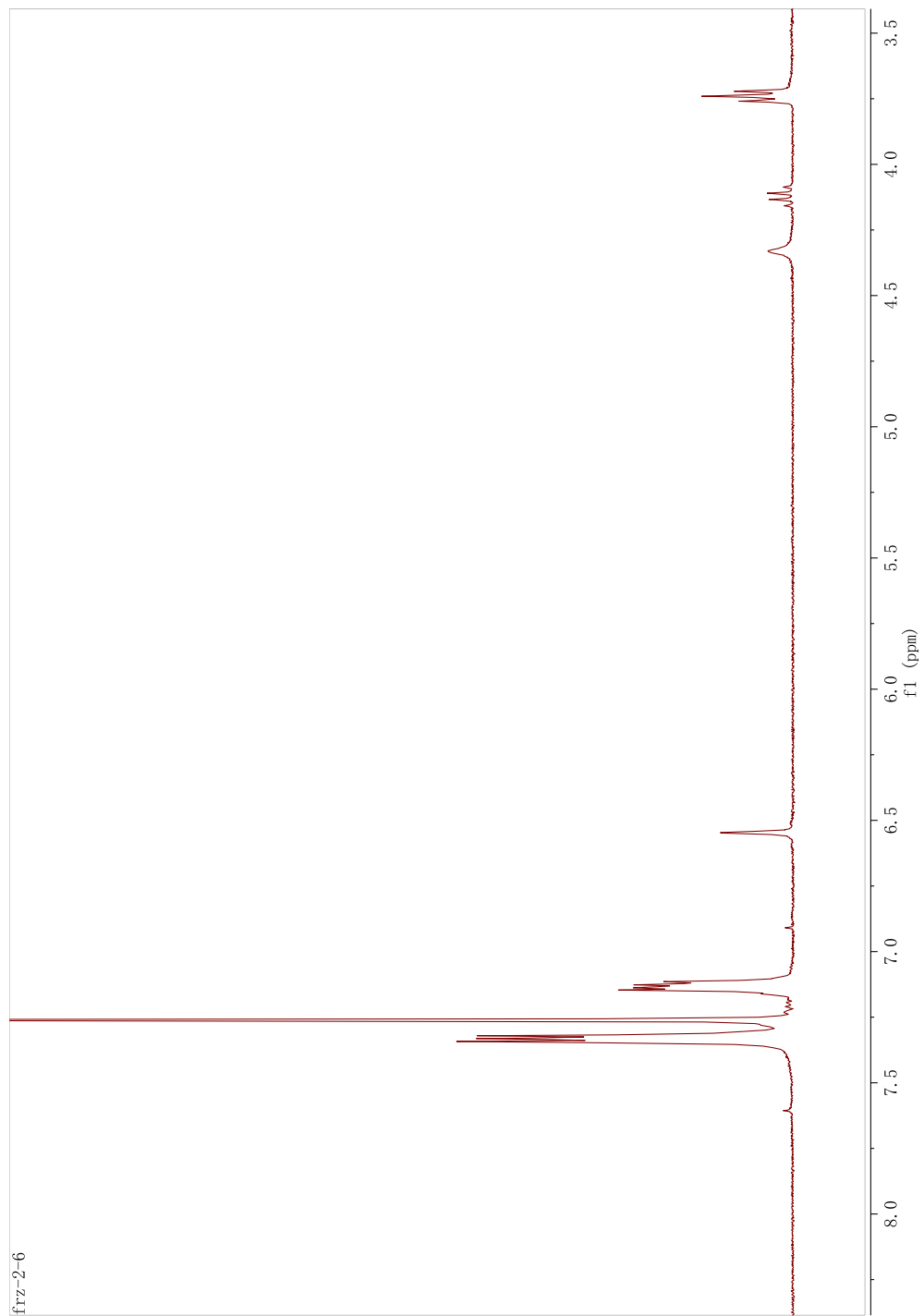
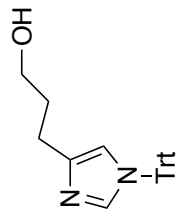
To move forward with the chemistry, it would be helpful to study a substrate that was both easier to make and cleaner in terms of the mechanistic possibilities available to the reactive intermediates involved. One strategy would be to study the substrates shown in Scheme 6.1. In these cases, the first cyclization reaction has just one option. In addition, the synthesis of the substrate avoids the more complex cyclic enones used in Chapter 4. In this way, the acyclic version of this oxidative radical vs radical cation intermediate pair would provide a quicker probe for answering questions about which intermediate is required for the electrochemical tandem cyclization.

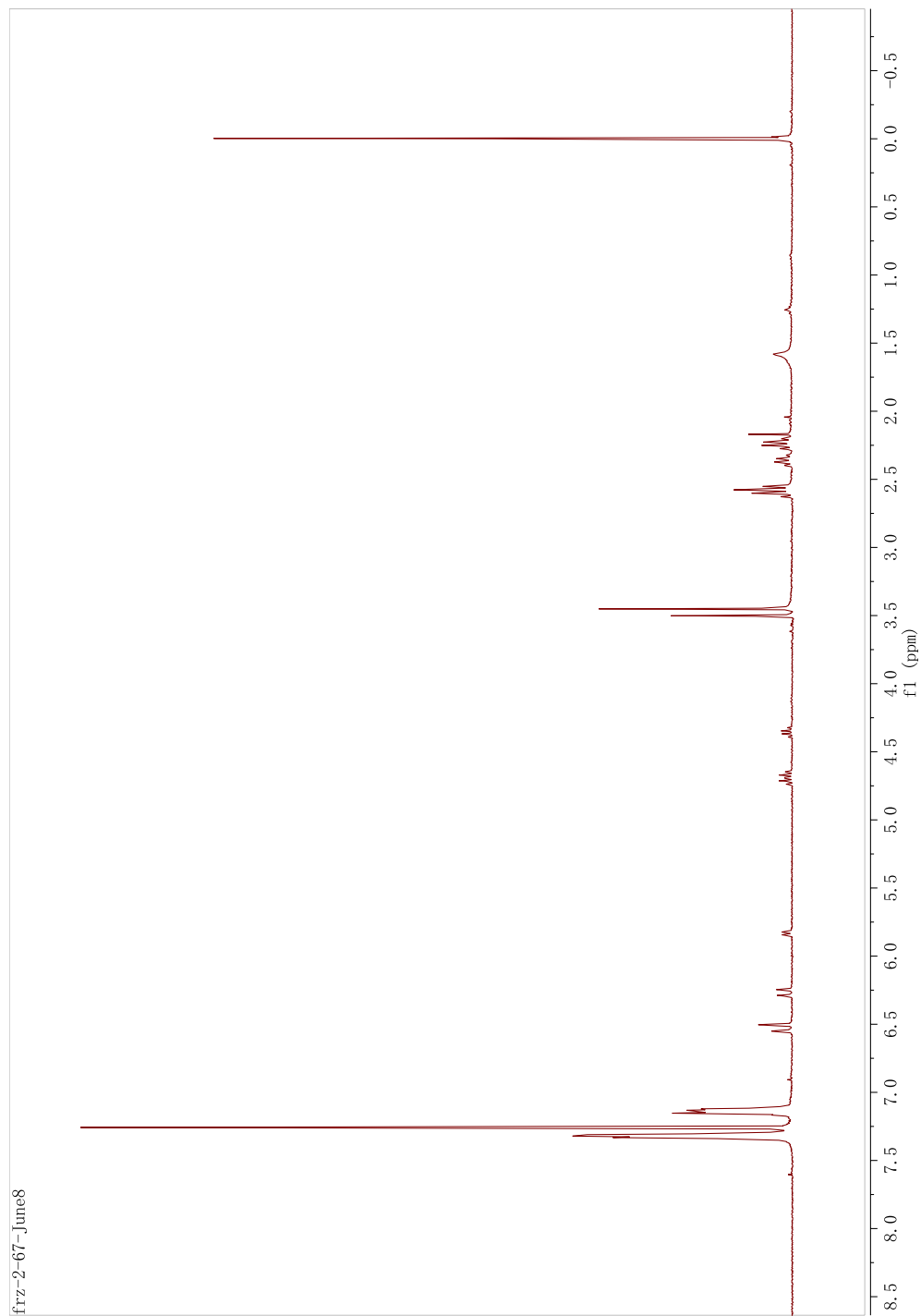
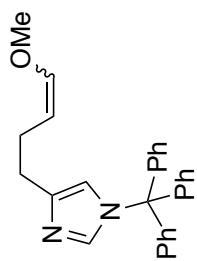


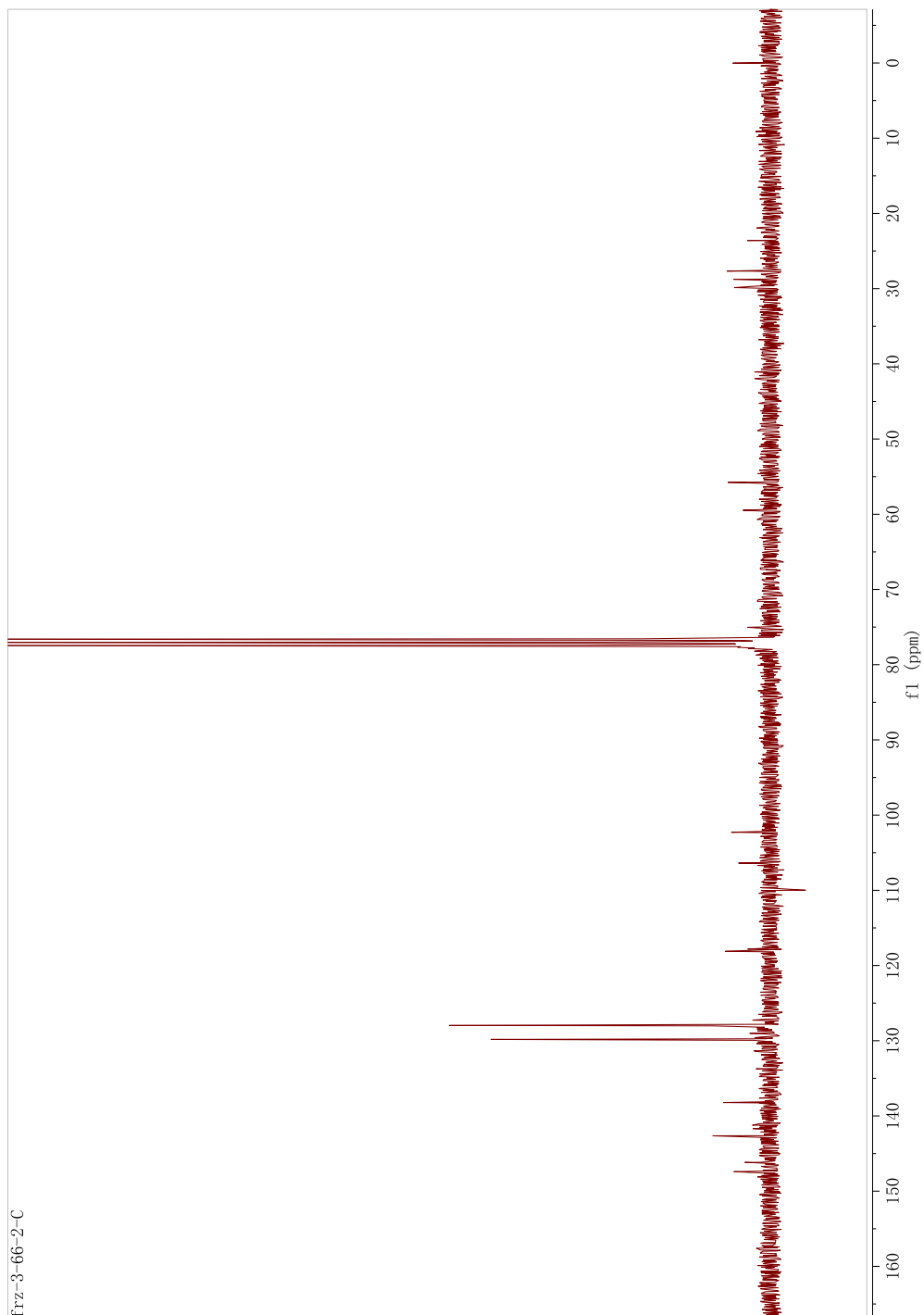
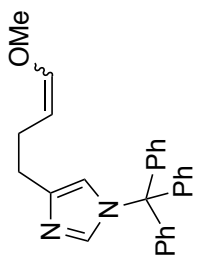
Scheme 6.1 Acyclic version of substrates for electrochemical Tandem cyclization

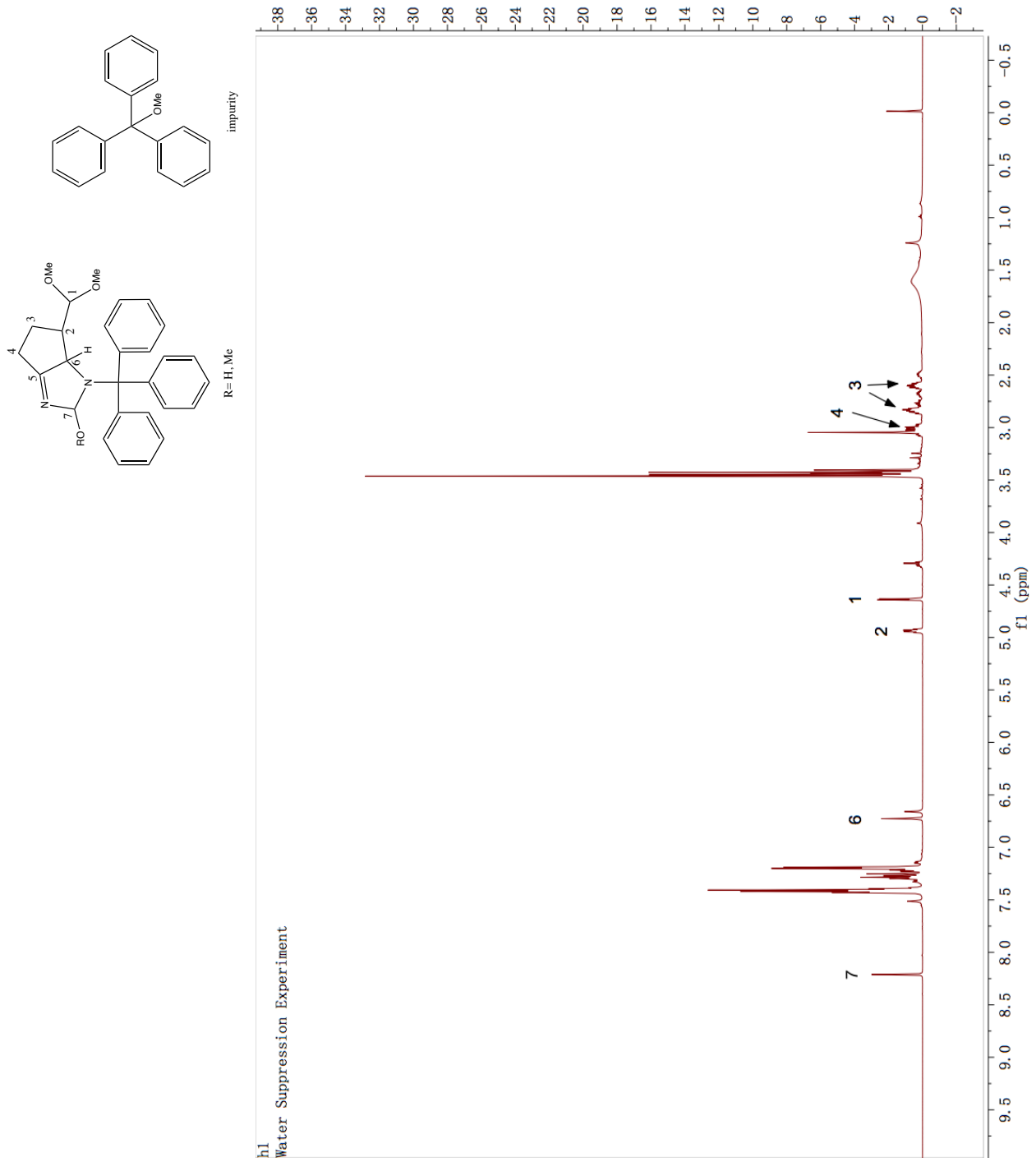
Appendix A

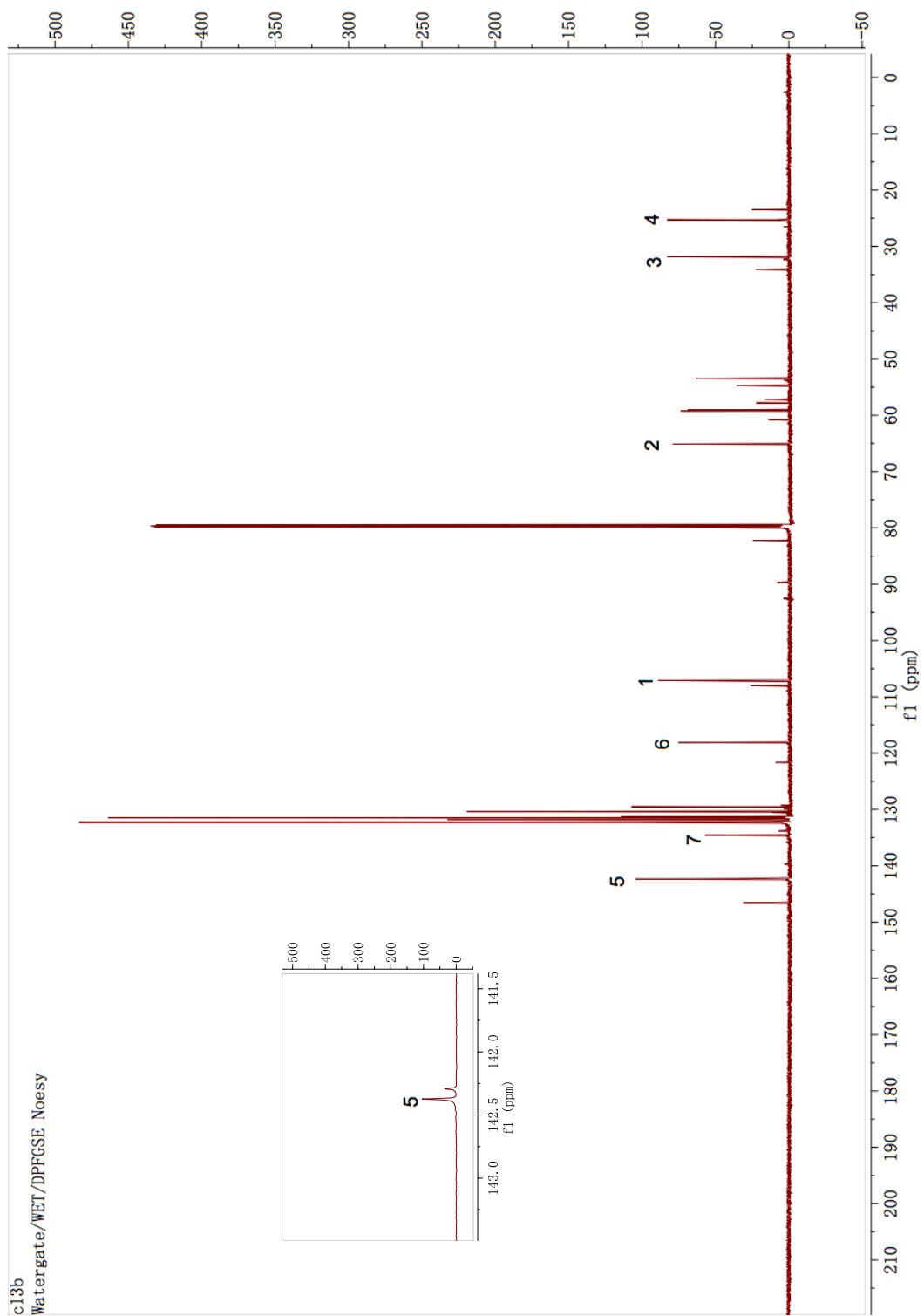
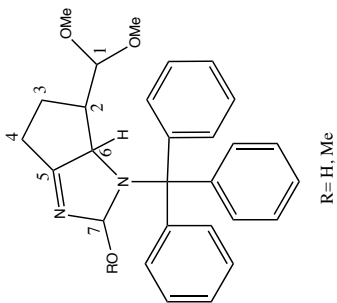


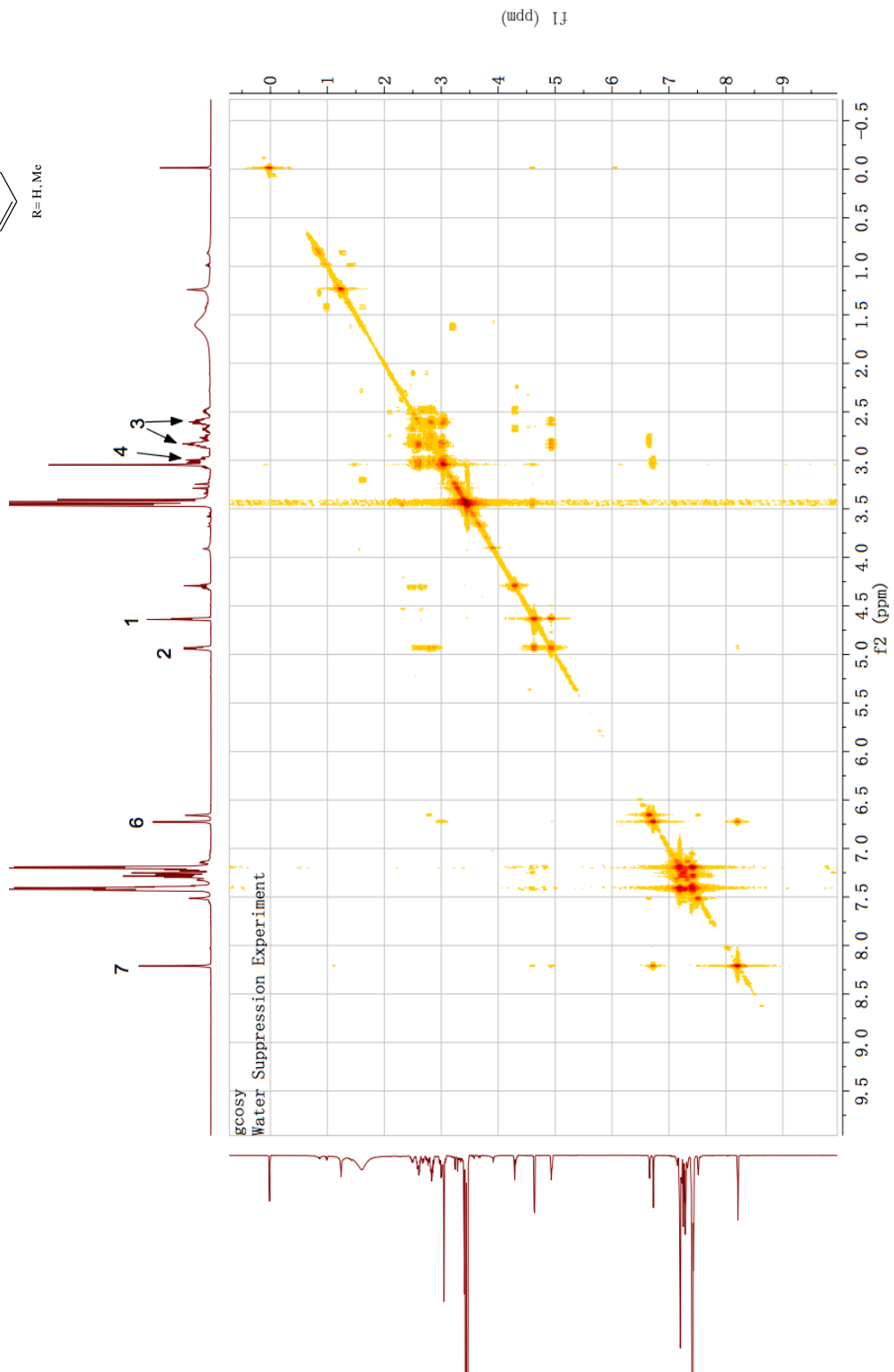
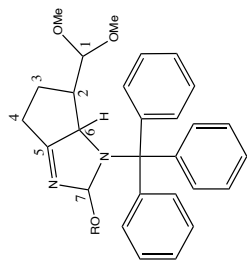


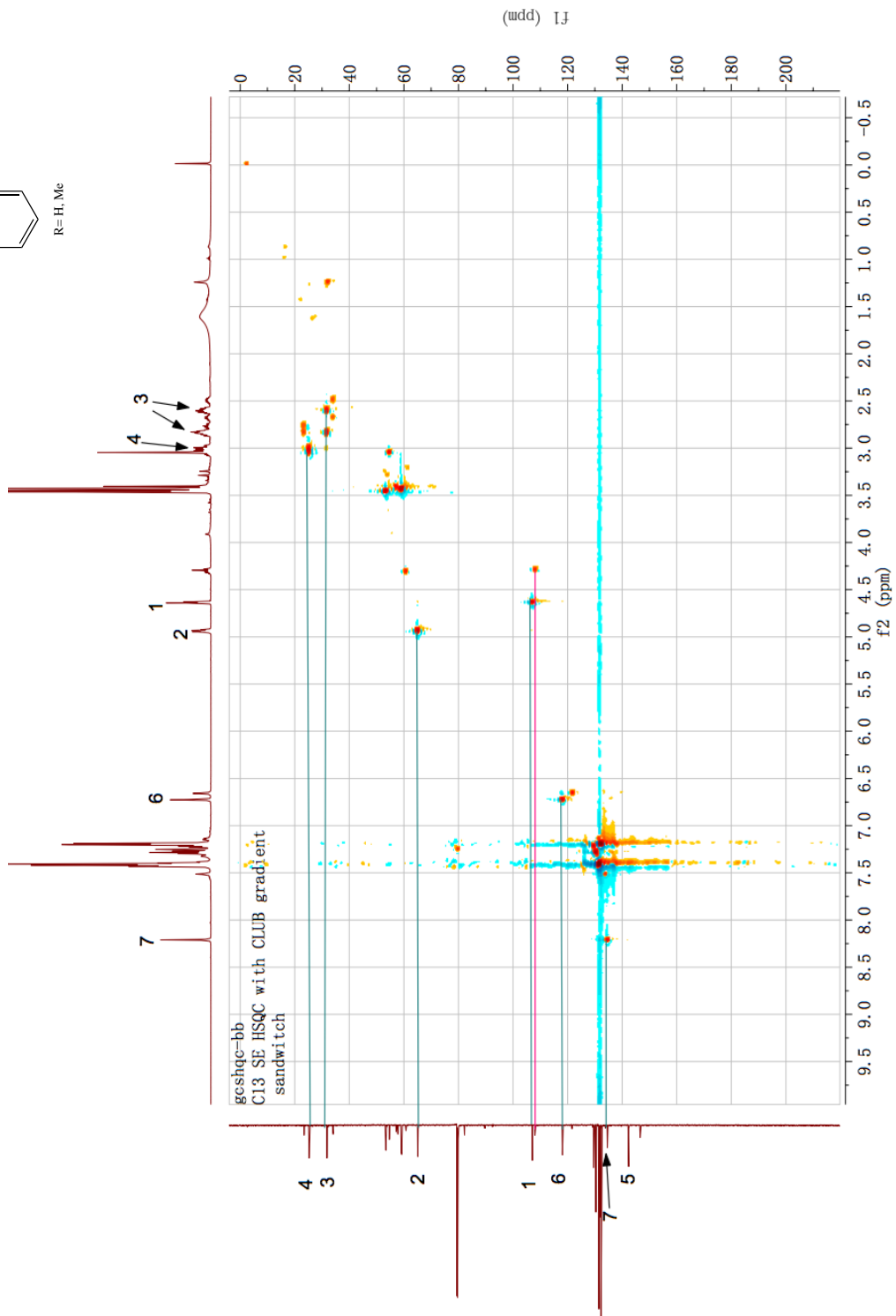
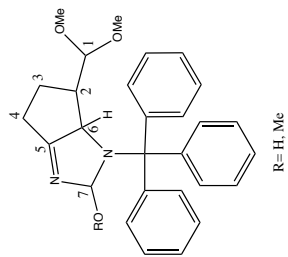


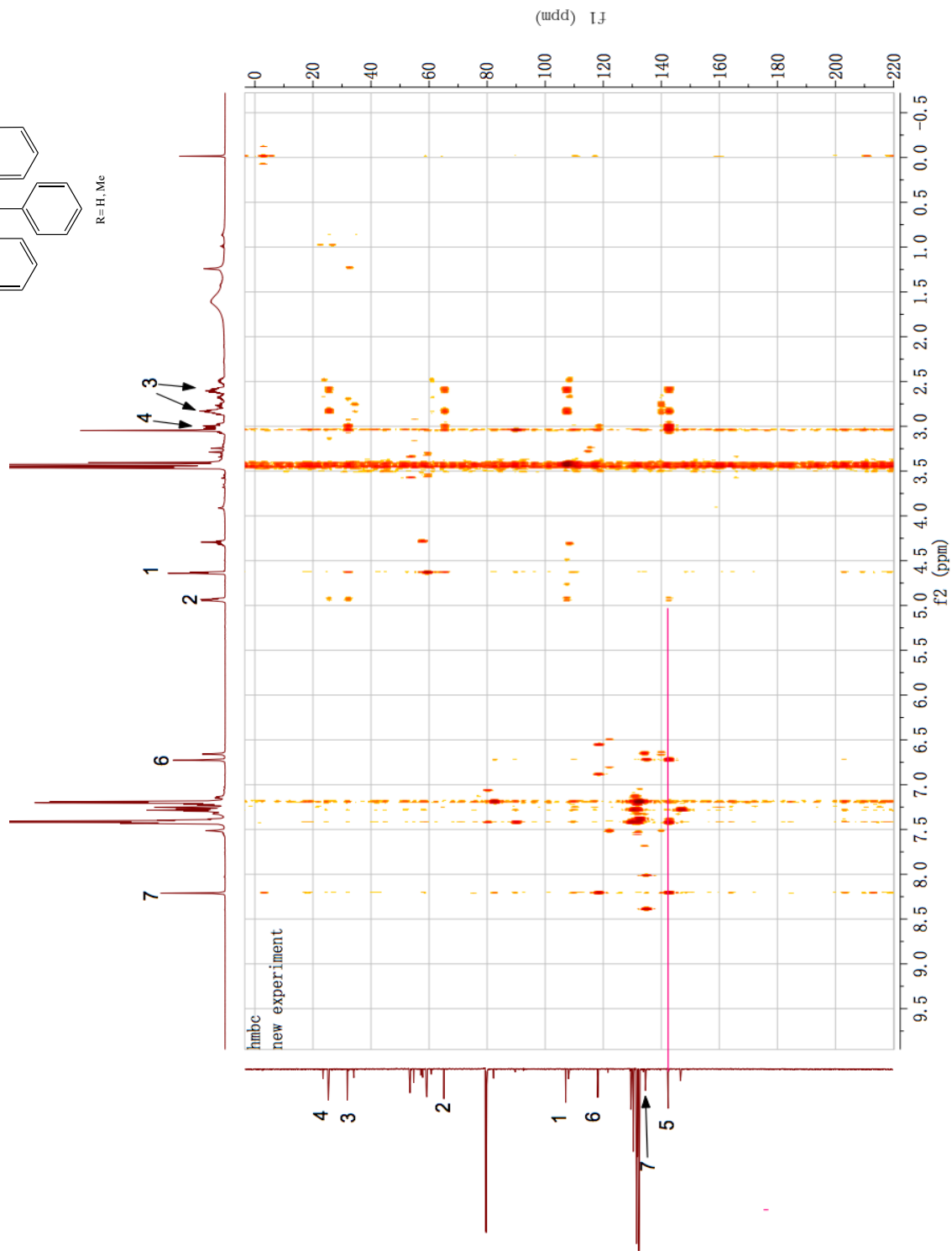
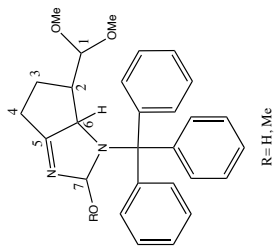




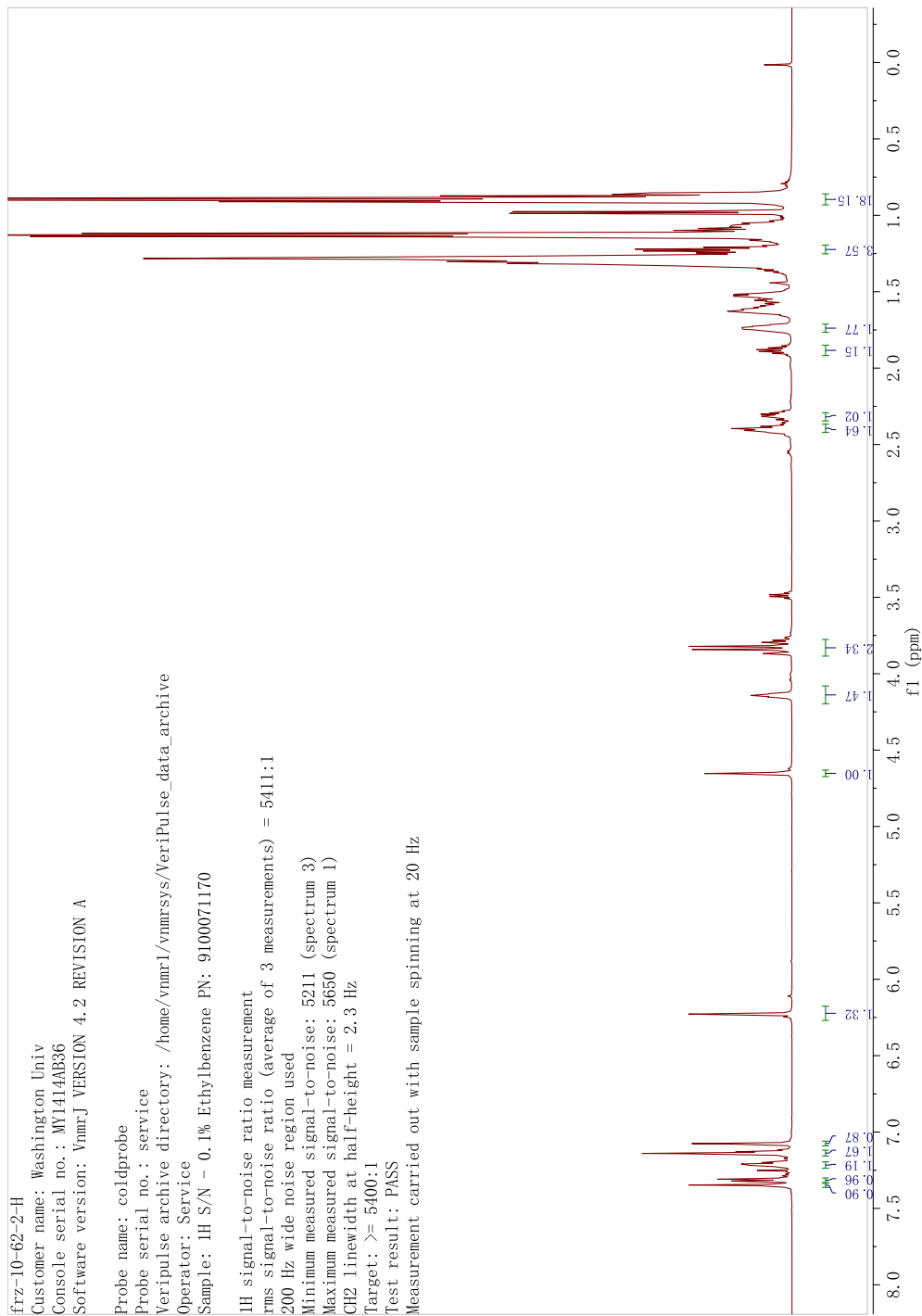
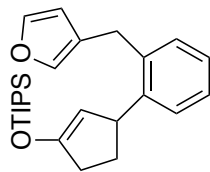


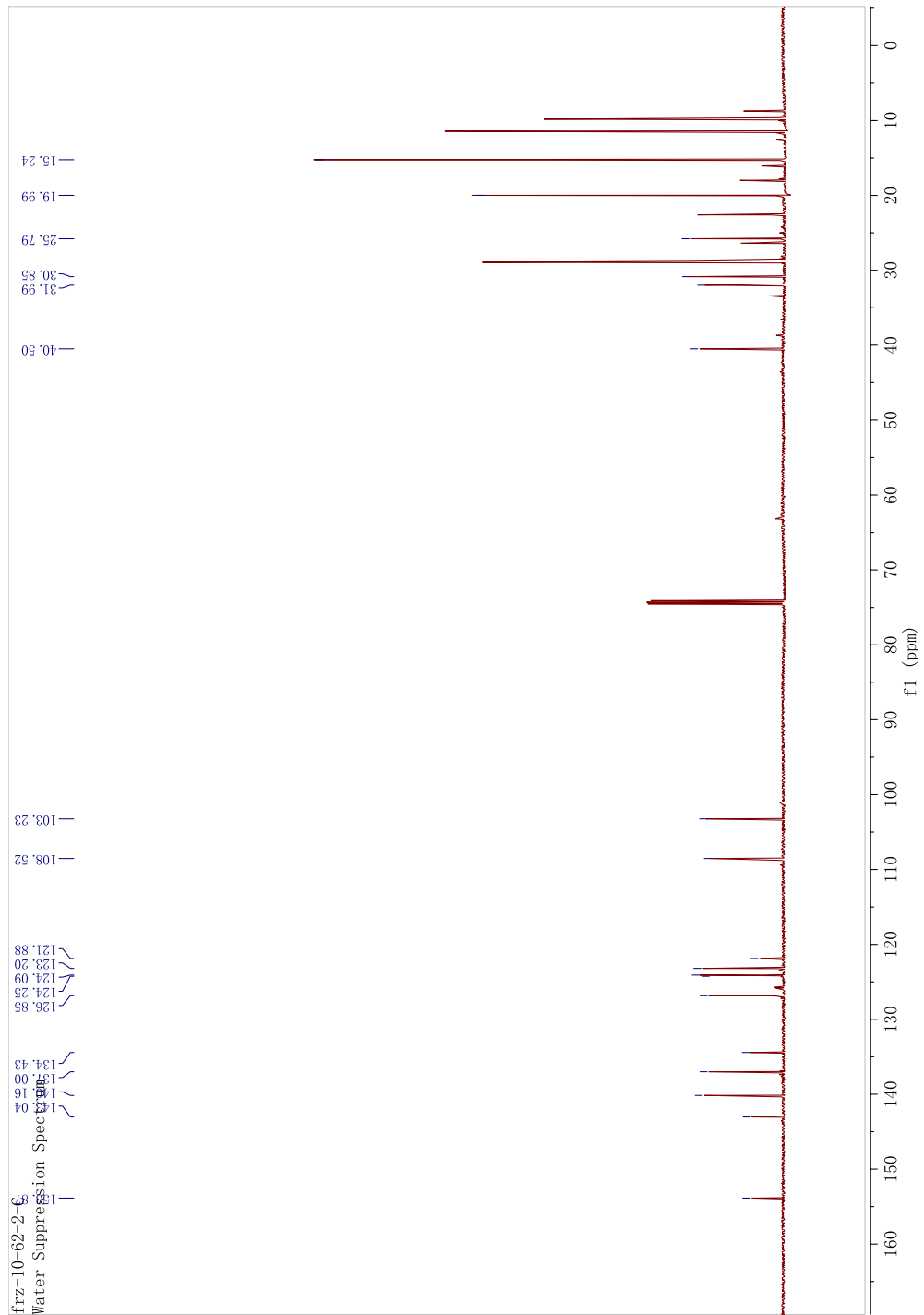
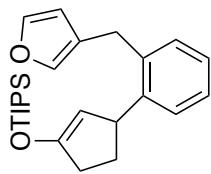


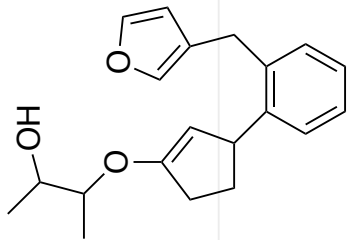




Appendix B

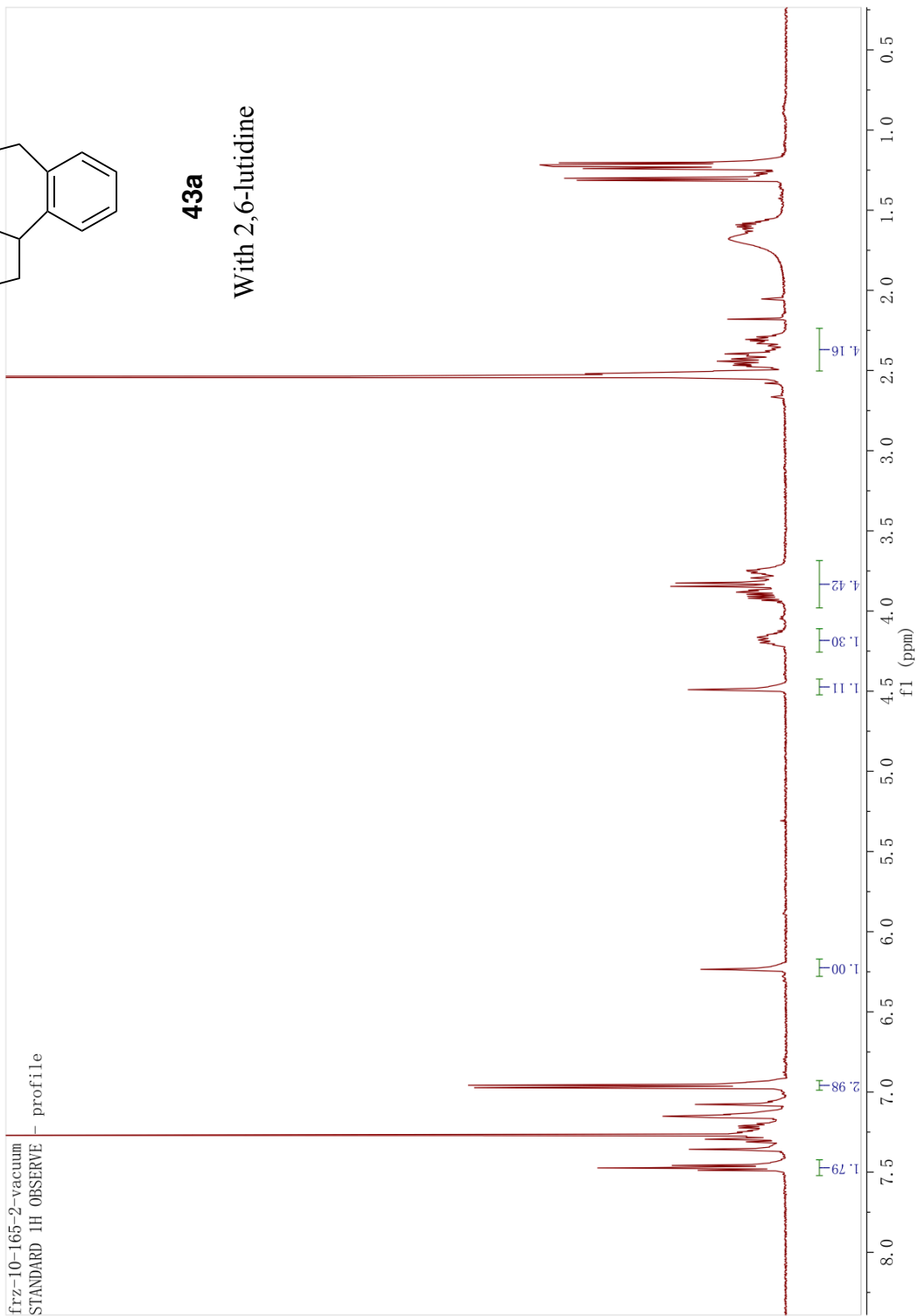


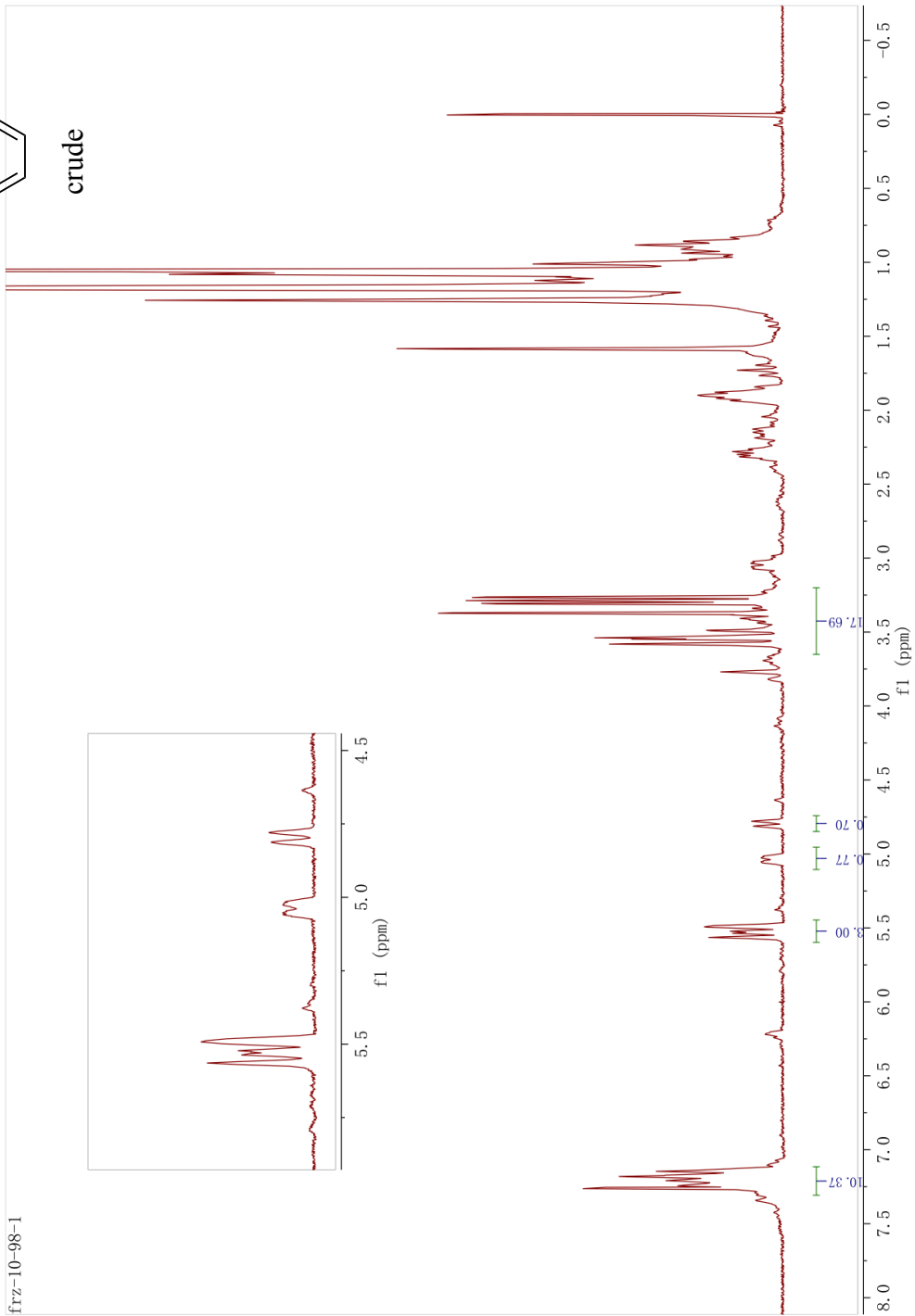
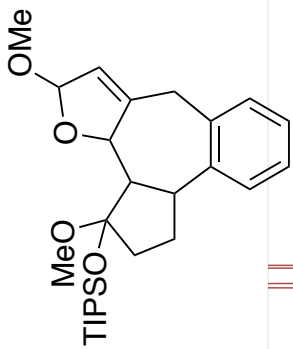


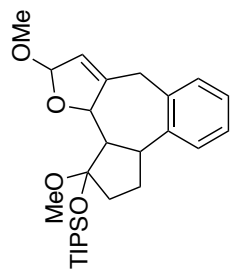


43a

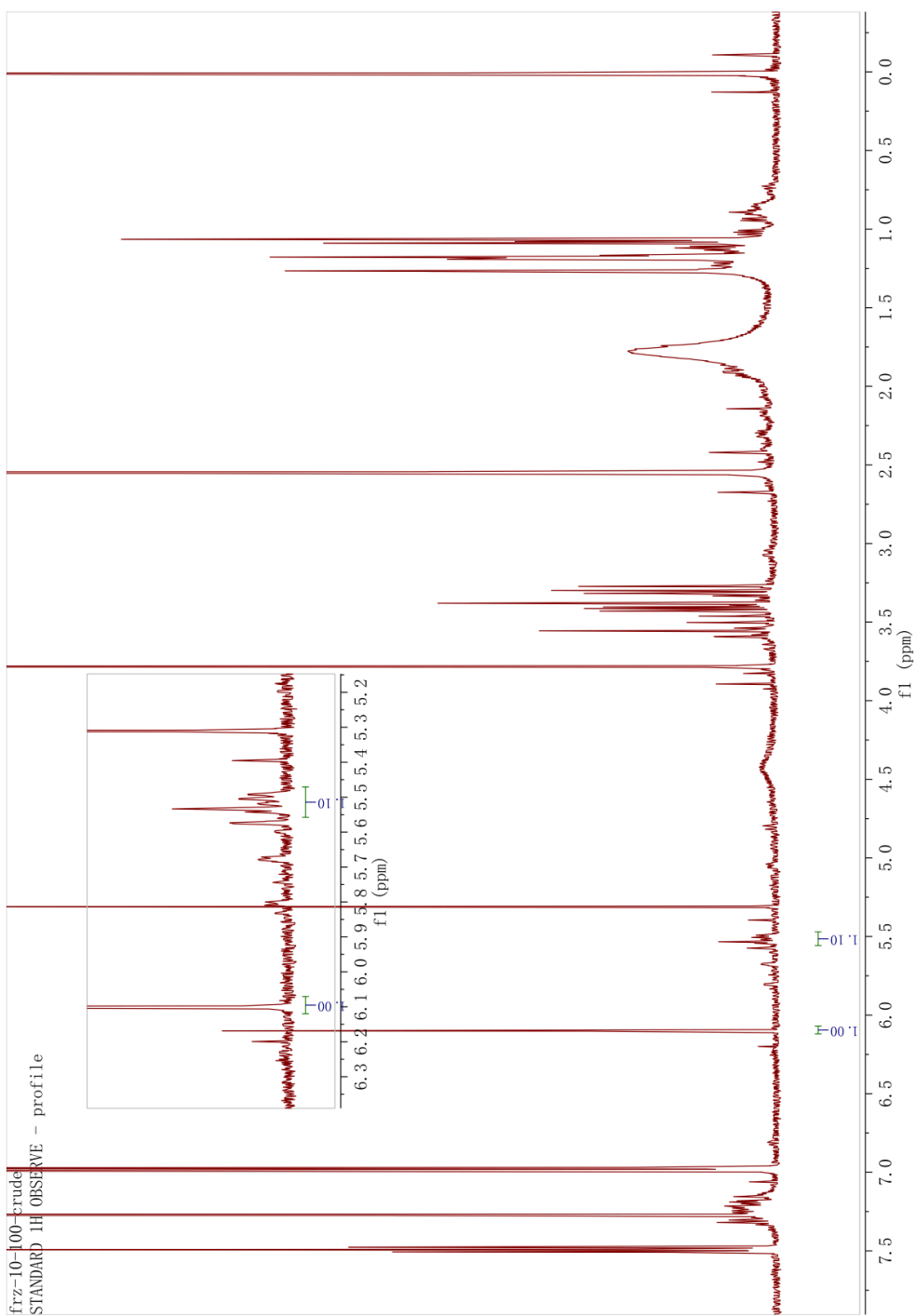
With 2,6-lutidine

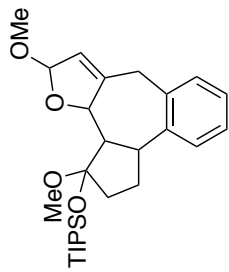




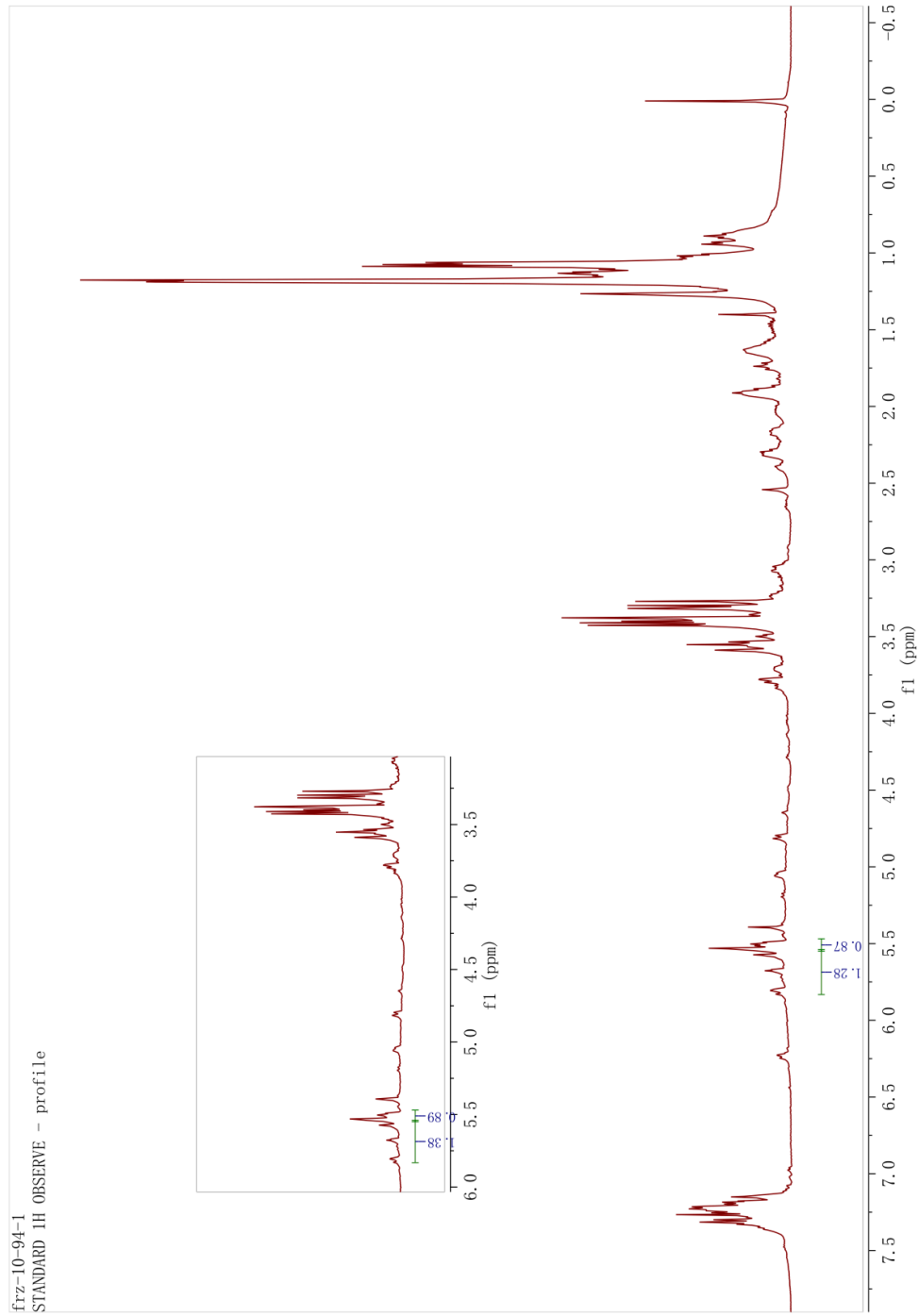


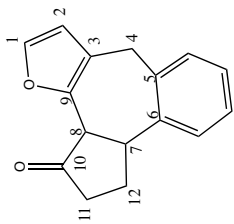
Crude, with Ph(OMe)₃ as internal standard



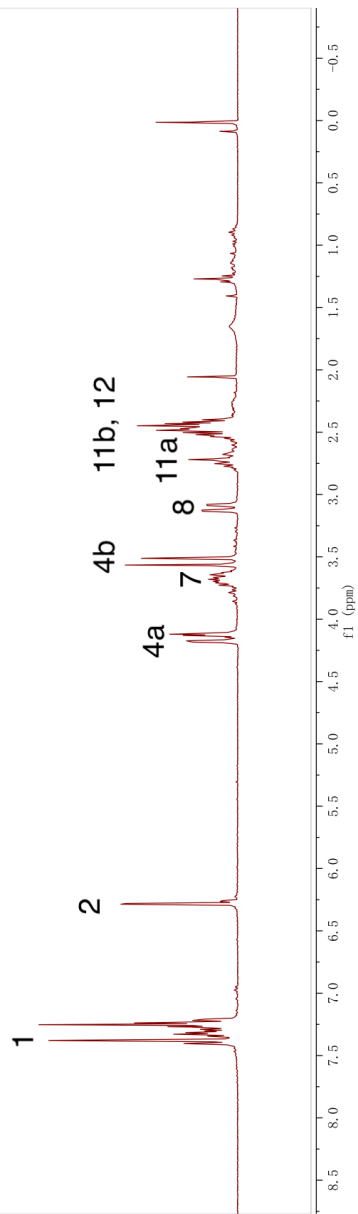


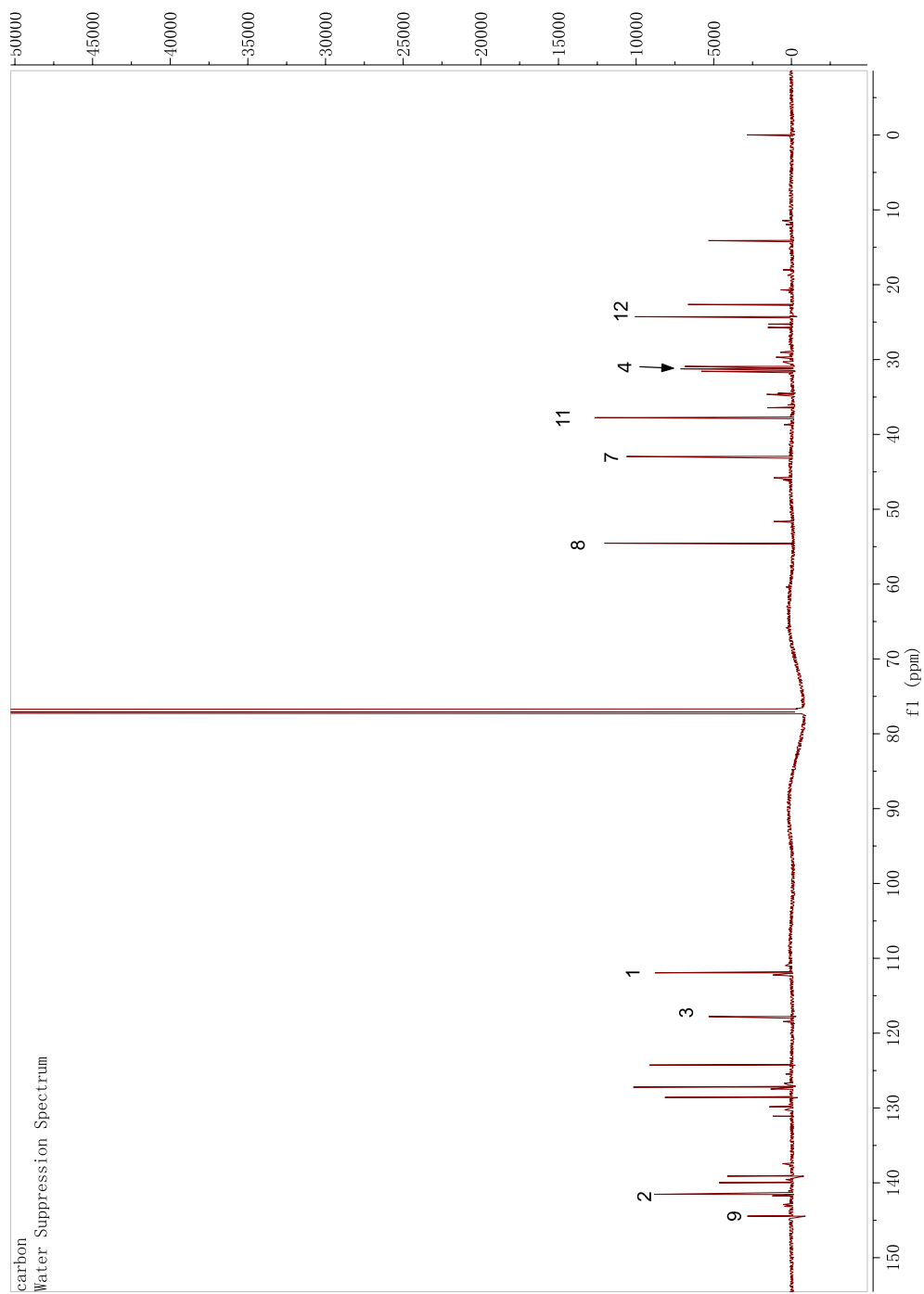
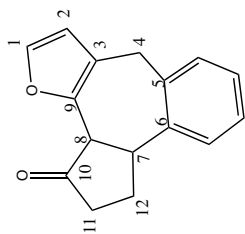
Crude, using Bu4NBF4 as electrolyte

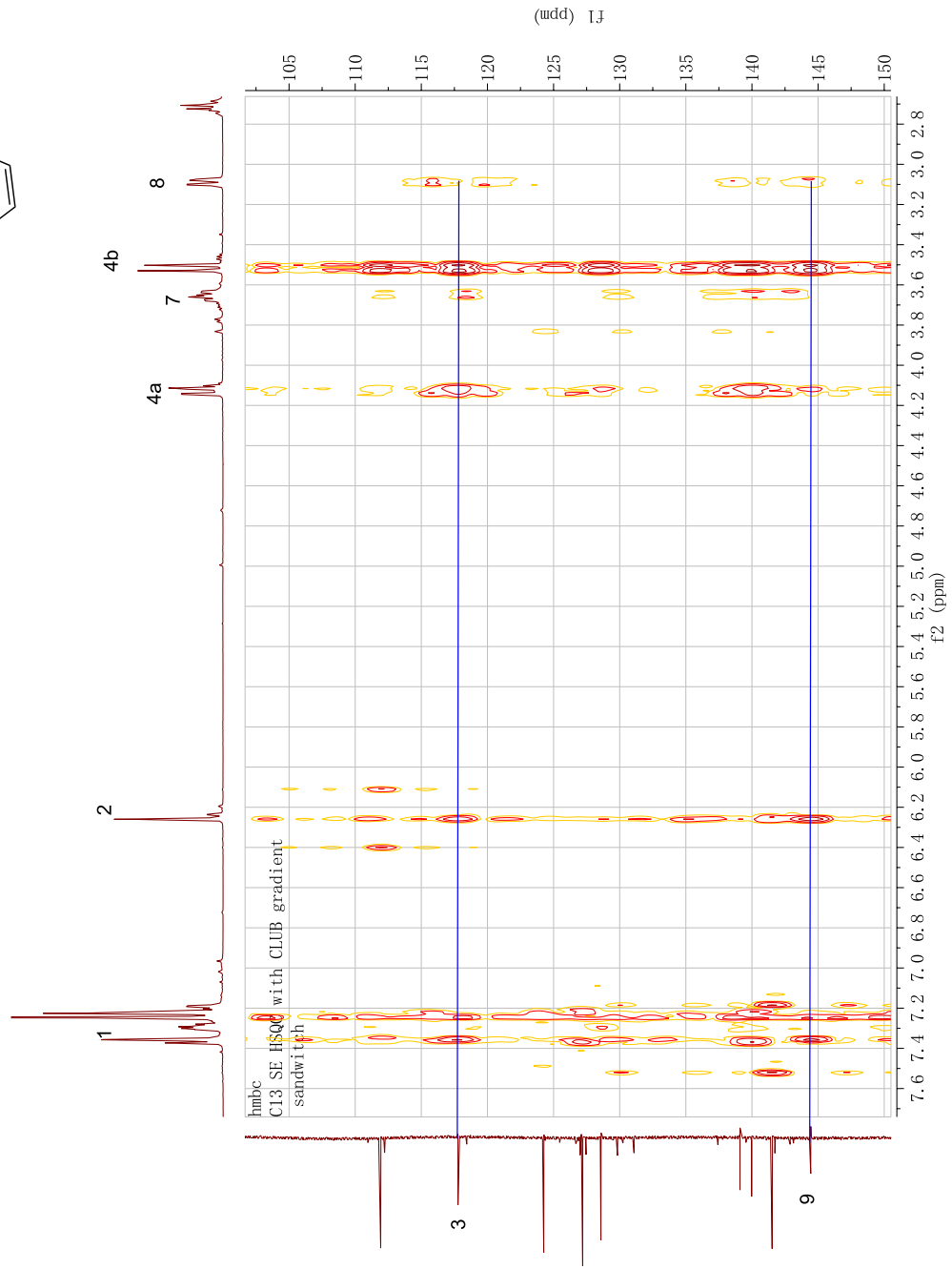
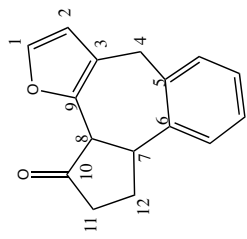


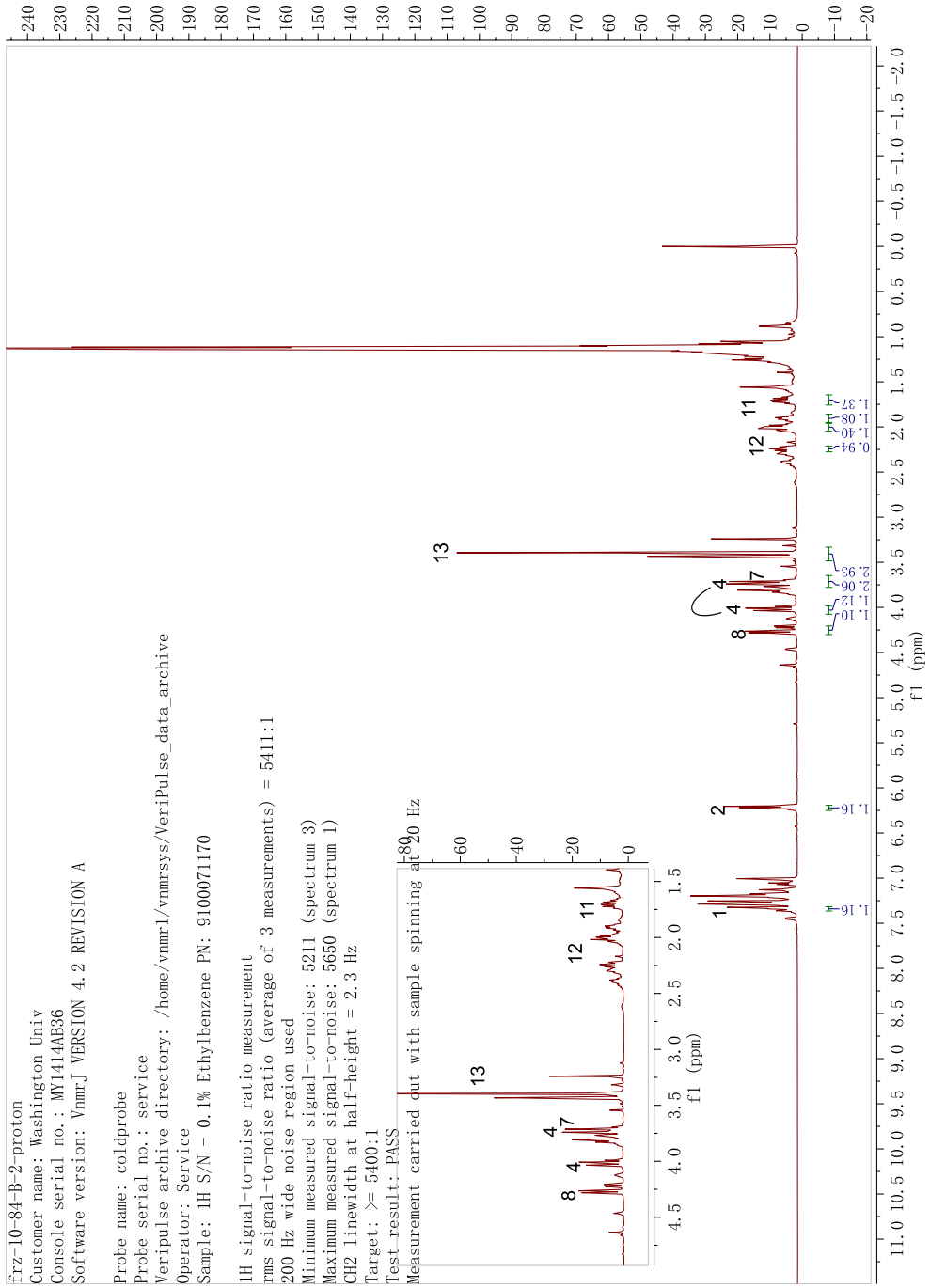
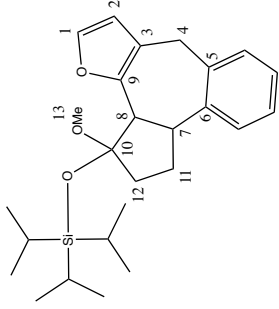


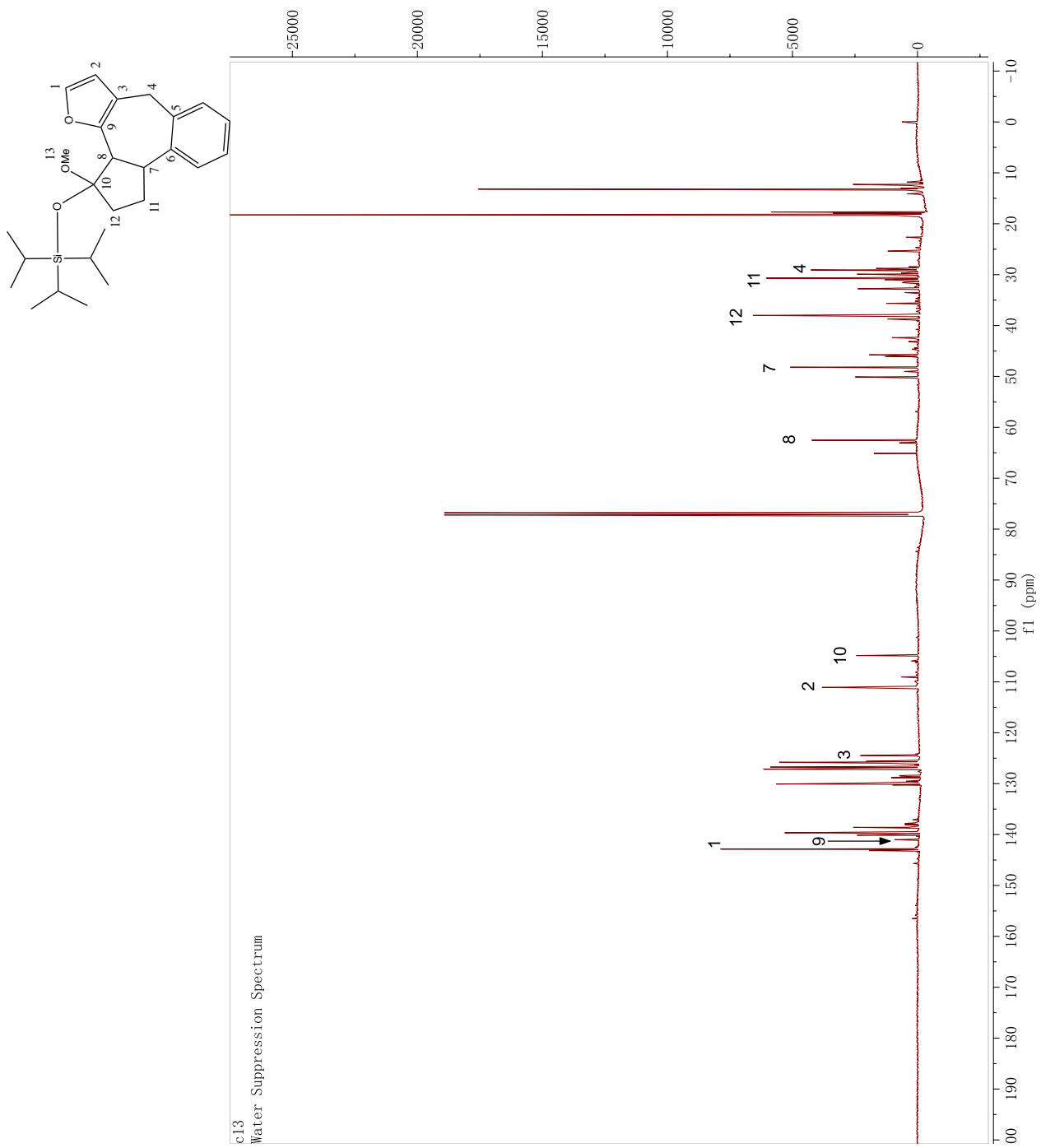
FRZ-10-112-TsOH-I

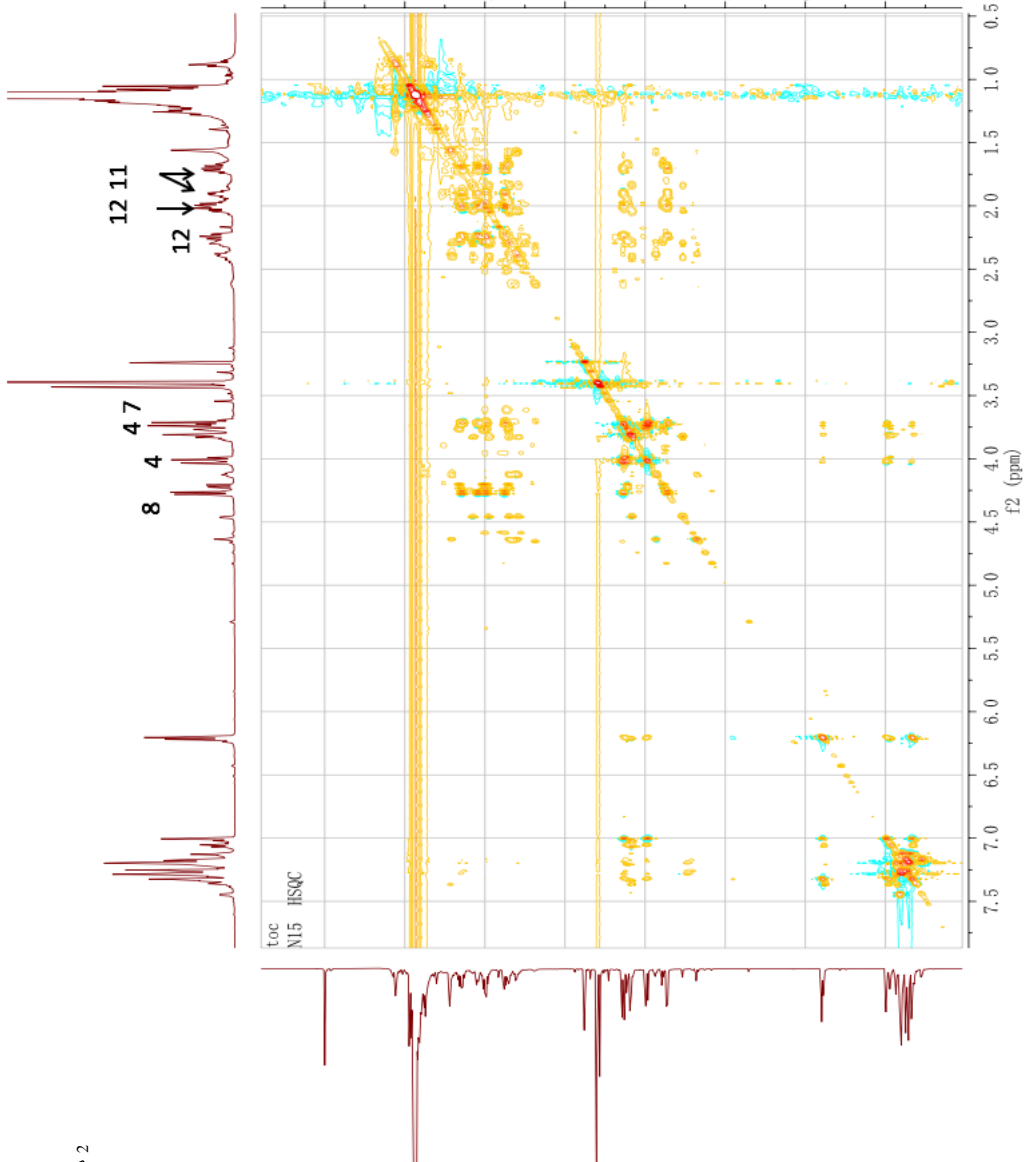
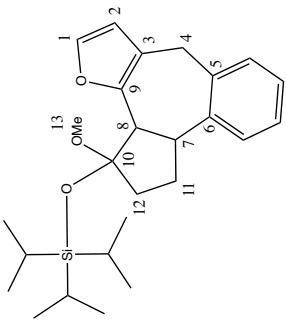


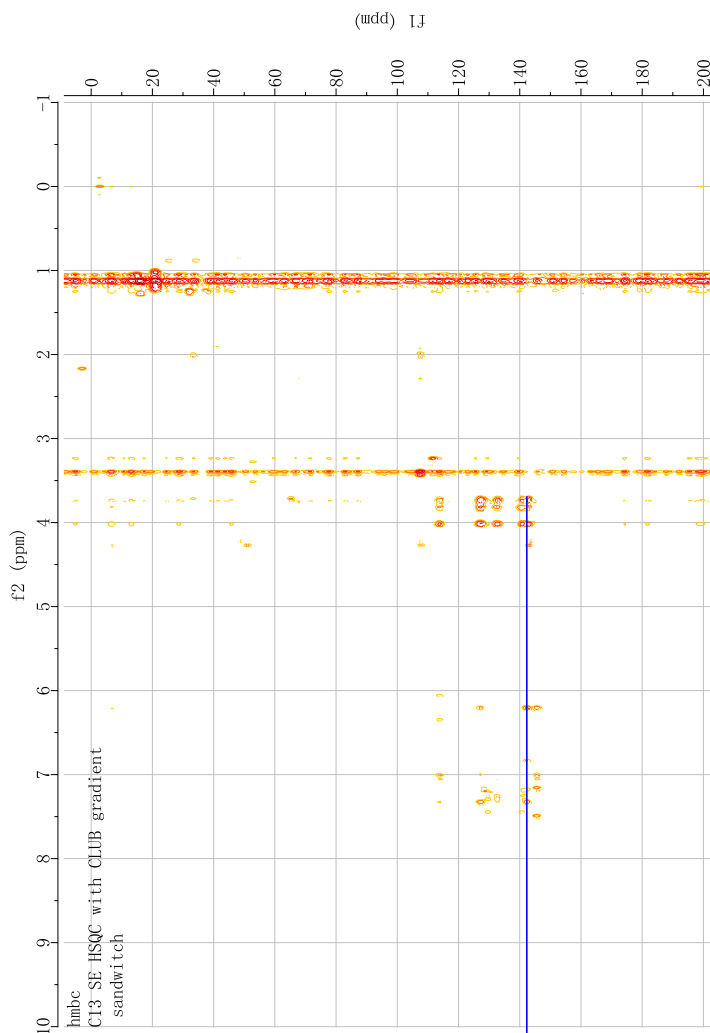
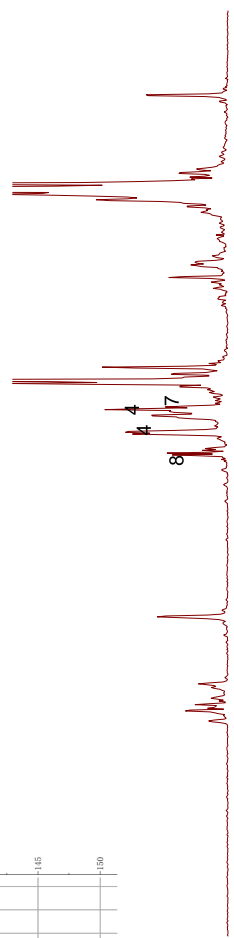
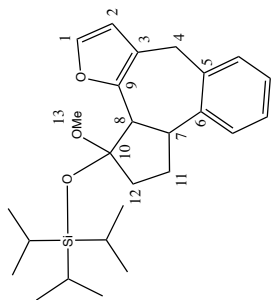
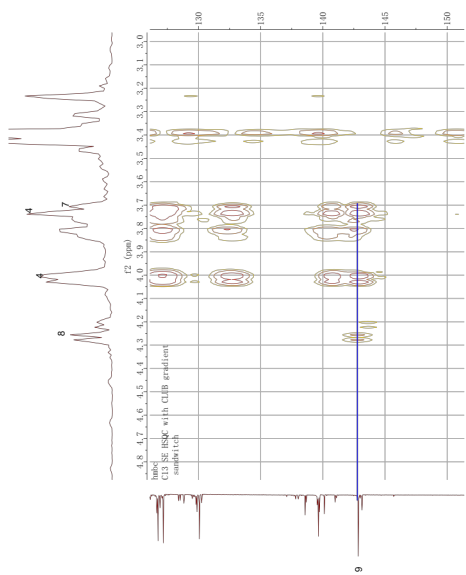


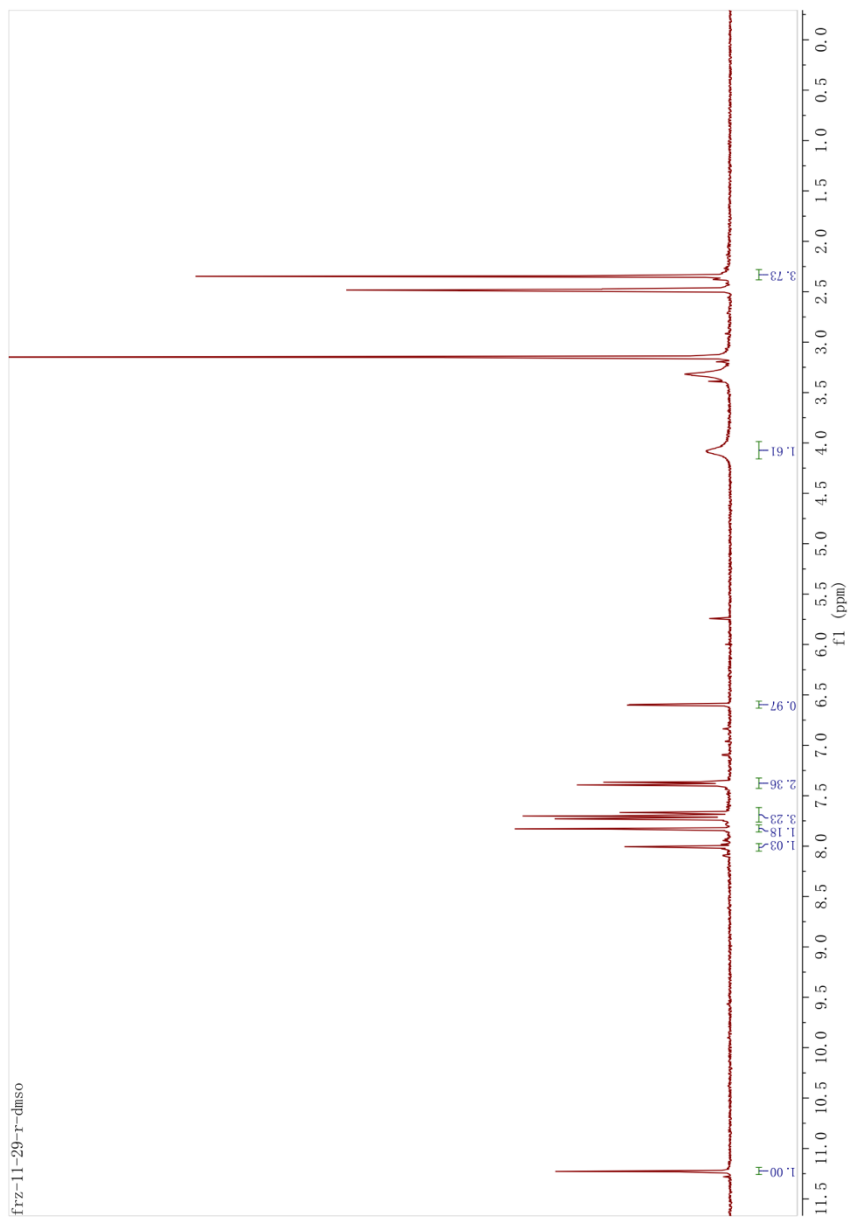
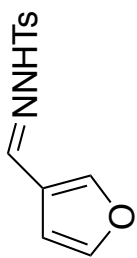


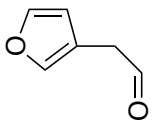




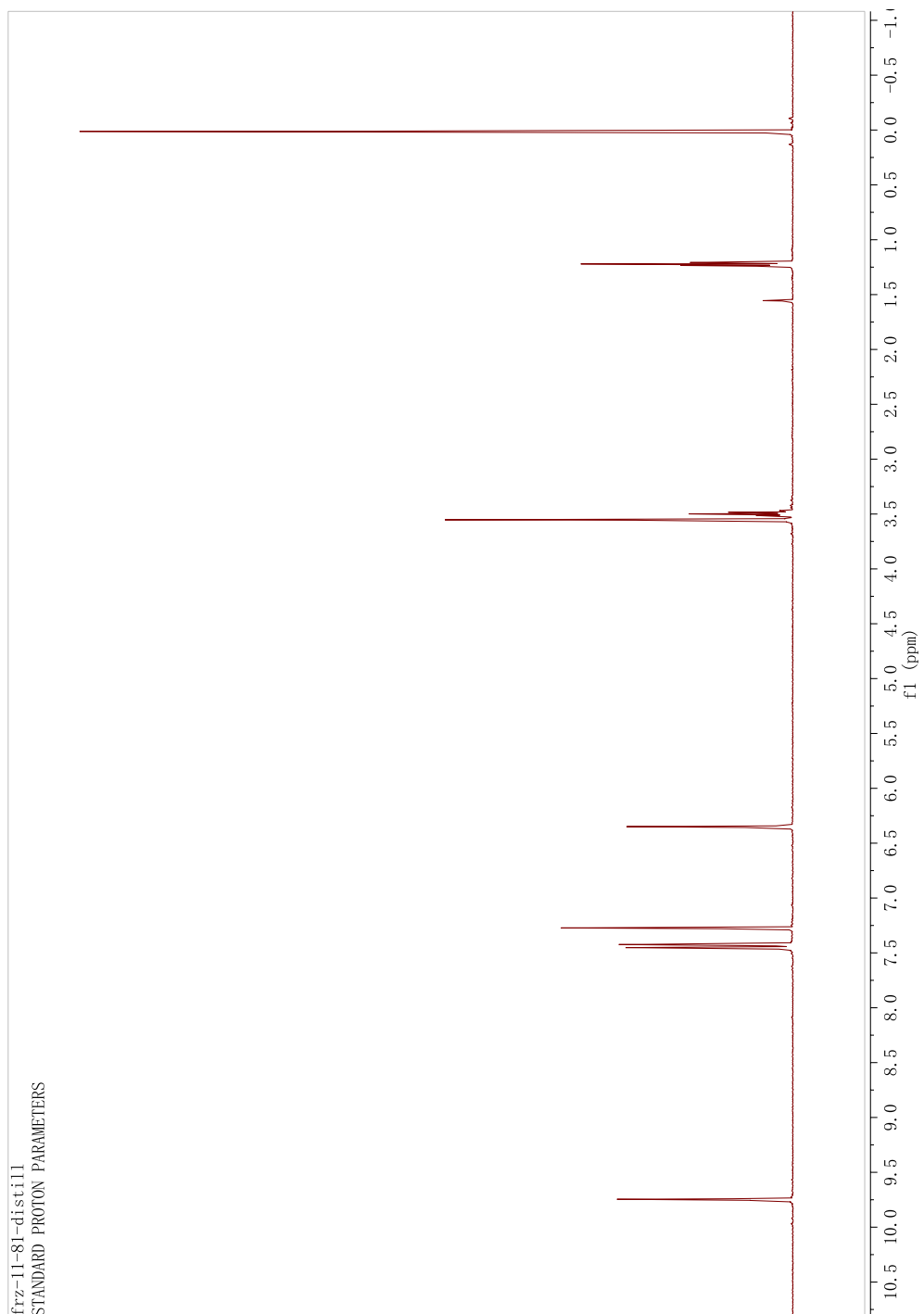




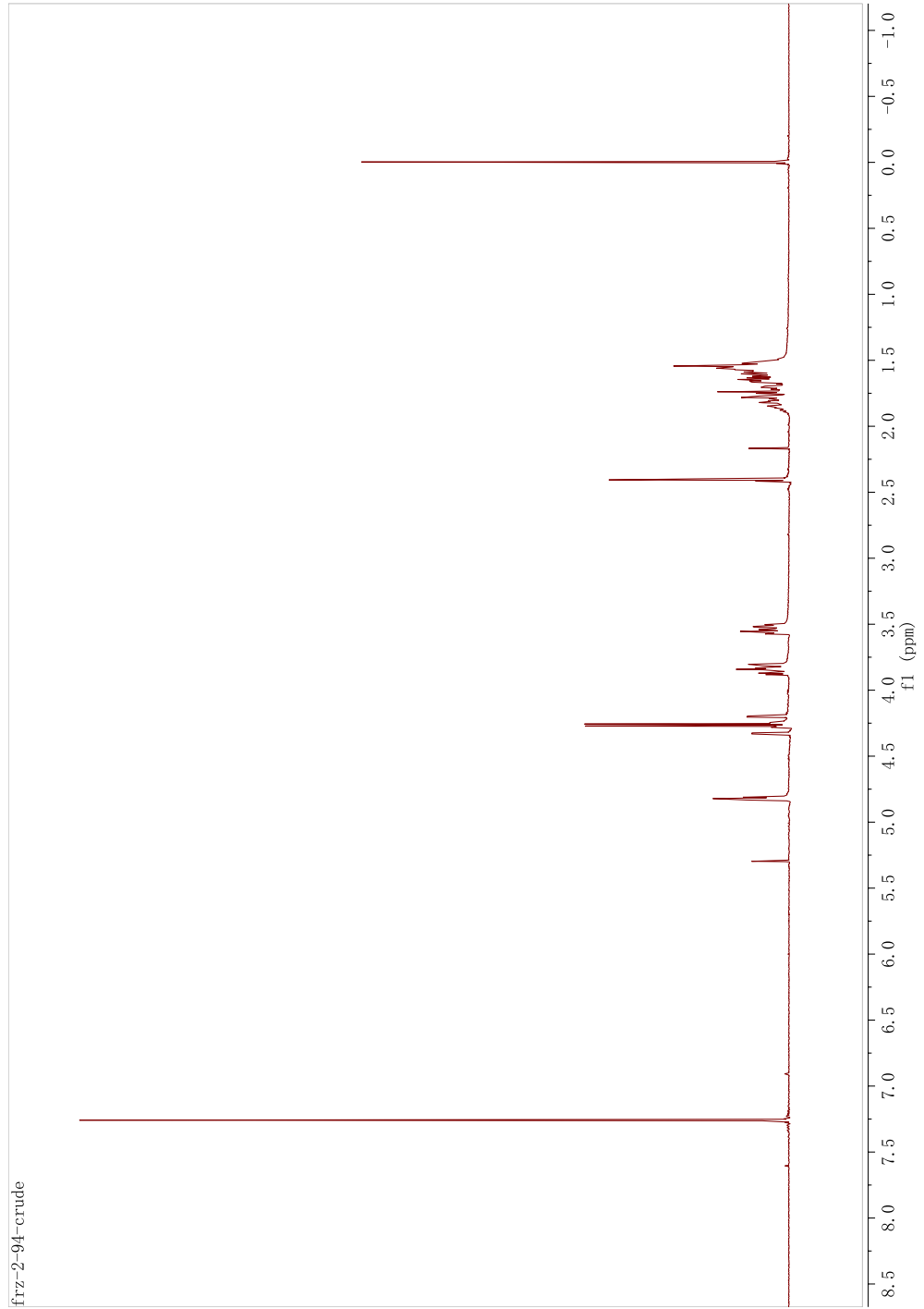
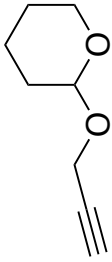


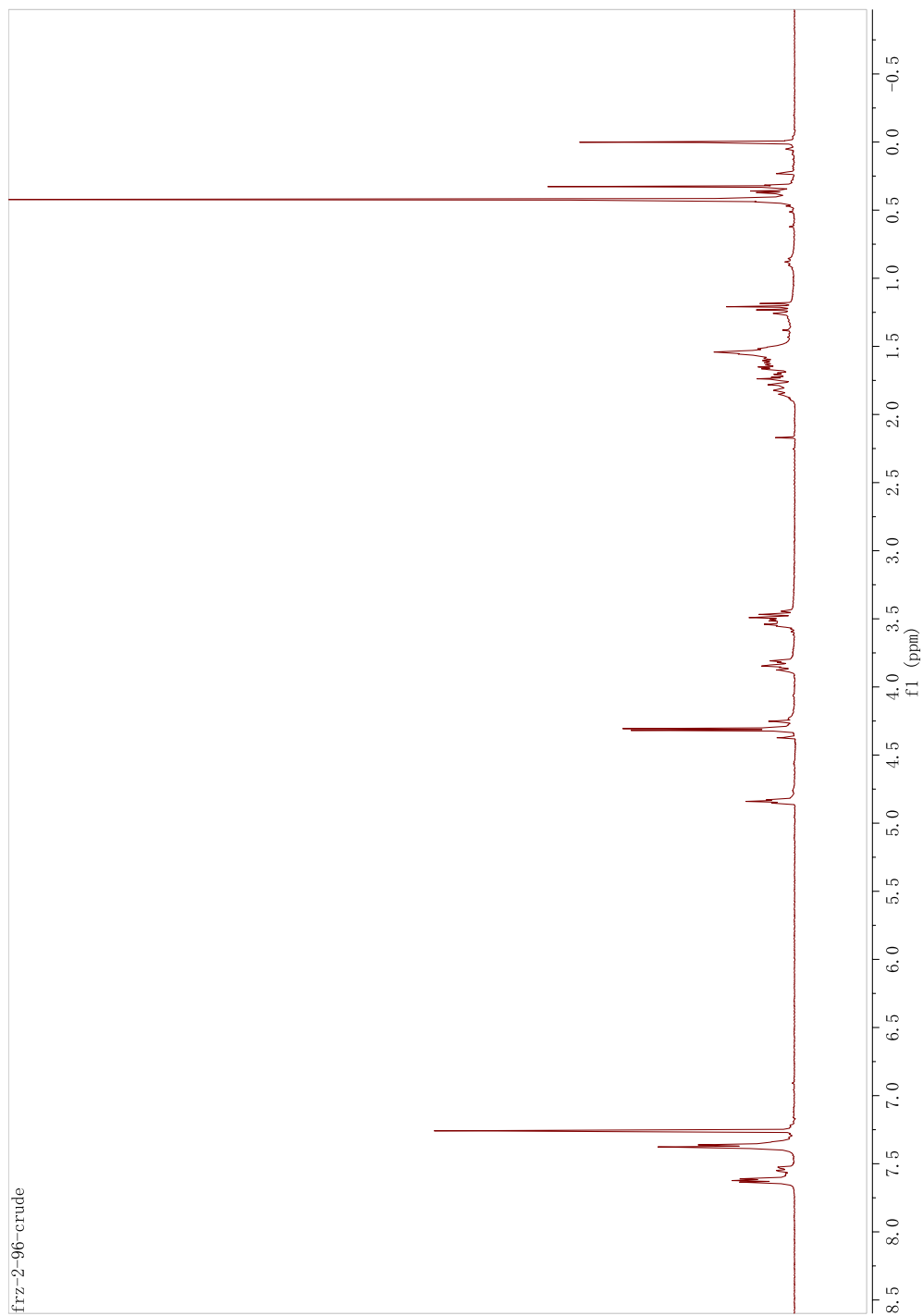
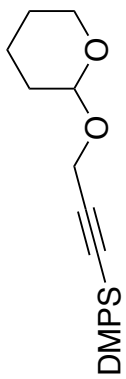


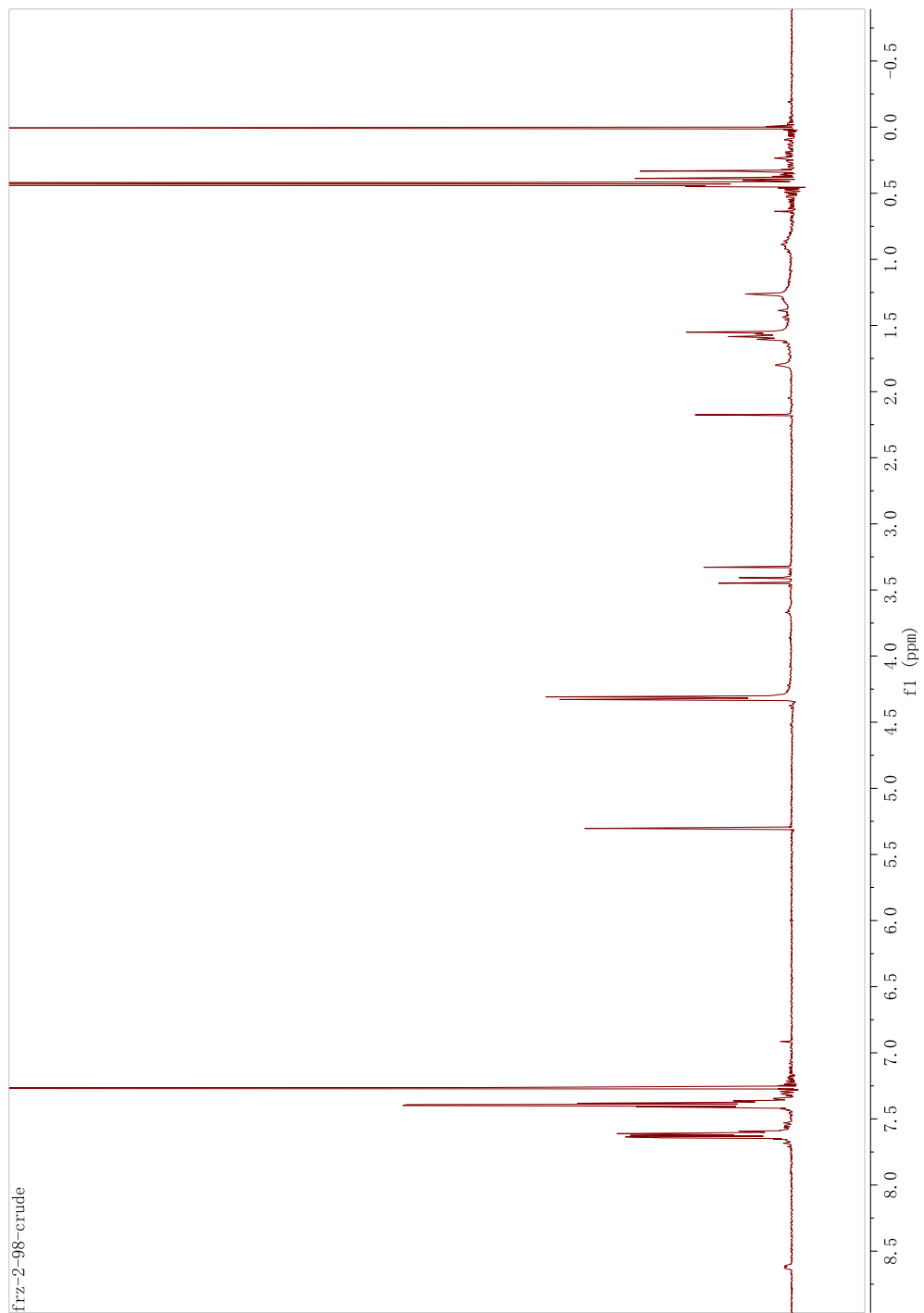
frz-11-81-distill
STANDARD PROTON PARAMETERS

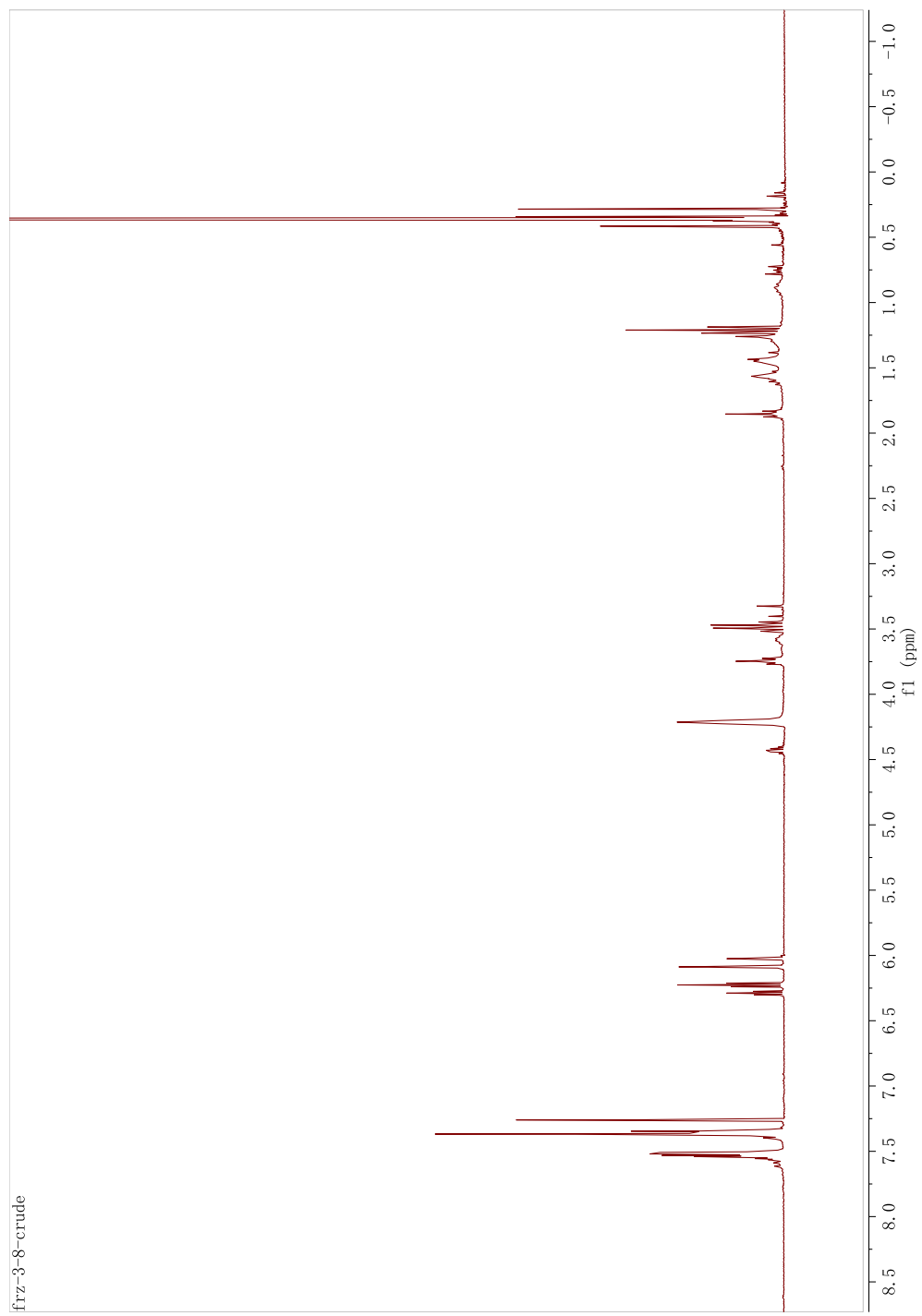
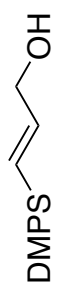


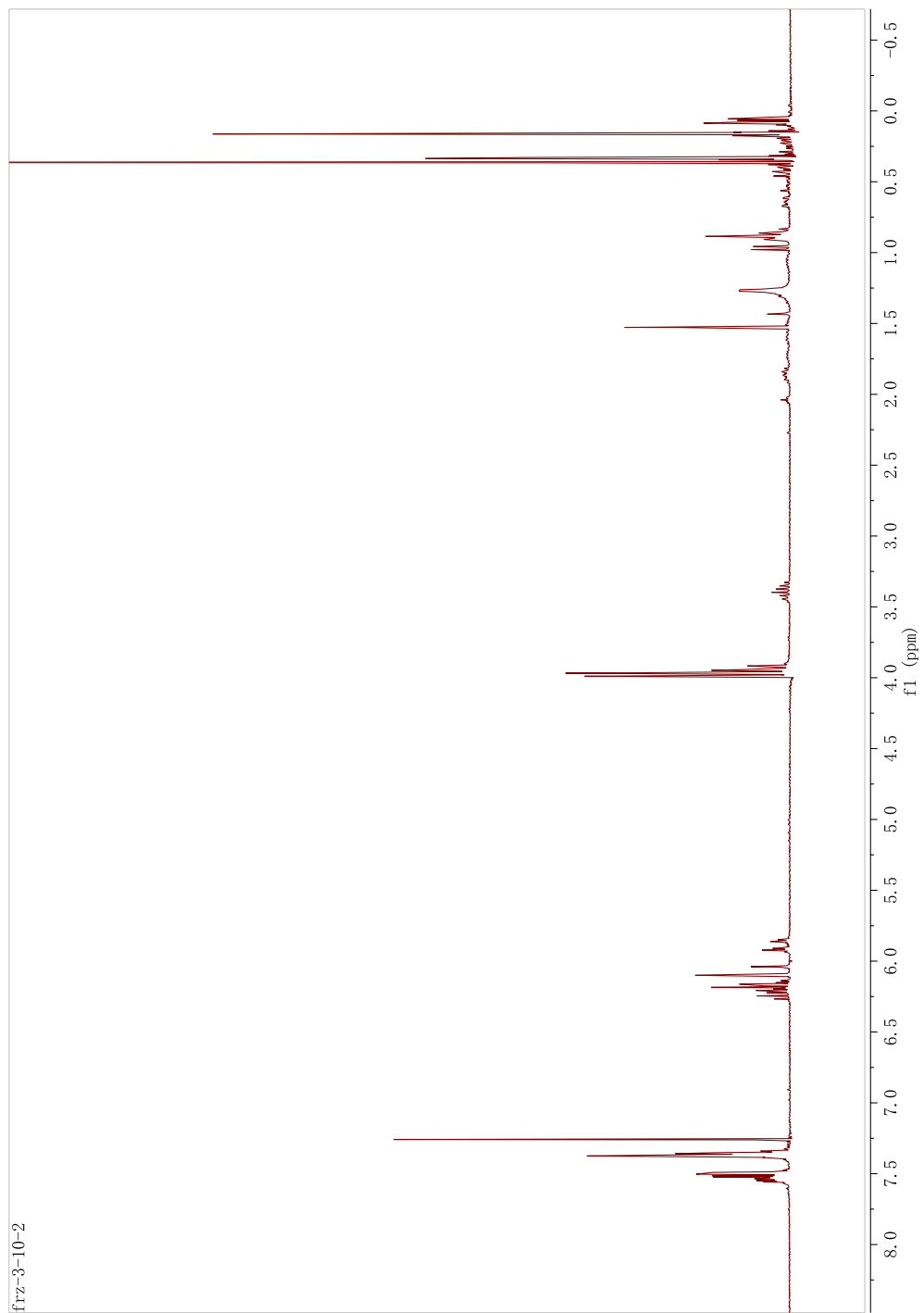
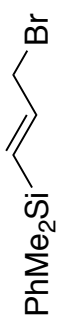
Appendix C

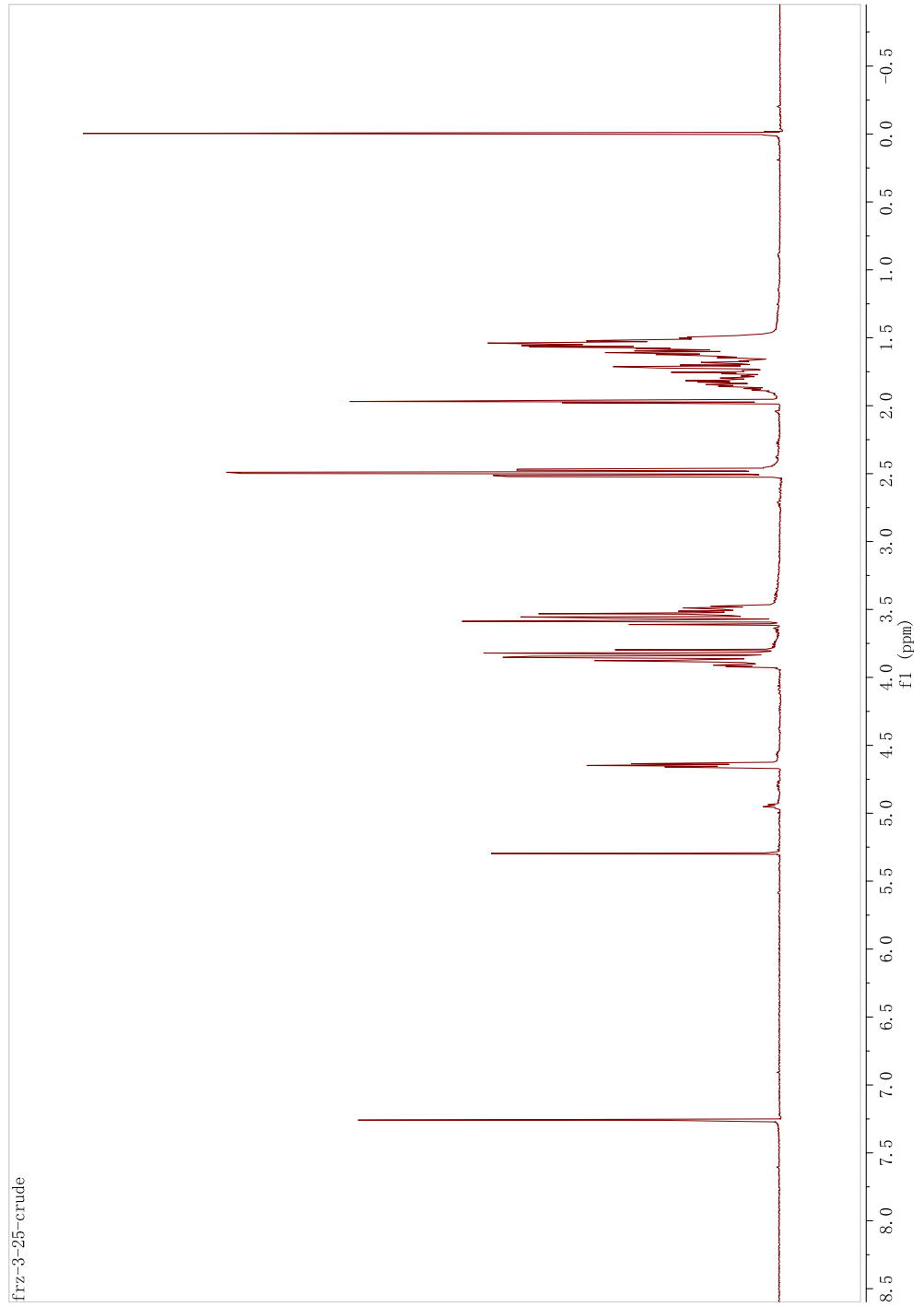
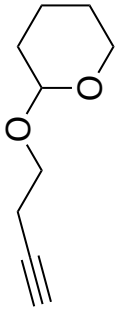


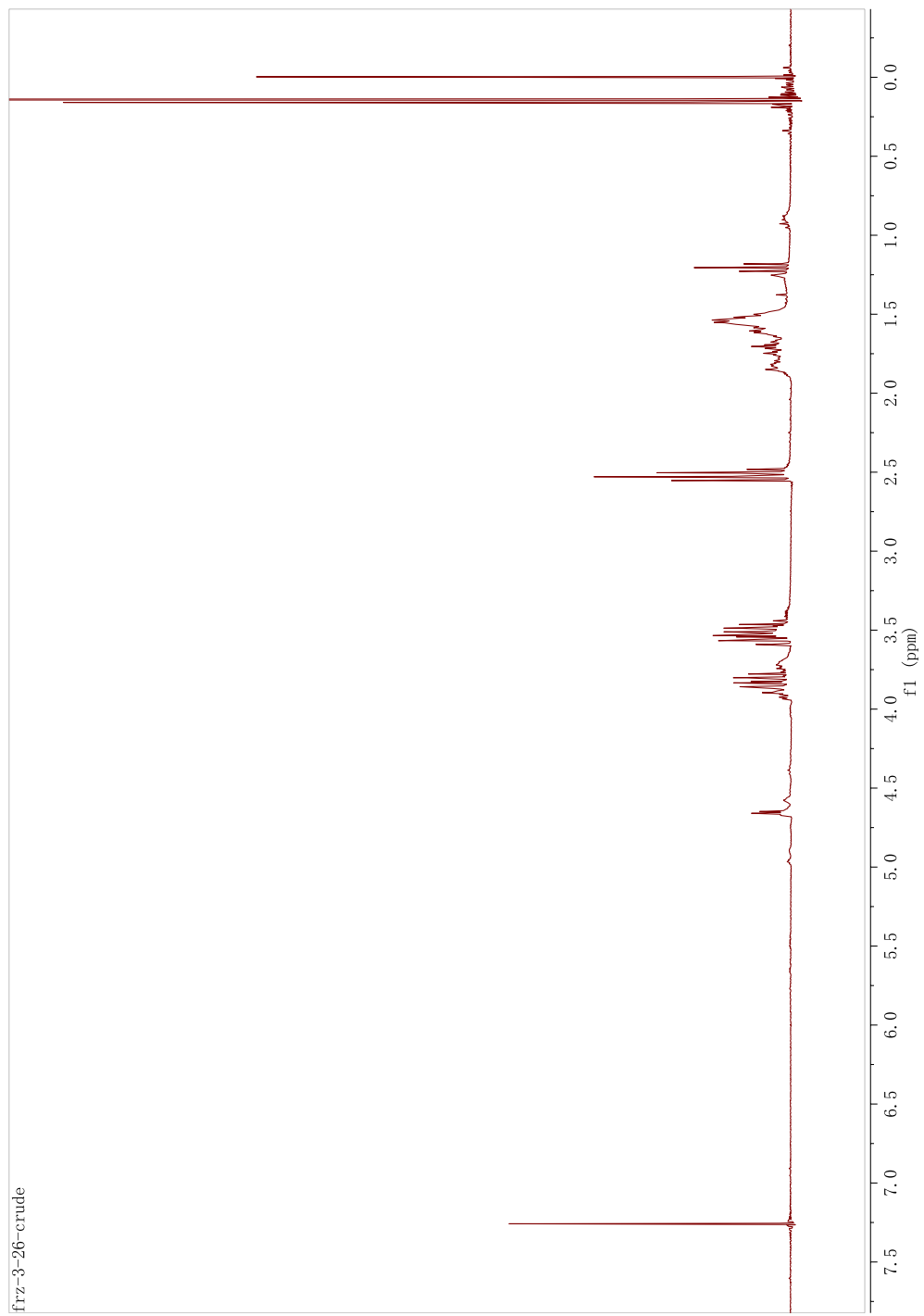
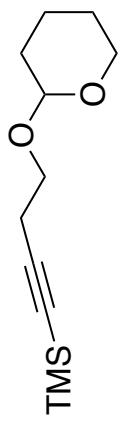


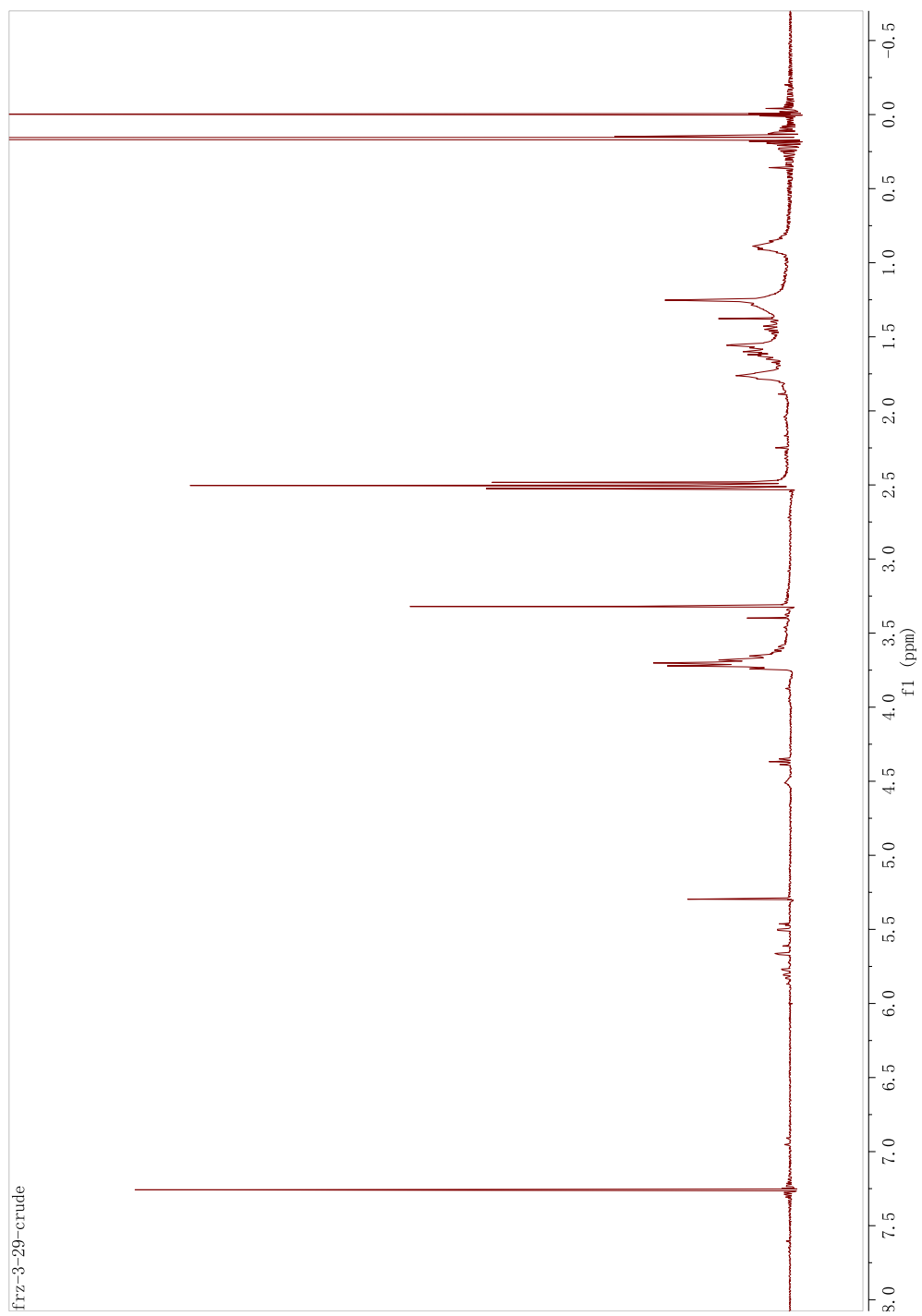


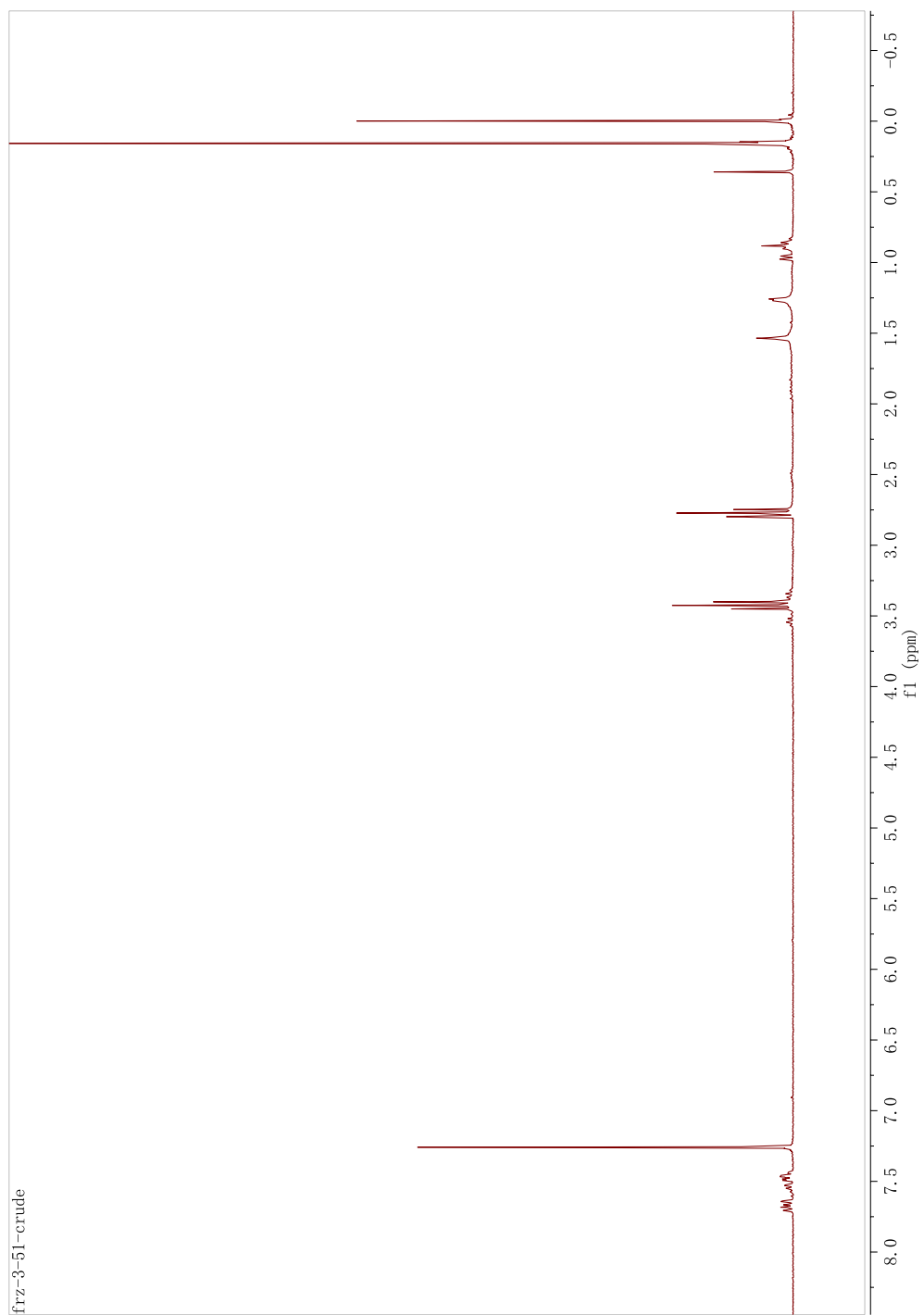


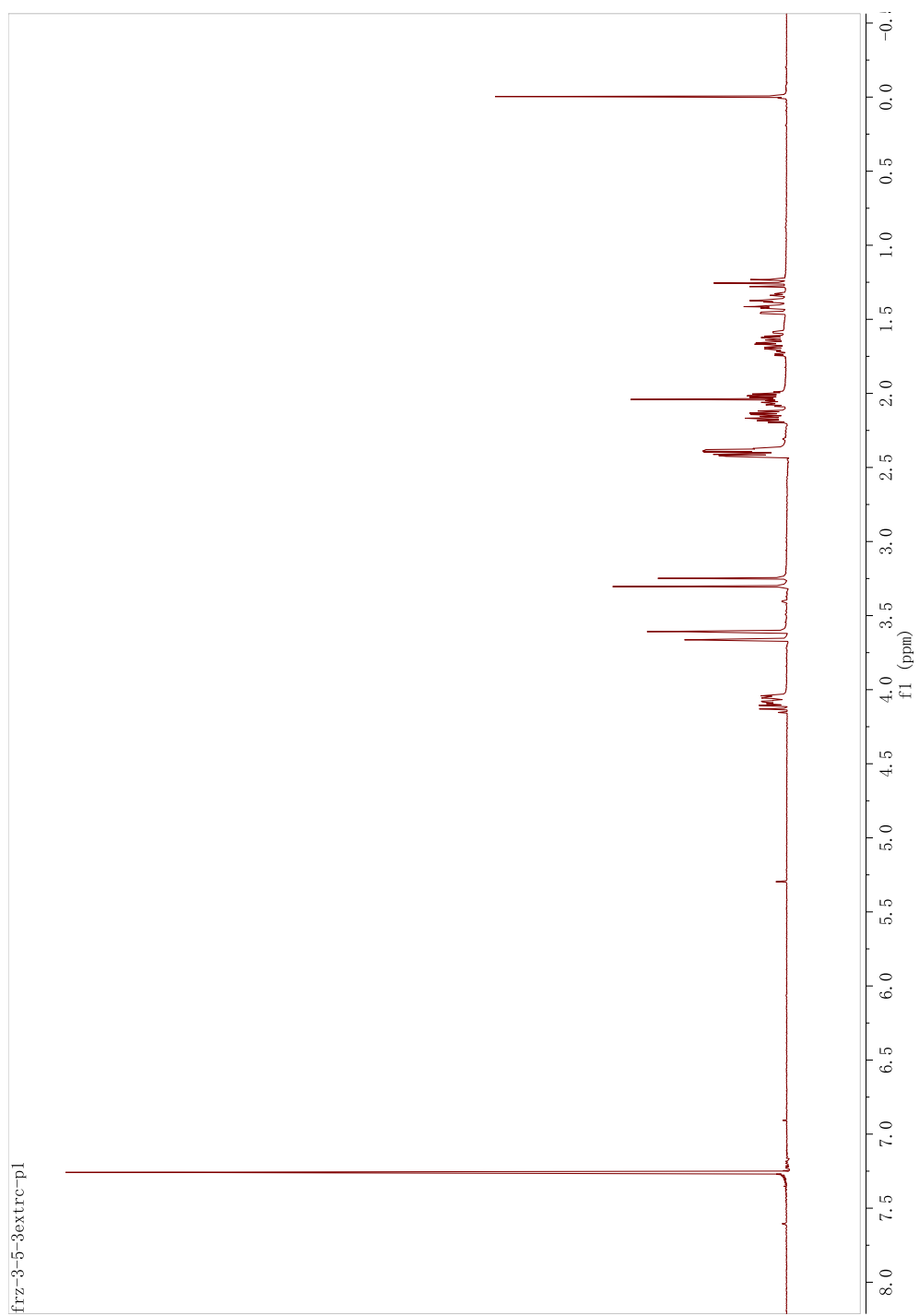
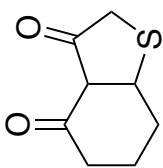




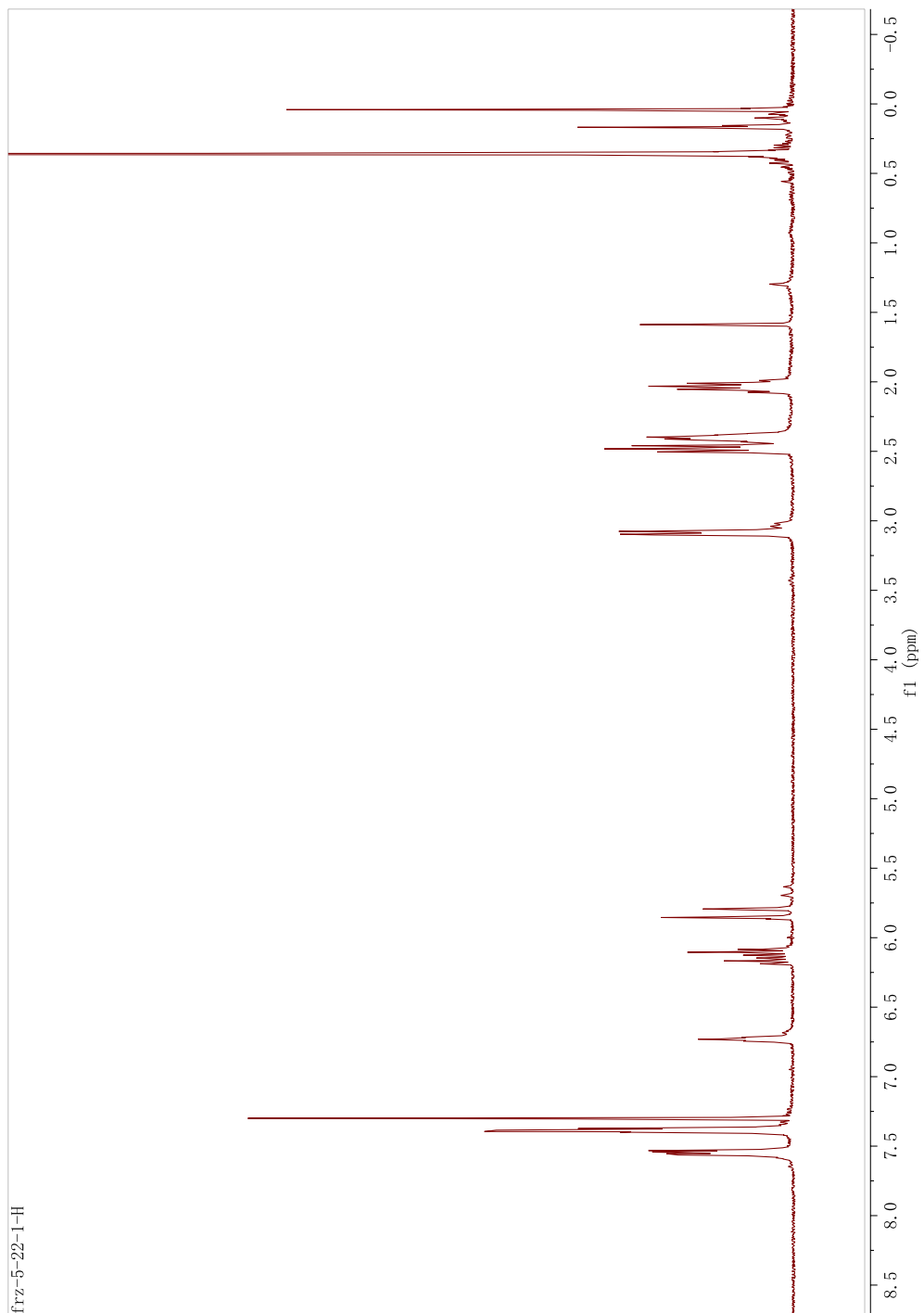
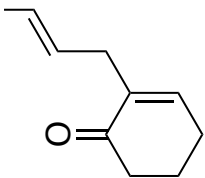




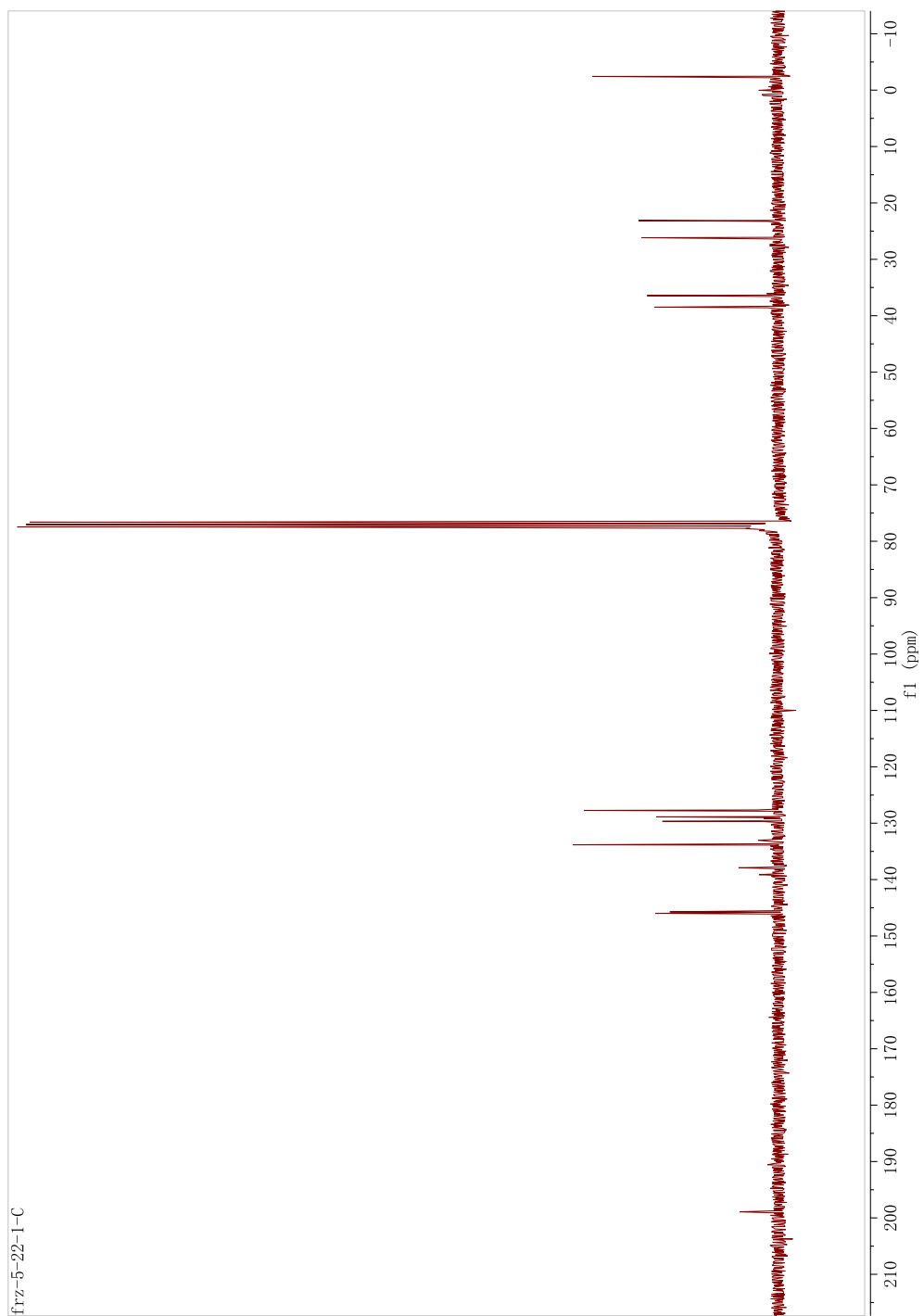
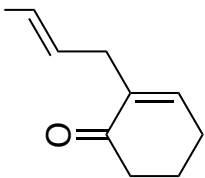


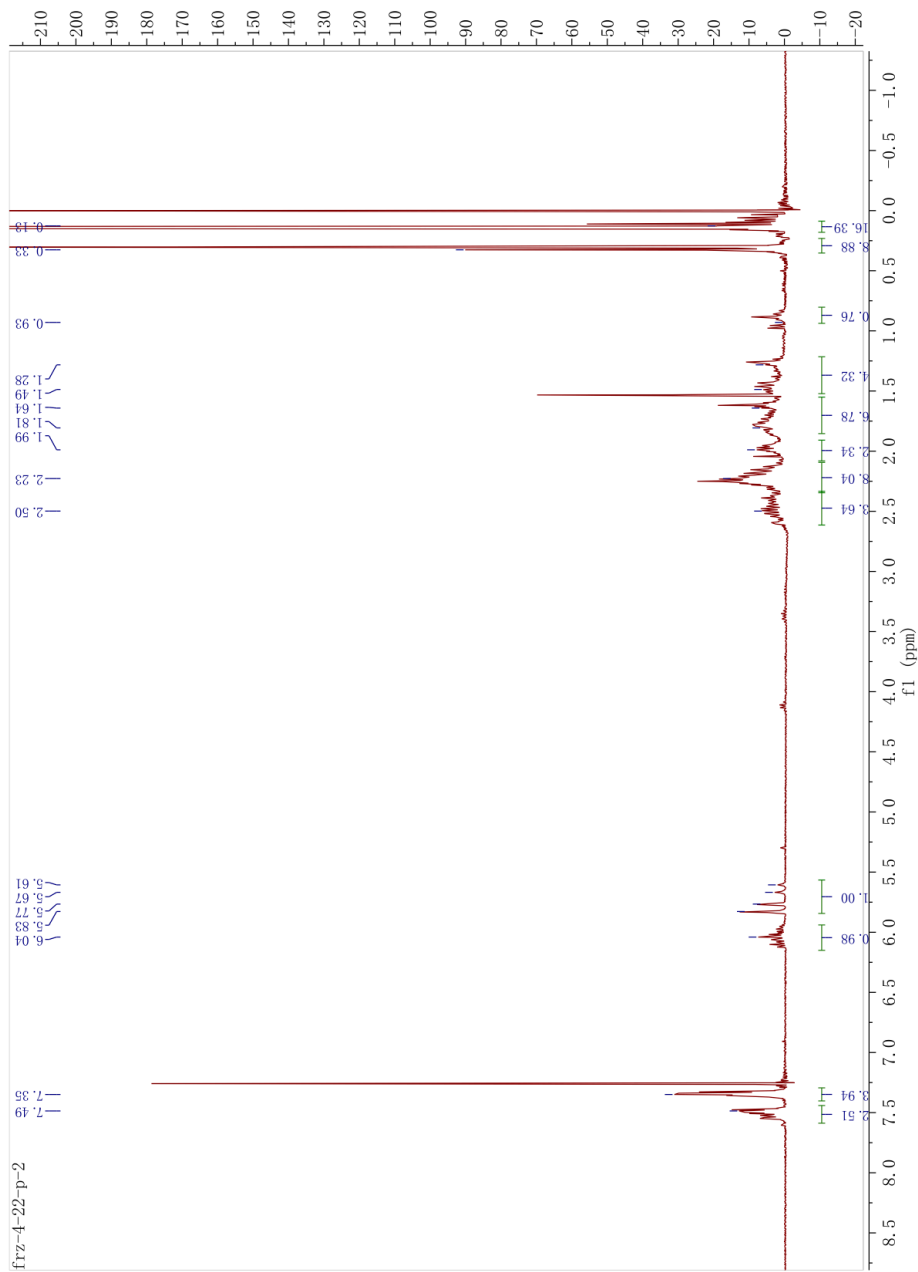
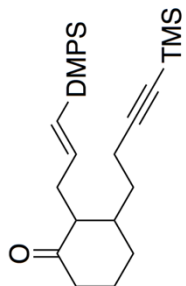


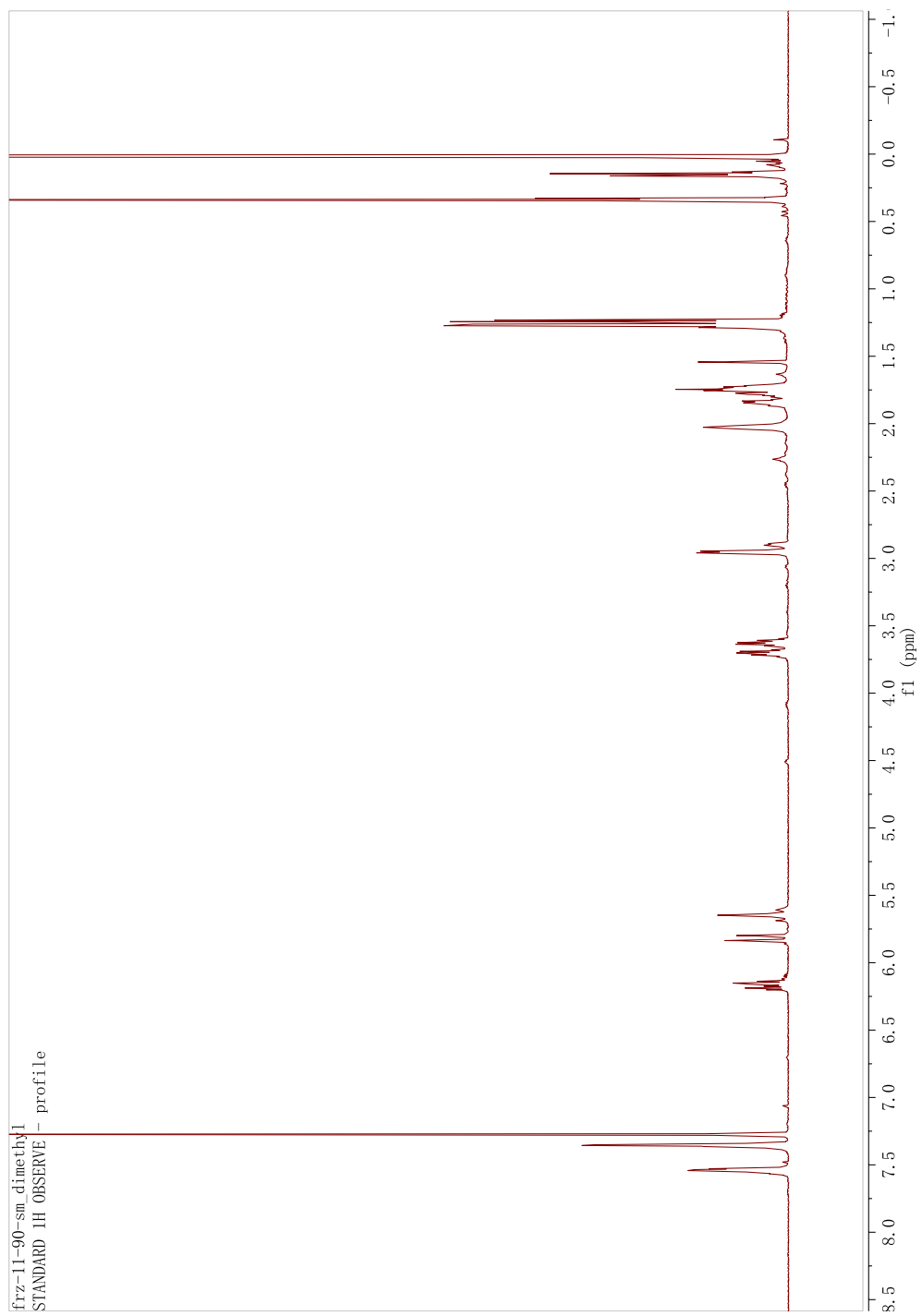
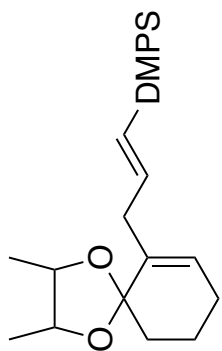
SiMe₂Ph

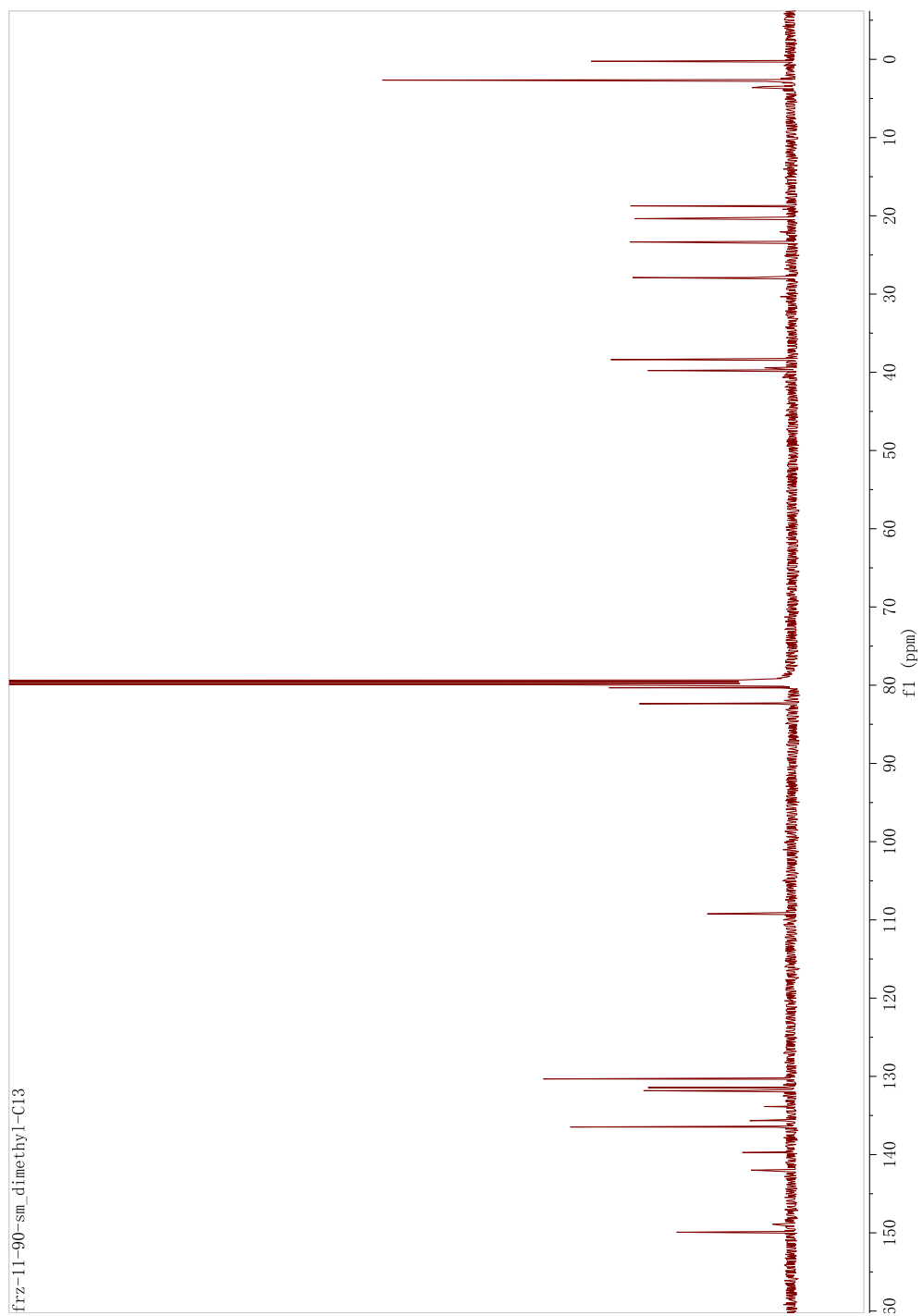
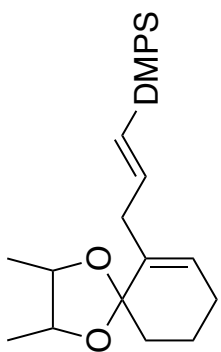


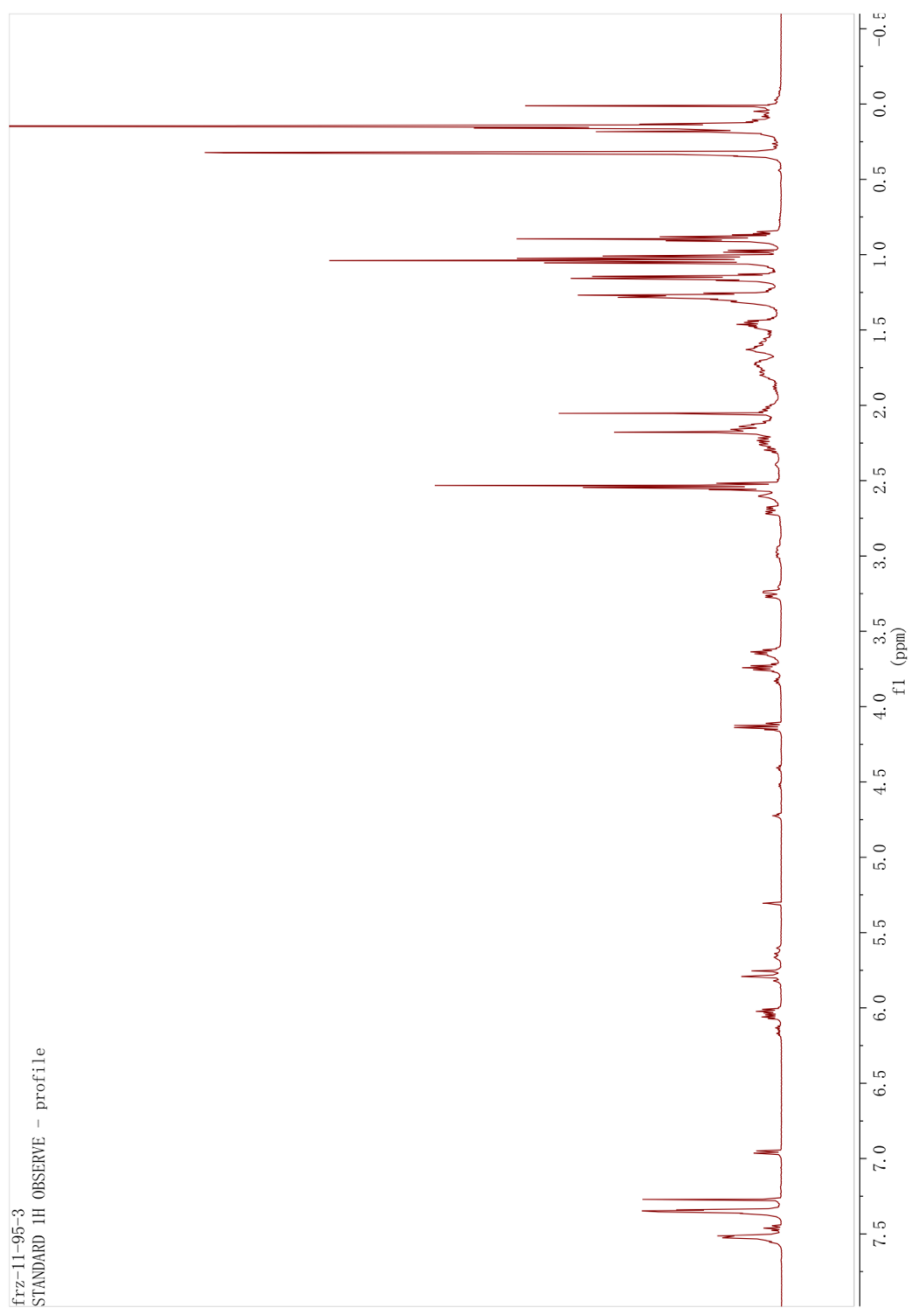
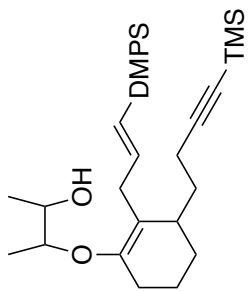
SiMe₂Ph

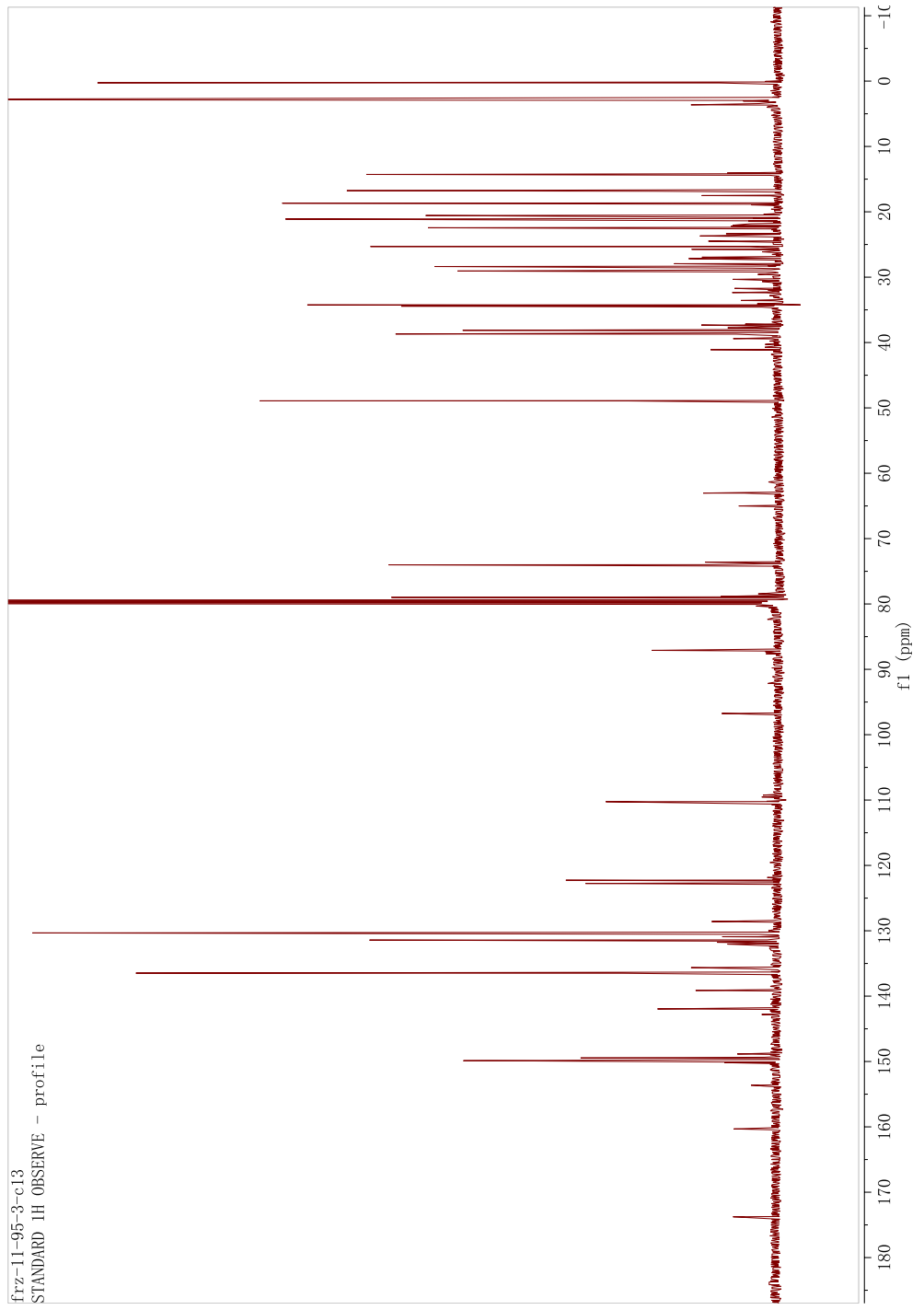
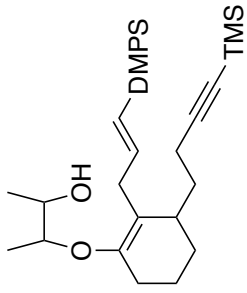


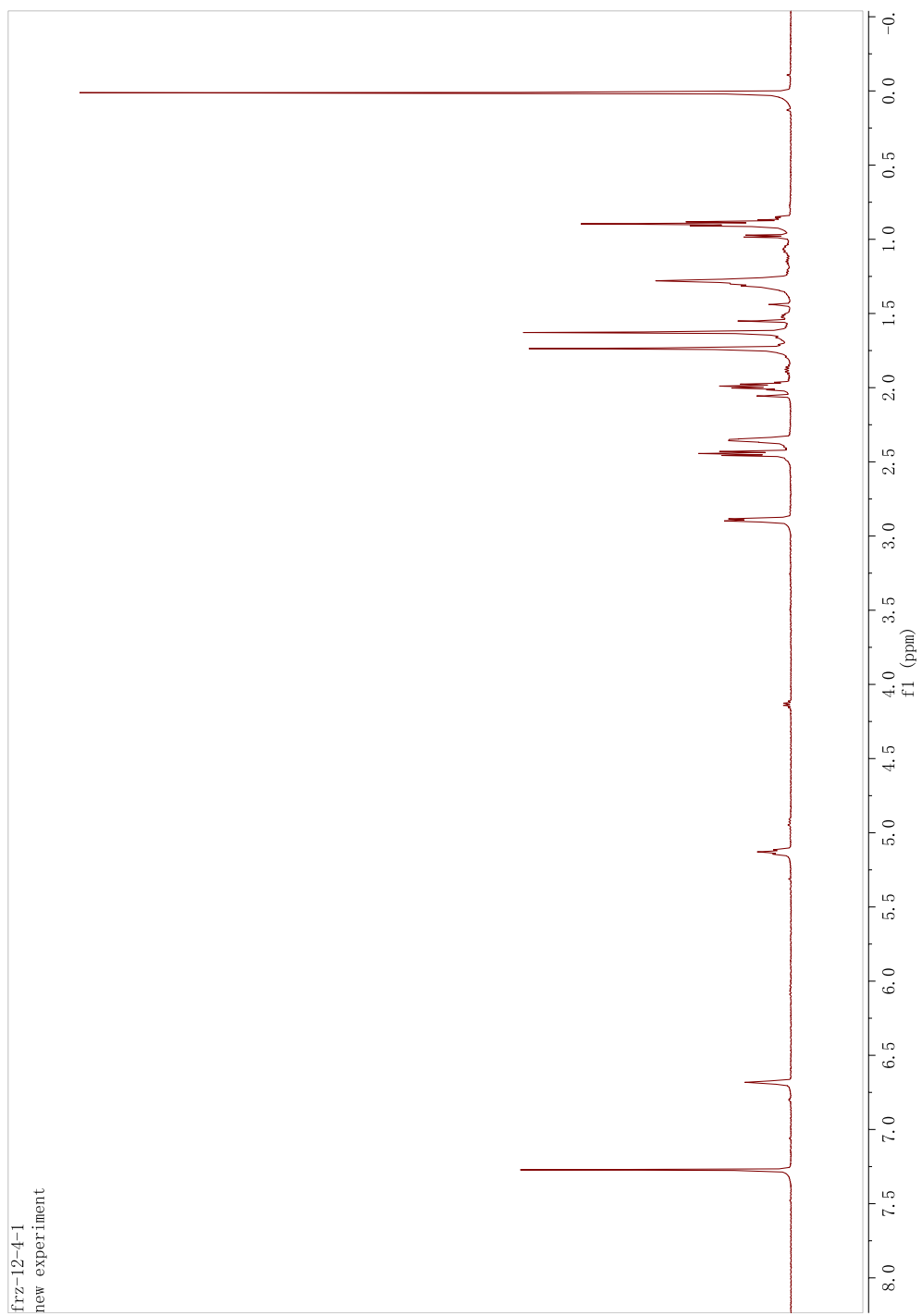
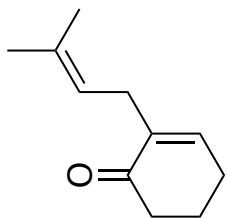


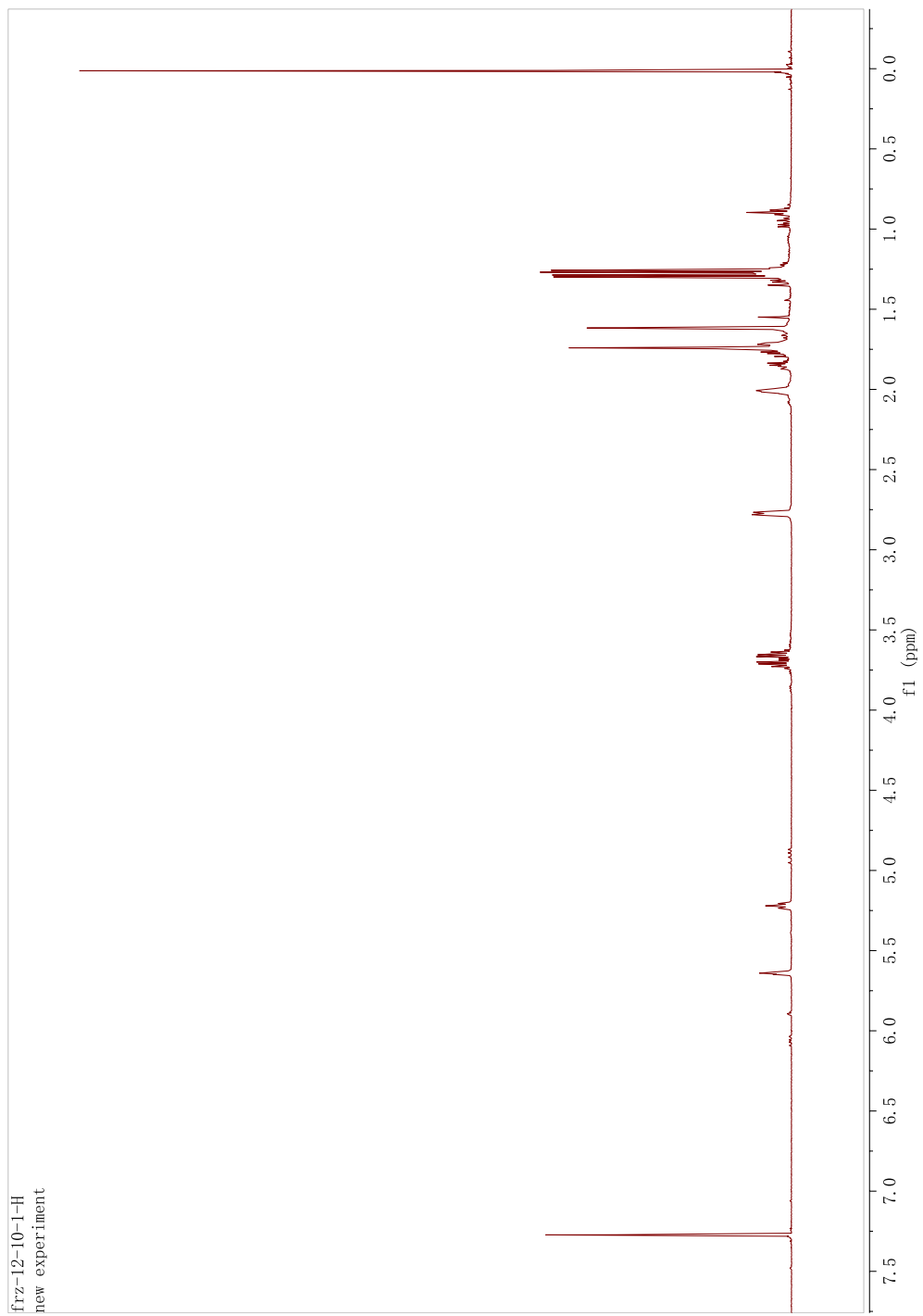
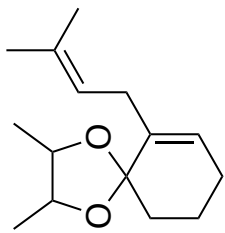


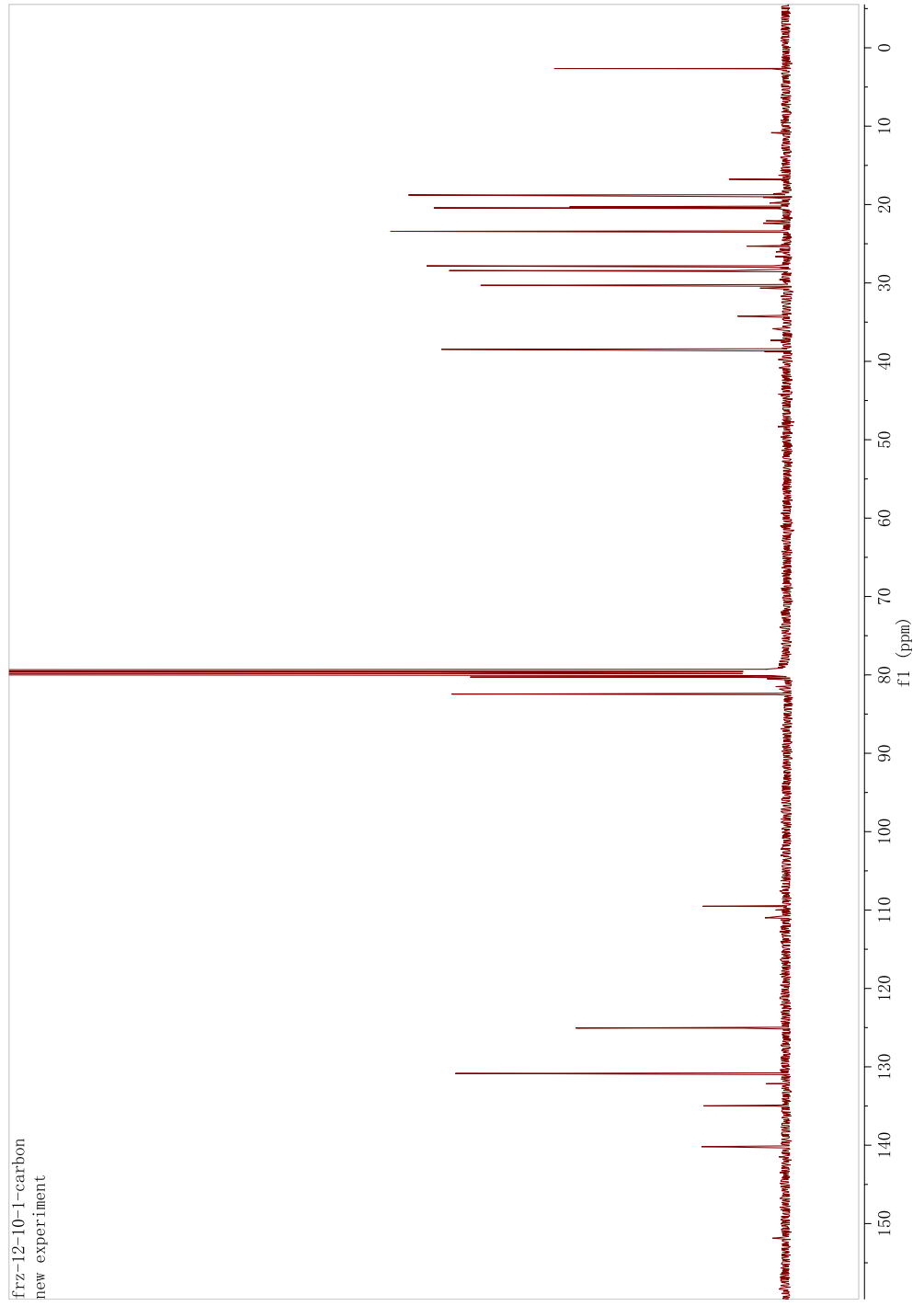
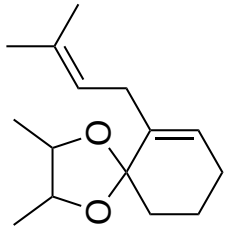


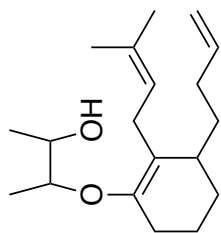




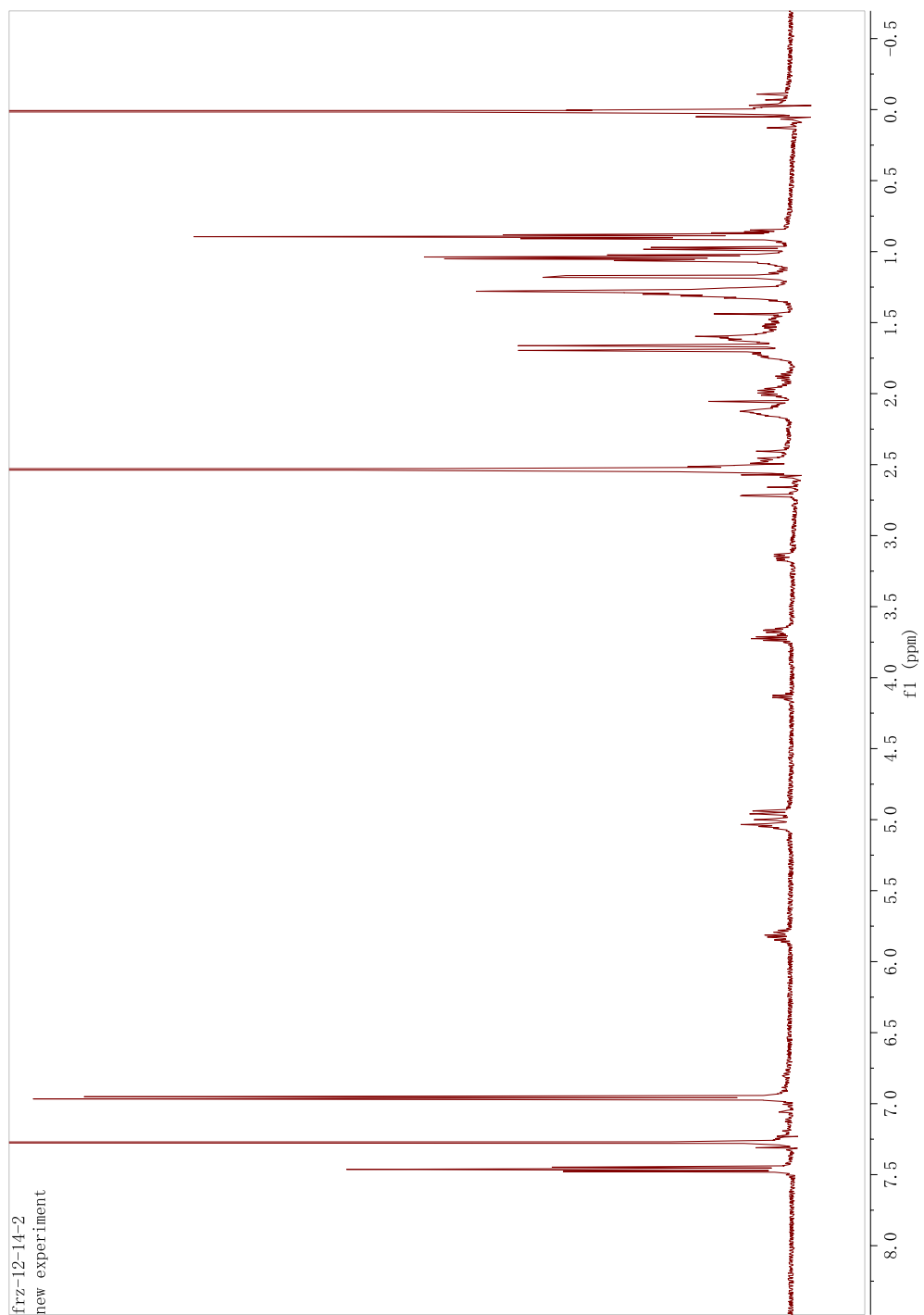


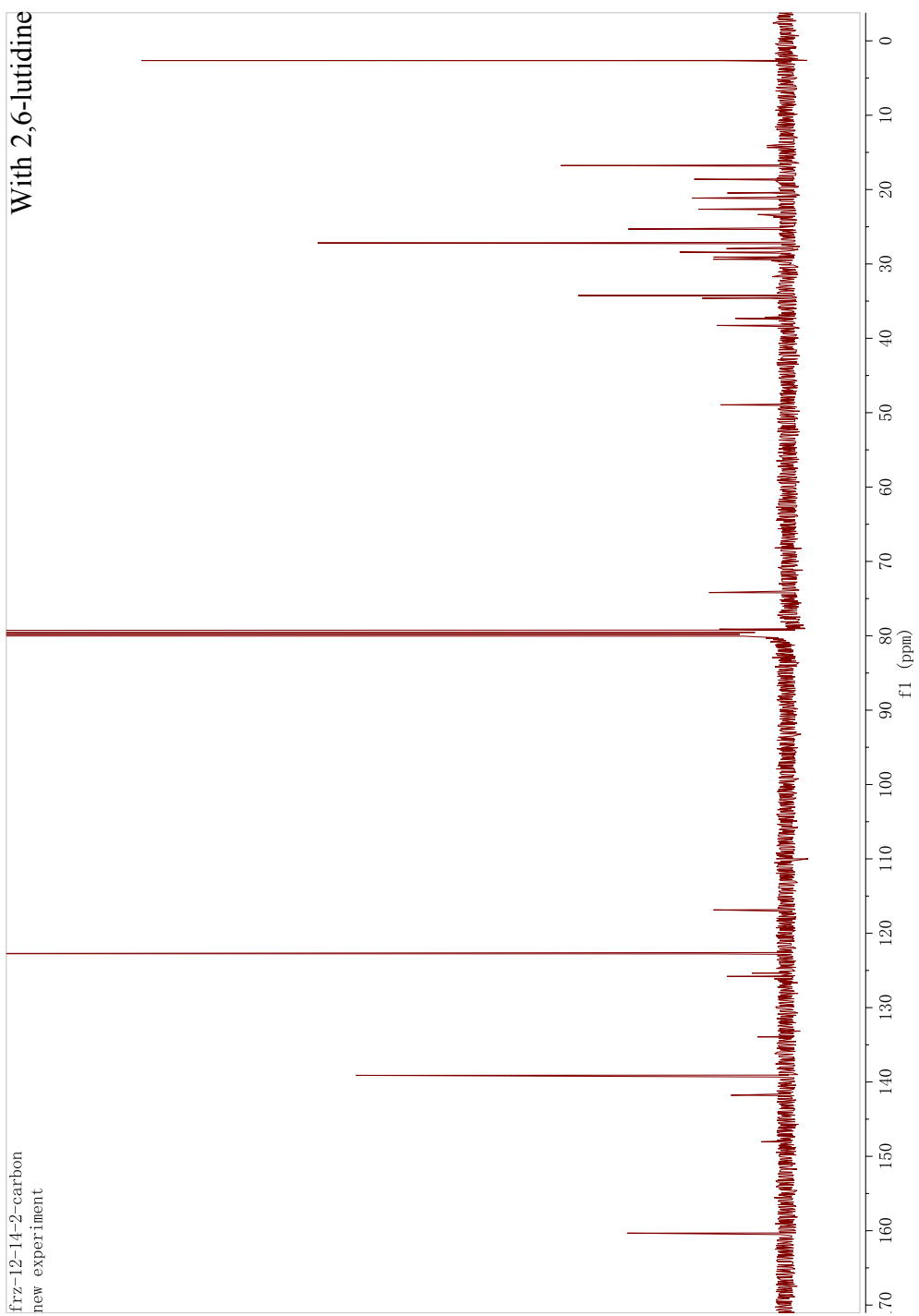
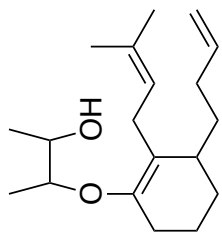


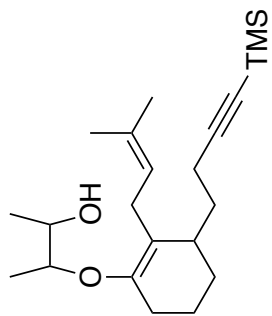




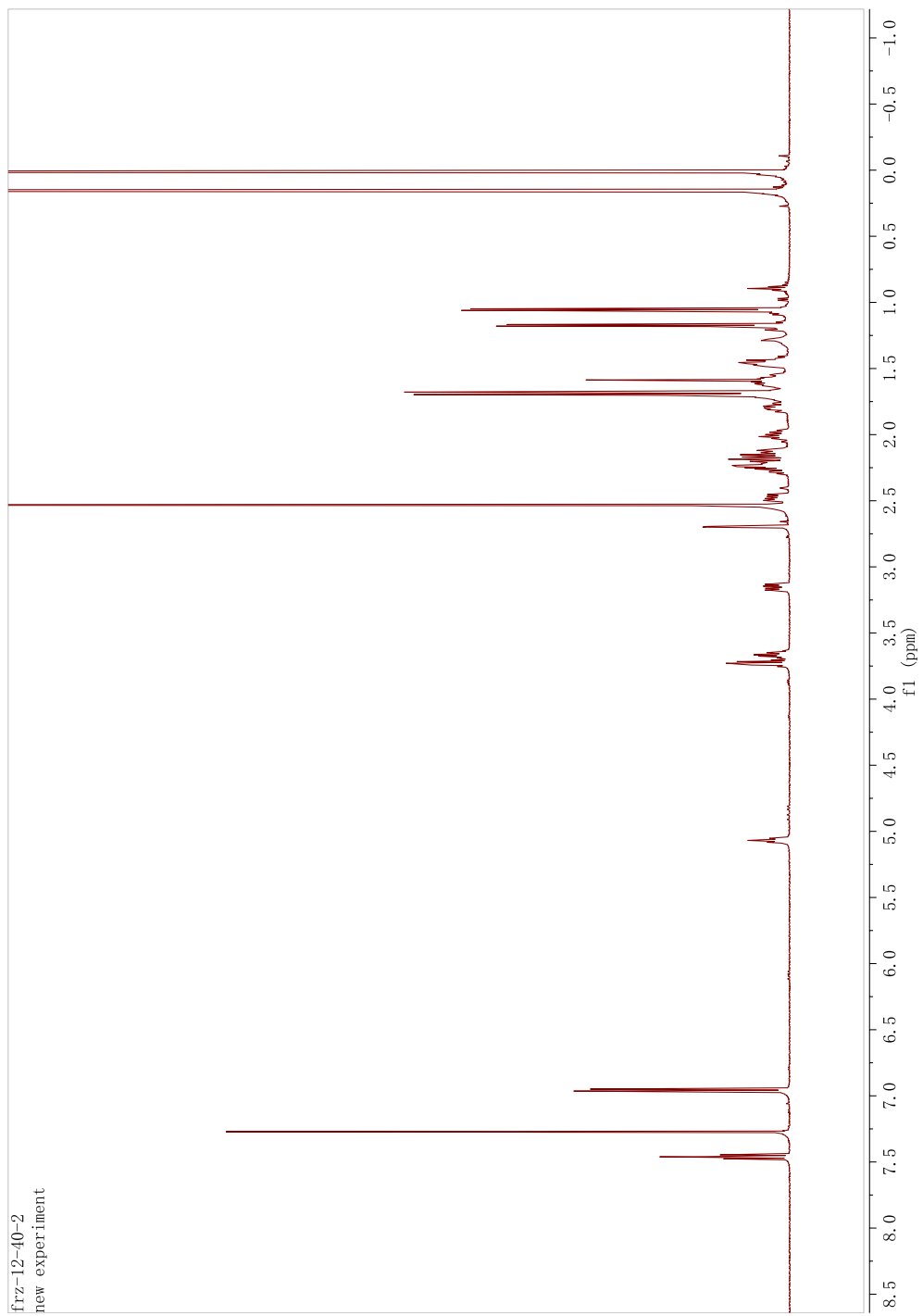
With 2,6-lutidine

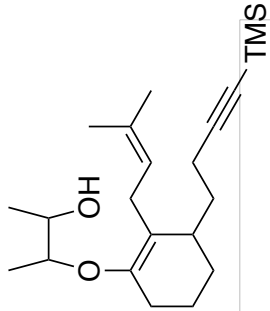






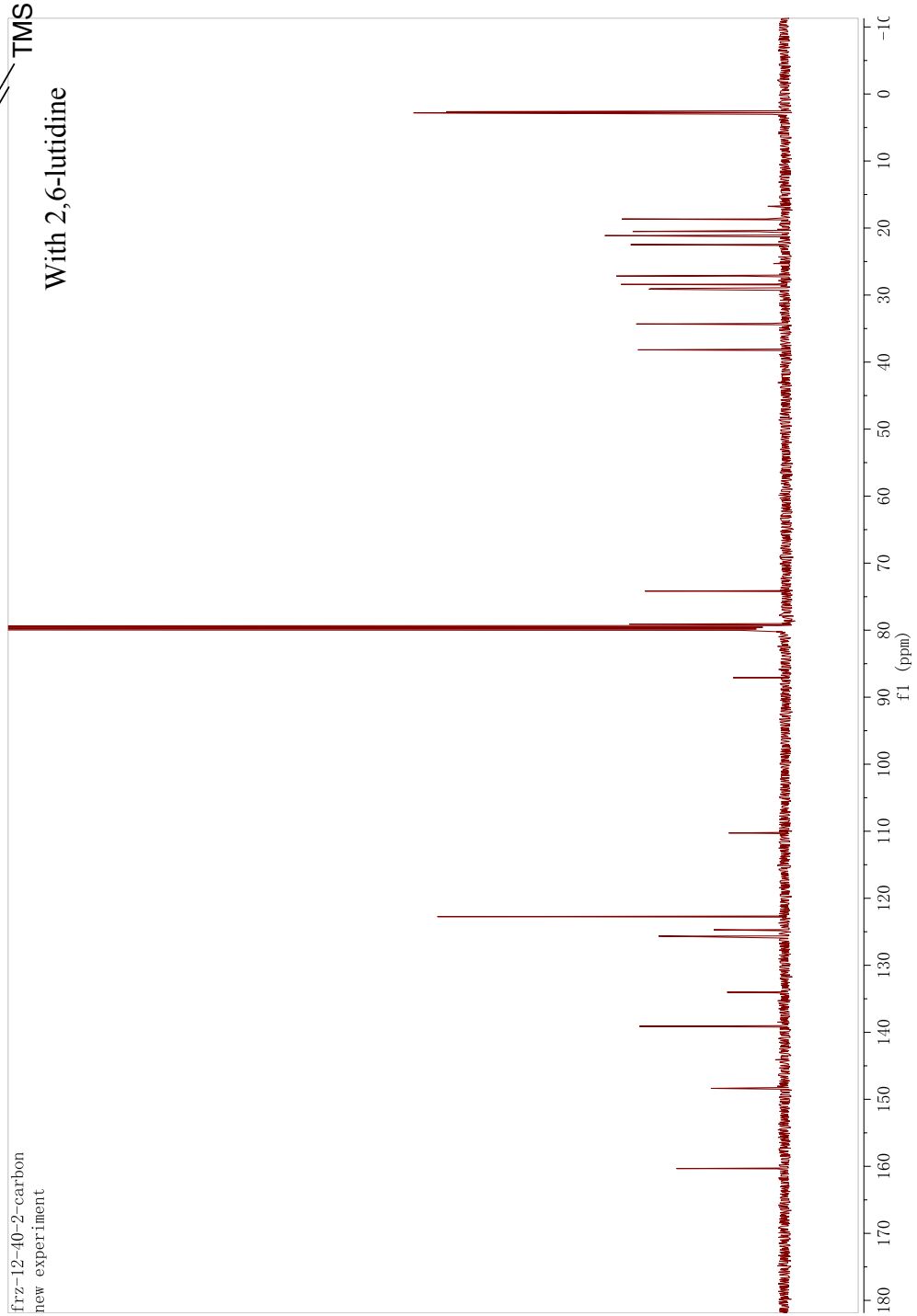
With 2,6-lutidine

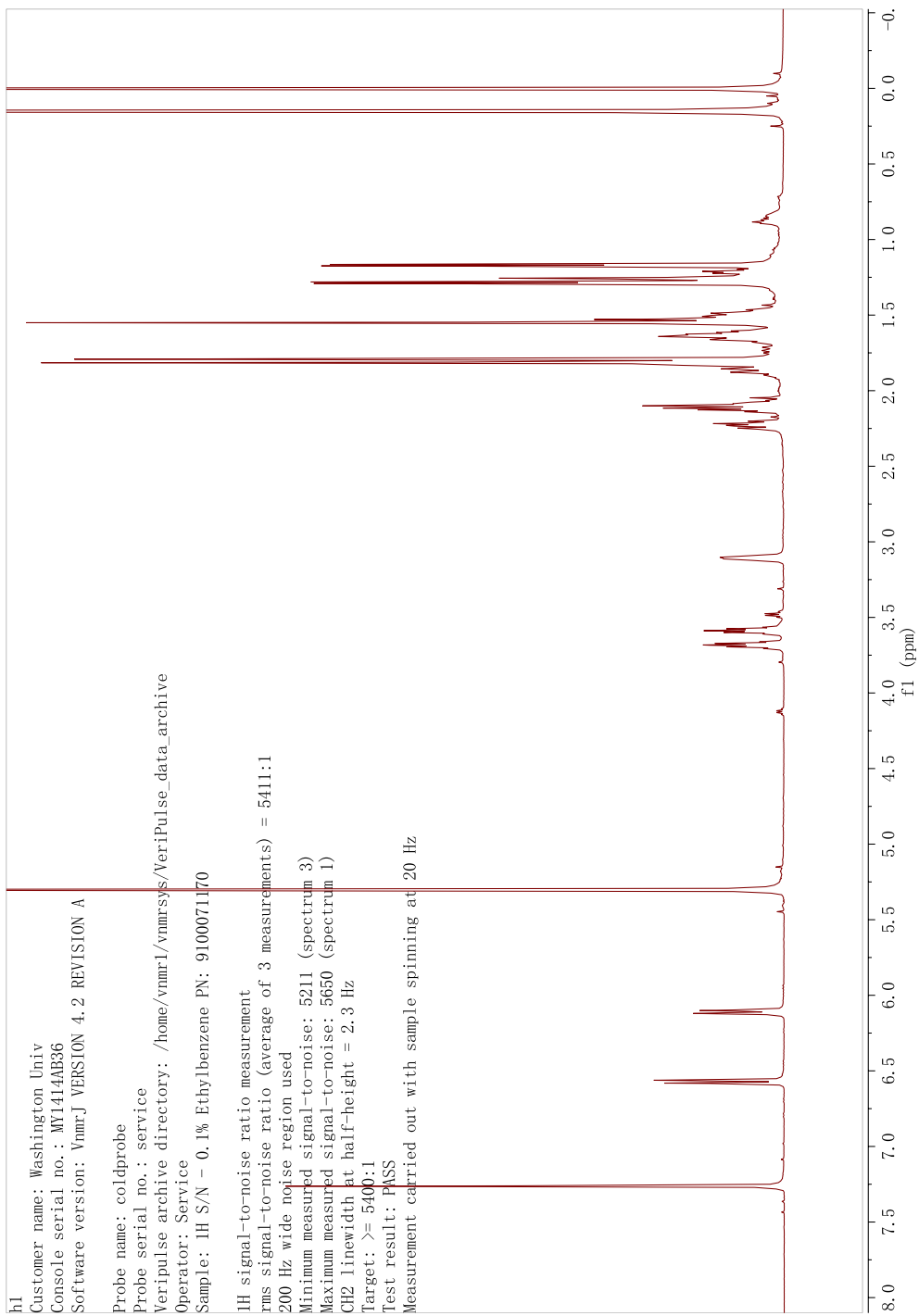
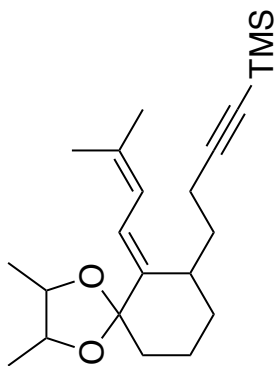


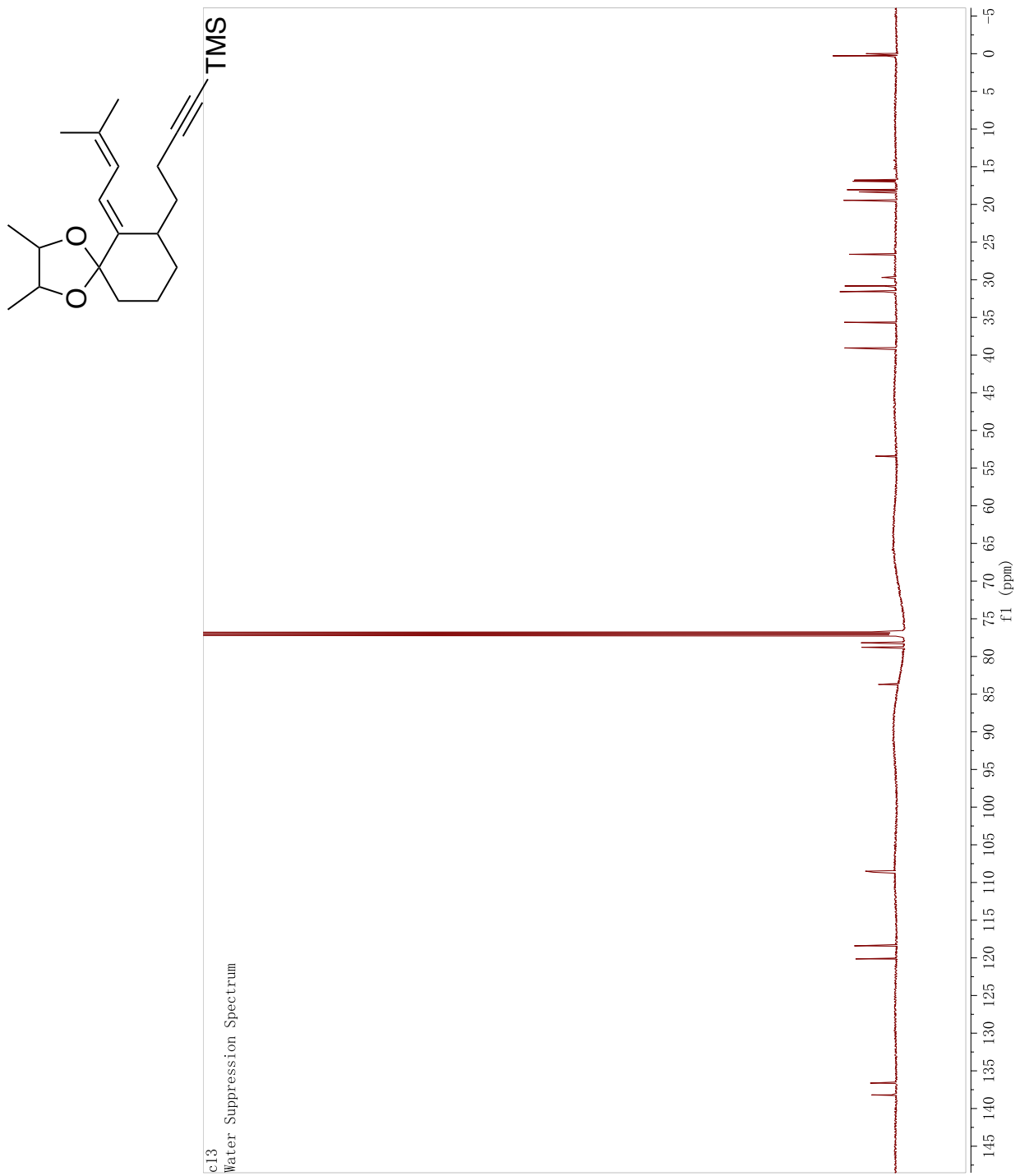


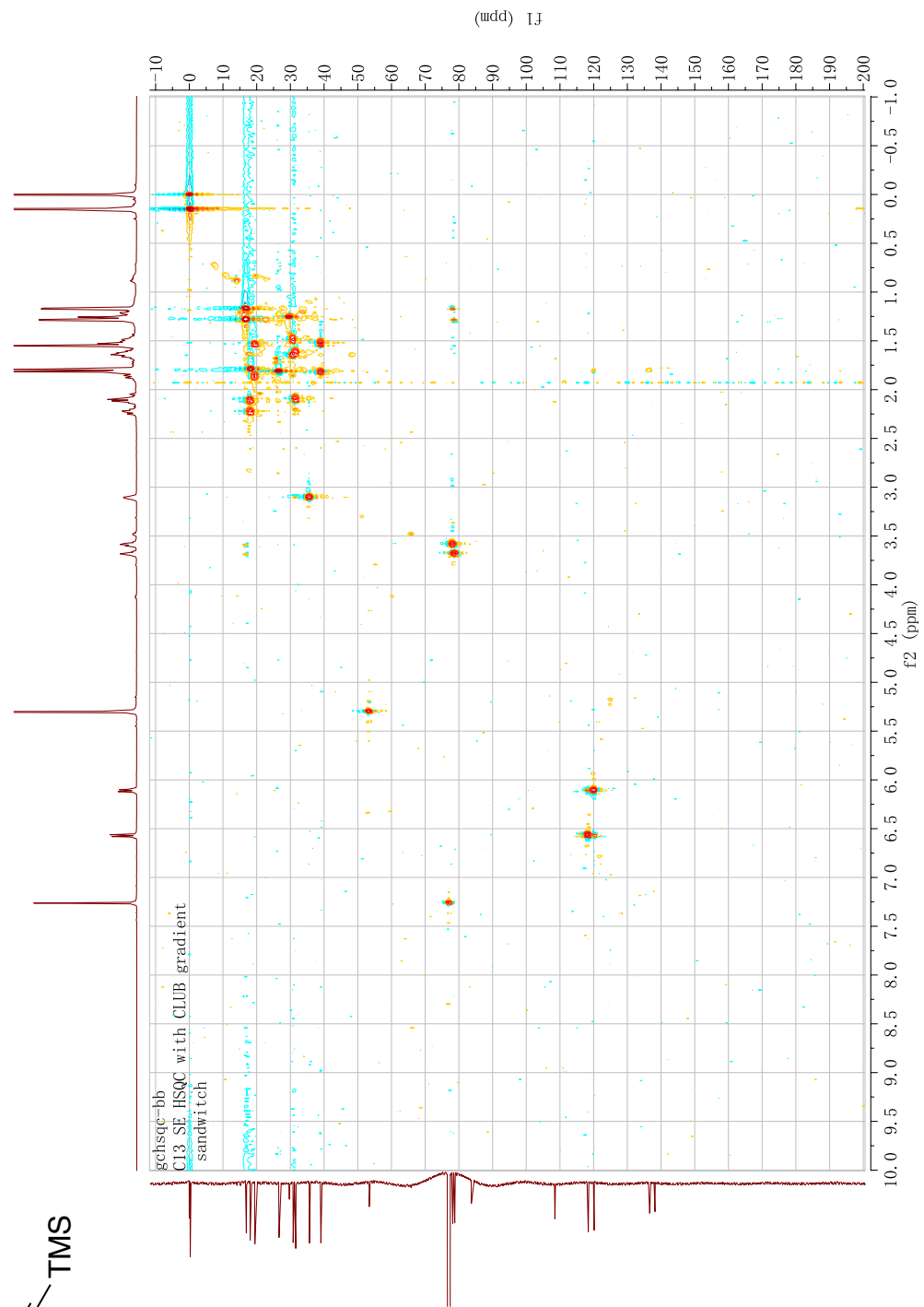
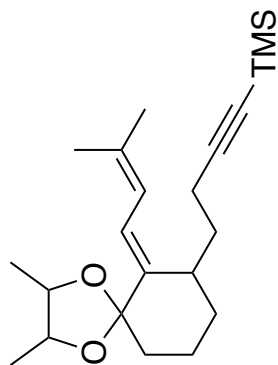
With 2,6-lutidine

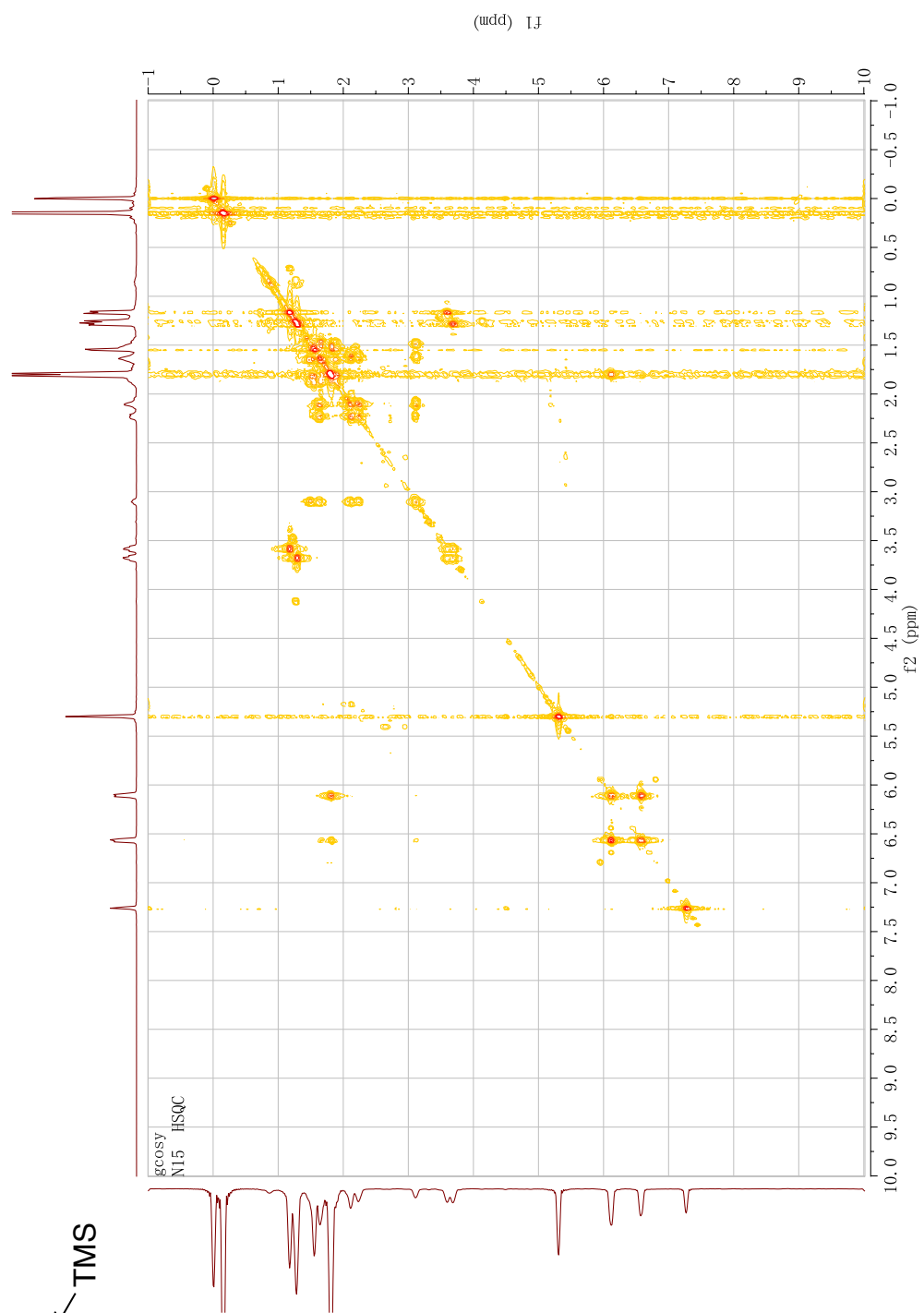
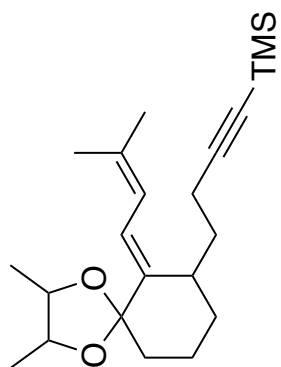
frz-12-40-2-carbon
new experiment

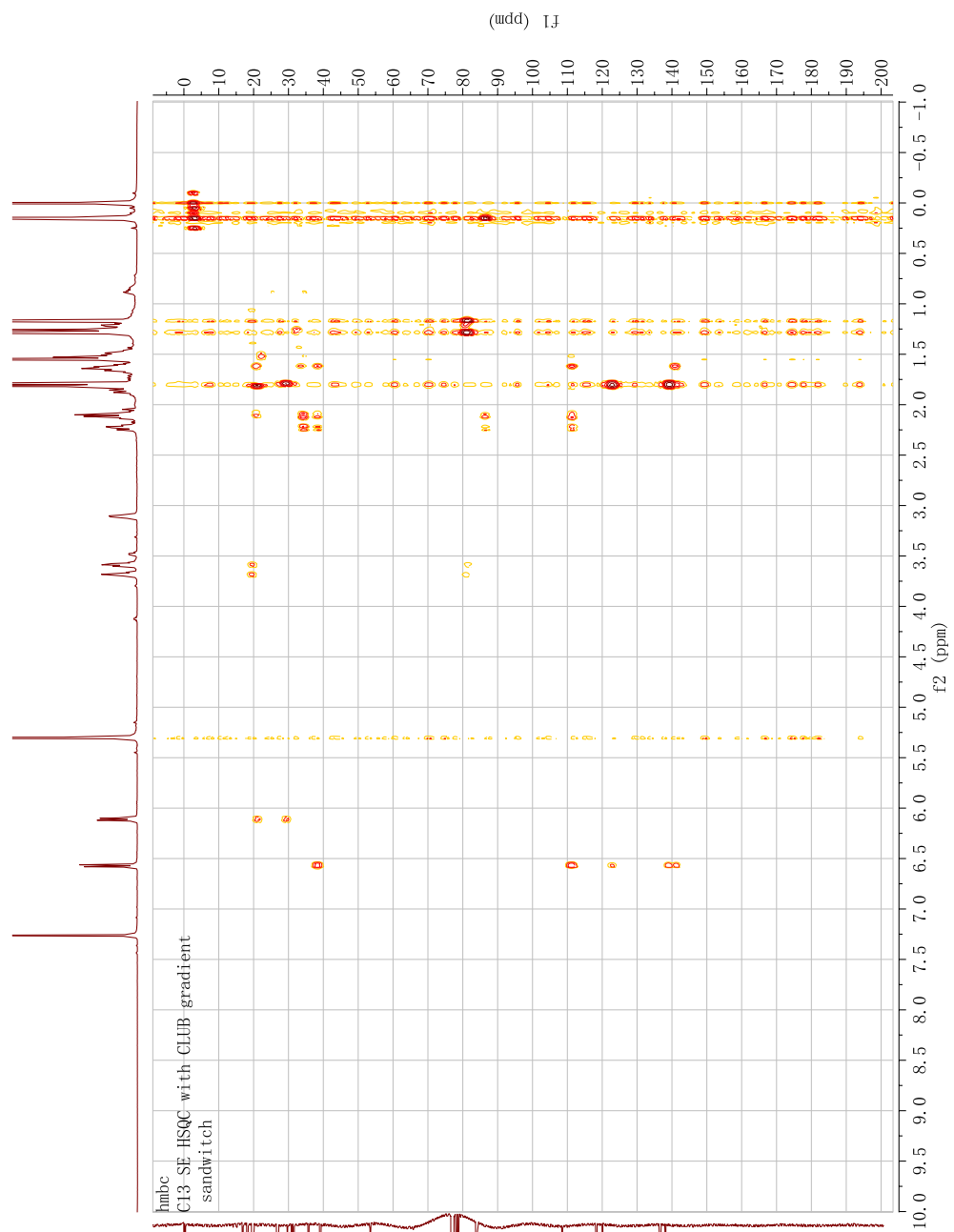
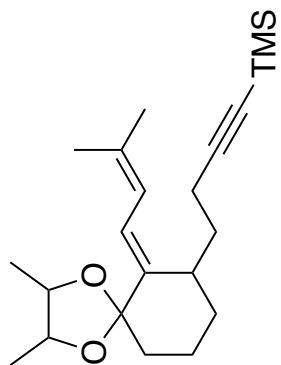


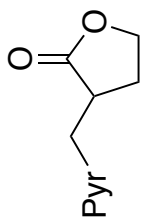




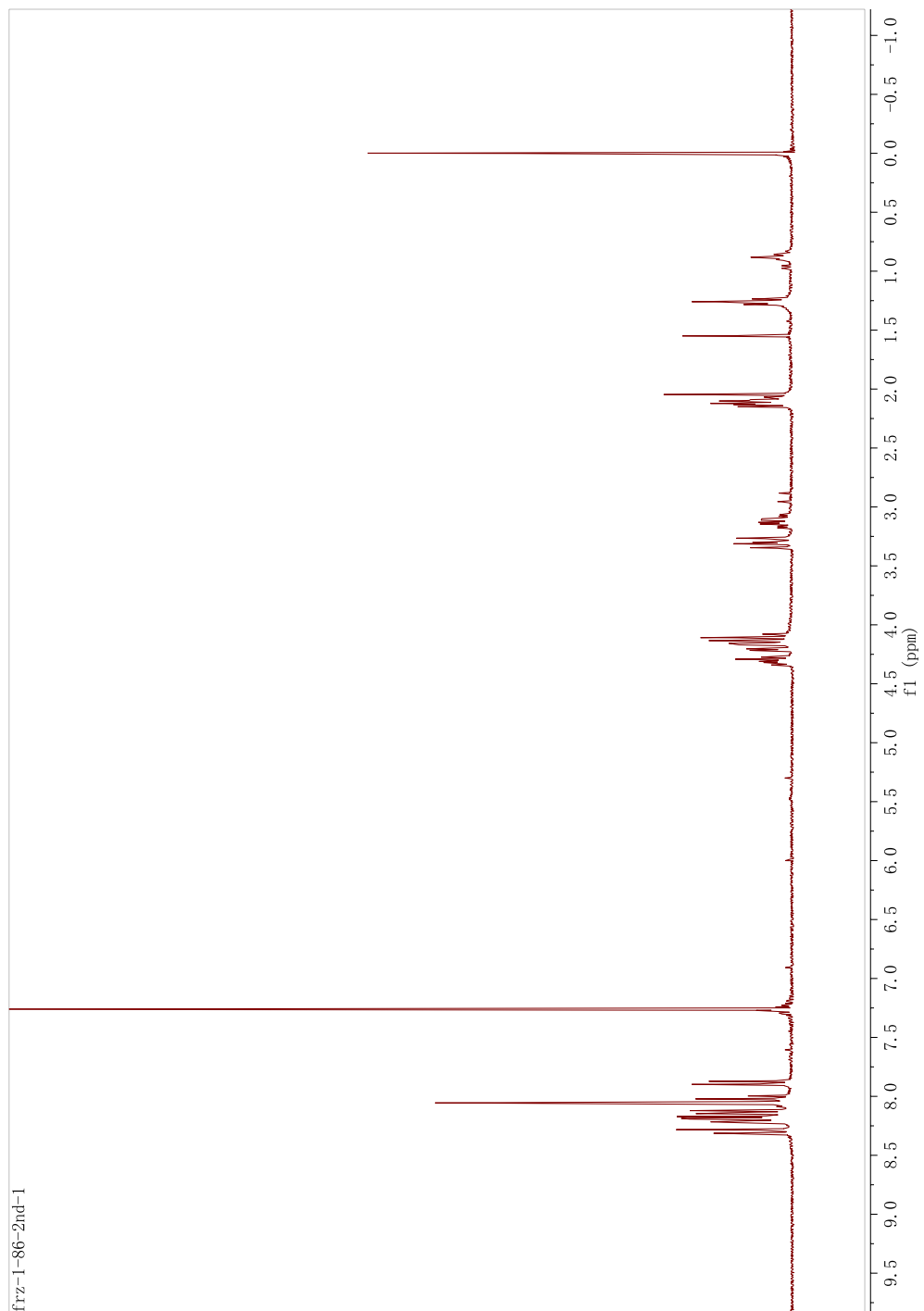


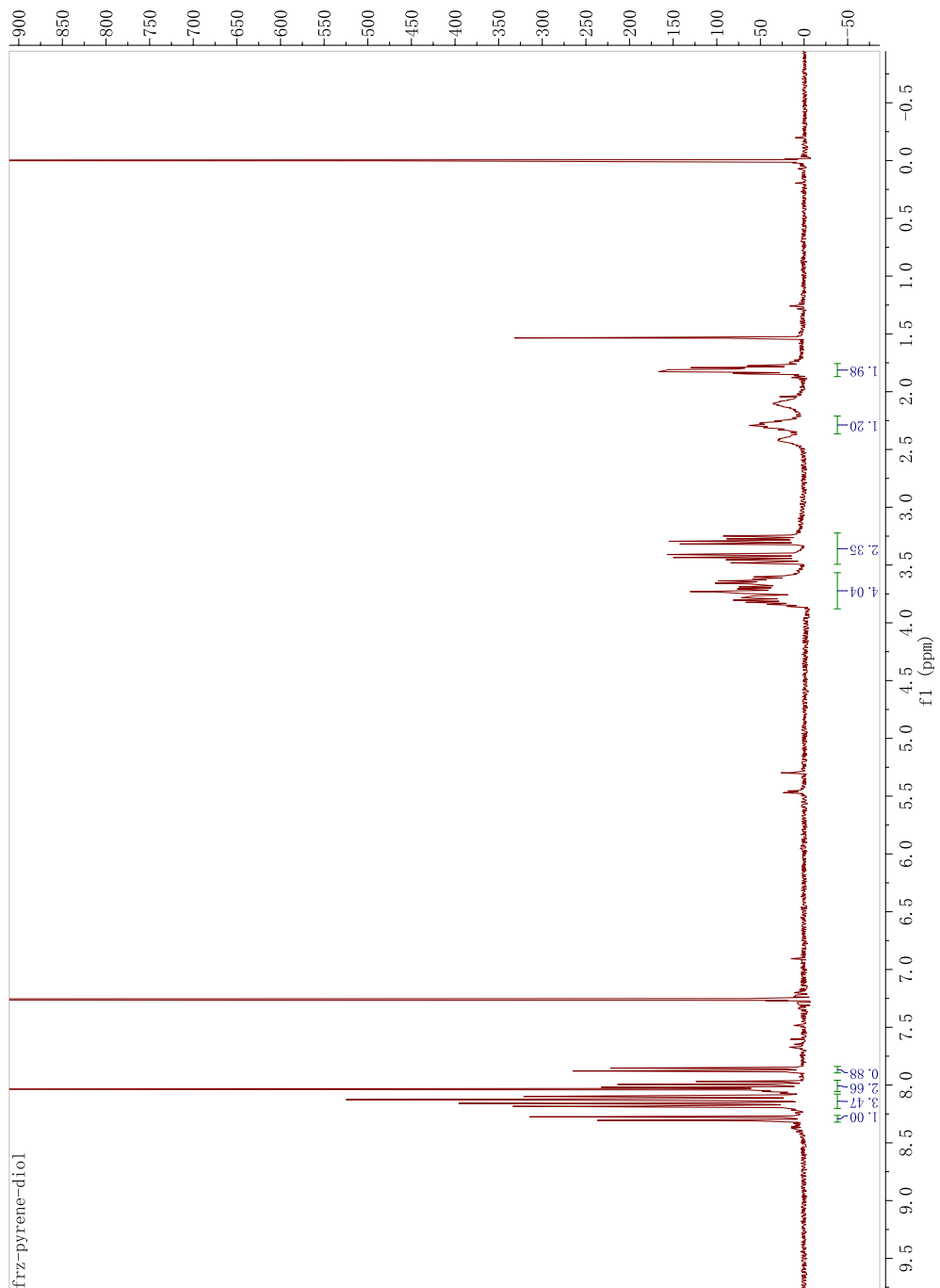
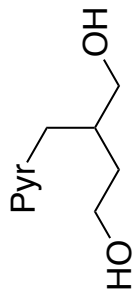


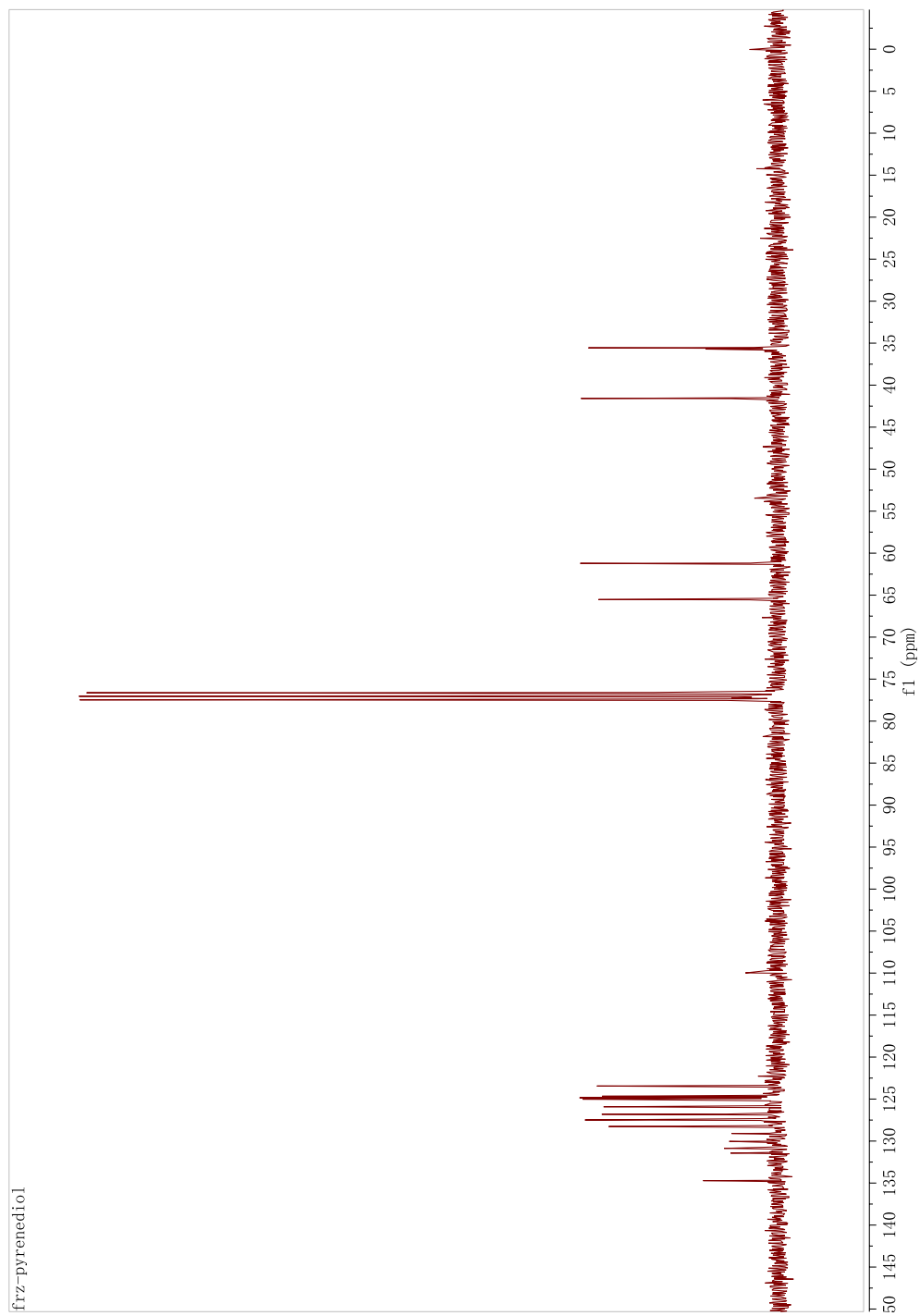
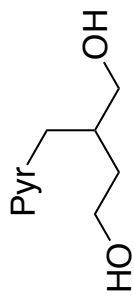


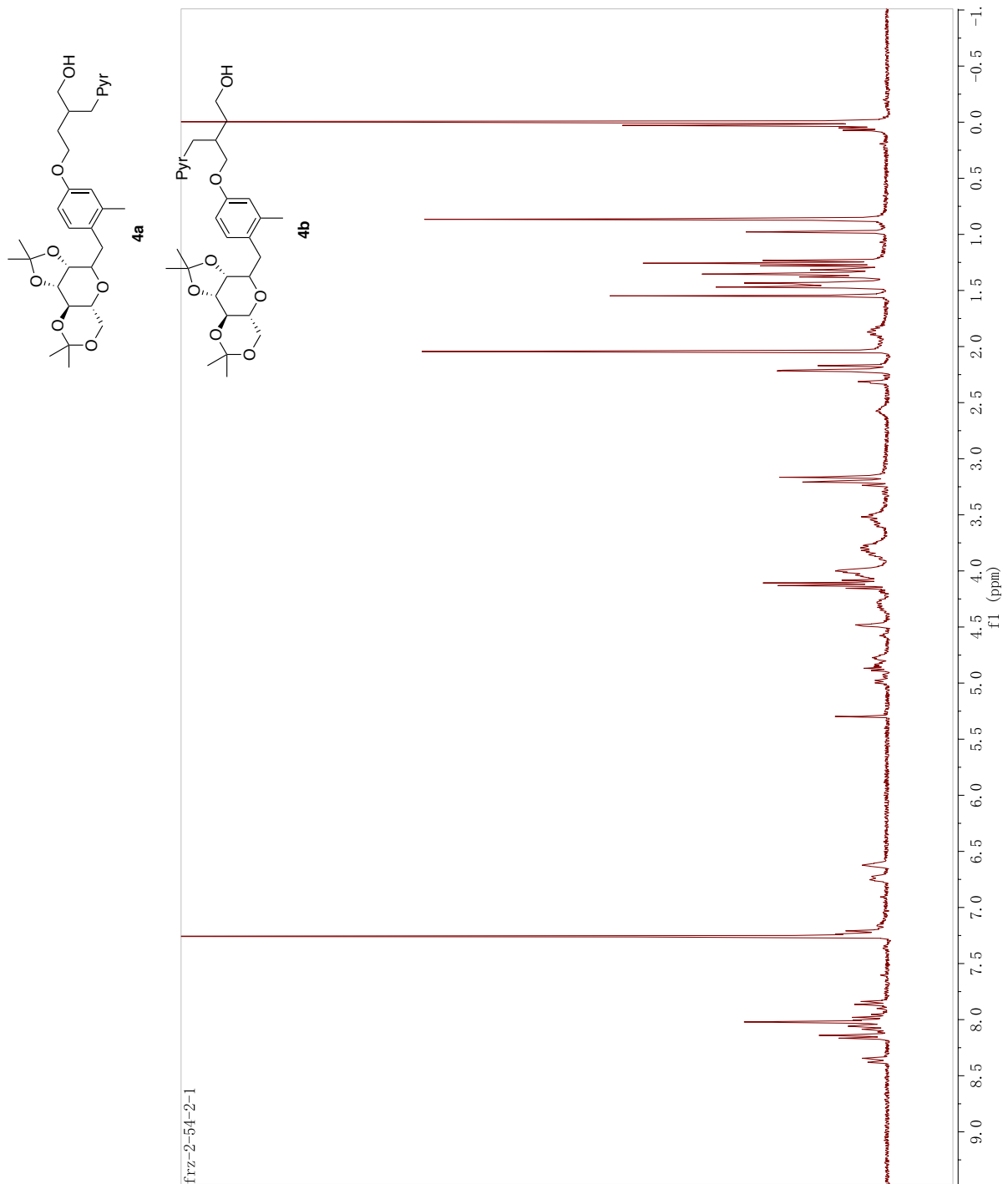


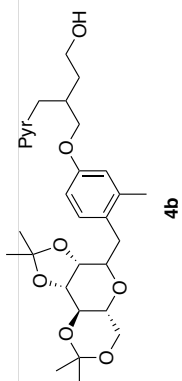
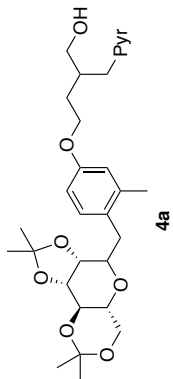
Appendix D











frz-2-69-purified-C

